In-Situ Determination of Buildings' Thermo-Physical Characteristics

Rasooli, Arash

DOI
10.7480/abe.2020.07

Publication date
2020

Document Version
Final published version

Citation (APA)
Rasooli, A. (2020). *In-Situ Determination of Buildings' Thermo-Physical Characteristics*. [Dissertation (TU Delft), Delft University of Technology]. A+BE | Architecture and the Built Environment. https://doi.org/10.7480/abe.2020.07

Important note
To cite this publication, please use the final published version (if applicable).
Please check the document version above.

In-Situ Determination of Buildings' Thermo-Physical Characteristics

Method Development, Experimentation, and Computation

Arash Rasooli

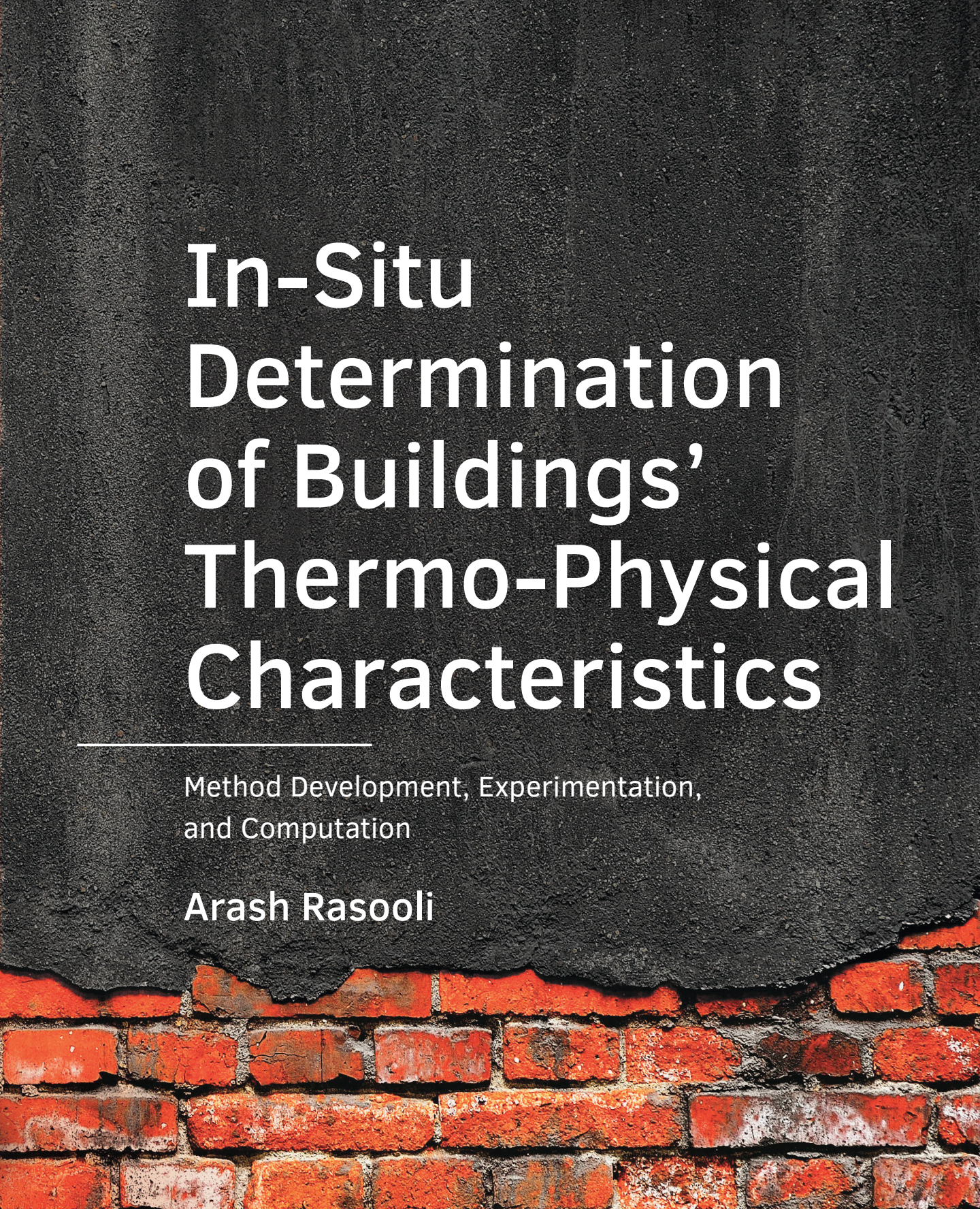

In-Situ Determination of Buildings' Thermo-Physical Characteristics

Method Development, Experimentation, and Computation

Arash Rasooli

TOC

A+BE | Architecture and the Built Environment | TU Delft BK

20#07

Design | Sirene Ontwerpers, Rotterdam

Cover photo | LiuNian

Keywords | In-Situ Measurement, Thermo-Physical Characteristics, Building Heat Transfer, Thermal Resistance

ISBN 978-94-6366-276-5
ISSN 2212-3202

Digital version freely available at **abe.tudelft.nl**

TOC

In-Situ Determination of Buildings' Thermo-Physical Characteristics

Method Development, Experimentation, and Computation

Dissertation

for the purpose of obtaining the degree of doctor
at Delft University of Technology
by the authority of the Rector Magnificus, prof.dr.ir. T.H.J.J. van der Hagen
chair of the Board for Doctorates
to be defended publicly on
Friday 5, June 2020 at 10:00 o'clock

by

Arash RASOOLI
Master of Science in Mechanical Engineering,
Delft University of Technology, the Netherlands
born in Tehran, Iran

TOC

This dissertation has been approved by the promotors.

Composition of the doctoral committee:

Rector Magnificus	chairperson
Prof.dr. L.C.M. Itard	Delft University of Technology, promotor
Prof.dr.ir. H.J. Visscher	Delft University of Technology, promotor

Independent members:

Prof. dr.-ing. U. Pottgiesser	Delft University of Technology
Prof.dr.ir.-arch. D. Saelens	KU Leuven, Belgium
Prof.dr.ir. J. L.M. Hensen	Eindhoven University of Technology
Dr.ir. O. Guerra Santin	Eindhoven University of Technology
Prof.dr.ir. P.M. Bluyssen	Delft University of Technology, reserve member

Other members:

Dr.ir. C.A. Infante Ferreira	Delft University of Technology

Rijksdienst voor Ondernemend Nederland

TU Delft

This project has partly been executed with help of “Topsector Energy Subsidy” of the Ministry of Economic Affairs and Climate Policy. TKI iDEEGO and Rijksdienst voor Ondernemend Nederland (The Netherlands Enterprise Agency, RVO) are acknowledged.

Dedicated to my beloved parents

Acknowledgements

This book was prepared and finalized during the pandemic COVID-19. My first and foremost acknowledgment goes to all the clinical staff and healthcare professionals who have heroically put our lives before their own, during this critical time.

My PhD path has been a wonderful journey and as I always say “It is not only about your work, but it is also about good people you get to know during your work “. I am very grateful to many good people who, in small-to-large scales, have had contributions to my growth and accomplishment of this PhD. Thus, rather than a formal script, I would like to take my time and appreciate a number of these people.

The first time that I attended the class Indoor Climate Control Fundamentals, I never thought that our instructor would be the one to entirely change my life. I would like to start with my dear promotor, mentor, teacher, and supervisor, Laure Itard, who is truly phenomenal. She has inspired me and conveyed to me a higher level of strength, confidence, knowledge, and wisdom. I do not think anyone has ever made me push my limits so far to grow and become a better version of myself. She has guided me to obtain invaluable skills and knowledge I will forever use in my professional and personal life. I am absolutely thankful and grateful to have had the pleasure of working with such a genius person, of the smartest people I have ever known. Laure, apart from my Master thesis and my PhD dissertation, my personal life including my residence in the Netherlands, my European network, and even my future job, almost everywhere there is a sign of you and obviously I cannot thank you enough for that. As always, words fail to express my gratitude towards all you’ve done for me. I also wish to thank you very much for trusting me and letting me teach independently during your master classes, the same course where we first met, and the edX online program. I trust to continue our collaboration in the future with great pleasure.

Secondly, I would like to thank my second promotor. Henk, thank you for supporting me during my PhD. As our ex-section director, you have fully succeeded in making us ex-DWKers feel like a family and I want to thank you for that. I also wish to distinctly thank you for trusting me and helping my friend Shima.

I wish to separately thank our partners in the OPSCHALER project: W/E Adviseurs, Enexis, DEMO BV, Technolution, Almende, Huygen Instalatie Adviseurs, and the

Hague University of Applied Sciences. I also wish to thank RVO for providing us financial support through OPSCHALER project. I wish to acknowledge all people involved in the execution of the large-scale campaign, including the installers, the secretaries, people from ICT department, facility management, and the logistic point of the faculty of A+BE, TU Delft.

I also want to acknowledge Truus, Monica, Mary, Martine, and Jeanet for their continuous help. Separately and very specially, I wish to thank Elianne, for her excellent support and kindness towards me during all the years of my work, and for her valuable help during the OPSCHALER project.

During my work, I have had the pleasure of working amongst the most wonderful colleagues: Tasos, Frits, Queena, Ad, Hongjuan, Youting, Jifang, Ling, Herman, Roger, Nico, Bo, Boram, Job, Alfred, Juan, Afua, Cynthia, Gust, Zoheir, Zahra, Ali, Marja, Marietta, Sylvia, John, and Paul. Thank you all for always being kind to me. I want to thank Arjen separately also for his contribution to the OPSCHALER project and his cooperation during the supplementary measurements. From the other departments, I would like to thank Erwin for being of the top nicest colleagues I have ever had. I would also like to thank Anna for the wonderful relaxing tea breaks we had together.

Carlos, apart from your help for the article and the patent, I want to thank you for teaching me very important lessons ever since I was a master student. Your attention to details is exemplary and through your critical perspective towards scientific work, I have learned much. I also appreciate the detailed review you carried out for this work which improved it to a higher level.

During the time I carried out the experimental part of my work, a number of very kind people have given me technical support. I wish to thank Martin Verwaal from the lab of the faculty of Industrial Design, TU Delft, for providing me with equipment for a critical part of my research and for teaching me about measurement instruments. I wish to appreciate Staf Roels and Willem Bertels from the faculty of Civil Engineering, KU Leuven, Belgium, for their very kind technical and scientific support and the practical arrangements for my experiments. I want to also thank Kees Van Den Bosch, the director of Hukseflux Thermal Sensors B.V. for being open for scientific and practical discussions and cooperation, and Robin Winters and Heerco Walinga, the managers of Delta OHM and Mierij Meteo for providing technical and scientific support.

I want to thank Kees Hoegendijk, the director of EKO Instruments Europe B.V. and my future boss, for his support, his interest in my work ever since I was a master student, and for offering me my next job without questioning my capabilities.

I would like to thank Stefanos, who has been a wonderful assistant to me during my work with the large set of measurement equipment. You have been a wonderful help, and a lovely friend. I want to really thank you and Ahmed, not only for the OPSCHALER project, but also for the “Linear-to-Go” control system you made for me with the help of Milad and Kevin.

I want to appreciate TVVL, especially Hans Besselink and John Lenz for supporting me and involving me in the jury activities of TVVL student competition. I also like to thank REHVA especially Nathalie Wouters, Manuel Carlos Gameiro da Silva, and Frank Hovorka for involving me in REHVA activities. Further, I wish to acknowledge Mrs. Véro Crickx for her excellent work and support during the preparation of my book for publication.

Back home in Tehran, and in many other places on this planet, many people, whose names will not fit in paper, have helped me to reach my current state. I have countless friends who I truly mutually love and care about. They have been giving me endless love and support and I want to truly thank them. Elham, you have played a key role in my life abroad. Thank you for being the best English teacher I could ever have. Babak, your contribution to my English, my applications for universities abroad and my life aboard is very bold and I want to deeply thank you for that.

I further wish to acknowledge all my dear teachers from school to university, who encouraged me and taught me much of what I know today, and all the academic staff who have contributed to my education till today.

Ever since I came to the Netherlands, I expanded my family with the most wonderful friends. These people have been caring for me and giving me moral support. To all my dear friends: Farid, Fariborz, Milad, Hassan, Ameneh, Sam, Antje, Farhad, Maryam, Mostafa, Maryam, Mohsen, Mahtab and all the ones missing in my list I am absolutely grateful to have had your friendship and support. You all are my lovely friends who I am blessed to have. I want to acknowledge Prins family, especially Marlies, for being the loveliest and best neighbors ever, always caring for us. I also wish to thank my first neighbor in the Netherlands, and lovely friend, Lilia, for always caring for me and my mother, and for what she has taught me during these years.

Anna L, I cannot imagine how I could miss you in my life. I owe you all you taught me from the language, culture, and the mind-set of the Dutch society. I am grateful to know you and your wonderful family, which I consider mine too. Lessons, meals, walks, camping, and trips, kerstavonds, and dining with Heijn, Luna, Daniel, and Jeff, are what I will keep in the most valuable memories of my life.

Gianis, I am very grateful to our friendship and to have known you much better in the recent years. You have shown me how strong a man can be and I look up to you in that. I have learned many important life lessons from you. Thank you for being my lovely friend and for supporting me. Faidra, you have supported me for all these years, ever since we met in the old OTB office. I owe you much in my life and for this PhD. Whenever I had an important moment, I looked around and you were there with me. I can never thank you enough for taking me to Greece and really treating me as your own family, whom I too truly love and miss. During our friendship, I have learnt so many things from you. You have also changed many of my important perspectives in life and taught me important lessons and I thank you for that and for always caring for me. Paula, thank you for being my single closest and by far the best "Landgenoot" friend. I am very grateful to our friendship and I want it to last forever. Also, as colleagues, the path we have been following together, has been very inspiring to me, because we did it together. I would also like to thank you for your contribution to the OPSCHALER project and to have helped me through our many scientific discussions. I have learnt many lessons from you, especially about the "actual-and not theoretical" meaning of the strength and independence of women, something I promise you to forever fight for.

Being a single child, I have had no brothers or sisters. To that end, I have always been collecting the bests of them from the people around me. Marzieh, I want to thank you for caring for me these years and also for fighting and trying for our friendship. You have shown me how one can learn, adapt, and change to find a new balance in life. I will always have our many trips together (especially Madeira) in my mind and still enjoy the memories. Also, thank you very much for making me correct my pyjamas-looking Excel graphs. Ahmadreza, I want to thank you for caring about our friendship and always prioritizing it. I am very happy and grateful to have a smart, artistic, poetic, and amazing friend like you. You are of the few people I continuously enjoy my time with. Mirhossein, had it not been for your help, I had suffered many times during my education abroad. Thank you for teaching me how to study, to program, to think, and to process information. I want to very specially thank you for all the adaption you went through to improve our friendship. You are truly valuable to me. Soheil, you have really given me an experience of being an elder brother, loving and caring for a younger one. I am very grateful to our friendship. Thank you for supporting me and caring for me all these years. Arghavan, I wish to thank you for all the lovely trips, meals, and times we have had together. Since the beginning of my life in the Netherlands, we have had many wonderful memories together and I thank you for that. Sadaf, you have been a lovely friend for me who has always cheered me up. I am proud of you and impressed by your achievements and growth during your life abroad.

Saman, despite the many kilometers, my heart is always with you. Thank you for showing me your courage and freedom. I did really learn much from you. The start of our friendship happened at the beginning of our university life. After our many trips together, we traveled to the Netherlands, lived, and grew up together. We have traveled countless trips and spent the most important years of our lives together. Thank you for being my lovely brother. Amirali, I owe you much more than one can imagine. Thank you for being my representative back home and taking care of all my family who see and love you similar to me. Thank you for showing me the real meaning of brotherhood and friendship. Thank you for that trip when you helped us move. I am truly grateful to the highest amount of unconditional love and support you have given me all these years. I am blessed to have you in my life and my greatest wish is that we can one day live in the same town together again. I want to particularly acknowledge my three beloved aunts: Jamileh, Fereshteh, and Fariba, not only for raising me as their own child, but also for continuously giving me their infinite love and always having taken care of my family back home during my absence. I also acknowledge my three lovely cousins, Setareh, Shayan, and Anna, who I truly love as my own brother and sisters. I also thank my very dear cousin Solene for bringing lots of love and joy to my life. I wish to separately appreciate Ali's family for truly treating me as their own member, especially his mother, Zahra: I would like to thank you for teaching me the ultimate level of strength, patience, and hope and for always giving me motherly love and care ever since we have known each other. You are always in my heart. A very special gratitude goes to my dearest Azar, for all the love and care she has always provided me with, and for all the critical lessons she has taught me in my life. Thank you for always giving me hope and for having my back during my most difficult times in life. Thank you for being of my best and closest friends ever, despite our age difference, and thank you for the best times of my life. My memories with you and my dear mother lighten my heart.

Shima, I want to especially acknowledge you for having my back despite my occasional attitude during the past years. Thank you for the unconditional support, help, love, and care you have provided me with during these years. You have gained my real trust and made me feel like having a true lovely sister, always encouraging me, flattering me, and cheering me up. Thank you also for always accompanying my mother during her trips to the Netherlands. Besides our friendship, I want to thank you for being a wonderful colleague whom I have truly enjoyed working with.

My dearest Ali, I have never had any brother, but if I had the best possible one ever, he would still miserably fail against you and due to your competitive spirit, I know you are happy for that. The fact that I am writing this text now in the Netherlands is simply because of you. Thank you for always being my "the-one-and-only" reference point during the past 16 years. Thank you for all the journeys we traveled together,

above all, the journey of brotherhood. Thank you for the good moments, the sad moments, the laughter's, the cries, and everything we have been sharing together. You are my best friend, family, and without question, my true treasure in life. I want to thank you for caring for me, tolerating my attitude, and for always having my back unconditionally. I hope to have not misused it unintentionally. Further than our friendship I really want to thank you for always helping me generously during my work and projects. Thank you for the -occasionally extreme- criticism which really made me improve my work. I am also thankful for the extreme competitive spirit we share, which has made me do so much more in life, including sports.

The accomplishment of this PhD and every other good I have gained in life would have been impossible without the support of my beloved parents whom I am truly blessed to have.

My dear and beloved, best father in the world, Baba, you have shown me the true meaning of unconditional love and support. I remember as a little kid, you always put me on your shoulders and carried me above you. During the rest of my life, I realized that you continued doing this even as I became an adult. I appreciate all the sacrifices you have made for me. You have delivered the greatest deal of effort to make my life a better one and I cannot thank you enough for that. Thank you for continuously having my back, even when you did not completely agree with my decisions. Thank you for always wanting the best for me, tolerating my absence and also thank you for a lifetime caring for our family. Without your help, love, and support it would have never been possible for me to reach my current state in life. Obtaining my PhD degree, I really hope I have made you and your father, my grandfather, Prof. Rasooli, proud.

There is no being in the world whom I love more than my dear mother. Maman, you have been my greatest treasure for my entire life, which is meaningless without you. Here I begin to write about you and having a lump to my throat, I get too emotional. I cannot thank you enough for loving me and caring for me ever since my first breath. You have made all possible sacrifices for my success and happiness in life. You have also been my most important teacher ever, who inspired me and taught me not only occupational lessons, but also about life itself. Thank you for teaching me discipline, precision, ethics, and principles of work and education. I really hope to have made you happy with the paths I have chosen in my life. I cannot thank you enough for the level of strength you revealed, which I had never ever seen anywhere in my entire life. Thank you for prioritizing our family above anything else in the world and thank you for your impeccable patience during all these years.

Finally, I want to thank whoever else who helped and supported me, being missed in my list.

Contents

List of Tables

List of Figures

Summary

Ever since the introduction of energy conversion systems in the built environment, buildings have become responsible for a considerable share of global energy consumption. Many countries have therefore aimed to invest on buildings' energy efficiency plans to reduce the depletion rate of the fossil resources and the CO2 emissions associated with them. In this context, accurate determination of building's thermo-physical characteristics is a necessity in the processes which lead to execution of energy conservation strategies in existing buildings. These characteristics are the essential inputs for buildings' thermal modelling, quality control, energy audits, and energy labelling, the results of which are determinant for energy renovation decisions and policies. In practice, the values of these parameters are not always available because the current determination methods are time-and-effort-expensive, and consequently rarely used. In accordance with the large deviations observed between the in-lab and in-situ thermal behaviour of building components, a special attention is laid on in-situ methods. This thesis aims at developing and testing different in-situ determination methods and approaches at different levels. Theories, simulations, and experiments, are combined for determination of a number of buildings' most important thermo-physical characteristics.

Transmission losses through the façades are known to be responsible for a significant portion of heat loss in buildings and consequently are investigated in all standard energy calculation methods. Thus, the major part of the thesis is dedicated to the thermal behaviour of exterior walls. The exact construction of existing walls is generally unknown. Consequently, the estimation of their thermal resistance, thermal conductivity, and volumetric heat capacity can be erroneous. Later, the attention is upscaled to the building level where rather than local characteristics, global characteristics are determined.

At the first stage, the walls' in-situ determination of thermal resistance has been examined. Despite the advantages of the existing standard method, "ISO 9869 Average Method" for measuring this parameter, two problems have been pointed out: long duration and imprecision. Accordingly, this phase describes and demonstrates how the simplest modifications to this standard method can improve it in terms of solving these problems. Heat transfer simulations and experiments in a variety of wall typologies have been applied to show the effect of using an additional heat

flux sensor, facing the first one, installed on the opposite side of the wall. Three estimations of thermal resistance based on either indoor or outdoor heat fluxes, and the average of the two values are then defined. It is shown that one of these values satisfies the convergence criteria earlier than the other two, leading to a quicker in-situ determination of thermal resistance with a higher precision.

To further shorten the measurement period, in the second phase, a new transient in-situ method, Excitation Pulse Method, EPM, is developed and examined experimentally on three walls. The method is inspired by the theory of thermal response factors. In EPM, a triangular surface temperature excitation is applied at one side of the wall and the heat flux responses at both sides are measured and converted into the wall's corresponding response factors which then leads to the wall's thermal resistance. To validate, the results are compared to the ones obtained following the ISO 9869. The good agreement of the results confirms the possibility of measuring the Rc-value within a couple of hours. Applying this method, the overestimation of around 400% between the actual and estimated values (in practice, often based on the construction year) of thermal transmittance was resolved. Thus, EPM is believed to significantly improve the required time and accuracy in determination of the thermal behavior of walls with unknown constructions. Experimental and practical details regarding the design and construction of the method's prototype as well as its application range are demonstrated subsequently. EPM has been patented in the Dutch patent office (Patent No. 2014467) and can be applied on in-lab and in-situ circumstances.

Following the success in the proof of principle, in the third phase, detailed conditions for correct application of EPM in heavy and multi-layered walls are further studied. Heat transfer theories, simulations, and experiments are combined to evaluate the method's performance for different types of walls. A specific attention is devoted to the relationship between the walls' thermal response time and the response factors' time interval, affecting the accuracy of Rc-value determination. Additionally, other hidden information in the response factors of the walls such as the possible construction are revealed. It is moreover demonstrated that in addition to the thermal resistance, the two main thermo-physical properties of a wall, the thermal conductivity and the volumetric heat capacity, as well as the wall's thickness can be determined using inverse modelling of the Response Factors. The accuracy and precision of the method is tested in many different ways, fortifying the confidence for future application of this method.

In the last phase, the advancement of smart metering and monitoring systems in buildings are considered. Such smart technologies have led to utilization of the data from, for instance, home automation systems. This data acquisition is referred to

as “on-board-monitoring” category of measurements, which removes the hassle, cost, and intrusion associated with locally-conducted experiments. The problem is then observed from a perspective wider than the component level. This time, the thermo-physical characteristics are studied for a whole building rather than just the walls. It is presumed that the current and future houses and their HVAC installations are by default, equipped with basic sensors, providing on-board monitored data. Therefore, the expected available data is measured and used as input parameters. A case study of an occupied apartment, in which air temperatures, humidity, and CO2 concentrations, gas consumption, and meteorological data have been measured for one year is investigated. Global characteristics such as the heat loss coefficient and thermal capacitance are estimated through inverse modelling of a 1st order circuit analogous to the thermal model of the building, and fed by the measurement data. In addition, using construction information, winter daily air change rates leading to ventilation and infiltration heat losses are estimated from the results of the inverse modelling. These results can be used to tailor the energy efficient use of the building.

In summary, the in-situ determination of walls’ thermal resistance is conducted by two methods in this thesis. The first one calls for longer measurement methods (minimum three days), but includes a straight-forward, well-known procedure. This method is highly suitable for high temperature gradients across the wall. The second method, EPM, requires more complicated instrumentation, but in return, in addition to rapid (couple of hours) determination of the Rc-value, it provides the walls’ response factors which are required for a dynamic thermal building simulation. In addition, using the results of this method, the thermal conductivity and volumetric heat capacity can be determined. EPM is most suitable for light-to-medium weighted walls and for homogeneous walls of known thickness. Stable heat flux profiles at the surfaces of the wall increase the accuracy of the method, especially when the temperature gradients across the wall are lower. Finally, as a less intrusive approach, the data from the HVAC installations’ existing sensors can be used. Global characteristics including the heat loss coefficient and the global capacitance can be then determined for a whole building, followed by ventilation and infiltration losses. Despite the low accuracy, this process is more suitable when the smart meter data is available and measurements at component level are not desired.

By introducing and testing new experimental and computational methods and approaches for reliable determination of buildings’ local and global thermo-physical characteristics, this thesis pays a significant contribution to the accuracy of the energy-related predictions and operations, especially within the built environment.

TOC

Samenvatting

Energieconversiesystemen voor gebouwen en de gebouwde omgeving zijn verantwoordelijk voor een aanzienlijk deel van het wereldwijde energieverbruik. Veel landen investeren daarom in energie-efficiëntieplannen voor gebouwen om uitputting van de fossiele bronnen en CO_2-emissies te voorkomen. In deze context is een nauwkeurige bepaling van de thermo-fysische kenmerken van bestaande gebouwen noodzakelijk om efficiënte energiebesparingsstrategieën te bepalen en uit te voeren.

Deze thermo-fysische kenmerken zijn essentiële voor energiesimulatie, kwaliteitscontrole, energie-audits en energielabeling van gebouwen, waarvan de resultaten bepalend zijn voor beslissingen over en het vaststellen van beleid voor energierenovatie. In de praktijk zijn de waarden van deze kenmerken niet altijd beschikbaar omdat de huidige bepalingsmethoden tijd en moeite kosten en daarom zelden worden gebruikt. Als gevolg van de grote afwijkingen die zijn waargenomen tussen het in-lab en in-situ thermisch gedrag van bouwcomponenten, wordt in dit proefschrift speciale aandacht besteed aan in-situ methoden. Dit proefschrift is gericht op het ontwikkelen en testen van verschillende in-situ bepalingsmethoden op verschillende niveaus. Theorieën, simulaties en experimenten worden gecombineerd om de belangrijkste thermo-fysische kenmerken van een aantal gebouwen te bepalen.

Transmissieverliezen door de gevels zijn verantwoordelijk voor een aanzienlijk deel van het warmteverlies in gebouwen en worden daarom meegenomen in alle standaard energieberekeningsmethoden. Het grootste deel van het proefschrift is dan ook gewijd aan het thermische gedrag van buitenmuren. De exacte constructie van bestaande muren is over het algemeen onbekend. Daarom kan de schatting van hun warmteweerstand, warmtegeleiding en volumetrische warmtecapaciteit onjuist zijn. Daarna wordt de aandacht opgeschaald naar het gebouwniveau waar, in plaats van lokale wandkenmerken, globale eigenschappen worden bepaald.

In de eerste fase is de in-situ bepaling van de thermische weerstand van muren onderzocht. Ondanks de voordelen van de bestaande standaardmethode, "ISO 9869 Gemiddelde methode" voor het meten van deze parameter, treden er twee problemen op: lange meetperiode en onnauwkeurigheid. Dienovereenkomstig beschrijft en demonstreert het onderzoek hoe de eenvoudigste aanpassingen aan deze standaardmethode een deel van deze problemen al oplost. Simulaties en

experimenten met warmteoverdracht in verschillende wandtypologieën zijn toegepast om het positief effect van het gebruik van een extra warmtefluxsensor, geïnstalleerd aan de andere kant van de muur aan te tonen. Drie bepalingen van de thermische weerstand worden dan gemaakt op basis van binnen- en buitenwarmtefluxen en het gemiddelde van de twee. Aangetoond wordt dat een van deze waarden eerder voldoet aan de convergentiecriteria dan de andere twee, wat leidt tot een snellere in-situ bepaling van de thermische weerstand met een hogere precisie.

Om de meetperiode verder te verkorten, wordt in de tweede fase een nieuwe transiënte in-situ methode, Excitation Pulse Method (EPM), ontwikkeld en experimenteel onderzocht op drie wanden. De methode is geïnspireerd op de theorie van thermische responsiefactoren. In EPM wordt een driehoekige excitatie van de oppervlaktetemperatuur toegepast aan één kant van de muur en worden de resulterende warmtefluxen aan beide zijden gemeten en omgezet in de corresponderende responsiefactoren, waaruit vervolgens de thermische weerstand van de muur berekend kan worden. Om te valideren worden de resultaten vergeleken met de resultaten verkregen volgens ISO 9869. De goede overeenstemming tussen beiden bevestigt de mogelijkheid om de Rc-waarde binnen een paar uur te kunnen meten. Dit is handig omdat de snelle inschatting van de Rc-waarde op basis van het constructiejaar –zoals vaak in de praktijk gedaan wordt- regelmatig leidt tot grote verschillen (tot 400%) met de werkelijke thermisch weerstand. Derhalve wordt gedemonstreerd dat EPM de vereiste meetperiode bij het bepalen van het thermische gedrag van muren met onbekende samenstelling aanzienlijk verkort en de nauwkeurigheid aanzienlijk verbetert. Vervolgens worden experimentele en praktische details met betrekking tot het ontwerp en de constructie van het meetprototype en het toepassingsbereik gedemonstreerd. EPM is gepatenteerd bij het Nederlandse octrooibureau (patentnr. 2014467) en kan worden toegepast in-lab en in-situ omstandigheden.

Na het bewijzen van de haalbaarheid van het EPM concept, worden in de derde fase de gedetailleerde voorwaarden voor een correcte toepassing van de methode in zware en meerlaagse muren verder bestudeerd. Theorieën, simulaties en experimenten met warmteoverdracht worden gecombineerd om de prestaties van de methode voor verschillende soorten muren te evalueren. Er wordt speciale aandacht besteed aan de relatie tussen de thermische responstijd van de muren en het tijdsinterval van de responsiefactoren, omdat die de nauwkeurigheid van de bepaling van de Rc-waarde beïnvloedt. Bovendien wordt andere verborgen informatie in de responsiefactoren van de muren, zoals de mogelijke constructie, onthuld. Er wordt aangetoond dat naast de thermische weerstand, de twee belangrijkste thermo-fysische eigenschappen van een muur: de thermische geleiding en de volumetrische warmtecapaciteit, evenals de wanddikte kunnen worden bepaald met behulp van

het invers modelleren van de responsiefactoren. De nauwkeurigheid en precisie van de methode wordt op veel verschillende manieren getest, wat het vertrouwen voor toekomstige toepassing versterkt.

In de laatste fase wordt de ontwikkeling van slimme meet- en besturingssystemen in gebouwen meegenomen. Dergelijke slimme technologieën hebben geleid tot het gebruik van de data van bijvoorbeeld domoticasystemen en wordt "ingebouwde-monitoring" genoemd. Het maakt metingen in woningen makkelijker en reduceert de kosten en inbreuk op privacy. Het probleem wordt dan bekeken vanuit een breder perspectief dan het componentniveau. Deze keer worden de thermo-fysische kenmerken bestudeerd voor een heel gebouw in plaats van alleen de muren. Aangenomen wordt dat de huidige en toekomstige woningen en hun installaties standaard zijn uitgerust met basissensoren waarvan de meetdata systematisch opgeslagen worden. Deze gegevens worden gebruikt als invoerparameters van een invers model Het model wordt getest op de casestudy van een bewoond appartement, waarin gedurende één jaar luchttemperaturen, vochtigheid en CO_2 -concentraties, gasverbruik en meteorologische gegevens zijn gemeten. Globale kenmerken zoals de warmteverliescoëfficiënt en thermische capaciteit worden bepaald door het invers modelleren van een 1e-orde circuit, analoog aan het thermische model van het gebouw en gevoed door de meetgegevens. Bovendien wordt aangetoond dat met behulp van extra constructie-informatie de dagelijkse gemiddelde luchtverversingsdebieten voor ventilatie en infiltratiebepaald kunnen worden, ook op basis invers modelleren. Deze resultaten kunnen worden gebruikt om het gebouw energiezuiniger te maken.

Samenvattend wordt in dit proefschrift de in situ bepaling van de thermische weerstand van wanden onderzocht met twee methoden. De eerste vraagt om langere meetmethoden (minimaal drie dagen), maar omvat een eenvoudige, bekende procedure. Deze methode is zeer geschikt wanneer grote temperatuurgradiënten over de muur aanwezig zijn. De tweede methode, EPM, vereist meer gecompliceerde instrumentatie, maar in ruil daarvoor levert het, naast een snelle (paar uur) bepaling van de Rc-waarde, de responsiefactoren van de muren die nodig zijn voor dynamische thermische gebouwsimulatie. Daarnaast kunnen met behulp van de resultaten van deze methode de warmtegeleiding en de volumetrische warmtecapaciteit van de muur worden bepaald. EPM is het meest geschikt voor lichte tot middelzware muren en voor homogene muren met een bekende dikte. Stabiele warmtefluxprofielen op de oppervlakken van de muur verhogen de nauwkeurigheid van de methode, vooral wanneer de temperatuurgradiënten over de muur klein zijn. Ten slotte, als een minder ingrijpende benadering, kunnen de gegevens van bestaande sensoren van installaties en slimme meters worden gebruikt. Globale kenmerken, waaronder de warmteverliescoëfficiënt en de globale capaciteit,

kunnen vervolgens worden bepaald voor een heel gebouw, gevolgd door ventilatie en infiltratiedebieten-en verliezen. Ondanks de lage nauwkeurigheid is dit proces geschikter wanneer de slimme metergegevens beschikbaar zijn en metingen op componentniveau niet gewenst of mogelijk zijn.

Door het introduceren en testen van nieuwe experimentele methoden en inverse rekenmodellen voor een betrouwbare bepaling van de lokale en globale thermo-fysische kenmerken van gebouwen, levert dit proefschrift een belangrijke bijdrage aan de nauwkeurigheid van energie-gerelateerde voorspellingen en maatregelen in de gebouwde omgeving.

Nomenclature

Symbols

a	thermal diffusivity (m^2s^{-1})
C	electric capacitance (F)
C_{eq}	equivalent global thermal capacitance ($Jkg^{-1}K^{-1}$)
c	specific heat capacity ($J\ kg^{-1}K^{-1}$)
D	common ratio between two consecutive RFs
$\boldsymbol{Dep}$	departure from the expected value
DEV	deviation between two values
f	function of parameters
H	wall's height (m)
I	electric current
i	time step (h)
j	secondary time step (h)
k	thermal conductivity ($Wm^{-1}K^{-1}$)
L	wall thickness (m)
m	minimum required measurement period (h) - index of constant RFs ratio
N	maximum required number of RFs
n	required number of RFs - maximum number of data points fed to the RC model
P	global solar irradiance (Wm^{-2})
q	heat content (Jm^{-2})
$\dot{q}$	heat flux (Wm^{-2})
R	electric resistance (Ω)
R_c	conductive thermal resistance (m^2KW^{-1})
R_{eq}	equitant global thermal resistance (m^2KW^{-1})
R_{eq}^{-1}	building's heat loss coefficient (WK^{-1})
R^2	coefficient of determination
S	surface area between a curve and the x-axis
S_0	solar radiation fraction parameter
S_1	internal gain parameter
T	temperature (K)
t	time (s) – time interval (half of the triangle's base)
U	thermal transmittance ($Wm^{-2}K^{-1}$)
U	multi-layered wall RF at excitation side ($Wm^{-2}K^{-1}$)

TOC

u	model input
V	multi-layered wall RF at the opposite side of excitation ($Wm^{-2}K^{-1}$)
V_0	voltage (V)
$\forall$	volume (m^3)
$\dot{\forall}$	air volume flow rate (m^3s^{-1})
W	width of the wall (m)
W	multi-layered wall RF at excitation side ($Wm^{-2}K^{-1}$)
X	single layer response factor at excitation side ($Wm^{-2}K^{-1}$)
x	along the x-axis orientation
Y	single layer response factor at the opposite side of excitation pulse (Wm^2K^{-1})
y	along with the y-axis orientation
Z	single layer RF at the exterior excitation side ($Wm^{-2}K^{-1}$)
z	along with the z-axis orientation

Superscripts

ac	actual value
∞	associated with fluid medium (air)
t	time (h)
th	theoretical value
*	obtained from the measurements
**	summation of the surface temperatures
–	mean surface temperature

Greek letters

α	convective heat transfer coefficient ($Wm^{-2}K^{-1}$)
δ	magnitude of the triangular excitation signal (K)
Δ	difference
η	efficiency of the heating system
θ	model parameter vector
κ	conductance ($Wm^{-2}K^{-1}$)
λ	reduction factor for thermal response time (%)
μ	model output
$\mathcal{O}$	linearization error
ρ	density (kgm^{-3})
σ	norm of the predicted error
$\tau_r\|_{1-\lambda}$	thermal response time for $1-\lambda$ (s)

Indices

A	associated with indoor surface (excitation side)
acc	accumulation of heat
ave	average
B,C	associated with outdoor/middle surface (opposite side)
eq	equivalent
f	floor
gen	heat generation
gl	glazing (whole window)
H	heating provided for the SH
H/C	heating and cooling demand
h	associated with horizontal surface
i	response factor number, summation counter, indoor
j	response factor index
in	associated with the interior surface
inf	infiltration loss
n	*nth response factor - nth data point*
o	outdoor
out	associated with the exterior surface
r	roof
s	surface
sol	solar radiation
ss	steady state
v	associated with vertical surface
vent	ventilation loss
w	wall
1	associated with the interior surface, layer number in a multi-layered wall
2	associated with the exterior surface, layer number in a multi-layered wall
1,2	associated with both surfaces

Abbreviations

ACH	Air Change Rate per Hour (h^{-1})
B1	Bedroom1
B2	Bedroom2
DEP	Departure (%)
DHW	Domestic Hot Water
ELP	Electricity Power meter
EPBD	Energy Performance of Buildings Directive
EPM	Excitation Pulse Method

FEM	Finite Element Method
GA	Genetic Algorithm
HFS	Heat Flux Sensor
HTC	Heat Transfer Coefficient (Wm^{-2})
IR	Infrared
K	Kitchen
LR	Living Room
MAE	Mean Absolute Error
ODE	Ordinary Differential Equation
PDE	Partial Differential Equation
RC	Resistance-Capacitance model
RF	Response Factor
RH	Relative Humidity
RMSE	Root Mean Square Error
SH	Space Heating
TRHC	Temperature, Relative Humidity, CO_2
VHC	Volumetric Heat Capacity ($Jm^{-3}K^{-1}$)

1 Introduction

1.1 Background

The depletion of fossil energy resources as a consequence of population growth, along with the increase in energy demand, calls for special attention to be devoted to global energy consumption – of which the building sector is accountable for a considerably large share. Consequently, the potential of this sector for saving energy, of which a considerable fraction is dedicated to heating, is significantly high. To achieve energy efficiency in the built environment, a deep understanding of the buildings' thermal behavior is of the essence. To this end, much effort has been made to study, develop, and test computation programs and software to generate building energy models. A building can generally be physically modelled as an assembly of mathematical operations, fed by several inputs. The heat transfer phenomena, taking place amongst various components (i.e. walls), are mathematically modelled, and upon feeding this model with inputs (e.g. thermal properties of components) and assumptions, energy-related output parameters can be extracted (Fig 1.1). In this context, the core outputs of a building's energy model are the heating and cooling energy demands and the heating and cooling capacities.

TOC

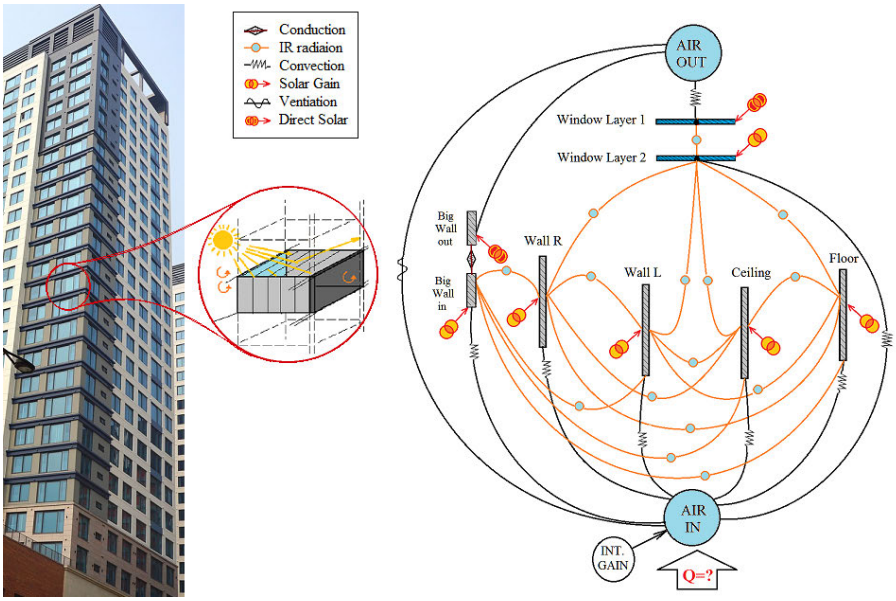

FIG. 1.1 A building's energy model: a unit in a block can be modelled by studying the heat transfer between its various components. The output of the model is the heating energy demand.

The importance of these values and therefore the dedication of numerous studies to this matter stems from the fact that these parameters are the basis of the building installations design. More importantly, many national and international policies are drawn based on these calculations. For instance, as reflected in the Energy Performance of Buildings Directive, EPBD [1] the main EU policies ought to target acceleration of the cost-effective renovation of existing buildings, aiming for a decarbonized building stock by 2050. Energy labels, energy saving potentials, energy renovation decisions and many other energy-related notions are closely related to the (estimated) energy demand.

Through sensitivity analysis of the conventional energy models [2], many studies have shown the estimated energy demand to be very sensitive to a number of specific input parameters, the accuracy of which is consequently critical to estimate the energy demand more accurately. Amongst various parameters to which the outputs of the models are sensitive, a number of buildings' thermo-physical characteristics such as the walls' thermal resistance (which determine the transmission losses) are of the most prominent ones [2–4]. The exact construction, the exact thermo-physical properties, and consequently the actual in-situ behavior of the building components are generally unknown. As a result, significant deviations observed between theoretical and actual values of energy consumption [5] cast a shadow of

TOC

doubt on the accuracy of the input values regarding the buildings' thermo-physical characteristics. Accordingly, numerous studies have sought to find solutions to determine these properties accurately. Most importantly, standard methods have been developed to test and measure these values in the labs. However, this has shown to not to be a suitable solution to the problem. Experience has shown that the in-situ behavior of building components as-built is also different from their predicted and in-lab behavior. Time, dynamic effects of climatic conditions, moisture, and many other parameters result in different-than-expected in-situ thermal behavior of building components. Subsequently, conducting in-situ measurements has become an inevitable solution.

Aiming for a general global solution to this problem, in-situ measurement standards have been developed and can be applied worldwide. The most important standard method for in-situ measurement of walls' thermal resistance is the ISO 9869 [6]. Similarly, American standards such as ASTM [7, 8] follow a similar prescription. These methods are quite straightforward and therefore can be widely applied. However, since they are time-expensive and constrained to fulfil many conditions, their application is limited to certain boundary conditions. Such barriers have caused these methods to be dismissed in many situations and replaced by simple calculations — and in the case of unknown constructions, by guess-based approximations. This has led to inaccurate estimations, calling a demand for developing and improving in-situ methods for determination of thermo-physical characteristics of the buildings.

In this thesis, new characterization methods are developed, determining some of the buildings' most important thermo-physical characteristics including: the façades' thermal resistance, thermal conductivity, volumetric heat capacity, the buildings' heat loss coefficient, global thermal capacitance, and daily air change rates. The estimation of some parameters reveals other crucial thermo-physical characteristics. For instance, determination of thermal conductivity discloses the thermal resistance R_c-value and thermal transmittance U-value of the façades, known to be of the key parameters in determination of buildings' heat loss. Since the façades have a large surface area, a substantial amount of heat loss rate belongs to transmission losses from these components. Therefore, it is of absolute necessity to characterize the exact thermal properties of the façades and other boundary components. These values can then be used to make the most cost-effective choices when deciding about thermal renovation of a building (e.g. for insulation of the walls), which is generally expensive. They can for instance lead one to reach a conclusion of giving the priority of investment to extra wall insulation, or to the change of a window.

On a higher level, accurate thermal properties can be fed into buildings' energy models, leading to more accurate estimations of buildings' energy demands and installation capacities. This results not only in better designs of HVAC installations and indoor climate systems, but also in making more reliable energy-related policies of which the effective ones can be made when the predicted energy consumptions are closer to the actual values. Obtaining accurate values of thermo-physical characteristics can be an essential part in the quality control processes and commissioning. Furthermore, these values can be used to determine the actual in-situ performance after the delivery procedure.

1.2 State-of-the-art

To determine buildings' thermo-physical characteristics, numerous studies have been dedicated to development and application of computational and experimental methods [9]. For the properties of exterior walls, which draw the focus in a large part of this thesis, the existing standard ISO 6946 [10] prescribes a calculation method based on the construction of the walls. Accounting for complex details such as thermal bridge calculations [11] and dynamic characterizations [12], the calculation methods still fail to reflect the actual thermal transmittance of some heterogeneous opaque elements [9]. Consequently, there has been an urge to lay emphasis on measurement methods. Amongst the most well-known conventional measurement methods, the guarded hot plate [13], the guarded and calibrated hot box [14], the heat flow meter method [6], and infrared (IR) thermography [15] can be named. In contrast with the last two which are in-situ methods, the first two measurement methods are suitable and applicable in the lab conditions. As the in-situ and in-lab thermal performance of the walls can be entirely different, a more special attention is given to the in-situ category of the measurement methods. As the most important in-situ method for determination of the walls' thermal resistance, the standard methods [16] ISO 9869 [6] and ASTM [7, 8] suggest and prescribe the heat flow meter method. In this method, based on heat flux and temperature values, the thermal resistance that converges to a certain value after a long-enough period is estimated. Many studies have aimed at improving the quality of this method's performance [17-23]. However, the majority of the proposed methods such as inverse modelling [24, 25] are based on infeasible circumstances and a level of knowledge (e.g. mathematics) beyond average user. Furthermore, many improvements are based on the construction information which are to remain unknown during non-destructive

experiments. Accordingly, the standard method is still most often followed globally by professionals and practitioners as is. The long waiting periods and the very specific conditions [26] in this method are the main barriers to its application. As an alternative, IR thermography [27] has been under progress for many years. The quantitative applications of this method are recently being used more often than in the past. Amongst a variety of problems are associated with this method, the high cost of its equipment and the need for specially-trained people [28], even for its qualitative approach, introduce practical barriers to its wide application. A new ISO 9869 (part 2) standard [15] is recently published to prescribe a quantitative application of this method for determination of thermal transmittance and thermal resistance in specific light buildings. Despite the many studies being carried out using IR thermography, due to its convinience, the level of uncertainty introduced by this method is under doubt. The emmisivity and the reflection of the surface and the air is rarely known and the IR camera measures the IR heat flux emission and not the net heat flux (e.g. including surface convection). Therefore, a number of researchers have tried to combine this method with other ones (e.g. heat flow meter method). Following the survey of the literature, the demand for improvement of the current standard method, the heat flow meter method, and the development of quicker alternative in-situ methods is evident.

Despite the emphasis laid on the necessity of measurements, making intrusive in-situ tests are not always desirable in occupied houses [29]. Accordingly, parallel to the rapid growth of sensor technologies [30], the use of the spontaneously-available on-board monitoring data (e.g. available from the home automation systems and smart meters) has raised a special attention [31]. Thus, numerous studies have aimed at using such data in combination with a variety of models and approaches [32-42] to extract buildings' thermo-physical characteristics such as the heat loss coefficient [31, 43-47] and to predict the energy demand. Of the main challenges faced in this category of studies is the use of real data [48] from occupied residential houses. The majority of the studies in this area have avoided this challenge in two ways: The use of synthesis software-generated data, or the use of actual data from commercial and office buildings. The synthetic data lacks the effects of the "reality" such as occupant behavior and in-situ circumstances, but is an essential tool in method development at early stages. The non-residential buildings are generally governed by a much more confined occupant and system behavior. Variables such as occupancy hours, HVAC settings, ventilation rates and the energy usage have constrained patterns, reducing the "unknown effects" in the mathematical modelling process. Accordingly, studies targeting occupied residential buildings (which are less often carried out) are in demand. The subjects studied in this thesis are in-line with the ones covered in the two IEA Annexes 58 [49] and 71 [29].

1.3 Research Questions

Reflecting on the limitations and barriers of using the standard and other conventional methods, the core question to be answered in this thesis is as follows:

What feasible in-situ methods can be developed, advanced, or modified, to determine buildings' local and global thermo-physical characteristics more accurately, more rapidly, and more efficiently?

To elaborate the strategies built up to answer the main question, the following key questions are to be addressed individually:

1. How is it possible to modify the equipment and the calculations of ISO 9869 standard's "Average Method" to improve its performance in terms of the required time and precision?
2. How can a new rapid transient in-situ method be developed, based on the theory of response factors, and be used as an alternative to ISO 9869 to measure the thermal resistance of the existing walls?
3. What are the constraints and the validity domain of the developed method in walls of various constructions?
4. What other properties and information other than the thermal resistance can be measured and derived by the alternative method?
5. What framework can be followed to estimate the global thermo-physical characteristics of a building, using the air temperature and energy consumption measurements?

The thesis answers to the mentioned questions in the same order. To carry out the required research, the following methods are applied.

1.4 Methodology

The thesis tackles the mentioned problem in four phases. Heat transfer theories are combined with simulations, experiments, and inverse modelling algorithms to develop, test, and validate the proposed methods and approaches. At first, as

the most intuitive approach, the existing standard method is improved to perform quicker and more precisely. Second, to reduce the measurement time much further, a new dynamic method is developed as an alternative to the standard method. Third, consequent to the success of the new developed method as a proof of principle, a prototype is built and more experiments are carried out in a test sample to find additional thermo-physical properties. In the first three mentioned phases, heat fluxes and temperatures are measured at the surface of the wall on site and analyzed according to the heat transfer theories. This might not always be feasible in real houses, due to the hassle, intrusiveness, and difficulties associated with on-site experiments. Thanks to the recent advancement and expansion of monitoring systems, a considerable attention is given to on-board monitoring systems and how to use the already existing measurement data. Accordingly, presuming the availability of specific data in the future, in the last phase, air temperatures and gas consumption patterns are measured globally and fed into a simple thermal model to find the global properties of a building. The general methods applied in this thesis are explained in the following.

1.4.1 Developing an Extension to the ISO 9869 Standard's Average Method

The ISO 9869 [6] standard's "Average Method" is of the most important topics in this thesis. It is used not only as the basis of the first part of the thesis, but also applied as the most reliable benchmark to validate the other in-situ measurements, using the alternative method developed in chapter 3. The importance of this method due to its straight-forward procedure is the acceptability by professionals and experts leading to its worldwide application. Therefore, at the very first stage, this standard method is improved by introducing a simple extension. The new extension simply improves this method, allowing it to perform much better in terms of time-duration and precision. The advantage of this approach rather than using a completely different measurement method is that applying this extension requires neither additional knowledge (e.g. beyond-average mathematics) nor new types of equipment. Accordingly, following the same principles of the standard method, the chances of using the extension in the future are higher than in case of a new method.

According to the ISO 9869 Average Method, the R_c-value can be determined based on loggings of surface temperatures and average heat flux. The R_c-value is obtained after a sufficiently-long period (at least 72 hours) when certain convergence criteria [50] are met. The standard prescribes installation of one heat flux meter at one side of the wall and two thermocouples each at one side of the wall. As mentioned before,

TOC

this procedure may take many weeks of measurements. In the second chapter, it is shown that by using an additional heat flux meter, it is possible to speed up this process to accomplish an earlier determination of the thermal resistance. For this purpose, simulations have been carried out in COMSOL Multiphysics 5.3a [51] to study the effect of adding an extra heat flux meter to the equipment of the ISO 9869 [6] standard method. Five different typologies are modelled as being exposed to indoor and outdoor conditions (simulation of in-situ circumstances). The proposed extension (in-situ measurements) has been modelled, with attention to the guidelines in the ISO 9869 Average method. Upon installation of an extra heat flux sensor at the second side of the wall and measuring the heat flux at both sides, three estimations of R_c-value can be done: 1) based on indoor heat flux, 2) based on outdoor heat flux, and 3) the average of the two values. It is shown in which possible cases the first, the second, and the third estimations can lead to a much quicker determination of thermal resistance by comparing the convergence times. In addition to the required time contribution, the extension solves a precision problem, when the two R_c-values fulfil the requirements of the ISO 9869 and therefore can be reported, while differing from each other. Following the simulation of the five typologies, the aforementioned equipment and the proposed extension is demonstrated on site to measure the R_c-values experimentally in actual case studies.

1.4.2 Excitation Pulse Method, EPM, Based on the Theory of RFs

The time required in the standard method and its extension, still being a couple of days, may still be too long in practice. To this end, a new in-situ transient method is developed, introduced, and tested on three case studies. The Excitation Pulse Method (EPM) is based on the theory of Response Factors (RF). The theory of RFs, is the most important topic and thus the most frequently addressed one in this thesis. Chapters 3, 4, and 5 are based on this heat transfer theory. The theory of RFs states that if a wall of two sides 1 and 2 is exposed to an excitation triangular surface temperature pulse of T_1= [0 1 0 0 …] at side 1, and a flat surface temperature T_2= [0 0 0 …] at side 2, specific heat flux profiles are generated simultaneously, called RFs X and Y respectively (Fig 1.2). Based on this theory, the surface heat flux at any moment can be translated based on the surface temperature history, using a transfer function of RFs. To model and simulate the heat dynamics in solid components, the theory has been widely applied in heat transfer modelling processes such as building simulation software, as an alternative to the time-consuming finite difference method.

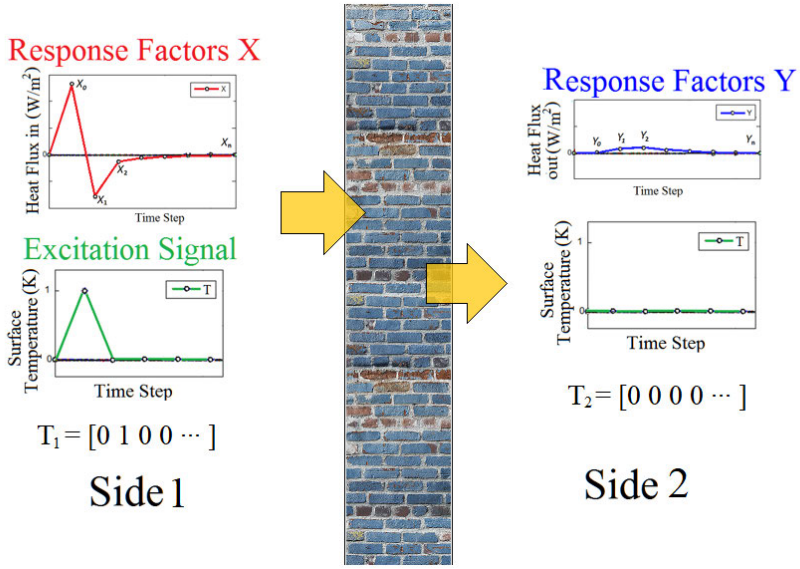

FIG. 1.2 Theory of RFs: generation of RFs X and Y as a response to signals T_1 and T_2

EPM is inspired by the theory of RFs and therefore, an experiment is designed and adapted to mimic this theory in a real-life application. In this method, a triangular surface temperature pulse is applied to one side of a wall, and the heat fluxes and temperatures at both surfaces are measured. Drawing on the theory of RFs, the heat flux at the excitation side is controlled in such a way that a surface temperature profile is formed in a shape of a triangle, this time with a magnitude (height) much larger than the one mentioned in the theory of RFs (1 K). The triangle is followed by a constant temperature equal to the initial value, representing the zero-line part of the pulse in the theory. Dividing the heat flux by the magnitude of the pulse, and following a proposed equation, the Rc value of a wall of unknown construction can be estimated in a short period of time. To validate the findings, the results obtained via this method are compared to the ones obtained following the ISO 9869 standard method. Finally, the advantage of using this method, at least in light walls of unknown construction has been illustrated by comparing the theoretically estimated and experimentally determined thermal transmittance in three case studies.

TOC

1.4.3 Experimental Aspects and Practical Considerations in EPM

Unless seeking proof of principle, testing the method in only three samples is never enough. Accordingly, to further validate the method, a prototype is built to ease the application of the method in further experiments. In the fourth chapter, first, the details of the prototype as well as its performance in the experiments are explained. As any new method, the developed method has many practical considerations that are important to take into account. To study this matter, heat transfer fundamentals associated with this method are illustrated and examples are simulated using COMSOL Multiphysics. The simulations have been made to represent actual experiments as much as possible. Accordingly, practical circumstances such as the effect of noise, the size of the pulse magnitude, and the temperature gradient across the wall are studied in the simulations. The possibility of using different combinations of pulse magnitude and RF time interval is demonstrated by modeling a wall exposed to different temperature pulses. Similarly, the sensitivity of the method to the number of RFs is explained using different numbers of RFs in calculation of the R_c-value from the results of a simulated experiment. Finally, the risk of 3D heat transfer effect in real walls is studied. At first, the practical considerations are explained theoretically and thereafter, simulations have been carried out to show the effect of 3D heat transfer in the method and to demonstrate how to deal with it.

1.4.4 Advancement of EPM and its Supplementary Applications

Following the experimental illustrations, EPM is then further studied through simulations and experiments to find the validity domain and its additional benefits in practice. The built prototype is used to conduct more experiments to explore new aspects of the EPM. Theoretically, the behavior of the method in multi-layer slabs is evaluated. A number of computer simulations have been carried out to show different aspects. Using COMSOL Multiphysics [51], the models are tested and validated following different approaches. Firstly, the possibility of using different combinations of time interval and pulse magnitude is theoretically and experimentally demonstrated and the relevant aspects for application of the method are accordingly mentioned. Secondly, the wall's response time is defined and its role in the validity of the experiments is thoroughly illustrated using a number of simulations in single layered and multi-layered walls. Thereafter, with aid of mathematics and more simulations, the information hidden in the common ratio between two consecutive *X* RFs are revealed. It is shown how the change of the slope of the curve and the change in the common ratio can bare information about the approximate composition of an unknown wall.

At a later stage, EPM is used to extract thermo-physical properties other than the thermal resistance. In this case, the thermal conductivity, volumetric heat capacity, and the thickness of a homogeneous wall have been determined by inverse modelling of the measured RFs. Accordingly, an RMSE (Root Mean Square Error) objective function is defined based on the measured and computed *X* RFs. The optimization problem is then solved via Brute-force search method in simulation examples. To prove the validity of this method, EPM and inverse modelling have been applied to a real case study and the results of the experiments are used to estimate the mentioned properties in the first layer of the wall. For a future follow-up, the required approaches for multi-layered walls are explained.

Further experimental validation of EPM has been conducted at first by measurement of the heat flux and deriving the *X* RFs and comparing them with their theoretical expected values. Then the results of four experiments are studied to show the validity of the theoretical approaches. To confirm the precision of the method, two similar experiments are compared and the determined values in different experiments on the same sample have been compared. Finally, the accuracy of the method is tested by making a comparison between the theoretical expected values of thermal conductivity and VHC (Volumetric Heat Capacity) and the ones obtained from the experiments.

1.4.5 Determination of the Buildings' Global Thermo-Physical Characteristics

In the final phase of this thesis, a different approach is taken and the problem is investigated for a whole house (defined as the whole system) rather than a single component (a wall). In contrast with the three previous chapters, where the parameters (surface temperature and heat flux) are measured on the boundaries of the component, other parameters (air temperature and gas consumption) are measured and processed at a whole building level. An occupied apartment of which the room air temperatures and energy consumption and some other parameters are measured over a long period of time (12 months) is studied. The building has been monitored and inspected during a large-scale measurement campaign of 100 Dutch dwellings. First, the details regarding the cleaning and preparation of the data are explained. These data series are coupled to feed a simple physical-based 1R1C (one resistance and one capacitance) building model formulated in MATLAB [52]. Accordingly, the average thermo-physical characteristics of the building are determined through inverse modelling of the energy conservation equation. Four parameters, the heat loss coefficient, equivalent thermal capacitance, solar radiation

fraction, and internal gains are estimated by solving an optimization problem. The RMSE function of indoor air temperature is optimized using Genetic Algorithm. The problem has been solved several times by using different periods, period lengths, and granularity levels (hourly, daily, and weekly data). Later, it is assumed that the majority of the deviations in daily heating demand are mainly the result of the variations in the variable part of the heat loss coefficient, the air flow rates. Accordingly, the daily approximated values of heat loss coefficient are recalculated by fixing the other parameters. Finally, using the construction information, the heat loss coefficients are translated into daily air change rates for the coldest and therefore the most critical months of the year. As this kind of study is by nature not of high accuracy, the findings are evaluated using construction data and known physics-based phenomena. The advantage of this approach is the much higher feasibility in practice when in-situ tests are not allowed and on-board monitored data (e.g. smart meter data and air temperature) is available.

1.5 Thesis Outline

The next chapter, Chapter 2, presents the extension to the ISO 9869 standard method through simulations and experiments. By using this extension, the thermal resistance of walls can be measured quicker, following the same procedure as the standard method. In Chapter 3, EPM, is presented and investigated in three case studies. The method is used to rapidly measure the thermal resistance and other thermal properties of walls of unknown construction. In contrast with the standard method, which requires a timeframe ranging from minimum several days to more than a month, with this method it is possible to find the thermal properties, specifically the R_c-value, in only a couple of hours. In Chapters 4 and 5, EPM is further studied to find more properties rather than only the R_c-value. A prototype is built, and the details of various aspects regarding the application of this method are given. Additional experimental aspects of the method are further investigated. The function of the method in multi-layered walls becomes clear, showing how the results of the experiments can be used to extract information about the construction of an unknown multi-layered wall.

Finally in Chapter 5, an apartment from a large-scale measurement campaign of 100 Dutch houses, explained in detailed in Appendix C, is studied. The on-board data such as the indoor air temperature and energy consumption patterns are measured

during a year and fed to a thermal model. Through inverse modelling, the global thermo-physical characteristics of the building are determined.

In appendix A, the mathematics behind the requirements of ISO 9869 standard method are demonstrated. Appendix B offers two additional modelled wall examples in addition to the ones shown in Chapter 2, and Appendix C presents details of a large scale measurement campaign from which the data of Chapter 6 are

2 Improving the Existing Standard Method

The most straight-forward and therefore globally-trusted method to determine the walls' in-situ thermal resistance is the one prescribed by the ISO 9869 standard. In this chapter, the problem of this standard method regarding its long measurement time is tackled using the most intuitive approach: modifying it to shorten this long time. It is shown how the simplest adjustments to the measurement equipment and the calculations can lead to significant reduction in the required measurement time.

This chapter is published under the following:

Rasooli, A., & Itard, L. (2018). In-situ characterization of walls' thermal resistance: An extension to the ISO 9869 standard method. *Energy and Buildings*, *179*, 374-383.

2.1 Introduction

Buildings are known to be responsible for a considerable share of worldwide energy consumption [53]. Apart from the occupant behavior, a building's individual energy consumption is highly dependent on the thermo-physical characteristics of its envelope [4, 54]. One of the most critical characteristics is the walls' thermal resistance R_c-value, whose accuracy of determination can significantly influence the accuracy of buildings' total energy consumption prediction [2, 3]. The accuracy of these predictions is critical in the sense that they are generally used as the basis for the majority of decisions and policies [55]. Therefore, accurate estimation of the actual R_c-value of the wall sections is known to be of high importance. Numerous experimental and computational studies [56, 57,58] have aimed at accurate

determination of this parameter using in-lab/in-situ and static (steady state)/ dynamic (transient) approaches. On one hand, calculation of the R_c-value can be quite simply done according to ISO 6946 [10], in which the computation methods for thermal resistance estimation based on the construction of the samples are provided. The exact construction of the existing walls is generally unknown and thus, in such cases, this calculation method is not appropriate. On the other hand, many studies have shown the difference between the thermo-physical characteristics calculated or claimed as the design values and the ones measured experimentally during measurement campaigns [26, 59-63], implying the necessity of performing measurements and the investigation of these measurements for being accurate enough. Regardless the numerous studies being carried out to accurately measure the actual thermal resistance of walls on site, the heat flow meter method suggested by the ISO 9869 [6] and ASTM 1046 and 1155 [7, 8] standards, which are very similar, are the ones being applied the most. Despite the advantages of these methods, two problems have been seen in practice: long duration and imprecision. The present chapter describes and demonstrates how modifications to ISO 9869 can improve the results of the in-situ measurements in terms of duration and precision.

2.2 State-of-the-Art

Various measurement techniques have been developed including steady state and transient methods applied in-situ [64, 65] and in-lab [14, 66-71] to estimate the accurate thermal resistance, with and without relying on steady state (and quasi-steady state) assumption. The steady state and the quasi-steady state assumptions, which are the basis of R_c-value measurements, tend to become problematic when the temperature and heat flux fluctuations are extreme (e. g. unsteady climatic conditions). Therefore, in case of static-based methods, usually additional modifications such as on-site data corrections for large temperature drifts [17] and including the wind velocity effects [18] are addressed to improve the measurement accuracy. Other advanced transient data analysis methods such as regression modelling and ARX (Auto-Regressive eXogenous)-modelling have been used to improve the reliability and robustness of the results [19]. In the recent past, applying the measurement data to mathematical models has become more popular. This type of methodology includes stochastic grey box modelling and inverse modelling [25, 72]. For instance, lumped thermal mass models and Bayesian statistical analysis of temperature and heat flux measurements, have been applied to estimate reliable thermo-physical properties of walls [21].

In summary, there is a large variety of scientific theoretical and practical methods available to determine the R_c-value of existing walls. However, if such determination is to be carried out in large scale (e. g. nationwide monitoring campaigns), a common trusted procedure is needed to be followed as a reference. For this purpose, standards have been developed and applied widely [22, 26, 60] to characterize the walls' thermal resistance via in-situ measurements. The standard practices for in-situ evaluation of wall's thermal resistance include the international standard ISO 9869 [6] and the American standard ASTM 1046 and 1155 [7, 8]. Beside small differences in details, the principles of the two standards are the same. In 2017, these two methods have been compared [16] in detail for different case studies finding out the time requirements, measurement conditions, and constraints to improve the results. In these methods, the thermal resistance of a wall is measured using two thermocouples mounted opposite to each other on two sides of the wall and a heat flux sensor (HFS) mounted next to the thermocouple on one side, preferably the interior side because of higher stability in temperature. For accurate post processing of the data, information about the construction is required to include the effect of heat storage and dynamic heat accumulation. In case of unknown construction, if a non-destructive inspection is to be carried out, such information is not available [23] and therefore, corrections cannot take place. This is known to significantly influence the accuracy, leading to a less reliable result. According to the studies in which the method has been applied, there are two main problems which the method can be associated with: First, the long duration of the measurements due to unstable boundary conditions [6, 26] and second, the problem of R_c-value precision. The duration required for the R_c-value to be reported, fulfilling the criteria of ISO 9869 [6], can be very long. This becomes a barrier and therefore, makes it difficult for the method to be applied often in practice. The results of the ISO 9869 [6] Average Method are highly dependent on the temperature and heat flux circumstances. The profile of heat flux and temperature determine the final value and the time required for the convergence to occur. According to ISO 9869 [6], presuming that all conditions are taken into account, in order to report an acceptable R_c-value, the main criteria to fulfill and stop the measurement include the following:

1. The measurement period should take at least 72 hours with a specific range of sampling and logging intervals
2. The R_c-value obtained from the last two measurement day should not differ by more than 5%
3. The difference between R_c-values obtained from the first and last certain number of days [6] is within 5%

Other criteria such as heat content and dynamic data processing [73] are generally not applicable in in-situ measurements as the exact construction is unknown and

sampling is almost never allowed. The cumulative R_c-value is reported for each day (including the average of the previous days). As this process continues, the curve of the reported R_c-values converges to a certain value, which is the average of the whole measuring period, fulfilling the aforementioned conditions.

Practical experiments, however, in which a second heat flux was installed [64] on the opposite side of the one recommended by ISO 9869 have shown that the two R_c-values are measured based on two heat fluxes (indoor and outdoor wall surface) could converge to two different final values (not in the same range) while both fulfilling the criteria of ISO 9869. As seen also in other studies [26, 64], it may happen that if the test continues, the final convergence value starts moving towards another convergence point, or that the two R_c-values do not converge to the same value even after a relatively long period. This poses a question about which of the values to report as the actual R_c-value, and if it would not be better to report the average of the two values.

According to the ISO 9869 [6] Average Method, the R_c-value of a wall, based on measurements of ΔT (the surface temperature gradient), $\dot{q}$ (the heat flux), and t (the time interval) , can be derived as follows:

$$R_c = \sum_{t=0}^{m} \Delta T^t \,/\, \sum_{t=0}^{m} \dot{q}^t \tag{2.1}$$

In which $\dot{q}$ is the net value of the total resulting heat flux (IR radiation, convection, and solar radiation in balance with the conductive heat flux) towards the wall. The heat flux meter measures this net value at the surface of the wall. According to (1), the instantaneous R_c-value at each side is different because the two instantaneous heat fluxes $(\dot{q}^t)_1$ and $(\dot{q}^t)_2$ at two sides of the wall vary, thanks to the thermal mass (resulting in $\dot{q}_{acc}$ in Fig 2.1), and temperature and heat flux fluctuations on two sides of the wall. However, in long term, based on energy conservation, the summations of $(\dot{q}^t)_1$ and $(\dot{q}^t)_2$ are equal. According to ISO 9869 [6], such summation is to be done in a long enough time period (at least 72 hours for light elements and more than a week for heavy elements [6]). In this case:

$$\sum_{t=0}^{m} (\dot{q}^t)_1 = \sum_{t=0}^{m} (\dot{q}^t)_2 \tag{2.2}$$

The validity of (2.2) depends highly on the construction, time period, and the boundary conditions (climatic conditions). In short term, by measuring the heat flux on either side of the wall, one may find a different R_c-value than by measuring the heat flux on the opposite side. The two R_c- values are expected to converge to the same final value over a long-enough period (See Fig 2.1):

$$R_{c1} = \sum_{t=0}^{m} \Delta T^t / \sum_{t=0}^{m} (\dot{q}^t)_1 = R_{c2} = \sum_{t=0}^{m} \Delta T^t / \sum_{t=0}^{m} (\dot{q}^t)_2 \tag{2.3}$$

Where $R_{c\,1}$ and $R_{c\,2}$ are the R_c-values obtained based on cumulative heat flux at the interior and exterior surface, respectively. In appendix A, a mathematical demonstration, based on the theory of Response Factors is presented to show the conditions which contribute to the occurrence of (2.3).

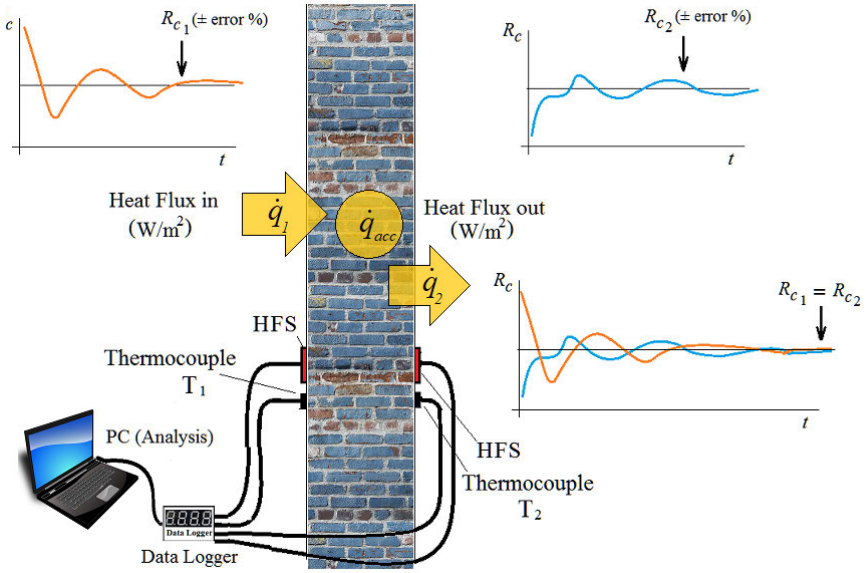

FIG. 2.1 General configuration of ISO 9869 standard measurement with one extra HFS added. The two R_c-values based on each HFS differ and in short term converge to different values.

The main aim of this study is to address the two aforementioned problems (long period and precision) in simulations and in practice, and to show the effectiveness of using an additional HFS in ISO 9869 [6] "Average Method" (equivalent to "Summation Method" in ASTM 1046 and 1155 [7, 8]), on the opposite side of the

TOC

first one, and measuring the heat flux in both sides instead of only one (See Fig 2.1). The focus is strictly laid on the usage of the standard method because of its advantage as being the most well-known and applied (due to its simplicity) reference method. Accordingly, in contrast with other aforementioned methods, there is neither the need for a prior knowledge (e.g. transfer functions, grey box modelling, advanced mathematics), nor a new type of equipment (e.g. heater, hotbox). The results of this research can be easily implemented in ASTM 1046 and 1155 as well.

The further organization of this chapter includes the research set-up in section 2.3, followed by the simulations and their results in section 2.4. Later, the experiments and their results are shown in section 2.5 and from all results and discussions, conclusions are drawn in section 2.6.

2.3 Research Set-up and Method

The set-up of this research consists of two different phases. At first, finite element simulations are carried out to investigate and demonstrate on different types of walls the difference between the results obtained from the heat flux at each side of the walls. In addition, the results obtained using an average R_c-value as defined below and the advantage of reporting this value instead of the two other values (R_{c-in} and R_{c-out}) in specific cases values are discussed.

$$R_{c-ave} = \left(R_{c-in} + R_{c-out}\right)/2 = \left(\sum_{t=0}^{m} \Delta T^t / \sum_{t=0}^{m} (\dot{q}^t)_1 + \sum_{t=0}^{m} \Delta T^t / \sum_{t=0}^{m} (\dot{q}^t)_2 \right)/2 \qquad (2.4)$$

Secondly, experiments have been carried out to show the benefit of measuring the heat flux at two sides in practice. During the simulations and experiments, the two problems (precision and long monitoring period) are addressed and the benefit of two-sided measurements is illustrated.

2.4 Heat Transfer Simulations and Results

For computational investigation and demonstration, heat transfer simulations have been carried out using COMSOL Multiphysics® 5.3a [51]. This software applies Finite Element Method (FEM) to simulate heat transfer problems. In transient heat transfer, issues such as homogeneity and the position of insulation affects the heat flows significantly [74]. Accordingly, for sake of demonstration, five typologies of walls have been studied: Two homogeneous walls, three insulated walls (insulation placed on the inside, in the middle, and on the outside), and a four-layered cavity wall. The properties and construction of the five types are depicted in Fig 2.2 and summarized in Table 2.1.

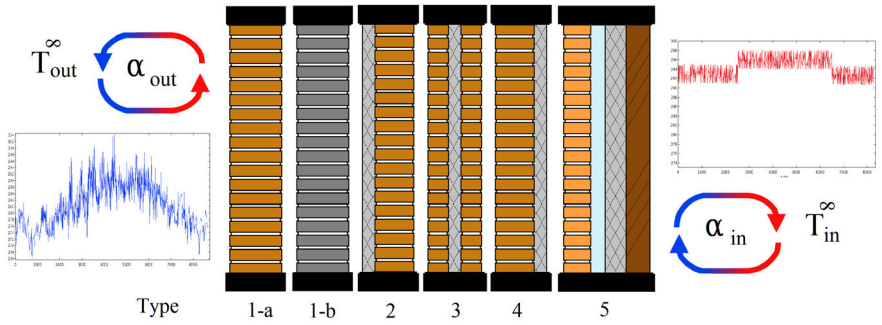

FIG. 2.2 Five typologies modelled in the simulations- All the walls are exposed to forced convection due to two air temperature profiles for 8760 hours.

The walls' boundary conditions for the simulations include the following:

- Initial Condition: initial temperature 291 K for all solid domains (average of indoor and outdoor temperature)
- Convective heat transfer coefficient 25 $Wm^{-2}K^{-1}$ with outdoor air (lumped convection and IR radiation)
- Convective heat transfer coefficient 7.5 $Wm^{-2}K^{-1}$ with indoor air (lumped convection and IR radiation)
- Insulation on all lateral sides (1D heat transfer assumption)
- Indoor temperature: winter and summer temperature of 293 K and 296 K (white noise of ±2 K amplitude).
- Outdoor temperature: reference Climate Year de Bilt 64-65 (one of the typical climate years in the Netherlands)

TOC

- Solar radiation, except in Section 2.4.4, according to the standard (the use of artificial screening), is not included.
- In 2.4.4, solar radiation is taken into account in late spring period only to show its negative influence (in other periods of the Dutch climate there is no long-term strong solar radiation to considerably affect the method).
- Rain and snow are neglected as explicitly mentioned in the ISO 9869 [6]

Software settings include time-dependent study, fine, finer, and extra fine mesh, strict hourly time step, and backward differentiation formula time stepping [75]. All simulations have been done for one climate year (hourly temperature data). The calculation of the R_c-value from the simulated data has been done for the Dutch heating season (winter, beginning of spring, and end of fall) to assure the reliability of the results. The results presented in sections 2.4.1 to 2.4.3 belong to winter season (February). As mentioned in the standard, the performance of the method is poor during the summer period and the minimum temperature difference between two sides should be 5K. Accordingly, this period is not investigated. The duration of the calculation of the cumulative R_c-value is up to the time when the test's convergence criteria have been met.

TABLE 2.1 Summary of the five wall types, their dimensions, and their thermal properties

Typology	Layer/property	l (m)	k ($Wm^{-1}K^{-1}$)	ρ(Kgm^{-3})	c ($J\ kg^{-1}\ K^{-1}$)	$R_{c^{th}}$ (m^2KW^{-1})
Type 1: Homogeneous	**a: Brick**	0.5	0.9	2000	840	0.55
	b: Concrete	0.5	1.8	2400	880	0.27
Type 2, 3 and 4: Brick and Insulation	**Brick**	0.2	0.9	2000	840	4.00
	Polyurethane	0.08	0.021	35	1320	
Type 5: 4-layer Cavity wall with insulation and exterior brick façade	**Facing brick**	0.10	0.900	2087	87	5.31
	Air cavity	0.04	$k = k(T)$	$\rho = \rho(T)$	$c = c(T)$	
	Polyurethane	0.10	0.021	35	1320	
	Wood-cement	0.09	0.350	1250	1470	

For each typology, the wall is simulated for one year with hourly air temperatures. The indoor and outdoor heat flux is evaluated at two surface cut-points in the middle of each side of the wall, where the HFSs and the thermocouples are supposedly mounted. The output is analyzed according to the ISO 9869 [6] Average Method in different periods of the year to check the accuracy and precision. Every 24 hours, the two hourly cumulative R_c-values (for each side) and their average are reported, using (2.1). This process continues for a long enough period for a perfect convergence of the three graphs to one actual value (as expected from Table 2.1), regardless of the mitigation of the ISO 9869 [6] convergence criteria (which happens earlier). Finally,

the minimum time required for the ISO 9869 [6] criteria to be met are reported and compared in all cases.

The six modelled walls are categorized as homogeneous and heterogeneous walls. The heterogeneous ones are divided into symmetrical and asymmetrical categories. The results for the R_c-value calculation according to (2.1) are shown for each category. In all figures, solid orange and solid blue lines are R_c-values based on inside ($R_{c\text{-}in}$) and outside ($R_{c\text{-}out}$) heat flux respectively and the dashed black line refers to the average R_c-value ($R_{c\text{-}ave}$). The arrow gives the point where convergence of R_c is achieved the quickest, according to ISO 9869 criteria. For further illustration, two additional simulated typologies are shown in Appendix B.

2.4.1 Homogeneous Walls (Types 1a and 1b)

The first typology is the homogeneous wall (type 1, see Table 2.1). For sake of simplicity, minor heterogeneities are neglected (e. g. the mortar joints are considered the same as brick because of their similar thermal properties). The R_c-values obtained for the two homogeneous walls are plotted in Fig 2.3 For the day of convergence and deviation from theoretical value, see table 2.7.

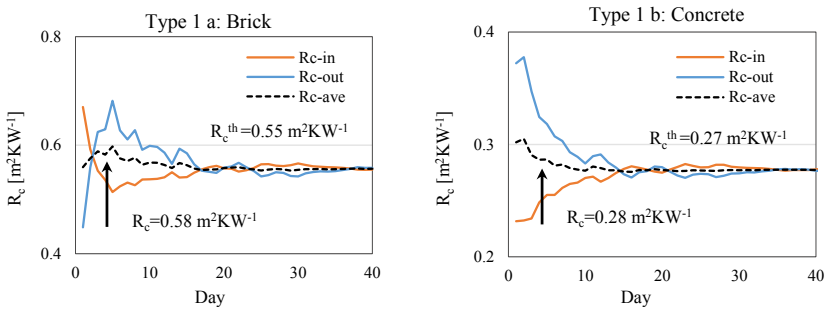

FIG. 2.3 R_c-values obtained from each of the two homogeneous walls made from brick (left) and concrete (right). The average Rc-value converges quicker to the final value.

As seen in both figures, in case of homogeneous walls, the two R_c-values converge to the same value, with a similar speed. Mostly, these profiles have a quasi-symmetric shape relative to each other. Therefore, the average of these two will converge quicker to the actual R_c-value (R_c^{th}). The temperature and heat flux disturbances on each side influence the results on either side whereas the average of the two R_c-

TOC

values shows higher stability. For instance, in the right graph, one would find the R_c-value at the 4th day of measurement, using the average R_c-value. Using the R_c-value based on heat flux on either side, more than 11 days are needed to fulfill the ISO 9869 [6] criteria (See also Fig 2.7). In other periods of the year, this duration may be much longer (see Section 2.5.5).

2.4.2 Heterogeneous Walls (Types 2, 3, 4, and 5)

Four heterogeneous walls are modelled. The two first models are two-layered walls with one layer of brick and one layer of polyurethane insulation, once at the interior (type 4) and once at the exterior (type 2) side. The third wall is a cavity wall (type 5) and the fourth one is similar to the first two, with the insulation in the middle (type 3). The walls are presented in a different order than the number of their types, due to their behavior.

2.4.2.1 Heterogeneous Asymmetrical Walls (Types 2, 4, and 5)

The two two-layered walls (insulation at inside and outside) and the four-layered cavity wall are presented here as non-homogeneous asymmetrical samples. Although types 2 and 4 are not exactly realistic (in practice, a plaster layer covers the insulation), they are modelled for sake of demonstration of the hypothesis in similar configurations. In Fig 2.4, the insulation on the exterior surface, Type 2 (left), makes the exterior R_c-values graph much more stable and converging very quickly, whereas for the case of Type 4, having the insulation on the interior side (right), the one from the interior side is more stable and converges quicker. Using the heat flux at the side closer to the insulation in these two cases results therefore in finding the R_c-value in a considerably shorter amount of time. All graphs converge in the end to a value of 4 m^2KW^{-1}, as expected from the construction (Table 2.1).

The result of type 2 (insulation at the outside surface) shows the opposite of what is recommended in ISO 9869, installing the HFS at the side with more stable temperature (indoor). In this case, one would need much longer time to find the R_c-value. The reason for this can be referred to the fact that the heat flux at the side with insulation is much more stable than at the side without. As the temperature gradient in two graphs is common, the stability of the heat flux can determine at which side the R_c-value graph is more stable, leading to a quicker convergence and therefore earlier estimation of the R_c-value. Therefore, in case of only one HFS

available, it would be better to place the HFS on the outdoor surface of the wall than on the indoor side. This however, cannot be known in advance and can only be detected by using two HFSs.

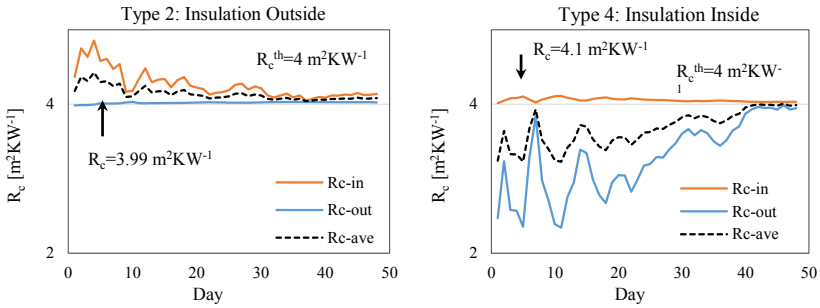

FIG. 2.4 R_c-values obtained from each of the types 2 and 4: a homogeneous brick layer with one layer of insulation on the outside (left) and on the inside (right). The R_c-value of the side having insulation converges much quicker to the actual value (R_c^{th}) in both cases.

The cavity wall is then analyzed. This construction belongs to an existing wall in a lab in Leuven, Belgium. In Fig 2.5, the result of the R_c-value simulations of the cavity wall is presented. The theoretical R_c-value is 5.31 m²KW⁻¹ as also reported in [20] (Table 2.1). The air cavity is modelled with an equivalent thermal conductivity, considering the thermal resistance of the air layer (0.180 m²KW⁻¹ as estimated by [20] and [76]) to include conduction, convection, and IR radiation).

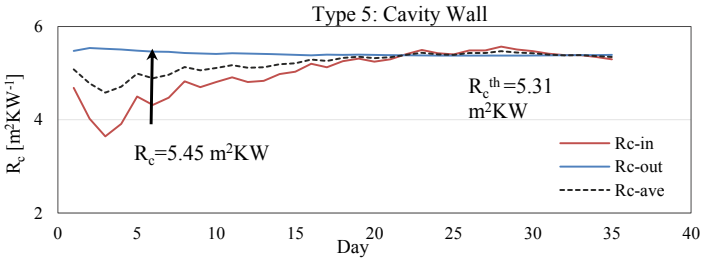

FIG. 2.5 R_c-values obtained from type5: 4-layered cavity wall consisting of (from interior to exterior) wood cement, polyurethane, air, and facing brick. The outdoor R_c-value has converged much quicker.

TOC

In the modelled cavity wall, similar to type 2 (insulation outside), measuring the HFS at the outer surface of the wall leads to a quicker estimation of the R_c-value. This, similar to type 2, in terms of time efficiency, is in contrast with what the ISO 9869 recommends regarding the placement of the sensors at the interior side. This example is underlining again the importance of using two heat flux meters at both sides of the wall for a quicker gain of the R_c-value with the same level of accuracy.

2.4.2.2 Heterogeneous Symmetrical Walls (Type 3)

The symmetry is formed by placing the insulation layer in the middle of the wall in between the two brick layers. In Fig 2.6, the result for the simulation of the symmetrical heterogeneous wall (type 3) is shown:

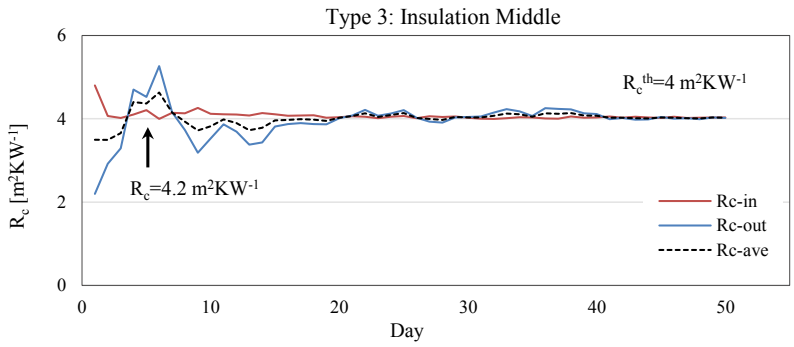

FIG. 2.6 Fig 2.6- R_c-values obtained from the type-3 wall: two homogeneous brick layers connected via insulation in the middle. The effect of the insulation is divided and thus, the side with more stable temperature converges earlier.

As seen in Fig 2.6, the interior R_c-value converges more quickly than the one from the outdoor. This is due to the fact that the effect of the insulation on the stability of the heat flux is divided between the two surfaces. Therefore, the stability of the temperature plays the dominant role of determining which side results in a quicker and more stable R_c-value. Thus, the indoor side R_c-value converges more quickly to the actual value of 4 m^2KW^{-1} (Table 2.1).

TOC

2.4.3 Minimum Required Convergence Times

For sake of comparison, the results of the simulations according to the ISO 9869 [6] criteria are summarized in Fig 2.7. The convergence time according to ISO 9869 are assessed and compared and in each case, and the inaccuracy of the measured R_c-value (in terms of deviation from the theoretical value) is reported:

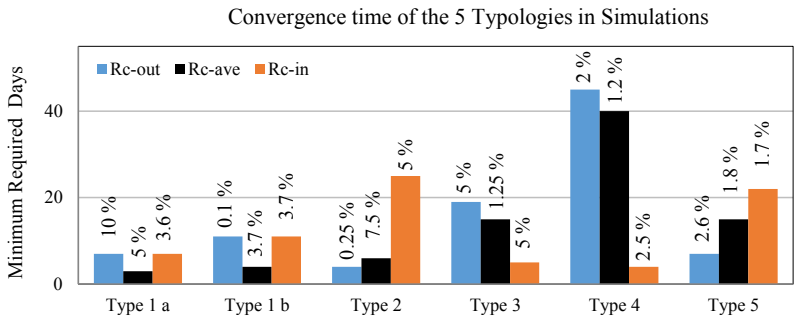

FIG. 2.7 Minimum required time for each typology to fulfill ISO 9869 convergence criteria. The case of which graph converges earlier in case of unknown construction is unpredictable. Inaccuracies are reported in terms of percentage deviation from theoretical value.

As conveyed in Fig 2.7, for an unknown construction, it is not possible to predict in advance about which graph will converge earlier to the final value. In types 1 a, and 1 b, the R_c-ave has converged respectively in half and one-third of the required time (if either of the two heat fluxes were used). In types 2 and 5, R_c-out has converged much more quickly than R_c-in (in less than one sixth of the time in type 2) whereas in types 3 and 4, in agreement with the standard method, the R_c-in has converged much more quickly. However, note that all values reported fulfill the converge criteria of ISO 9869, as described in section 2.

2.4.4 Parameters Influencing the Convergence Time and Stability

Generally, two different aspects affect the stability and convergence of the R_c-value graph: The construction (e. g. thermal mass) and the boundary conditions (e. g. solar radiation). In Fig 2.8, two examples are shown. The first graph (left) is a concrete wall exposed to solar radiation (which was excluded in the preceding examples). The presence (in solid and dotted black) and absence (in orange and

blue) of solar radiation are shown to compare the stability and convergence of the R_c graph. It is also recommended in the standard to use artificial screening or to exclude the daytime measurements from the results in low thermal mass samples [6]. The second graph (right) shows the effect of thermal mass on the time and quality of the convergence. In case of lower thermal mass ($l = 0.2$ m), the graph (in solid and dotted black) converges much more quickly and the results are more stable than in case of high thermal mass ($l = 0.5$ m) (in orange and blue).

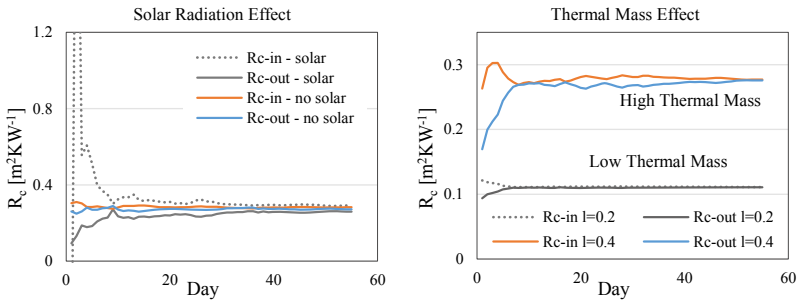

FIG. 2.8 Parameters influencing the convergence of R_c graph. Solar radiation (left) and high thermal mass (right) have negative effects (in grey) while in the absence of these effects, the R_c graphs are more stable and converge earlier

2.4.5 R_c-value Precision Problem

The uncertainty of simulations according to ISO 9869 should be around at least 10% (Except temperature and heat flow variation error, Other errors concern operational, equipment, and calibration error which do not concern simulations). In Fig 2.7, all inaccuracies (in terms of deviation from theoretical value) and all precisions (in terms of deviation of the R_c-values) were below 10 %. However, in certain types of construction, during certain periods of the year, the two R_c-values converge, fulfilling the criteria of ISO 9869 (mentioned in section 2), to two different values which differ by much more than 10%. This happens most often in homogeneous walls with high thermal mass where stability occurs at the same level on two sides (See Fig 2.9). If the extraction of the R_c-value continues, the two values take a very long time to reach the same value, the actual R_c-value, (See the right part of Fig 2.9). This is problematic because both values may be reported while not being within the expected precision range. In such cases, it would be advantageous to use the

average R_c-value, as it is in the common bandwidth of the two uncertainties and it is closer to the expected value.

In Fig 2.9, two cases are shown in which the R_c-values have converged to two different values, fulfilling the ISO 9869 criteria at the same time, but differing by more than 10% in precision. These walls (type 1: 0.5 m brick on the left and 0.5 m concrete on the right) are the same walls shown before, in a different period of time (beginning of fall). The issue has also been occasionally observed in the other types in different periods when temperature and heat flux fluctuations are extreme or when the temperature gradient of the two surfaces becomes small. The arrow gives the point where convergence of R_c is achieved, according to ISO 9869 criteria.

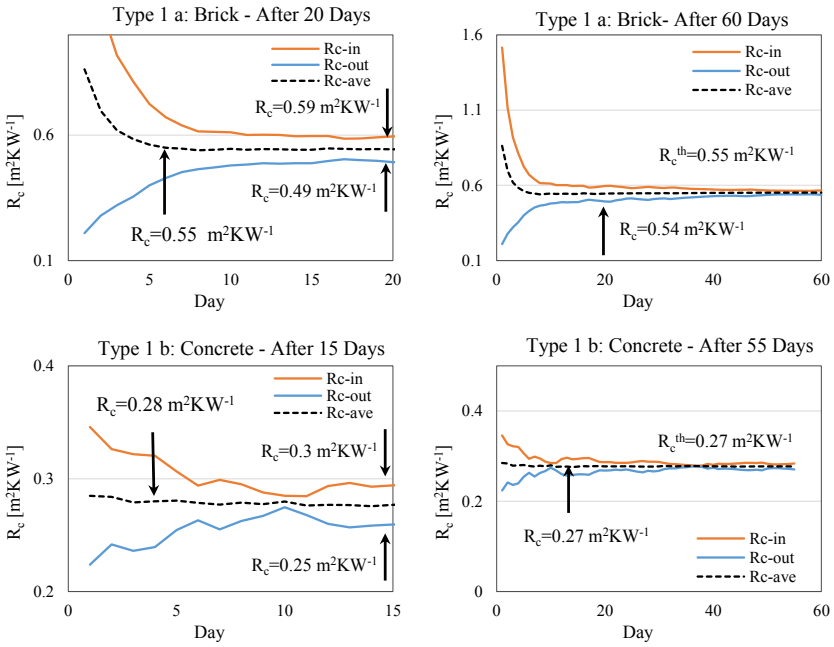

FIG. 2.9 The problem of R_c-value precision: Two different R_c-values (left) are obtained instead of one, both fulfilling the criteria of ISO 9869. The average R_c-value is closest to the actual one which the two graphs will converge to, after a very long time (right)

As seen in Fig 2.9, the R_c-in and R_c-out graphs converge to different values at the same day, both fulfilling the standard criteria before reaching the final actual value. For the brick wall $R_{c\text{-}in}$ has an inaccuracy of 7.3% and 10% for $R_{c\text{-}out}$. Both values

TOC

differ by more than 10%. For the concrete wall $R_{c\text{-}in}$ has an inaccuracy of 11% while it is 7.4% for $R_{c\text{-}out}$ which is within an acceptable range. Both values differ by more than 10%. The average of these two graphs in both cases converges much earlier (6th day vs 20th day for the brick wall and 4th day vs 15th day for the concrete wall), with an inaccuracy of less than 4%. Therefore, using the average R_c-value is a suitable alternative to waiting for the two graphs to meet at the actual value (far beyond the time to satisfy the convergence criteria of I SO 9869). The occurrence of this problem is not known beforehand, due to the unknown construction and unknown boundary conditions. Therefore, in these cases, it is also of high benefit to measure the heat flux at both sides and if the precision problem is observed, the average value is reported instead of the other two. To even increase the accuracy of the measurement, one can continue the measurement of the average value for a few days more after achievement of the ISO 9869 convergence criteria. This will still be shorter than using the RC-in value, and more accurate.

2.5 Experimental Setup and Results

Experiments have been carried out on two case study walls, to show the effectiveness of performing two-sided measurements of heat flux. The first wall is similar to type 3 (insulation inside - the construction is estimated from the appearance). The R_c-value is claimed to be 3.5 m^2KW^{-1} according to the value reported in the building permit. The second case is type 1 (homogeneous brick) with the R_c-value estimated based on construction (0.21 m wall made of Dutch brick with thermal conductivity of 1.2 WmK^{-1} [77]) as being 0.175 m^2KW^{-1}.

Two T-type thermocouples (accuracy 0.5°C) and two HFP01 HFSs (accuracy 5%) by Hukseflux Thermal Sensors [78] have been mounted on two sides of the wall. The faces of the sensors are covered by paper tape whose emissivity is close to the one from the surface of the wall. Thermal imaging (using FLIR E5 thermal camera) has been employed at first to find the spot which is representative for the whole wall and second, to check if the emissivity's of the sensors' surfaces are the same as the whole wall. This is to avoid different radiation heat transfer, as also recommended by ISO 9869. As explicitly noted in ISO 9869 [6] to protect the exterior surface (e.g. by artificial screening), the exterior surface of the wall is covered with a covering box to minimize the temperature and heat flux perturbations. The box is a square of 60×60 cm^2 made from Polystyrene and covered with reflective shield to protect the sensors

from solar radiation disturbances. The effect of the box has been tested beforehand to ensure limiting the temperature and heat flux noise. The ratio between the area under the box, the area of the sample, and the thickness of the sample is such that the box covers a considerable surface around the sensors while minimizing the 3-D heat transfer effects. In case of high levels of solar radiations and/or larger surfaces, larger protections must be used. Measurements of heat flux and temperature have taken place every second with OMEGA SQ2010 data logger and the hourly averages have been logged. All equipment have been calibrated by the providers before the measurements. In Fig 2.10, the experimental setup as well as the IR thermography images are shown.

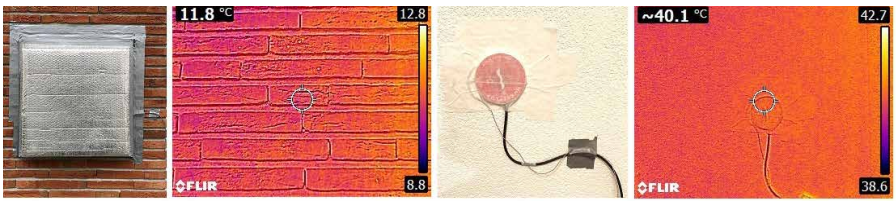

FIG. 2.10 From left to right: the insulation box covering the HFS and the thermocouple outside, the interior side HFS and thermocouple covered with same emissivity tape, IR thermography of the exterior and interior surfaces.

Measurements have been carried out for long enough periods until the two R_c graphs converge to the same final value. The outcomes of the measurements are presented in the following section.

2.5.1 Case Study 1

For the first case study, measurements have been carried out for 16 days. The cumulative R_c-value has been calculated by the end of each day using (2.1), converging to a final value. The results of the R_c-value s are plotted in Fig 2.11:

TOC

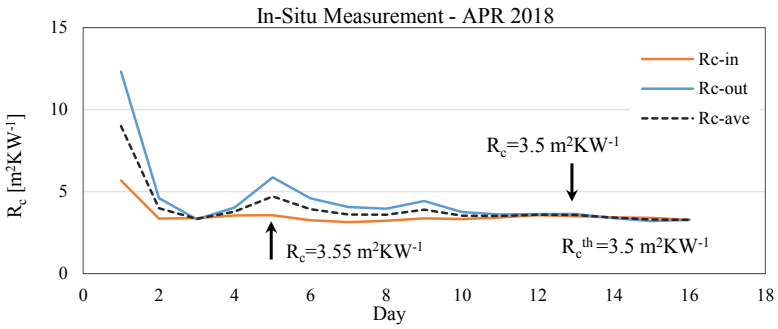

FIG. 2.11 R_c-value measurements from case study 1. The indoor heat flux has resulted in the earlier convergence of the R_c-value graph. Location: Delft, Netherlands, Apr 2018

Meeting the criteria of ISO 9869, the interior R_c-value has converged to 3.55 m^2KW^{-1} at the 5th day with a departure of 1.4% compared to the value reported in the EPC value report by the constructor. According to the criteria of ISO 9869 only the interior R_c-value is to be reported. The exterior R_c-value seems to need much longer time as it hasn't met the ISO 9869 criteria after 16 days. Despite not meeting the standard criteria, the three graphs have converged to the final value of 3.5 m^2KW^{-1} with an error of within 5%.

2.5.2 Case Study 2

During other experiments [79], a case study (Case study 2) of a Dutch homogeneous brick wall has been examined. The measurement has been carried out for 14 days and the R_c-values have been calculated by the end of each day using (2.1). The results of the R_c-value s are plotted in Fig 2.12:

TOC

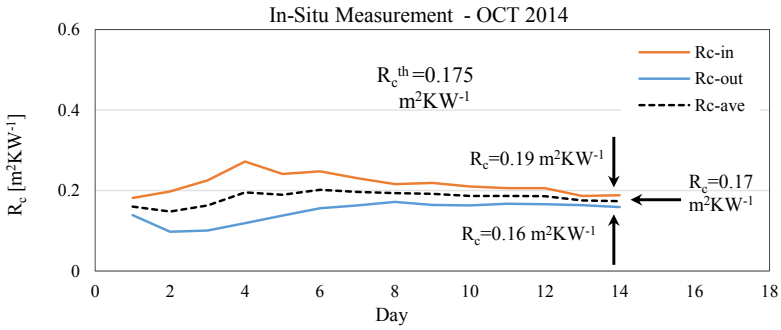

FIG. 2.12 R_c-value measurements from case study 2: Two different R_c-values are obtained, fulfilling the criteria of ISO 9869. Location: The Hague, the Netherlands, Oct 2014

The problem of precision (finding two valid R_c-values) has been observed in this case. The two interior and exterior R_c-values have converged within 2.5% at the 14th day. The two obtained R_c-values are 0.19 m^2KW^{-1} and 0.16 m^2KW^{-1} respectively, leading to an inaccuracy of 8.6% in both cases. The average R_c-value however, had converged earlier to 0.17 m^2KW^{-1}, which is closest to the theoretical value (inaccuracy of 2.9%).

In such cases, according to what has been shown so far and the mathematics demonstrated, it is recommended to use the average R_c-value as it seems to be the most reasonable solution. Especially in this case, because the wall is homogeneous, the average of the two R_c-value has converged much better than the other two which will require longer time to meet at the actual value.

2.6 Conclusion

Two problems associated with in-situ measurements based on ISO 9869 [6] have been assessed: duration and precision. The advantage of using two sides' different heat flux time series in R_c-value measurements was demonstrated through simulations and measurements. Five typologies of walls have been modelled, showing the advantage of measuring the heat flux at both sides instead of only one. Based on the results of the homogeneous walls, it can be concluded that due to the

TOC

symmetry of the R_c-value graphs, the average R_c-value will be closer to the final value and therefore, more reliable than either of the two. Accordingly, the measurement period can be reduced without compromising the accuracy. The average R_c-value contributes to solving the problem of R_c-value precision as well. In this case, the average R_c-value has shown to converge much quicker (up to 10 times quicker) to the actual value. While having the same accuracy, the averaging will avoid finding two different values which are out of 10% precision range.

In case of a heterogeneous wall, the stability of heat flux plays the key role in the convergence of the R_c-value graph. The indoor temperature is generally more stable than the outdoor and therefore, ISO 9869 implies placing the HFS in the indoor side. However, as explained in Section 2.4.2, the effect of heat flux is more critical than the one from temperature. For instance, the effect of outdoor insulation on the stability of the heat flux can become dominant and therefore overcome the negative effect from instability of the outdoor temperature. Accordingly, in case of an insulation layer on exterior side of the wall, or in a cavity wall, it may happen that the outdoor heat flux would result in a much more stable and quicker R_c-value whereas the interior heat flux converges much later.

In summary, it is highly recommended that in the in-situ R_c-value characterization of unknown constructions, the heat flux would be measured on both sides of the sample rather than only one. This way, three graphs are generated: R_c-values based on inside heat flux, outside heat flux, and the average R_c-value. In case one of the $R_{c\text{-}in}$ and $R_{c\text{-}out}$ is more stable and converges earlier than the other, the R_c-value from that side should be reported. In case both graphs are instable and symmetrical, mostly happening in homogeneous samples, the average of the two ($R_{c\text{-}ave}$) will converge much quicker and it is the closest to the actual R_c-value. This way, the two mentioned problems are tackled. Observing both R_c graphs also provides qualitative information about the possible construction of the wall (e.g. homogeneous, insulation inside, etc.)

The additional costs associated with the suggested modification are generally not high (roughly 5% - 20% addition to the total cost). This cost difference (an additional HFS) can be compensated by the fact that by applying the second HFS to the set, the final R_c-value can be obtained more quickly, leading to shorter measurement periods. A short measurement period becomes advantageous by allowing more samples to be measured in the same period of time.

3 Developing a New Alternative Rapid Method, Excitation Pulse Method, EPM

The time required for the modified version of the standard method cannot be less than couple of days. This time can be considered as to be still too long in practice. Accordingly, in this chapter, a new rapid transient in-situ method is developed, by which the thermal resistance of some walls can be determined within a couple of hours.

This Chapter is published under the following:

Rasooli, A., Itard, L., & Infante Ferreira, C. (2016). A response factor-based method for the rapid in-situ determination of wall's thermal resistance in existing buildings. *Energy and Buildings*, *119*, 51-61.

3.1 Introduction

The building stock in the European Union accounts for nearly 40% of total EU energy consumption [5]. In accordance with the EPBD (Energy Performance of Building Directive), it is mandatory for all European countries to define Energy Labels for buildings. In the Netherlands, such energy labels are based on calculation methods described in ISSO 82.3 [80], developed as a part of EPBD, leading to a theoretical value of gas and electricity consumption. Referring to studies by Majcen et al. [5], and Ioannou and Itard [3], it turns out that the actual energy consumption

for heating, strongly deviates from the predicted values. The poorer the energy label, the worse is the prediction. Generally, poorer energy labels are given to the older buildings with poor insulation in which the heating energy consumption is shown to be strongly overestimated (up to 50%). In a sensitivity analysis carried out by Majcen et al. [2], it was illustrated that one of the very sensitive parameters in predicting energy consumption is the U-value of the walls. Even slight changes in the U-value result in considerable changes in heating demand [5]. It is much more difficult to estimate the U-values in old buildings than in new ones. In the newer buildings, the wall construction is generally known whereas in old ones, it is often impossible to know even if an insulation layer is present or not.

In the Netherlands, the U-value and the R_c-value of the walls are seldom measured but rather estimated following the descriptions available in [80], based on calculations and procedures in [81] which suggests thermal resistances for different types of construction materials. However, in old buildings, the construction and the material of the walls are often unknown. Hence, the procedure will lead the inspector to use R_c-values based on the year of the construction, tabulated in [82]. Accordingly, it is very well possible that this method currently used for several years leads to a very poor estimation of the thermal transmittance in old buildings with unknown construction. The valid measurement techniques available today for in-situ R_c-value measurement include the international standard ISO 9869 [6] and the American standard ASTM [7, 8]. These methods require long periods of measurement (up to 2 or more weeks) which is obviously an obstacle to making measurements. Hence, new methods are required to measure the R_c-value of unknown constructions on-site with a good level of accuracy in a short time. The topic of this research has become so far crucial that the International Energy Agency's program Energy in Buildings and Communities (EBC) has dedicated the ongoing (2011-2015) project Annex 58 [49] to "Reliable building energy performance characterization based on full scale dynamic measurements" [83].

In this chapter, a transient method is presented for in-situ measurement of the thermo-physical properties of the walls including thermal resistance. The method is based on the principles of the thermal Response Factors (RFs) method by Mitalas and Stephenson [84].

In section 3.2, a state-of-the-art about relevant measurement techniques is presented. Section 3.3 describes the theoretical part of the method, the experimental set up is introduced in section 3.4, and in section 3.5 the results of the measurements are analyzed. Conclusions and recommendations are drawn in section 3.6.

3.2 State-of-the-Art

In principle, the R_c-value of an existing building component can be obtained by applying the standard method of measuring the heat flow rate on one side and the temperatures on both sides of the element under steady state conditions. However, since static conditions are never achieved on site in practice, other approaches are necessary to overcome this issue.

3.2.1 Lab Methods

The use of steady state methods such as application of hotbox apparatus [14] in labs and transient methods are common approaches for measurement of the R_c-value. For example, large scale devices such as ORNL hotbox apparatus [85] have been used for large building components reliably [86]. In the large scale, other specific kinds of hot boxes can be used as well to assess the dynamic performance of walls by simulating outdoor conditions in the lab. These experiments include the static and dynamic tests by Sala et al. [67] and later on by Martín et al. [66] which were done via an air chambered hot box in the lab. Along the same line, outdoor test cells are developed to measure the thermal characteristics of building components [87]. Jiménez et al. [88] used such a large scale cell to characterize a wall exposed to actual weather conditions.

3.2.2 In-Situ Methods

Regardless of the benefit of aforementioned lab methods in including the actual weather conditions, they cannot be applied in existing residential buildings. Therefore, in the recent past, in-situ measurements have become more popular and numerous in-depth studies have been conducted regarding in-situ evaluation of thermal characteristics such as thermal resistance, effective thermal mass [60], and specific thermal conductance [59].In-situ measurements are performed by measuring the heat flow rate at the surface of the wall and surface temperatures over a long enough period. By application of a dynamic theory [60, 62] in the analysis of recorded data the fluctuations of the heat flow rate and temperatures can be taken into account. In accordance with the literature and relevant technical reports, although various in-situ measurement methods [62] have been proposed till today,

the challenge remains for handling the fluctuations of the temperatures and heat fluxes on both sides of the building walls, in addition to the time delay in thermal response of the ones with higher thermal mass due to which static conditions are never achieved.

3.2.2.1 Methods Based on ISO 9869 and ASTM standards

ISO 9869 [6] and ASTM [7, 8], using the same principles, prescribe the standard measurement method for in-situ measurement of R_c-value and U-value of building components. The analysis of the measured data is done via "Average Method" (Summation method in ASTM) and via "Dynamic Method" (or by "Least Squares Method" in ASTM), which does not shorten the minimum measurement period in heavy elements (walls). Especially in heavy walls, when using the Dynamic method, the measurement time required for obtaining the U-value is the same as in the Average method [89]. Including the dynamic effect of thermal mass of unknown constructions in ISO 9869 [6] requires sampling and endoscopic inspection by drilling which is generally not allowed by the dwellings' occupants. A desirable on-site measurement method should not only be reliable, but also non-destructive to be applicable during the building inspections [23].

After at least 72 hours of monitoring, if the termination criteria has been met [6], the measurements may stop [90]. Ahmad et al. [22] studied hollow reinforced precast concrete walls based on standards ASTM C1155-95 [8], ASTM C 1046-95 [7], and ISO 9869 [6] in Saudi Arabia finding 6 days enough for satisfaction of the convergence criteria. However, such short period is generally insufficient for obtaining results, especially, in countries with less stable climate [91]. Smaller temperature gradients along two sides [23] and heavy construction of walls leading to long measurement periods [92] are other shortcomings of such measurements. In Scotland, with a monitoring period of 17 days, Baker [63] compared the in-situ measurement results based on ISO 9869 [6] with the ones obtained in the lab, resulting in a good agreement. The study was further developed [26] by studying a larger number of case studies where he showed the necessity of longer periods of in-situ measurements for achieving satisfactory results. It turned out that in some cases, even 36 days of monitoring had not been enough to measure the U-value of the walls. The walls with heavier construction demand more time to stabilize the average heat flux and the average temperature gradient. Note that by long periods of measurement, more climatic fluctuations are included in the results, highly increasing the error probability.

3.2.2.2 Comparison between Calculated and Measured Values

In the United Kingdom, Doran [93] conducted a research to improve the building simulations by making comparisons between the measured and the standard calculated U-values [10]. It was shown that the U-values can be underestimated up to 30% by calculation. The same conclusion has been drawn more recently by Asdrubali et al. [94]. Based on ISO 9869 [6], Rye and Scott [95] published a technical report for SPAB (Society for the Protection Ancient Buildings), with their measurements based on Baker's [63] report on 77 old-constructed walls. The results were compared to the calculated U-values, showing that in 77% of the cases, the calculation software had overestimated the U-values. Along the same line, other studies [96, 97] also conclude that the measured U-values can be significantly lower than the ones being assumed. This possible overestimation is suspected [2] to be one of the reasons for the final overestimation in energy consumption predictions in poorer Dutch energy labels.

3.2.2.3 Other Methods

Other in-situ measurement methods include IR thermography. Concerning much emphasis on non-destructivity nature of inspections, the application of thermography for thermal diagnostics has been popular since early 90s. Grinzato et al. [98], and Balaras and Argiriou [99] illustrated some of the use and advantages of thermography in building diagnostics such as inspections of insulation problems. Fokaides and Kalogirou [100] applied infrared thermography for the determination of U-value in building envelopes in Cyprus. The results have been compared with ISO 9869 [6] method as well as calculations. Regardless of the advantage of this method to the others in shortening the measurement time, the data analysis is done by steady-state models. Furthermore, the required steady climate conditions such as indirect solar radiation, low wind speed, and complete evacuation of the building are the main obstacles of this method. The conditioning period prior to the test to achieve the quasi-steady state condition is considered 3 to 4 hours while it is well known that for high thermal mass (old buildings), such short period is never enough. Therefore, this method is limited to light constructions and steady climate conditions.

From the scientific perspective, regarding the U-values and R_c-values, measurements are generally preferred to calculations because they provide more realistic and accurate information necessary for prediction of energy use in buildings. While the need for accurate in-situ measurements has become evident, the only applicable

methods require long measurement periods which strongly restrain their practical use. Therefore, there is a certain demand for a new method to tackle this issue.

3.3 Methodology

The current reliable standard methods for in-situ measurement of the walls' thermal resistance are originally static-based with corrections to include the dynamic effects. However, in case of unknown structures, due to lack of information about thermo-physical properties, these corrections cannot be applied. Additionally, the problem of the need for long measurement periods becomes even more extreme for the case of the Netherlands where the climate is quite unsteady and the temperature and heat flow fluctuations are relatively large. The present chapter describes a fully transient method, the Excitation Pulse Method (EPM), by which only few hours of measurements are needed. In sections 3.3.1 and 3.3.2, the theory behind and the method itself are presented, in Section 3.3.3, the data processing method is described, and in 3.3.4, the validation of the method is explained.

3.3.1 Excitation Pulse Method, EPM

The idea behind EPM is based on the theory of RFs. Mitalas and Stephenson [84] developed the theory of RFs leading to methods that have been applied in building simulation software (e.g. ENERGYPLUS, TRNSYS) till today [101]. The RFs method is used as an alternative to solving sets of partial differential equations. The benefit of the method is that it is independent from the wall's internal temperature. The RFs are calculated from the wall thermo-physical properties. The heat fluxes $\dot{q}_1$ and $\dot{q}_2$ at two surfaces of the wall can be calculated then as a function of surface temperatures, X being the inner heat flux time-series RFs to a triangular surface temperature pulse of 1 K, and Y being the outer heat flux time-series RFs to the same pulse ((3.1) and (3.2)). In Fig. 3.1, the concept is illustrated, with $\dot{q}_1$ the heat flux from the excitation pulse, and $\dot{q}_2$ the heat flux on the wall's outer surface.

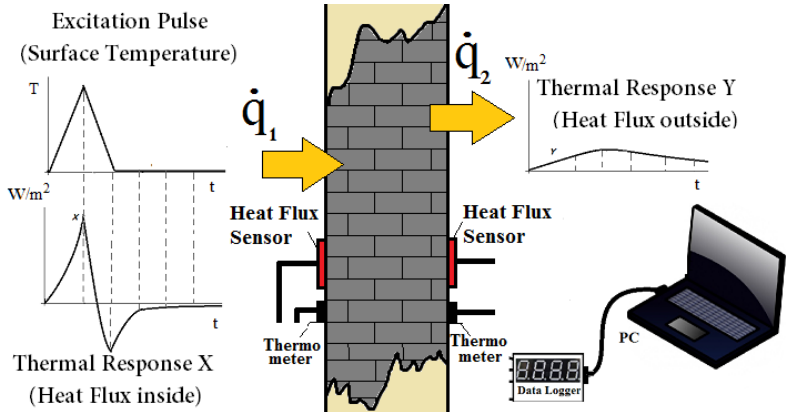

FIG. 3.1 The general concept of EPM – applying a triangular temperature pulse to the surface and measuring heat flux responses on two sides of the wall

The heat fluxes on the wall's surfaces based on RFs are obtained by the following equations [84].

$$\dot{q}_1 = \sum_{i=0}^{\infty} X_i T_1^{t-i} - \sum_{i=0}^{\infty} Y_i T_2^{t-i} \tag{3.1}$$

$$\dot{q}_2 = \sum_{i=0}^{\infty} Y_i T_1^{t-i} - \sum_{i=0}^{\infty} X_i T_2^{t-i} \tag{3.2}$$

Where $\dot{q}_1$ and $\dot{q}_2$ are the heat fluxes of two sides of the wall with surface temperatures T_1 and T_2. The variable t is the RF time interval defined here as the time for the pulse to start from zero and reach its peak (half of the triangle). X and Y are the RFs either calculated by equations in [84] or obtained via EPM.

In EPM, the problem is reversed: if it is possible to control the wall's surface temperature to form a triangular profile, then it is possible to determine the RFs X and Y by measuring the heat fluxes $\dot{q}_1$ and $\dot{q}_2$. Therefore, in EPM, the wall's interior surface is linearly heated and cooled, generating a triangular surface temperature profile. Meanwhile, the heat fluxes on two sides of the wall are measured leading to the RFs to this excitation pulse. Not only can these RFs be used directly in dynamic simulations, but also, they can lead to the determination of the R_c-value and other thermal properties. A patent has been granted on the method by the NL Patent Office.

3.3.2 Determination of the Wall's RFs by EPM

In actual conditions, temperature and heat flux fluctuations always exist on the surface of the walls. Temperature fluctuation range, generally higher than 1 K, prevents measurements to take place accurately. However, since the RF method is based on Fourier's conduction equation and Laplace transform [102], it allows applying the superposition principle [84], allowing generation of a triangular pulse with a magnitude much greater than 1 K. Having a greater magnitude allows neglecting the small magnitude temperature and heat flux fluctuations while easing the application and control, assuring sufficient heat penetration through the wall. Of course, the magnitude should be such that it doesn't affect the inside finishing of the wall (e.g. paint or wallpaper). According to the superposition principle, the measured heat flux should be divided by the magnitude of the triangular pulse in order to obtain the RFs of the equivalent wall (RFs are defined for a triangular pulse with a magnitude of 1 K). The equivalent wall here means a homogeneous wall with same thermal behavior according to its equivalent thermo-physical properties. Let δ be the magnitude of the triangular pulse. The RFs can be calculated from the results of the EPM as:

$$\begin{cases} X_i = \dot{q}_1 / \delta \\ Y_i = \dot{q}_2 / \delta \end{cases} \tag{3.3}$$

Where X_i and Y_i are the RFs. $\dot{q}_1$ and $\dot{q}_2$ are the heat fluxes measured at interior and exterior surfaces respectively.

According to the theory of RFs, time interval is a very important variable. Different time intervals for the excitation signal result in different time series of RFs. The smaller the time interval is, the greater the RFs will be. This is logical because for reaching the desired temperature earlier, a greater amount of heat is required. On the other hand, it is possible to convert the RFs from one time interval to another. For instance, RFs with the time interval of 1/2 hour can be converted to RFs with time interval of 1 hour as following [84]:

$$\left(RF_i\right)_{t=2t} = \left(0.5RF_{2i-1}\right)_{t=t} + \left(RF_{2i}\right)_{t=t} + \left(0.5RF_{2i+1}\right)_{t=t} \tag{3.4}$$

Where $\left(RF_n\right)_{t=t}$ is the nth RF at time interval t and $\left(RF_n\right)_{t=2t}$ is the same RF at time interval $2t$. The relation between the time interval and the first X RFs of a 0.2 m brick wall (k =1.2 Wm^{-1}K^{-1}) is presented in Fig. 3.2:

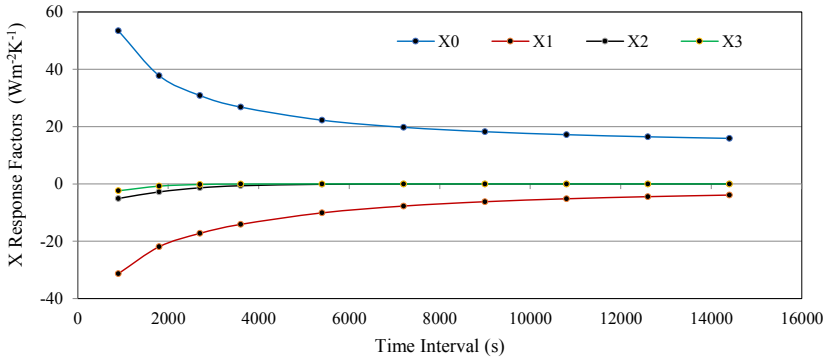

FIG. 3.2 The relation between time interval and the X thermal response factors

As seen in Fig. 3.2, greater time intervals result in smaller response factors. This implies that in EPM, a greater time interval can be chosen instead of a greater magnitude of the excitation pulse. The main criterion of choosing EPM's time interval is that the heat response (temperature rise) should be observed from the opposite side of the wall. This can be checked with the heat flux/temperature data. In this case, it can be concluded that the information (heat conduction) has been received by the other side.

3.3.3 Determination of the Wall's Thermo-Physical Properties

According to the definition of $\dot{q}_1$ and $\dot{q}_2$, a derivation for R_c-value based on RFs is demonstrated:

$$\left(\dot{q}_1+\dot{q}_2\right)/2=\frac{1}{2}\left[\sum_{i=0}^{\infty}X_iT_1^{t-i}-\sum_{i=0}^{\infty}Y_iT_2^{t-i}+\sum_{i=0}^{\infty}Y_iT_1^{t-i}-\sum_{i=0}^{\infty}X_iT_2^{t-i}\right]=$$
$$=\frac{1}{2}\left(\begin{bmatrix}X_0\\ \vdots\\ X_n\end{bmatrix}+\begin{bmatrix}Y_0\\ \vdots\\ Y_n\end{bmatrix}\right)\times\left(\left[T_1^t\ \ldots\ T_1^{t-n}\right]-\left[T_2^t\ \ldots\ T_2^{t-n}\right]\right) \quad (3.5)$$

TOC

(3.5) is always true. Therefore, it is also true when the wall is in steady state condition. Let the wall be in a steady state condition with constant surface temperatures T_1 and T_2 for n hours. This assumption does not influence the results and it only helps in mathematical simplifications. Then with a constant temperature gradient $T_1 - T_2$ from time $t-n$ to time t:

$$\begin{aligned}&\frac{1}{2}\left(\begin{bmatrix} X_0 \\ \vdots \\ X_n \end{bmatrix}+\begin{bmatrix} Y_0 \\ \vdots \\ Y_n \end{bmatrix}\right)\times\left(\begin{bmatrix} T_1^t & \dots & T_1^{t-n} \end{bmatrix}-\begin{bmatrix} T_2^t & \dots & T_2^{t-n} \end{bmatrix}\right)\\ &=\frac{1}{2}\left(\begin{bmatrix} X_0 \\ \vdots \\ X_n \end{bmatrix}+\begin{bmatrix} Y_0 \\ \vdots \\ Y_n \end{bmatrix}\right)\times\begin{bmatrix} T_1^t - T_2^t & \dots & T_1^t - T_2^t \end{bmatrix}\end{aligned} \tag{3.6}$$

$$\frac{1}{2}\left(\begin{bmatrix} X_0 \\ \vdots \\ X_n \end{bmatrix}+\begin{bmatrix} Y_0 \\ \vdots \\ Y_n \end{bmatrix}\right)\times\begin{bmatrix}1 \dots 1\end{bmatrix}_{1\times n}\times\left(T_1 - T_2\right)=\frac{1}{2}\left(\sum_{i=0}^{n} X_i+\sum_{i=0}^{n} Y_i\right)\times\left(T_1 - T_2\right) \tag{3.7}$$

By definition of the steady state $\dot{q}_{ss}=\dot{q}_1=\dot{q}_2$, (3.7) leads to:

$$\left(\dot{q}_1+\dot{q}_2\right)/2=\dot{q}_{ss}=\frac{k}{L}\left(T_1 - T_2\right)=\frac{1}{2}\left(\sum_{i=0}^{n} X_i+\sum_{i=0}^{n} Y_i\right)\left(T_1 - T_2\right) \tag{3.8}$$

Therefore:

$$\frac{1}{2}\left(\sum_{i=0}^{n} X_i+\sum_{i=0}^{n} Y_i\right)=\frac{1}{2}\sum_{i=0}^{n}\left(X_i+Y_i\right)=\frac{k}{L}=1/R_c \tag{3.9}$$

The R_c-value therefore can be obtained by the sum of the measured RFs.

$$R_c=2\times\left(\sum_{i=0}^{n}\left(X_i+Y_i\right)\right)^{-1} \tag{3.10}$$

The benefit of (3.10) is not only the direct conversion of the EPM results into R_c-value, but also, is the significant shortening of the measurement time without affecting the accuracy. The reason behind is that the term $\sum_{i=0}^{n}(X_i+Y_i)$ converges much more quickly than each of the terms $\sum_{i=0}^{n}Y_i$ and $\sum_{i=0}^{n}X_i$ (which also individually approach the inverse of R_c-value). Fig. 3.3 shows an example of the response factors (X in red, Y in blue, and the $X+Y$ in black) of a sample Dutch brick wall (k=1.2 $Wm^{-1}K^{-1}$) of 0.2 m thickness.

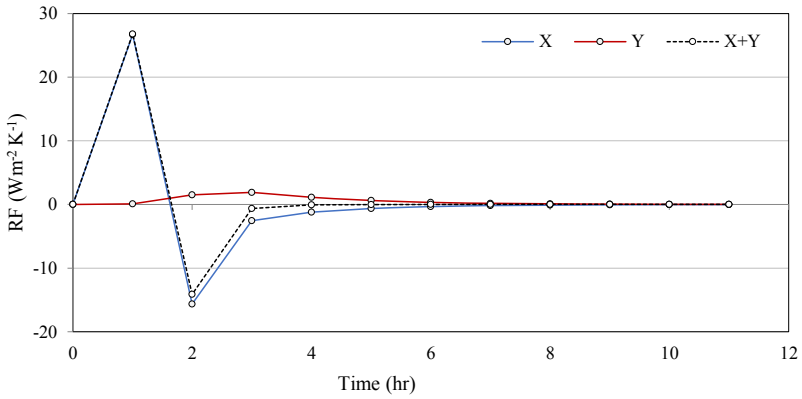

FIG. 3.3 Comparison between the convergence time of X, Y, and the $X+Y$ curves

As shown in Fig. 3.3, while X and Y factor curves (in blue and red) converge to zero at time $t=9$ h the curve of $X+Y$ (in black) converges to zero at time $t=4$ h which is five hours earlier. Consequently, the R_c-value can now be obtained even quicker. If the thickness of the wall is known (this can generally be estimated on site quite accurately), the equivalent thermal conductivity of the wall (k) can also be determined. Afterwards, it should be possible by solving the set of equations of the RFs [84], to determine the Volumetric Heat Capacity (VHC). These equations can be solved either for both properties VHC and k or only for VHC when k is obtained from the R_c-value based on (3.10) and the thickness of the wall. The specific heat capacity and the density are combined as one property VHC here since in the heat transfer equations, the aggregated variable is directly used. This is beneficial since three variables of density, specific heat capacity, and k can be reduced into two variables VHC and k.

3.3.4 Validation of the Method

The current standard methods include the international standard ISO 9869 [6] and the American standard ASTM [7, 8] with similar data analysis methods and different stopping criteria. The application of ASTM is explicitly noted to be limited to light to medium-weighted constructions. ISO 9869 though seems to be more applicable in the walls' typologies and structures. However, it still seems to be very dependent on the information about the construction. In this research, ISO 9869 [6] seems to be better for validation of EPM because of its structure and the fact that it is commonly used in studies alike. In case of unknown construction, the only sub-method to be used is the Average method of ISO 9869. Therefore, for validation of the measurement results, this method has been used for the three walls investigated. The obtained R_c-values by EPM are compared to the ones obtained by measurements based on ISO 9869 [6] method, and the relative difference is presented in order to assess the accuracy and validity of the EPM as a new method. In each case study, one in The Hague (Netherlands) and two in Delft (Netherlands), the two methods have been conducted at the same period of time.

The Measurement Method Based on ISO 9869

The ISO 9869 [6] method requires two thermocouples to be mounted on two surfaces of the wall and one heat flow meter on one side of the wall with more stable temperature. The steady-state assumption implies that only one heat flow meter is enough since the average heat flow on both sides are equal in a long-enough period of measurement. However, in the current study, two heat flow meters are used on two sides of the wall which have relatively equal steadiness in the surface temperature profile because a strong protective insulating shield (box) was designed and mounted on the exterior surface. It is well known that due to the thermal mass, differences always exist between internal and external heat fluxes. The inside surfaces were not exposed to direct solar radiation and heat convection. The duration of the measurement depends on the stopping criteria explained in ISO 9869 [6]. The duration of the test must exceed 3 days taking up to 7 to 14 days or even more than a month for heavy structures. For walls with unknown construction, the "Average Method" is to be used but without the heat accumulation corrections. The R_c-value based on this method is then obtained by (3.11):

$$R_c = \sum_{t=0}^{m} \Delta T^t \,/\, \sum_{t=0}^{m} \dot{q}^t \tag{3.11}$$

TOC

Where ΔT^t is the temperature difference between two sides and $\dot{q}^t$ is the heat flux in the same direction of ΔT^t and t is the time interval, chosen 5 minutes for data logging (average of 1-minute readings). Obviously, according to the heat accumulation by thermal mass, each R_c-value calculated based on each heat flux meter, converges to a different number. With a long enough measurement period (e.g. one month) and quasi-steady state conditions, both converge to the same value (See Chapter 2). This is due to the fact that according to the conservation of energy, the sum of the heat going through the wall, over a relatively long period, is equal to the sum of the heat flux coming out of the wall:

$$\sum_{t=0}^{m}(\dot{q}^t)_1 = \sum_{t=0}^{m}(\dot{q}^t)_2 \tag{3.12}$$

Where $(\dot{q}^t)_1$ and $(\dot{q}^t)_2$ are the interior and exterior heat fluxes with the same direction at time t. Hence, it is implied that by using an additional heat flow meter (two instead of one as in ISO 9869 [6]) and using the average of the two R_c-values, in accordance with the theory of RFs and Fig. 3.3, it should be possible to obtain the R_c-value slightly quicker.

3.4 Experimental Setup

The aim of the experimental set up is the proof of principle for the EPM. In Fig. 3.4, a schematic view of the experimental set up designed for EPM is shown. The heater is an infrared radiative type and the performer of the experiment (later, the dimmer and the cntrol unit) performs as a controller in order to adjust the heat flux to the wall's surface by maintaining a constant heat flux at a very short period of time (the heat flux sensor'sresponse time) and once stable, moving to the next desired temperature.

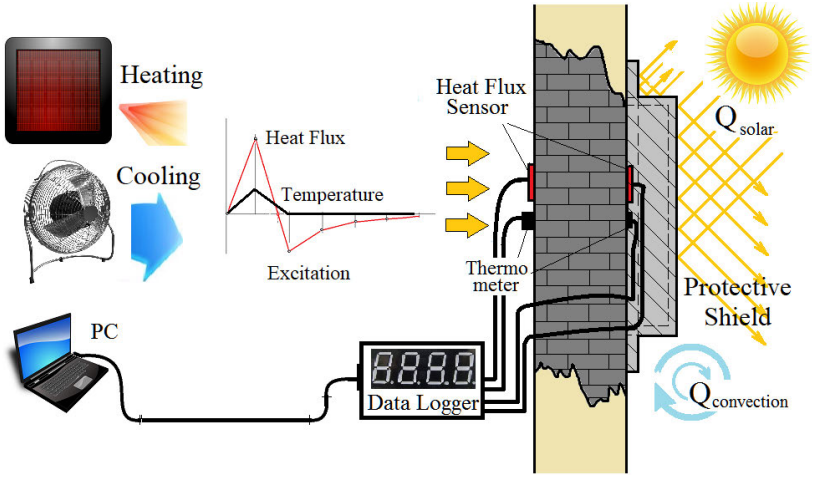

FIG. 3.4 The designed set up for the experiment: heating by radiative heater and cooling by a convection fan and an ice bag. Exterior surface of the wall is protected by a box and the data from heat flux sensors and thermometers is recorded in a data logger

The purpose of EPM is to observe the heat flow on two sides of the wall as responses to a triangular temperature pulse on the wall's interior surface. As mentioned before, the duration of exerting the excitation pulse and the maximum surface temperature to reach (the magnitude of the pulse) depend on the actual conditions such as sensitivity of the finishing of the wall to high temperatures. Since there is much emphasis laid on the "non-destructivity" nature of the inspection, this issue must be taken into consideration. In this case, as explained in Section 3.3.3, a greater time interval can be chosen instead of a higher surface temperature. Generally speaking, a range of 70°C to 90°C and a duration of 15 minutes (6 RFs in 1.5 hour) were found to be appropriate for the maximum surface temperature and the time interval. Note that a too short time interval will also make it difficult or even impossible to control the wall surface temperature linearly. Note also that if the exterior heat flux response (temperature rise) is not observed, a greater time interval must be chosen.

3.4.1 Locating a Proper Test Area by IR Thermography

Before starting the experiment, it is recommended to find an appropriate area to install the set up. It is well known that sometimes the walls are not thermally homogeneous. Therefore, as recommended in ISO 9869 [6], an IR thermography camera is used for the allocation of the area where the experiments should take place. If the surface temperature profile shows a range, it can be concluded that

TOC

multiple points of measurements should be chosen and the measured values should be corrected.

3.4.2 Generating a Triangular Surface Temperature Pulse

A triangular pulse is generated by taking a step-by-step procedure (each dsesired temperature is reached and maintained for a short time to stabilize, before moving to the next desired temperature) to make sure that the whole pulse signal is built up properly. Linear heating to the maximum temperature (e.g. 80°C) takes place by decreasing the distance between the heater and the wall's surface. Right after linear heating, linear cooling takes place immediately. This is very important because the wall reacts according to its "memory" and the type of the pulse that is previously given to it. Linear cooling takes place by increasing the distance between the heater and the wall, followed by cooling with a fan and an ice bag, respectively. According to the cooling rate, at some point, the heater must be switched off and then forced convection heat removal should start by using a fan with increasing air flow rate (Forced Convection). At final steps – when the temperature does not decrease with the convection, an ice bag must be held close enough to the wall's surface to remove heat by combined radiation and convection to maintain the pulse at a zero level. The surface temperature received from the thermocouple is read and compared to the desired linear data. According to the time interval, the heat flow is adjusted by varying the radiator's distance or dimming its power.

3.4.3 Protecting the Exterior Surface

The exterior surface of the wall is exposed to various thermal disturbances such as forced convection, solar radiation, etc. These effects are the main phenomena influencing the undesirable fluctuations of temperature and heat flow on the surface which in ISO 9869 [6], cause a demand for longer measurement periods. Therefore, it is desired to prevent such disturbances by insulating a considerable part of the wall which is under inspection. Additionally, the measurements of the heat flux response on the exterior surface of the wall have to be distinguished from the other heat flux disturbances such as solar radiation, wind convection, IR radiation, etc. This part of the wall is therefore isolated from the rest of the surface by a protective shield (box). The total thermal resistance provided by the box perpendicular to wall's surface is 4.41 m^2K/W. Experiments have shown that the presence of the box significantly reduces the temperature and heat flux fluctuations.

3.4.4 Heat Flux and Temperature Measurements and Data Acquisition

Two heat flux sensors (EKO Instruments MF-180) with individual calibration certifications are mounted on both sides of the wall under study. According to the temperature dependency of these sensors, a maximum error of 1.8% in high levels of heat flux has been possible. Two T-type thermocouples with an accuracy of 0.1 K are attached at the same spots of heat flux sensors. The data logger has an accuracy of 0.5 K in the temperature junction (reference temperature). Therefore, a maximum total error of 0.6 K in the temperature measurement is expected. The surface of the heat flux sensors and the thermocouples are covered with a layer of tape with the same color of the wall's surface for sake of radiative heat transfer. The linearity of the signal is controlled every 10 seconds. According to the chosen time interval, the data is read and analyzed to obtain the RFs.

3.5 Results

The experiments have been conducted for three case studies. The measurement results of one case study are shown explicitly here and the results of two other case studies are shown briefly in Table 3. The case study investigated in this research is an 8.5 cm thick wall with unknown construction in a bedroom of an 84 m^2 apartment located in Delft with an energy label of E. The year of construction is 1964. In Fig. 3.5, the whole building, the interior and the exterior surfaces are shown.

FIG. 3.5 Case study - The whole building (left), the inside surface of the wall (middle), and the outside surface and sensors covered by the box (right). Location: Delft, the Netherlands, Oct 2014

TOC

The results of IR thermography showed that for the three case studies of this research, only one point was sufficient for the measurements to take place.

3.5.1 EPM Results

The Results of the RFs and surface temperature measurements by EPM are presented in Fig. 3.6. For this type of wall, the inner heat flux response goes up to around 800 Wm^{-2}.

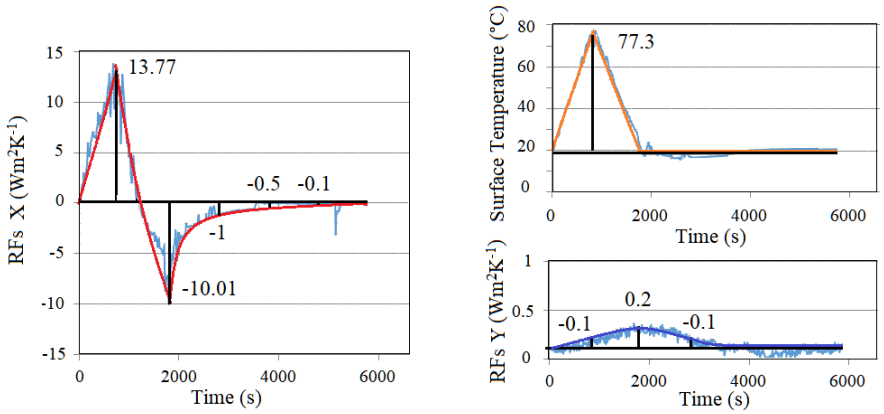

FIG. 3.6 Thermal RFs and the excitation pulse measurements in case study

The magnitude of the excitation pulse (in orange) is 57 K. Therefore, all of the measured heat fluxes are divided by 57 in order to obtain the RFs at the excitation side (in red) and at the other side (in blue). The peak of the interior RF curve (in red) is X_0, then comes the X_1 which is the minimum of the curve, and then the rest of the RFs. Plotting the connecting lines according to the theory explained and the values from the graphs, the RFs for the case study are obtained as given in Table 3.1.

TABLE 3.1 The results of measured thermal RFs by EPM, case study

RF	0	1	2	3	4	5
X	13.77	-10.01	-1	-0.5	-0.1	0
Y	0.1	0.2	0.1	0	0	0

According to (3.10), the R_c-value can be obtained using the sum of RFs.

$$R_c = 2\times\left(\sum_{i=0}^{n}(X_i + Y_i)\right)^{-1} \cong 0.78\ \left(\mathrm{m^2KW^{-1}}\right) \tag{3.13}$$

3.5.2 ISO 9869 Results

The heat flux and surface temperature measurements (every 5 minutes) by ISO 9869 method for the case study are presented in Fig. 3.7. As seen in the temperature graph, the surface temperature of the exterior surface of the wall has been successfully bounded by the protective shield and the undesired fluctuations and disturbances are damped.

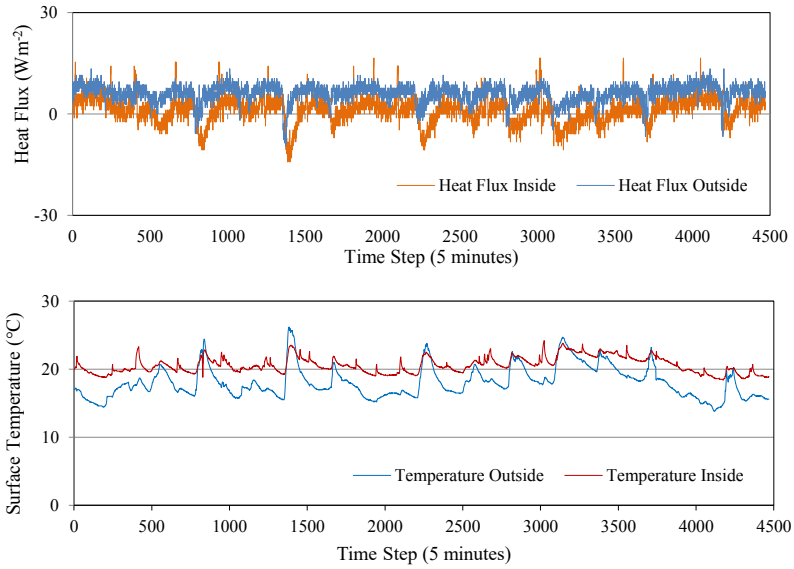

FIG. 3.7 Heat flux and surface temperature measurements on two sides of the wall (case study)

Results of R_c-value measurements based on ISO 9869 for the case study are presented in Table 3.2. $R_c\left(\dot{q}_1\right)$ and $R_c\left(\dot{q}_2\right)$ are the cumulative R_c-values calculated by interior and exterior heat fluxes $\dot{q}_1$ and $\dot{q}_2$.

TOC

TABLE 3.2 R_c-values in (m²K/W) obtained by ISO 9869 method using $\dot{q}_1$ (inner side heat flux) and $\dot{q}_2$ (outer side heat flux), case study

Day	1	2	3	4	5	6	7	8
$R_c(\dot{q}_1)$ (m²KW⁻¹)	0.80	0.83	0.80	0.94	0.93	1.07	1.07	1.05
$R_c(\dot{q}_2)$ (m²KW⁻¹)	0.49	0.48	0.45	0.44	0.44	0.44	0.44	0.44
Day	**9**	**10**	**11**	**12**	**13**	**14**	**15**	**16**
$R_c(\dot{q}_1)$ (m²KW⁻¹)	1.11	1.12	1.16	1.16	1.15	1.13	1.10	1.11
$R_c(\dot{q}_2)$ (m²KW⁻¹)	0.44	0.44	0.43	0.43	0.42	0.42	0.43	0.42

The final R_c-values based on $\dot{q}_1$ and $\dot{q}_2$ are obtained 1.114 m²K/W and 0.427 m²K/W respectively. The duration of the measurements has exceeded 72 hours and the R_c-values for $\dot{q}_1$ and $\dot{q}_2$ converge by 1.15% and 0.04% error, respectively, satisfying the first and second termination criteria of ISO 9869 [6]. The R_c- value obtained from the first 10 days deviates less than 5% from the R_c-value obtained of the last 10 days, fulfilling the third condition. The final criterion cannot be investigated though because of the fact that there is no information about the construction to calculate the stored heat. In Fig. 3.8, the variations of cumulative R_c-values obtained from the case study are plotted.

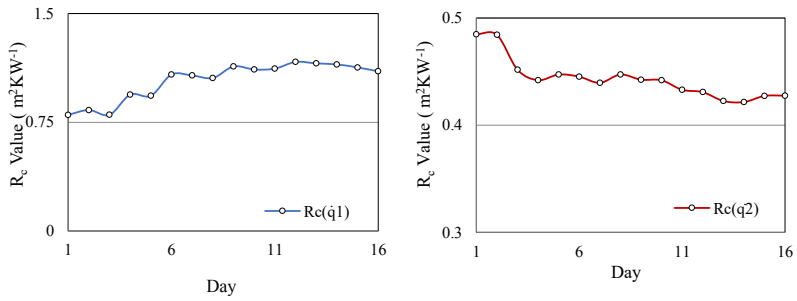

FIG. 3.8 R_c-values obtained by ISO 9869 method using $\dot{q}_1$ (inner side heat flux, left) and $\dot{q}_2$ (outer side heat flux, right), case study

After 10 days, the data starts converging to a certain value. It is very well known that by having a longer period of measurement, the two different R_c-values will converge to a common number. In Fig. 3.9, the average R_c-value is shown as a function of days. It can be seen that similar to chapter 2, the convergence occurs earlier in comparison with the previous graphs in Fig.3.8.

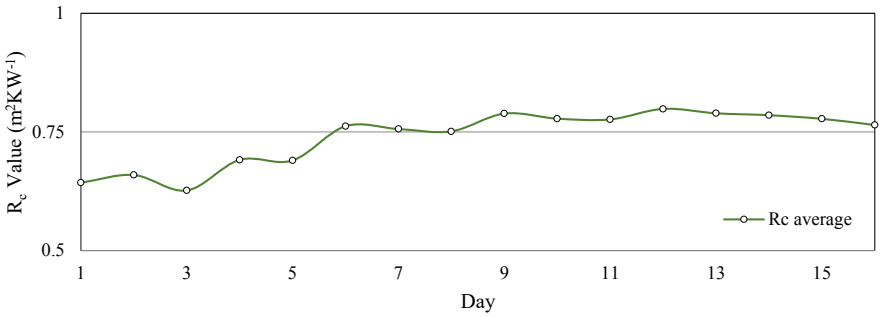

FIG. 3.9 The average R_c-value by ISO 9869 method between $R_c(\dot{q}_1)$ and $R_c(\dot{q}_2)$, case study

As mentioned before, the R_c-value (taken as the final average of two cumulative R_c-values) for the case study with ISO 9869 method can be obtained as following:

$$R_c = \left(R_c(\dot{q}_1) + R_c(\dot{q}_2)\right)/2 \cong 0.77 \ \left(\mathrm{m^2KW^{-1}}\right) \tag{3.14}$$

An R_c-value of 0.78 m^2KW^{-1} by EPM and 0.77 m^2KW^{-1} by ISO 9869 with an error of +1.2% shows a good agreement between the two methods. Note that using the ISO 9869 method based solely on one side's heat flux would have led to around 44.5% miscalculation in the R_c-value even though the required conditions had already been met.

3.5.3 Summary of the Results for the 3 case studies

The results of the three experiments are summarized in this section. For the three case studies with different conditions, EPM and the method based on ISO 9869 were applied. The results are summarized in Table 3.3. For the case study in which the construction of the wall was known (Dutch brick wall), the measured R_c-values are compared to the calculated R_c-value (k =1.2 $Wm^{-1}K^{-1}$ [103] and L=0.21 m).

TOC

TABLE 3.3 Comparison between the Rc-values by ISO 9869 and by EPM for three case studies

Case	Location	Duration ISO 9869	R_c by ISO 9869	R_c by EPM (Duration 1.5 h)	Predicted Rc (Calculation)	Departure
1	Delft	16 Days	0.77 m^2KW^{-1}	0.78 m^2KW^{-1}	-	+1.2%
2	The Hague	14 Days	0.173 m^2KW^{-1}	0.172 m^2KW^{-1}	0.175 m^2KW^{-1}	-0.6%
3	Delft	14 Days	1.57 m^2KW^{-1}	1.60 m^2KW^{-1}	-	+2.0%

As illustrated in Table 3, the results of EPM show a good agreement with the ones obtained by applying the method based on ISO 9869 [6]. Furthermore, by using an additional heat flux sensor it was possible to shorten the measurement period of ISO 9869 [6] method and increase its accuracy because the convergence of the final R_c-value occurs earlier in case of using the average R_c-value.

In Table 3.4, the results of the R_c-values by EPM are compared to the ones predicted by ISSO [80, 82] (in the framework of Dutch energy labeling) for unknown constructions. According to ISSO 82.1 [82] and ISSO 82.3 [80], the R_c-value is assumed based on construction period which is the same in all three cases (before 1965). Accordingly, the R_c-value for all three cases is supposedly equal to 0.19 m^2KW^{-1}.

TABLE 3.4 Comparison between the R_c-values by ISSO 82.1 (Dutch energy labelling method) and by EPM for three case studies

Case Study	Location	Construction year	R_c by ISSO 82.1	R_c by EPM	Departure
1	Delft	1964	0.19 m^2KW^{-1}	0.78 m^2KW^{-1}	-76%
2	The Hague	1933	0.19 m^2KW^{-1}	0.17 m^2KW^{-1}	+10%
3	Delft	1680	0.19 m^2KW^{-1}	1.60 m^2KW^{-1}	-88%

As shown in Table 3.4, the estimation of the R_c-value by ISSO 82.3 [80] can result in a considerable error. The ISSO estimations are compared to the ones obtained by EPM since EPM already showed a good agreement with the method based on ISO 9869 standard. Taking convective heat transfer coefficients of 7.6 $Wm^{-2}K^{-1}$ and 25 $Wm^{-2}K^{-1}$ for indoor and outdoor respectively in accordance with ISSO [103] and ISO 9869 [6] , the U-values for three cases by ISSO and by EPM are calculated in Table 3.5.

TABLE 3.5 Comparison between the U-values by ISSO 82.1 and by EPM for three case studies

Case Study	Energy Label	U-value by ISSO 82.1	U-value by EPM	Departure
1	E	2.76 $Wm^{-2}K^{-1}$	1.05 $Wm^{-2}K^{-1}$	+163%
2	F	2.76 $Wm^{-2}K^{-1}$	2.92 $Wm^{-2}K^{-1}$	-6%
3	F	2.76 $Wm^{-2}K^{-1}$	0.56 $Wm^{-2}K^{-1}$	+393%

As shown in Table 3.5, by using ISSO [80, 82] (Dutch energy labeling method), the U-values of the unknown walls can be extremely overestimated. This also might explain the overestimation of gas consumption in old dwellings with poor energy labels and unknown construction reported in [5]. However, three case studies are far from enough to prove so.

3.5.4 Error Analysis

For error analysis, the accuracy of EPM has been investigated here by incorporating the measurement aparatus uncertainties. The inaccuracy of the heat flux sensors (accordding to the producer's documents) has a positive corrolation with the temperature and heat flux magnitude. Accordingly, the maximum error is expected to occur in the case study with highest temperature and heat flux levels (The Hague). To estimate the total accuracy of the R_c-value measured by EPM, the fractional error analysis followed by quadrature error analysis approach [104] (heat flux divided by temperature and then the summation of RFs to obtain the Rc-value) is performed. For each parameter, the inaccuracy of the respective sensor is applied and finally the total error is calculated. The maximum relative error to occur (in the Hague) by the measurement equipment has been less than 6%. Since in the levels of temperatures and heat fluxes in two other case studies are lower in comparison with the aforementioned one, it can be concluded that the level of instrumental error in EPM in the three tests has been less than 6%. Note that this level of accuracy is so far only valid for the tested walls. For a more reliable accuracy analysis, more tests are needed, provided that the samples are within the application range of the method. For instance, a ventilated cavity wall will result in a high inaccuracy since it is outside the application range of this method (Chapter 5). The accuracy of R_c-value estimation through EPM is also dependent on test conditions and experimental circumstances (See Chapters 4 and 5). Note that the uncertainty of the estimation of the R_c-value by the standard method ISO 9869, as explained in the document, is between 14 to 28%.

3.6 Conclusion

3.6.1 Conclusions

A new in-situ R_c-value measurement technique was investigated and tested in three case studies. In one hour and a half of on-site measurements, it was possible to measure the R_c-value with an accuracy comparable to the one by weeks of ISO 9869 measurements. A difference of less than 2% was found in comparison between EPM and the method based on ISO 9869. Moreover, for one of the case studies EPM showed also a very good agreement with the calculated R_c-value of the wall. While there is still place for improvements, according to the first results, the concept of this method already shows to be working accurately enough to rely on. By comparison between the assumed R_c-values tabulated in ISSO 82.3 (the Dutch energy labeling method) and the ones measured, it was shown that the estimation of R_c-value in unknown constructions, based on construction period, can be very poor. Along the same line, from the comparison between the U-values obtained by EPM and the ones estimated by ISSO 82.1 [82] energy labeling method, up to 393% overestimation was found. Hence, in case of unknown constructions-which occurs quite often for inspection of old dwellings- it is recommended to apply EPM instead of referring to the construction period. Additionally, It was shown that in some cases with lack of information about the thermo-physical properties and the construction of the wall, the criteria of ISO 9869 can be fulfilled while the obtained R_c-value is substantially incorrect. It was also shown that it is possible to improve the method of ISO 9869 in terms of accuracy and time by using two heat flow meters instead of one and by averaging the two sets of results.

3.6.2 Recommendations for Future Studies

Further investigations on walls with different constructions should be carried out to test the validity of the EPM especially for the walls strongly inhomogeneous in the direction of the heat flux or for the two-dimensional heat transfer. It is also recommended to test further the reproducibility of the results through different seasons and conditions. Furthermore, it is highly recommended to design an advanced automatic-controlled prototype for the EPM. Currently, because the main emphasis was laid on the feasibility of the concept of this method, the experiments

were carried out manually (by hand). Along the same line, it would be beneficial to improve the cooling system by replacing the ice packs with a small adjustable cooling unit. A high quality automatic-controlled set up can strongly reduce the errors and ease the application for further measurements.

4 Experimental Aspects of the New Method, EPM

The concept of EPM was proven to be worth pursuing. Thus, in this chapter, a prototype is built for EPM to carry out further measurements on site. The triangular pulse's properties such as the relation between its magnitude and its time interval on its corresponding response are investigated. It is shown how changes in time interval can make the method sensitive to the number of residuals and affect its reliability. General constraints and validity domain of the method are studied. In addition, the effect of 3D heat transfer on the performance of the method is further illustrated in light and heavy constructions. It is shown in which cases it is possible to apply the method in-situ and measure the thermal resistance within a couple of hours.

This chapter is based on the following publication:

Rasooli, A., & Itard, L. (2019, May). Properties of the triangular excitation pulse and the 3D heat transfer effects in the excitation pulse method. In *E3S Web of Conferences* (Vol. 111, p. 04018). EDP Sciences.

4.1 Introduction

The high levels of energy consumption in buildings as a result of heating demand requests special attention as it consequently gives also a huge potential for energy saving [55]. Accordingly, many studies have been dedicated to finding out the most important parameters influencing buildings' thermal behavior and their energy demand [2-4]. Amongst various building components, exterior walls are responsible for a considerable rate of heat loss. Consequently, determination of their thermal

properties through theoretical [19, 10, 72], in-lab [66, 67], and in-situ [6-8, 22, 58, 61, 105] methods have been given much devotion. In 2016, a transient in-situ method, Excitation Pulse Method (EPM) [64], based on the theory of Response Factors (RFs) was developed and tested on three case studies [79] as a proof of principle. The method has shown to potentially aid in a reliable rapid measurement of walls' thermal resistance (R_c-value), within a couple of hours. As a potential was observed in the performance of the method, the research was continued to further test and validate it to elevate its performance for further measurements. In this chapter, new details regarding the application of the method are presented. A prototype is built and shown to further test the method in more samples in-situ and in the lab.

4.2 EPM and the theory of RFs

EPM is based on the theory of RFs. The same excitation pulse (linear heating followed by linear cooling and keeping the surface temperature at the initial level) as described in the theory of the method [106] is applied to the surface of the wall using a heater and a cooling unit. The two heat flux responses at two sides are measured via heat flux meters and the surface temperatures are measured via high accuracy thermocouples and controlled accordingly. The exterior surface of the wall is protected via a reflective semi-insulating cover to minimize the effects of outdoor heat flux disturbances on the measurement of the heat fluxes.

The RF theory is based on Laplace transform and therefore superposition is allowed. In order to overcome the noise in the temperature and the heat flux, the pulse is applied at a magnitude much higher than 1 K (as the RF theory prescribes). This way, the disturbances from heat flux and temperature become negligible. The consequent heat flux responses $\dot{q}$ at sides 1 (excitation side) and 2 (opposite side) are therefore, divided by the magnitude of the pulse to obtain the RFs (X_i at side 1 and Y_i at side 2). From the calculated RFs, the walls' main thermo-physical characteristics such as the R_c-value can be obtained based on both [64], or either of the surfaces as shown in (4.1):

$$R_c = \left(\sum_{i=0}^{n} X_i \right)^{-1} = \left(\sum_{i=0}^{n} Y_i \right)^{-1} \tag{4.1}$$

TOC

For a light wall, as it is usually possible to obtain the Y factors easily, the use of both sides' RFs is beneficial as it results in a quicker obtaining of the R_c-value [64]. For the heavily-constructed (high thermal mass) and highly insulated (high R_c-value) walls, as it is usually difficult to observe a significant rise in the exterior heat flux, it is better to use (4.1) only for the *X* RFs. As for some constructions it may take several hours for the *X* RFs to reach the end of the time-series *X* (time axis), it is possible to measure few of RFs and as use the constant ratio [107], to estimate the rest based on the ratio and the last measured RF.

4.3 Building the Prototype

As the method has shown to require a certain level of preciseness for the execution and the control [64], it is not appropriate to perform it manually. Consequently, a prototype is built to apply the triangular excitation pulse and control the desired surface temperature profile. While previously the variable heat flow was adjusted by moving the radiative heater, the prototype executes this step by continuous adjustment of heat flux through variable power, via a dimmer. Following the linear heating, linear cooling consists of four stages (Fig. 4.1):

1. Dimming down the heating
2. Heat removal via natural convection (no fan)
3. Heat removal via forced convection (fan)
4. Heat removal via forced convection (fan and coil)

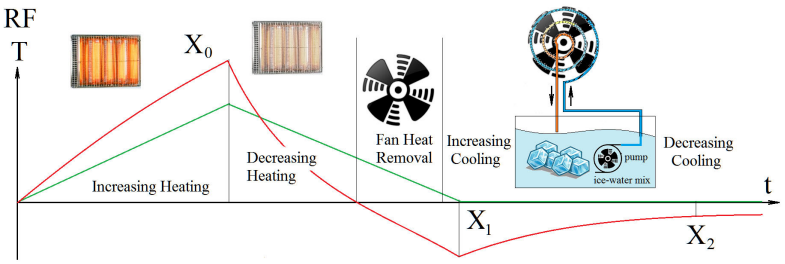

FIG. 4.1 Heating and cooling stages in EPM: The triangular pulse is generated using a heater and a cooling system.

TOC

In the prototype, a fan, cooling water, and ice bricks are integrated into one cooling system. The fan has been equipped with a spiral tube in which cool water is circulated by a pump. Ice bricks are placed in the water container to keep the temperature at 0 C. The fan applies a forced convection to the wall over the tube, decreasing the air flow temperature significantly. In Fig. 4.2, the schematic view of the system (on the right) and its actual photos (on the left) are shown.

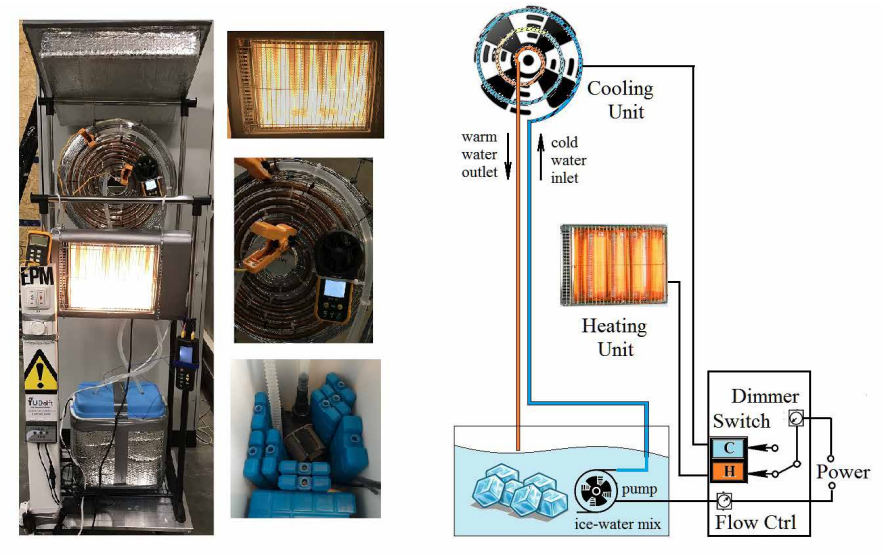

FIG. 4.2 Schematic view (right) and the actual photo (left) of the EPM prototype and its components

The prototype has been used and tested to carry out more measurements in a lab. The results of these experiments and their post processing are presented in chapter 5.

4.4 Heat Transfer Simulations and Results

Simulations of heat transfer based on finite element method have been carried out in COMSOL Multiphysics 5.3a [51] to study various possibilities for performing measurements. The simulations have been made in such a way that they represent actual experiments (inspired by experience and measured data) as much as possible.

TOC

Boundary conditions include surface temperature of 293 K) for indoor side and 288 K for outdoor side of the wall. The initial condition is an average temperature of 285.5 K for the solid domain. The indoor surface of the wall is given a pulse of δ K above the indoor surface temperature, after it has reached a quasi-steady state (as it is supposed to be during the experiment). The heat fluxes at indoor and outdoor sides are computed at the center and the opposite side of the heated area (where in the real measurements the heat flux sensors and thermocouples are mounted).

4.4.1 Time Interval vs Pulse Magnitude

As the feasibility of EPM includes a non-destructive approach, it is of great importance to prevent damage to the finishing of the indoor wall (e.g. wallpapers). Accordingly, if the surface is sensitive to the heat and high temperature, it is required to apply a pulse of a lower magnitude. To ensure that the heat imposed to the wall is of enough quantity, the base of the triangle should increase when the height decreases. This way, equal amounts of heat can be applied to the surface. In Table 4.1 and Fig 4.3, the results of three experiment simulations of a 0.2 m brick wall are presented. Three pulse magnitudes of 80 K, 40 K, and 20 K are combined with time intervals of 20 min, 40 min, and 80 min respectively. The X_0, being the first RF, derived from the peak of the heat flux decreases as the time interval becomes larger. R_c^{th} is the theoretical R_c-value, based on construction, R_c^{EPM} is the R_c-value resulted from an EPM simulation and calculated by (4.1).

TABLE 4.1 Combination of time intervals and pulse magnitudes modelled for a brick wall and the resulted Rc-value

t [min]	δ [K]	X_0 [Wm^{-2}K^{-1}]	R_c^{EPM} [m^{2}KW^{-1}]	R_c^{th} [m^{2}KW^{-1}]
20	80	26	0.24	0.24
40	40	19	0.25	0.24
80	20	13	0.25	0.24

The results of RFs generated by the various time intervals and pulse magnitudes are presented in Fig. 4.3.

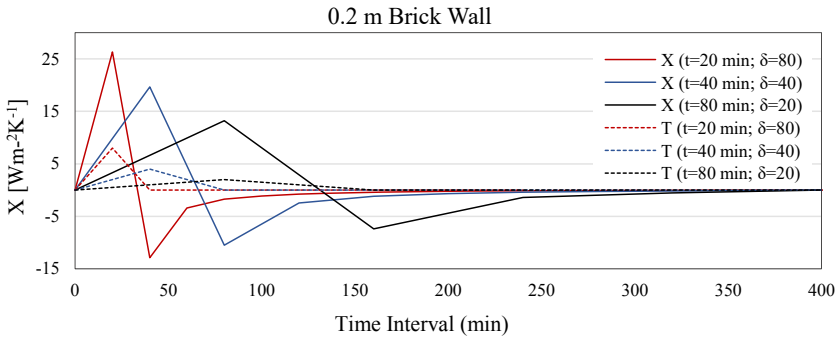

FIG. 4.3 Combination of various pulse magnitudes and time intervals in 0.2 m brick wall

As seen in Fig. 4.3, different time intervals can be combined and applied with different pulse magnitudes. The selectivity of different combinations allows higher flexibility and therefore higher efficiency in measuring components of various sizes and constructions. For instance, in a heavy construction, in order to ensure sufficient heat penetration, a larger magnitude with a longer time interval can be used. Note that in these cases, the heated area should be as large as possible and the measurement takes place at the center of the heated area.

4.4.2 Time Interval vs Number of RFs

As observed in Fig. 4.3, the number of RFs also changes as the time interval varies. The total time required for the wall to absorb and conduct the heat from the excitation pulse determines *N*. The total time is a function of thermal response time [108] which depends on the construction. The required number of RFs (defined as the minimum number of RFs needed in (4.1) to find an accurate R_c-value) increases as the time interval of the RFs becomes shorter. The required number of the RFs with an index greater than 3, as well as the dependence of the R_c-value to these RFs increases consequently. In Fig. 4.4, the results of the post processing of a simulation of a brick wall (*thermal conductivity* 0.9 $Wm^{-1}K^{-1}$, density 2000 kgm^{-3} and specific heat capacity 840 $Jkg^{-1}K^{-1}$) are shown. The dashed curves show how the minimum required number of RFs ($N_{required}$) decreases in different thicknesses as a longer time interval is chosen. Note that in EPM, not all the RFs are needed to be measured since using both sides, shortens the measurement time significantly. Additionally, RFs with indices higher than 3 can be estimated rather than measured when (4.1) is used.

TOC

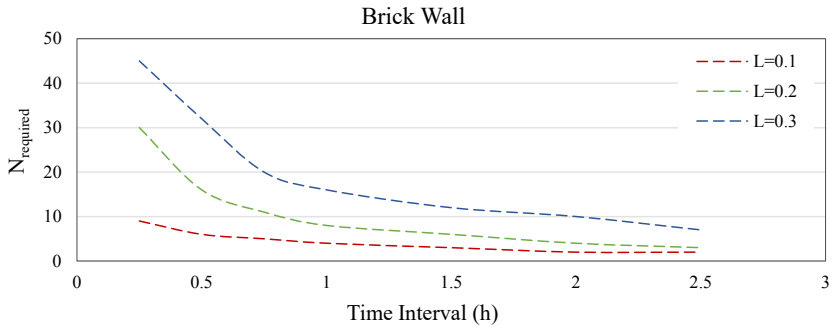

FIG. 4.4 Minimum required number of RFs vs time interval for a brick wall in different thicknesses L

The necessity of having a minimum number of RFs is based on the fact that if a lower number is used, the R_c-value is not accurate. This happens due to the fact that in such case, the *X* curve does not reach zero if *N* is smaller than the minimum required number of RFs. In Fig. 4.5, the R_c-value is calculated via (4.1), with the required number of RFs ($N_{required}$) in black dashed line, being accurate enough and therefore in-line with the actual R_c-value (dotted red line). The same procedure is repeated also for only 4 RFs ($N_{required}$ for the time interval of 2 h), resulting in a higher difference (solid black line) when a shorter time interval is chosen. The blue dashed-dotted line shows the error in finding the R_c-value from (4.1) if only 4 RFs (*N* for the time interval of 2 h) are used.

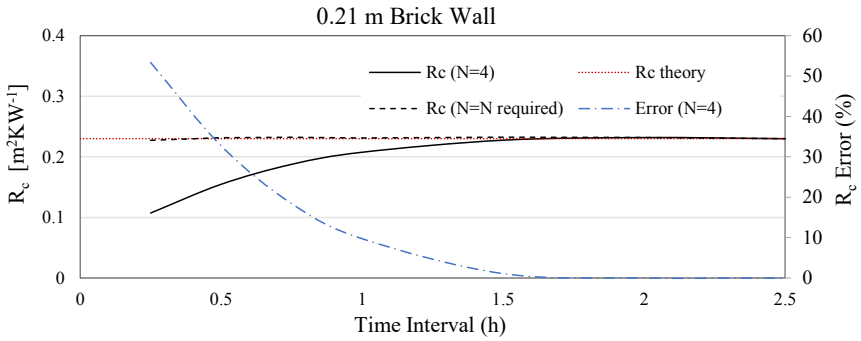

FIG. 4.5 Sensitivity of the R_c-value to the number of RFs in a 21 cm brick wall

TOC

4.4.3 Dealing with 3D Heat Transfer Effects

Since the heat pulse is applied only to a certain area of the wall, depending on the size of the heater, the risk of three-dimensional heat transfer exists. Especially, due to the fact that the temperature gradient between the heated domain and the non-heated domain is high, chances are that the heat flux in the directions of width ($\dot{q}_x$) and height ($\dot{q}_z$) of the wall become considerable and even comparable to the one in the direction of the thickness ($\dot{q}_y$). This issue is negligible in thin walls and becomes more important in thick walls. The heat transfer in any direction has the following rate:

$$\dot{q}_{x,y,z} = \left(\frac{1}{R_{x,y,z}} \right) \Delta T_{x,y,z} \tag{4.2}$$

Two parameters, the first one being the thermal resistance *R* and the second one being the temperature gradient contribute at the same time to the 3D heat transfer effects and in this case in the measurements carried out using EPM.

On the one hand, the whole body of the wall can be considered as a system (Fig. 4.6) of resistors (and capacitors) which can be divided into separate parts in lateral directions. The middle part (where the heating is applied in y direction) can be modelled as a control volume with same resistances (R_y) in all directions, bounded by much larger resistances in height (R_z) and width (R_x) direction.

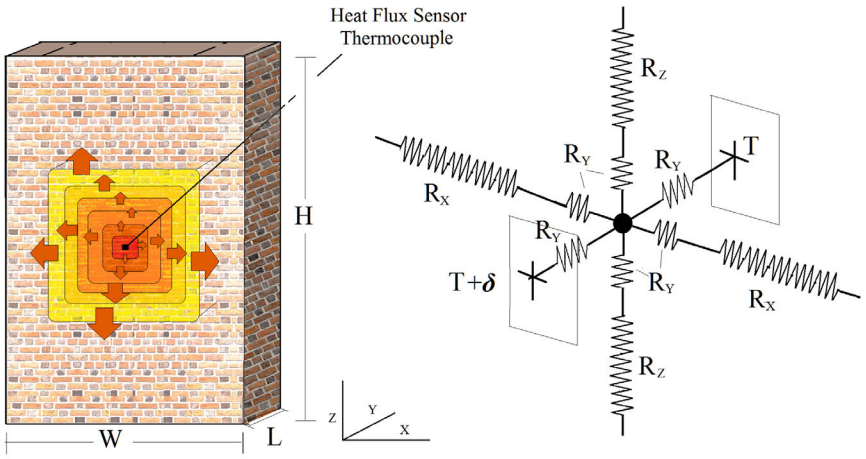

FIG. 4.6 The 3D heat transfer effect due to the resistance network: the wall modelled as a network of resistances

The resistances in different directions can be calculated as follows:

$$\begin{cases} R_y = \int_0^{\frac{L}{2}} k dy = \dfrac{L}{2k} \\ R_y = \int_0^{\frac{W-L}{2}} k dx = \dfrac{W-L}{2k} \\ R_y = \int_0^{\frac{H-L}{2}} k dz = \dfrac{H-L}{2k} \end{cases} \quad ; \quad H, W \gg L \tag{4.3}$$

Where R is the thermal resistance, and x, y, and z are space coordinates, and k is thermal conductivity. Since in a wall the height H and the width W of a wall are much larger than its thickness L, R_x and R_z are considerably greater than R_y. As the height and width directions include these additional large resistances, in normal conditions and constant temperature gradient ΔT in the whole domain, the heat $\dot{q}$ in the center line direction (y axis) has a higher tendency to flow towards the smaller resistance (R_y) and not towards the much larger lateral ones (R_y+R_z and R_y+R_x):

$$\begin{cases} \dfrac{\Delta T}{R_x} \ll \dfrac{\Delta T}{R_y} \rightarrow \dot{q}_x \ll \dot{q}_y \\ \dfrac{\Delta T}{R_z} \ll \dfrac{\Delta T}{R_y} \rightarrow \dot{q}_z \ll \dot{q}_y \end{cases} \tag{4.4}$$

TOC

Consequently, this matter becomes more important as the thickness L and consequently the resistance R_y increase. On the other hand, the temperature gradient is the driving force. When a large area is heated, the heat in the center has lower tendency to flow towards lateral directions because the lateral neighbor domains are also heated and therefore have a closer temperature (T^1_{High}) to the center (T_{High}). Accordingly, as the distance from the center is decreased, the heat will have a higher tendency to flow towards the depth direction, rather than the lateral directions. In Fig. 4.7, this concept is depicted.

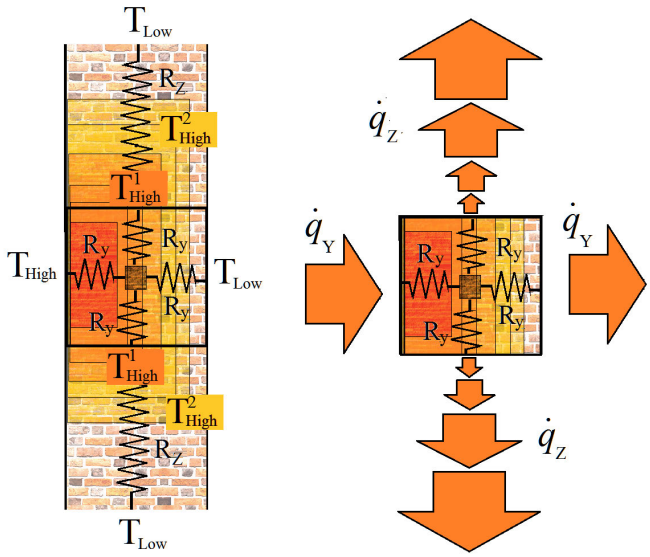

FIG. 4.7 3D heat transfer effect due to the temperature gradient

The heat flows in different directions can be estimated as follows:

$$\begin{cases} T^1_{High} < T^2_{High} \ll T_{Low} \\ \dot{q}_y = \dfrac{T_{High} - T_{Low}}{R_y} \\ \dot{q}_x = \dfrac{T^1_{High} - T^2_{High}}{R_x} \rightarrow \dot{q}_x \ll \dot{q}_y \\ \dot{q}_z = \dfrac{T^1_{High} - T^2_{High}}{R_z} \rightarrow \dot{q}_z \ll \dot{q}_y \end{cases} \tag{4.5}$$

TOC

T is the temperature of each domain. $T1_{High}$ is greater than $T2_{High}$ and the difference becomes greater as the distance from the central line increases. Accordingly, again in (4.5), $\dot{q}_x$ and $\dot{q}_z$ are much larger than $\dot{q}_y$. This aspect is directly affected by the area where the heat is applied and therefore, requires considerations.

In Fig. 4.8, a 0.3m concrete wall is modelled. EPM is applied to this wall at the center in a diameter of 1.2 m and the R_c-value can be obtained using (4.1). The heat flow in y direction (towards the thickness) in shown in solid black. The heat flows in z direction (towards the height) are shown in dashed lines. These values are much lower as the distance to the center line decreases.

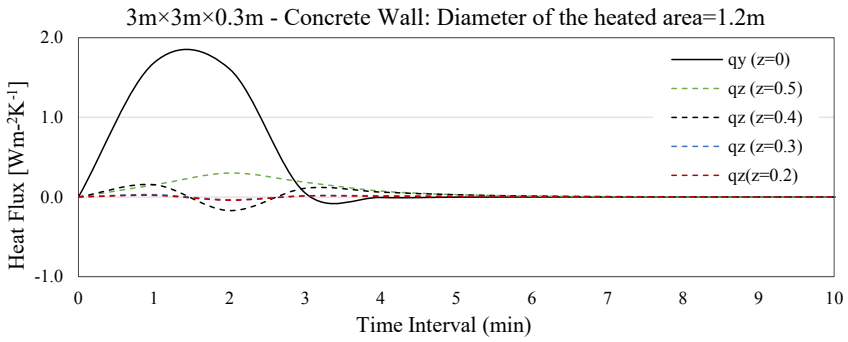

FIG. 4.8 Heat flux in z direction (dashed) in different distances from the y axis passing the center of the heated area in EPM and the heat flux in y direction (in solid black) at the same axis

Accordingly, in EPM it is always recommended to apply the pulse to an as large as possible area and measure the parameters only in the center of this area. This becomes more important when dealing with heavier walls. In Fig. 4.9, a concrete wall of height H=3 m and width W=3 m is modelled in different thicknesses of L= 0.1 m, 0.21 m, 0.35 m, and 0.5 m. The diameter of the heated area is varied by different ratios of the width.

TOC

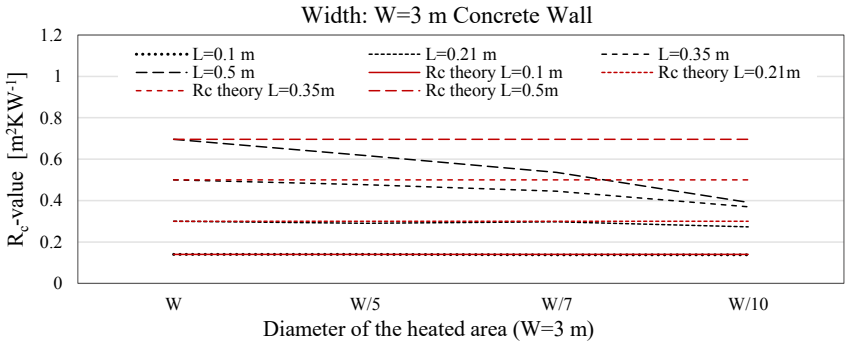

FIG. 4.9 Relation between the diameter of the heated area in EPM and the accuracy of the R_c-value measurement through EPM in different thicknesses of a 3×3 m² concrete wall

In addition to what was discussed so far, as long as the duration of the test is shorter than the thermal response time in lateral directions, the heat will flow towards the thickness direction before flowing in lateral layers and the measurement ends before the 3D heat transfer starts to affect it.

4.5 Conclusion

Further details of a rapid in-situ transient method, EPM, were introduced to apply it in large scale and a variety of constructions. The new control system has shown a more user-friendly application and the new cooling system has shown to be promising. Further experiments by this prototype are shown in Chapter 5. The RFs' time interval is investigated to show the possibility of combining various time intervals with different pulse magnitudes, allowing further flexibility and higher efficiency. As the number of RFs greater than 3 decreases with a higher time interval, the longer time interval is a better alternative as the residuals are difficult to record due to their small values. Additionally, the number of RFs shows to play an important role in the sensitivity of the results to the number of RFs. As demonstrated during the comparison of various pulse magnitudes and time intervals, it is concluded that for heavy constructions, a combination of largest possible signal and the longest possible time interval is better to be used. The analysis of the three-dimensional heat transfer effects showed a low tendency of the heat to transfer in lateral directions in light homogeneous walls. The effect of 3D heat transfer is generally rather

TOC

limited except in very heavy constructions, resulting in a general advice regarding the size of the heated area. For heavy homogeneous walls, it is recommended to heat an as large as possible area and measure the parameters in the center of this area in order to minimize the lateral heat transfer risk. In the light homogeneous constructions however, this is not the case. More research will be done in the future, regarding the application and performance of the method, especially in multi-layered constructions.

TOC

5 Advancement and Further Expansion of the EPM

As the new developed method EPM showed a success in the proof of principle, the prototype designed and built in the previous chapter is used in this chapter to make more measurements and pursuit further validation. The measurement of the Y response factors are difficult in practice and therefore, more focus is laid on X response factors. Many aspects of the response factors theory are translated into actual circumstances in EPM. Further experimental and theoretical aspects of the method, leading to the accuracy of the R_c-value determination are demonstrated. It is also shown how this method can be used to find thermal conductivity and volumetric capacity of homogeneous layers.

This chapter is published under the following:

Rasooli, A., & Itard, L. (2019). In-situ rapid determination of walls' thermal conductivity, volumetric heat capacity, and thermal resistance, using response factors. *Applied Energy*, *253*, 113539.

5.1 Introduction

Within the framework of the European Energy Performance of Building Directive (EPBD) [1], the lack of accurate input data regarding actual thermal performance of construction walls is considered as a bottle neck in the mandatory determination of buildings' energy performance. In addition to being the basis of policies and decisions regarding energy efficiency measures and energy saving targets [109], forecasting the buildings' energy performance is necessary for sizing of the HVAC

facilities [110]. Along the same line, accurate estimation of the critical thermo-physical characteristics of buildings' façades as a result of the urge for energy audits [9] and energy performance checks is essential. To improve the thermal performance of the buildings, the building envelopes' thermal characteristics have been the first to be targeted [111]. The existing assumed values of these characteristics, such as walls' thermal resistance (R_c-value) have shown to be of the most critical parameters [2] contributing to the large deviations between actual and theoretical energy consumption [5]. Underestimation of the R_c-value has shown to result in around 400% overestimation in wall's thermal transmittance [64], leading to a high overestimation of the buildings' energy consumption [3]. Due to the absence of accurate and reliable data regarding actual thermo-physical characteristics, till today, the standard in-situ measurement methods [6-8] have been the most reliable option to follow. However, due to long measurement periods on the one hand and the many constraints of the test conditions on the other hand, the required time and effort are seldom feasible in practice and therefore, has become a barrier to their application. Consequently, efforts have been needed to assess the issue by developing and testing alternative measurement methods. Recently, the proof of principle of the Excitation Pulse Method (EPM) was presented, which allows for a relatively quick and accurate in-situ estimation of light walls' thermal resistance [64]. The objective of this chapter is to extend the method towards heavy walls and multi-layer walls, illustrate its accuracy and performance, and to demonstrate the capability of the method in the determination of other thermal properties: thermal conductivity and volumetric heat capacity (VHC). Additionally, the practical application of the theory of Response Factors (RFs) [106] is demonstrated.

5.1.1 State-of-the-art

Several approaches have been set up to estimate building components' thermo-physical characteristics. For walls of well-known construction, the R_c-value can be calculated following ISO 6946 [10]. However, as shown in numerous studies, the actual R_c-values often do not agree with the calculated ones [19] and the ones declared by the manufacturers. Therefore, much emphasis has been laid on performing measurements rather than calculations, to determine a more realistic thermal performance of the building components. For instance, in-lab measurement methods including the famous hot-box method by ISO 8990 [14] guarded hot plate apparatus by ASTM [112] have been applied in many cases [113-115]. Due to the often large variations between the in-situ and in-lab performance of the building components, as a result of in-situ conditions (e.g. moisture content and material aging), various in-situ effects including wind velocity [18], emissivity of the sensors,

and large temperature drifts [17] have been included in the analysis of the test results, showing appreciable improvements.

As the most accurate approach in determination of buildings' actual thermo-physical characteristics, in-situ methods [7, 8, 16, 60, 64, 105, 116] have been given special attention as they measure and assess the realistic actual performance directly on site. Many pieces of research have been carried out during IEA Annex 58 (2011-2015) [49] and IEA Annex 71 (2016-2021) [29] regarding this topic as a result of its significance in the accurate indication of buildings' energy performance.

The non-contact measurement category of in-situ methods relates to IR thermography. This method has been applied by Fokaides and Kalogirou [100] to determine the thermal transmittance and later by Aversa et al. [117] to determine actual dynamic thermal behaviour of building components. Despite the advantage of being relatively simple to use, the quantitative application of this method is based on assumptions which may be far from actual circumstances. For instance, the emissivity of the surface as well as the air is required for an accurate estimation of the surface temperatures. Accordingly, Albatici et al. [118] improved this shortcoming by measuring and including the wind velocity and surface emissivity, showing how this method can be reliable in determination of thermal transmittance in heavy elements. More recently, Lucchi [27] reviewed 150 pieces of literature about this technique, suggesting relevant procedures and tool development for dynamic characterization of building components.

Direct contact, being widely applied, the most important in-situ wall characterization method is the standard heat flow meter method introduced in ISO 9869 [6] and ASTM [7, 8]. The method has been of preference as the international reference and it benefits from a quite straight-forward procedure. However, this method has often shown to rely on very long (up to more than a month) measurement periods [9, 26, 61, 63, 105, 119]. Moreover, low temperature gradients between the two sides of the walls have shown a significantly negative effect on the accuracy of the method. In line with the results of Desogus et al. [23] , Atsonios et al. [16] have shown that the method is not reliable in low temperature gradients. Accordingly, many studies have suggested and developed corrections by means of practical extensions [105] and dynamic data analysis methods to shorten the measurement periods and to overcome the accuracy drawback. Using dynamic data analysis and alternative interpretation methods [116], it has been possible to successfully calculate the thermal resistance [120] and thermal transmittance [121] in shorter periods of time.

Including materials' detailed thermal properties (which are often not required for the long measurements periods) to study the dynamic behaviour [122] of buildings has

resulted in significant improvements [123]. Lately, Petojević et al. [124] introduced a new mathematical framework by which the dynamic thermal characteristics of multi-layered walls (excluding cavity walls) can be determined, using days of heat flux and temperature measurements. In contrast with general findings in literature, Evangelisti et al. [125] found an acceptable agreement between the dynamic thermal behaviour of a homogeneous wall, which was modelled as an equivalent to a multi-layered one of the same thermal performance. Applying finite difference method and experimental data of 50 hours, the properties were found to be representative for the wall of unknown construction. Most recently, Šuklje et al. [126] calibrated a homogeneous equivalent wall model for inverse determination of thermo-physical properties in green façades. Along the same line, the use of other dynamic-theory-based methods such as signal-response methods have been suggested. The idea of using excitation of a system and studying its response is being used widely in the level of the whole buildings [127]. The main methods associated with this technique include the QUB [128] and ISABELE [129] which estimate the global heat lost coefficient of a whole building [130]. Similarly, for the scale of building components (e.g. walls) the RF method has been considered. The RF method, first developed by Mitalas and Stephenson [84] has shown to be a suitable alternative to solving heat equations. The method is solely based on a temperature excitation on a system and its corresponding heat flux response and in many situations is less expensive than the numerical methods, in terms of computation time [131]. Many studies have proposed alternative mathematical methods such as direct numerical integration [132] and state space method [133] for calculation of RFs in multi-layered walls [134] even more efficiently. Apart from walls' heat transfer analysis , the applications of the RF method ranges from the assessment of the thermal performance of capillary radiant floors [135] and earth-to-air heat exchangers [136] to thermal behaviour of food products [137]. The RF method has been experimentally applied in lab conditions on walls in 2008 via a calibrated hot-box by Sala et al. [67] to test a multi-layered heterogeneous wall. The study showed the significant difference in results when the heterogeneous layer of hollow brick is modelled as a homogeneous layer, equivalent to the heterogeneous one. Later in 2010, Martín et al. [66] used the same apparatus to measure and calculate the RFs of walls of low thermal resistance and medium thermal inertia. The R_c-value has been measured once through steady-state regime and once via the RFs through a dynamic regime. The method was compared to the computational model, showing a good agreement. The authors found the method to be a suitable alternative when the properties of the tested wall are unknown.

In-situ determination of thermo-physical properties has so far taken days of in-situ measurements. In the current chapter, a transient in-situ method is demonstrated, by which, at least in many cases (light to medium weighted walls), it is possible to

determine the thermal resistance R_c-value, thermal conductivity, Volumetric Heat Capacity, and an indication of possible construction of an unknown wall, within a few hours, without the many constraints required by the conventional methods.

5.1.2 Excitation Pulse Method, EPM

Aiming for rapid determination of the walls' thermal resistance R_c-value, a rapid transient-based in-situ measurement method, EPM, based on the theory of RFs, was developed and tested on three case studies [64, 79]. Applying the EPM, it was shown that by exposing one surface of a wall to a triangular temperature pulse under certain conditions, it is possible to estimate its thermal resistance in a few hours. In the theory of RFs, the excitation pulse is defined as a unit (1 K) magnitude (triangle's height) and the RFs time interval (half of the triangle's base) is typically one hour. The theory of RFs is based on Laplace transform, and thanks to superposition principle, the theory itself and therefore the EPM benefit similarly from temperature pulses of larger magnitudes. In EPM, the magnitude of the triangular excitation pulse (δ) is way above 1 K, in order to overcome the effect of walls' surface temperature and heat flux noise. The pulse magnitude δ is the difference between the initial value and the peak of the surface temperature at the excitation side.

Working Principles and the Control Circuit

The working principle of EPM is depicted in Fig 5.1. Either manually or automatically, the control of the heating and cooling units is performed to achieve a pre-defined triangular surface temperature profile T_1 as an excitation pulse on the wall. Here, the initial and the final wall's surface temperature are the equivalent of 0 K in the theory. A dimmer constrains and controls the voltage V_0 towards the EPM unit to control the power for heating and cooling heat flux $\dot{q}_1$ in such a way that a measured triangular surface temperature T_1^*, following a desired triangular surface temperature profile T_1 with a height of δ is formed on the excited side (1) of the wall. A peak indoor surface temperature of 80-90°C is generally found suitable for a safe experiment, not damaging the walls' finishing. Right after the peak, the surface heat flux $\dot{q}_1$ is decreased in such a way that the surface temperature profile declines linearly with an opposite slope. At the end of heat exertion ($\dot{q}_1 = 0$), the surface temperature is still above the base of the triangle (initial value), due to the effect of thermal storage. Therefore, at this point, to return to the initial temperature, heat removal takes place after switching the power from the heater to the cooler. The cooling is similarly controlled in such a way that the surface temperature reaches the base of

TOC

the triangle, following the previous slope. At the end of the triangle, the temperature is kept at base to resemble the pulse at a zero level. At the opposite side of the wall, a protective box (60×60 cm^2, polystyrene covered with bubble wrap and reflective coating) is mounted to cover and protect a large area of the wall from the outdoor heat flux and temperature disturbances. Despite the success in reaching the purpose with the current size, the area of the box may be as large as possible. This way, the outdoor surface temperature T_2^* can remain at a constant level and the outdoor heat flux response $\dot{q}_2$ can be observed and measured, similar to the theory of RFs. Due to the outdoor conditions and the small size of outdoor heat flux, the results of outdoor heat flux are seldom analysed for extraction of wall's properties.

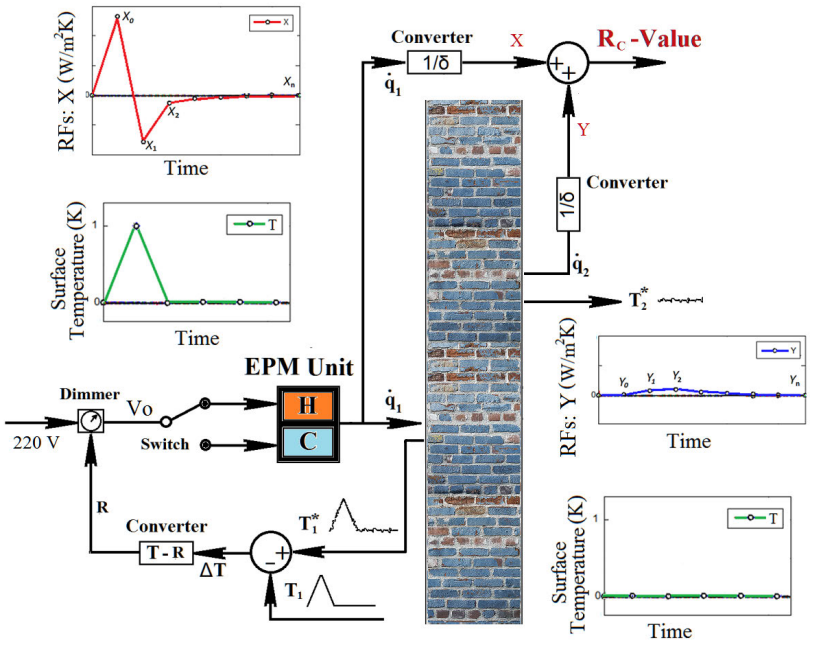

FIG. 5.1 Control system and working principles of EPM: The heat fluxes are controlled (and measured) in such a way that a triangular temperature excitation pulse forms on one side of the wall, while the other side is kept at constant temperature. The RFs are then calculated to be used for estimation of the wall's thermo-physical characteristic.

The whole control process takes place at very short time steps by comparing and minimizing the difference between the measured triangular surface temperature profile T_1^* and the pre-defined triangular temperature profile T_1. T_1^* is controlled via the converter that tunes the electrical resistance R of the dimmer. In the meantime, the surface heat fluxes at the excitation side ($\dot{q}_1$) and at the opposite side ($\dot{q}_2$) are

measured via sets of heat flux meters mounted on the surface of the wall. All controls and conversions can take place manually or by using electronic systems. To obtain the wall's RFs, at every time interval, the heat fluxes are divided by the magnitude of the pulse δ, whose value is obtained from the thermocouple mounted on the excitation side of the wall

$$X_j = \frac{(\dot{q}_1)_j}{\delta} \quad ; \quad Y_j = \frac{(\dot{q}_2)_j}{\delta} \tag{5.1}$$

Where X and Y are the RFs of the wall and j is the index indicating the time interval at which the heat flux must be used in terms of number of RFs (See Fig.5.1). The Rc-value can be then obtained, using RFs of one side of the wall:

$$R_c = 1/\sum_{j=0}^{n} X_j = 1/\sum_{j=0}^{n} Y_j \tag{5.2}$$

, or more quickly, when possible, using the RFs from both sides [64]:

$$R_c = 2 \times \left(\sum_{j=0}^{n} (X_j + Y_j) \right)^{-1} \tag{5.3}$$

In the current study, emphasis is laid solely on using *X* RFs for a variety of reasons. The *Y* RFs appear after the minimum response time (See section 5.3.1), making the experiment longer, resulting in less feasibility. In addition, in heavy constructions and high insulation values, *Y* RFs are unlikely to be observed. The operational and instrumental errors associated with *X* RFs are much lower since the interior side of the wall is generally exposed to fewer sources of heat flux disturbance and therefore is better controlled. Nevertheless, the Y factors can be used for light walls in stable climatic conditions or in labs where the conditions on the outdoor wall can be fully controlled.

Location of the Pulse and the Size of the Heated Area

So far, EPM has been successfully applied to light homogeneous walls [64]. The results of simulations and experiments carried out so far have shown negligible difference between theory, computations, and experiments, in terms of walls' thermal behaviour and determination of the thermal resistance. The location of the pulse has to be as far as possible from the areas potentially disturbing the 1D signal and its response by 3D heat sink effects (e.g. wall area close to a window). An IR thermography camera should be used to check the homogeneity of heat flux (an indication for homogeneous surface temperature). The size of the heated area needs to be as large as possible. The heat fluxes and the temperatures should be measured then in the centre of this area, where the occurrence of heat transfer towards lateral sides is minimum. In case of presence of high insulation, the risk of 3D heat transfer increases. This can also be dealt with, heating an as large as possible surface. Practical details regarding the built prototype, properties of the triangular pulse, and the size of the heated area in relation with their effect on the accuracy of the method are discussed in [138]. It has also been shown how the accuracy of the method in finding the R_c-value increases when larger numbers of RFs or longer time intervals are used.

Although EPM has been demonstrated on 3 samples (walls of relatively light construction) [64], further research has been required to examine the method in more detail regarding its overall reliability and performance in other typologies as well as its further new applications. In the current chapter, the remaining main questions are addressed:

1. With regards to the thermal response time, applying which combinations of signal magnitude and time interval can lead to an accurate determination of the thermal resistance?
2. To what extend can the RFs of a wall help to understand and illustrate its construction and thermal behaviour?
3. To what extent is it possible in EPM to concurrently measure thermo-physical properties other than the R_c-value?

At first, the effect of a wall's response time and the selected signal time interval on the wall's RFs in single-layered and multi-layered walls is studied and specific RF features are illustrated, focusing on clarification of experimental and practical aspects and the potential future benefits of EPM and other RF- measurement methods. Secondly, aiming for more reliable estimations of thermal properties, the method is extended from the determination of the R_c-value to in-situ determination of two main fundamental thermo-physical properties: thermal conductivity and VHC.

Unlike the R_c-value which is used in steady-state assumptions, these two properties are used in combination in dynamic modelling [122] of building components. It is shown to what extent the method at its current stage (manual control and basic equipment) can be used to determine the aforementioned material properties (as well as the wall thickness) for a tested wall.

5.2 Methodology

A combination of software simulations and experiments is used to answer the research questions and to explore boundaries, validity domain, and further application range of the method.

5.2.1 Simulations and Computations

To avoid too long experiments, a large part of the study has been conducted using virtual walls and a virtual triangular pulse excitation, all modelled using COMSOL Multiphysics 5.3a [51]. The models have been computationally tested and validated using different approaches:

1. A single layer wall is modelled in COMSOL Multiphysics 5.3a: A wall of which one surface is exposed to a triangular temperature pulse of 1 K height, while its other side is kept at reference temperature (0 K),is modelled. The heat fluxes at two sides are computed, representing the RFs.
2. These RFs are compared to the RFs from the theory [106] (calculated in MATLAB [52]) as a function of wall's thermal properties and same time interval, showing excellent agreement.
3. The models for multi-layered walls were first validated by using identical layers and comparing them with an equivalent homogeneous wall of same material which is already validated in 1 and 2.
4. The magnitude of the signal is increased and using realistic boundary conditions, the results are compared to the original model with 1 K magnitude, confirming the superposition rule with perfect agreement.

Other boundary conditions include lateral insulation. The initial condition of all solid domains is the reference temperature, 0 K.

To maintain high accuracy, the “finer” mesh setting has been used for all simulations. The time stepping is chosen according to the mesh size. In multi-layered walls, the effect of thermal contact between layers has been tested beforehand. Due to the size of the constructions, for this method, imperfect thermal contact has shown no difference with perfect contact and therefore has been used in order to shorten the computation time.

5.2.2 Experiments

For the experiments, two heat flux sensors (HukseFlux HFP01 [78]) for outdoor surface and EKO MF-180 [139] for indoor surface) and two high-accuracy (0.5 °C) T-type thermocouples, all pre-calibrated, have been used. The reason for using two different heat flux sensors is that the one for outside surface captures very small noise and the other for inside can handle high operational temperature. The two heat flux sensors have been calibrated and tested beforehand and had assured to give identical results. During the experiments, each thermocouple has been installed next a heat flux sensor, on both sides of the wall (Following the sensor installation guidelines of ISO 9869 [6]). Data have been logged using an OMEGA OM-SQ2010 high accuracy data logger. Before execution, IR thermography has been carried out using a FLIR E5 [140] IR camera to inspect and avoid possible discrepancies in surface temperature and heat flux. This check is necessary also after covering the sensors with a cover of same thermal emissivity as the wall’s surface, to assure the same radiative heat transfer on the sensor and the surrounding surface. In Fig 5.2, from left to right, the outdoor sensors (under the protective box), the IR image of the outdoor sensor, the schematic of the wall (Table 5.1) and the measurement equipment, and the indoor sensors are shown.

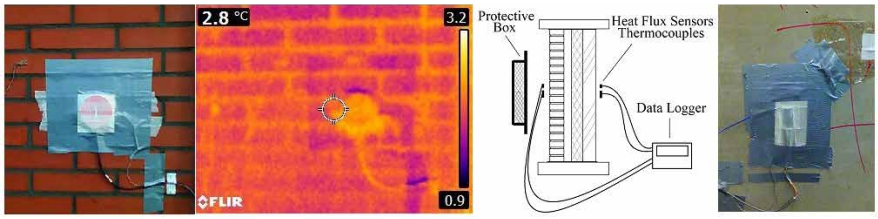

FIG. 5.2 From left to right: outdoor sensors and their IR image (under the protective box), the schematic of the equipment and the wall, indoor sensors, Dec 2018, Leuven, Belgium

TOC

Measurements have been carried out using a prototype on a wall in a test-building laboratory in KU Leuven, Belgium. The following tests have been carried out to further study and validate the method:

- Comparison between the in-situ measured heat flux and the one computed in a theoretical model
- Comparison between measured *X* RFs and time intervals for four different pulses
- Comparison between the results of two similar tests (precision)
- Comparison between the experimentally determined values for k and ρc in different pulses (precision)
- Comparison between the theoretical values k and ρc and the ones experimentally determined (accuracy)

In Table 5.1, the construction properties of the tested wall (from outside to inside) are tabulated in detail as presented in [20]. ρ is density, c is specific heat capacity, k is thermal conductivity, L is thickness, and $\tau_r|_{1\%}$ is the minimum response time (See section 3.2). The results of the tests are shown in Fig 5.5 and are used in the analyses carried out in sections 5.3 and 5.4:

TABLE 5.1 Thermal properties of the tested wall

Layer/property	L (m)	k [Wm^{-1}K^{-1}]	ρ [kgm^{-3}]	c [J kg^{-1}K^{-1}]	$\tau_r\|_{1\%}$ [min]
Facing brick	0.10	0.900	2087	870	34.3
Air cavity	0.04	-	-	-	-
Polyurethane	0.10	0.021	35	1320	37.5
Wood-cement board	0.09	0.350	1250	1470	72.5

5.2.3 Experimental Validation of the Models

To validate the experimental models, the tested cavity wall (Table 5.1) has been modelled in COMSOL Multiphysics 3a [51]. The lateral sides are insulated and the entire surface is excited with a temperature pulse. The model is fed with the experimental temperature pulse data (Fig 5.3, left), taken from the in-situ measurements from Test 4. The heat flux is then computed at the location of the heat flux sensors and compared to the ones measured on site (Fig 5.3, right).

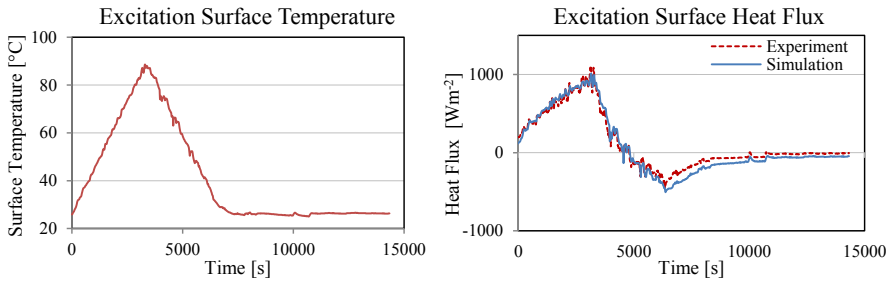

FIG. 5.3 Comparison between heat flux profiles (right) from the measurement (dashed red) and simulation (solid blue) from the surface temperature excitation pulse (left) being applied in the experiment and fed to the COMSOL model

As seen from the agreement of the two heat flux profiles, the simulation model is in good agreement with the experiment. The differences between the profiles can be minimized by decreasing the mesh size, at the expense of long computational time.

In section 5.3, the influence of the thermal response time on the required signal's time interval and its corresponding RFs is studied for single-layered and double-layered constructions. Experiments show the possibility of carrying out measurements using triangular pulses of different time intervals and magnitudes. In addition to the determination of the minimum thermal response time, the ratios of the *X* RFs have shown to give an indication of presence of different layers in a multi-layered wall.

In section 5.4, the results of the experiments have been used in an inverse modelling problem to determine the two main thermo-physical properties of a wall: thermal conductivity and VHC, as well as the thickness of a homogeneous slab.

5.3 RF Time Interval and the Walls' Thermal Response Time

5.3.1 EPM: RF Time Interval and Pulse Magnitude

To limit the required measurement time, the choice of the signal's time interval is critical for EPM. An appropriate time interval should be chosen before starting the measurements. The sufficiency of heat penetration through the wall depends on two aspects: time and heat flux. Accordingly, in practice, to ensure sufficient heat penetration (to observe the Y factors), to minimize the 3D heat transfer effects, and to overcome the surface heat flux noise, two different approaches can be followed: By exerting the excitation pulse on a large area, with a large magnitude δ (grey curves in Fig 5.4) and/or by choosing a long time interval. The quantity of heat q transferred to the wall during the pulse is equal to the area under the curve of heat flux-time.

$$q = \int_0^t \dot{q}(t)\,dt = \int_0^t \delta \;\; X(t)\,dt \tag{5.4}$$

As shown in Fig 5.4, for a light wall, by selecting a longer time interval (in light blue), in comparison to a shorter one (in orange) of the same pulse magnitude, a larger quantity of heat can be transferred to the wall. This has the same effect as imposing a larger magnitude with the short time interval (in dark red), resulting in a greater heat flux:

$$q = \int_A^C \dot{q}_{AB'C}(t)\,dt = S_{AB'C} = \int_A^E \dot{q}_{ADE}(t)\,dt = S_{ADE} \tag{5.5}$$

For a medium-weight wall, a larger time interval in combination with a large pulse magnitude (dark blue) can support sufficient heat penetration through the body of the element.

$$\int_A^E \dot{q}_{AD'E}(t)dt > \int_A^C \dot{q}_{AB'C}(t)dt > \int_A^C \dot{q}_{ABC}(t)dt \tag{5.6}$$

Finally, for heavy constructions, longest possible time intervals (longer than 1 hour) and largest pulse magnitudes (90–100°C) are to be used (in black).

$$\int_A^E \dot{q}_{AD''E}(t)dt \gg \int_A^C \dot{q}_{ABC}(t)dt \tag{5.7}$$

Applying such a large excitation pulse on a large area can increase the chance of observation of *Y* RFs, minimizing the risk of 3D heat transfer effects on 1D heat transfer of the pulse.

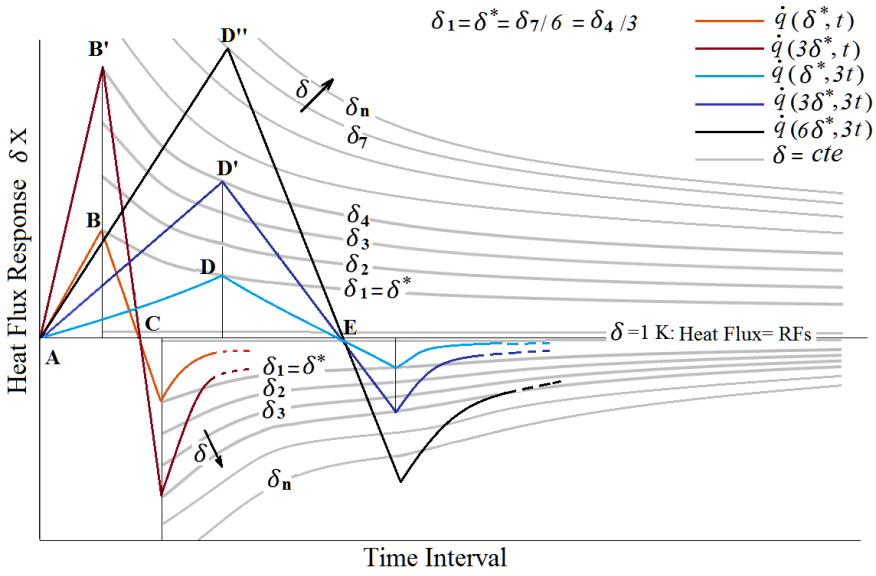

FIG. 5.4 Representation of excitation pulse magnitudes, time intervals and heat flux responses

The constant δ grey lines represent the variations of X_0 and X_1 when t is increased.

TOC

In Fig 5.5, the results of the measurements are presented. The red dotted curves are surface temperature pulse (above the initial and final surface temperature) at the excitation side and the dashed blue curves are the corresponding RFs (derived from the heat flux measurements and the pulse magnitude). It is shown how different combinations of δ the pulse magnitude, and t, the time interval, can be applied in EPM. Note that tests 1 and 3 are very similar in terms of the two aforementioned parameters. In section 5.4 it is shown how these two tests lead to the same results. Tests 2 and 4 are the shortest and longest experiments respectively.

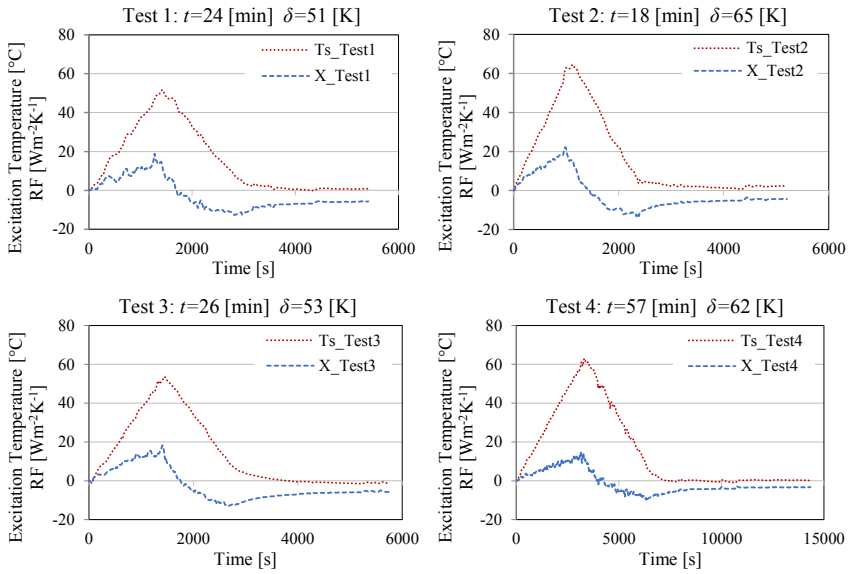

FIG. 5.5 Surface temperature (dotted red) and RFs (dashed blue) measurements in four experiments used in the analyses

By choosing a longer time interval, lower amplitude of heat flux is needed to take the surface temperature to 1 K. Accordingly, the RFs become naturally smaller. In Fig 5.6, a concrete wall, exposed to an excitation pulse of 1 K is simulated. As seen from the curves, the X factors decrease as the time interval of the signal increases.

TOC

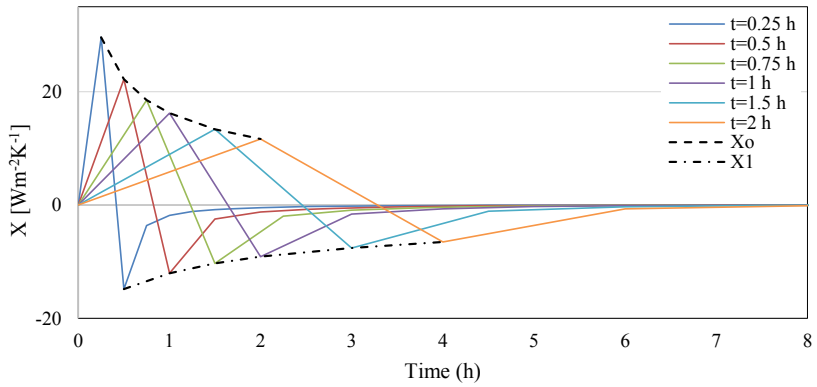

FIG. 5.6 Relation between different time intervals and RFs (X_0 in black dotted and X_1 in black dotted-dashed), data obtained from MATLAB computation of RF equations

Similarly, the relation between the time interval and the magnitude of the excitation pulse and the corresponding RFs has been studied in the experiments. The experimental results of the RFs are shown in Fig 5.7, where the black dashed and dotted-dashed lines present the X_0 and X_1 values. The *X* RFs become smaller as a larger time interval is applied.

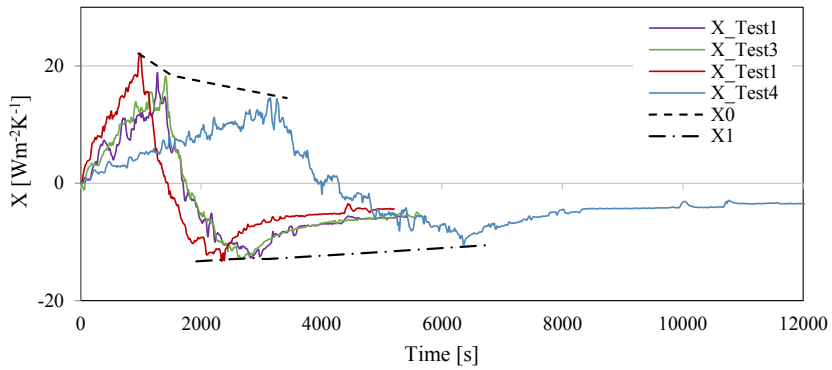

FIG. 5.7 Relation between different time intervals and RFs (X_0 in black dotted and X_1 in black dotted-dashed), data obtained from the experiments, Dec 2018, Leuven, Belgium

Using a larger time interval has shown to be advantageous in practice, as it leads to easier control of the triangular temperature profile. Since in this case the RFs are smaller, it is important to combine a longer time interval with large pulse magnitudes

TOC

to ensure the distinction between the heat flux and temperature noise and the pulse and its response.

5.3.2 Wall's Thermal Response Time

The correct understanding of a wall's thermal behaviour, when submitted to a triangular excitation pulse, is achieved by the analysis of the thermal response time. The response time of a system is defined as the time required for the output to reach a certain percentage of the input, when the input is increased with a step function. For a homogeneous wall, considering the input as heat flux at excitation side, and the output being the heat flux at the other side, the thermal response time can be obtained by solving Fourier's heat equation. Accordingly, the response time of such wall of thickness L and thermal diffusivity a can be obtained as follows [108]:

$$\tau_r\big|_{1-\lambda} = \frac{4}{a\pi^2} L^2 \ln\frac{4}{\lambda\pi} \tag{5.8}$$

λ is the reduction factor to determine for output heat flux $\dot{q}_2$ to reach $(1-\lambda)\dot{q}_1$ during its response time $\tau_r\big|_{1-\lambda}$, when $\dot{q}_1$ is increased by one step. In Fig 5.8, the response times of a brick wall (k=0.9 Wm^{-1}K^{-1}, ρc=1.36E7) of different thicknesses L are shown. At $\lambda = 0.37$ the response time $\tau_r\big|_{63\%}$ is called "time constant", a well-known concept used when analogizing the thermal systems with electrical systems.

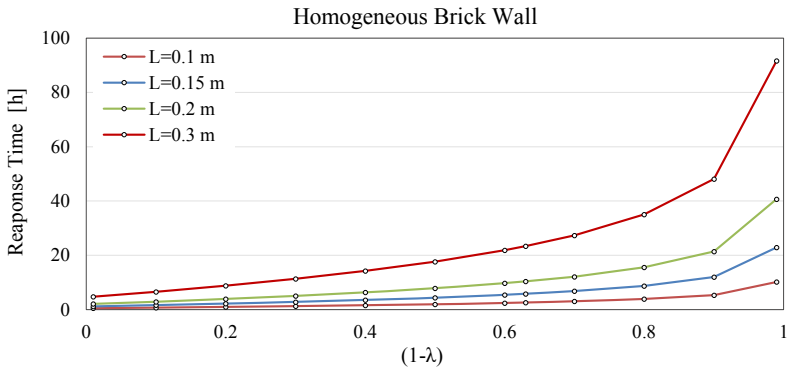

FIG. 5.8 Computation results: thermal response times of a homogeneous brick wall in different thicknesses (time constant is found at $(1-\lambda)=0.63$).

During a measurement using EPM and any other pulse-response-based method, it is highly important that the effect of the excitation side heat pulse reaches the other side. The minimum response time $\tau_r|_{1\%}$ (the required time for output heat flux at the other side- to reach at least 1% of the input heat flux) happening at $\lambda = 0.99$ is critical to be covered by the time interval during the experiment. The minimum thermal response time $\tau_r|_{1\%}$ in a wall exposed to EPM is equal to the time required for the Y curve to rise from zero to positive values. This can be found during an experiment, provided that an adequate amount of heat is transferred to the surface of the wall (See Section 5.3.1). In many cases it is of necessity or at least beneficial to choose the time interval based on minimum thermal response time in order to avoid repetition of the experiment. The minimum response time can always be observed from the rise of the *Y* RF curve. Alternatively, it can be simply measured in a test in advance, by applying any form of excitation heat pulse at one side and log the time duration taking the other side of the wall to show a heat flux response. Furthermore, the minimum response time can be found by studying the ratio of the *X* RFs of high indices (See Section 5.3.5).

5.3.3 Response Time and RFs' Time Interval: Single-Layered Homogeneous Walls

The effect of the excitation temperature pulse being applied to the first side of a wall needs at least a period of $\tau_r|_{1\%}$ to reach the second surface. When the second surface is reached, its heat flux increases (*Y* appears), acting as a heat flux pulse on this side. Similarly, this signal needs a period of $\tau_r|_{1\%}$ to reach back to the excitation side. If the time duration of the excitation signal is shorter than $2\tau_r|_{1\%}$, the effect of the second surface may not be transferred back to the results of heat flux response at the excitation side. For instance, consider a case where a time interval (time needed for appearance of X_0, the first RF) shorter than $2\tau_r|_{1\%}$ is used. At the time when X_0 is reached, the heat pulse effect is in the same location inside the wall, regardless of its thickness. Consequently, using such time interval will lead to identical X_0 values for the considered wall and a similar wall of much higher thickness. This implies that for very thick walls or the ones of high thermal mass (long response time), unless a very long time interval is used, X_0 does not depend on and therefore do not represent the thickness. In Table 5.2, the X_0 factors have been computed for different thicknesses and time intervals corresponding to the following conditions:

$$t<\tau_r|_{1\%}:\begin{cases}X_0\neq f(L)\\ Y_o=0\end{cases};\qquad t<2\tau_r|_{1\%}:\begin{cases}X_0\neq f(L)\\ Y_o\geq 0\end{cases};\qquad t\geq 2\tau_r|_{1\%}:\begin{cases}X_0=f(L)\\ Y_o>0\end{cases}\tag{5.9}$$

TABLE 5.2 X_0 computed with the simulation model, for a brick wall (k= 0.9 Wm^{-1}K^{-1}, ρc=136 E5 Jm^{-3}K^{-1}) of different thicknesses (and different response times) using different time intervals

	RF time interval [s]	t=10	t=600	t=1800	t=3600	t=180000
Wall Thickness [m]	$\tau_r\|_{1\%}$ [s]	$X_{0t=10s}$	$X_{0t=600s}$	$X_{0t=1800s}$	$X_{0t=3600s}$	$X_{0t=180000s}$
0.01	18	**438.0**	99.3	93.1	91.5	90.0
0.05	457	**438.0**	**56.6**	33.3	25.7	18.0
0.1	1827	**438.0**	**56.6**	**32.7**	**23.1**	9.3
0.2	7310	**438.0**	**56.6**	**32.7**	**23.1**	5.1
0.5	45687	**438.0**	**56.6**	**32.7**	**23.1**	**3.3**
0.8	116961	**438.0**	**56.6**	**32.7**	**23.1**	**3.2**
1 >	>182751	**438.0**	**56.6**	**32.7**	**23.1**	**3.2**

As seen in Table 5.2, as long as the selected time interval is shorter than $2\tau_r|_{1\%}$, the X_0 in walls of different thicknesses will be identical. Note that in all given conditions (except for $t=10s$ which is extremely short), it may still be possible to successfully extract the R_c-value from the RFs, provided that at some point in the rest of the RFs with higher index, $2\tau_r|_{1\%}$ has been passed in time, changing the rest of the RFs. This, in heavy walls may demand for a very long experiment time. Similarly, the aforementioned interpretation is valid for the RFs of higher index: If $2\tau_r|_{1\%}$ is not reached during the appearance of any X RF (of higher index), that X RF and the ones before (smaller indices) are also identical for walls of any higher thickness:

$$(j+1)t<2\tau_r|_{1\%}:\begin{cases}X_j\neq f(L)\\ Y_o\geq 0\end{cases};\qquad (j+1)t\geq 2\tau_r|_{1\%}:\begin{cases}X_j=f(L)\\ Y_o>0\end{cases}\tag{5.10}$$

This implies that when using a short time interval and measuring a limited number of RFs, the RF curves of walls of different thicknesses can be identical and therefore, the accuracy of R_c-value determination can become extremely poor as the RFs do not include enough information about the thickness of the tested wall.

Note that in theory, unlike in practice, numerous RFs can be used. Accordingly, the R_c-value can be derived from the RF curve of any given wall, using any arbitrary time interval, because the effect of the thickness, even in a short time interval, will

always appear in the RFs of much higher index. More explanations about this notion is found in Section 5.3.5. For short time intervals, the number of wall's needed RFs increases significantly. Therefore the accuracy of R_c-value determination drops, if fewer number of RFs are used in (5.2) [138]. This becomes problematic in practice because the experimental error associated with such approach can be higher than the necessary level of accuracy, when (5.2) is used. Therefore, it is of high importance to confirm the coverage of $2\tau_r\big|_{1\%}$ in the *X* RFs, either by observing a rise in *Y* RFs during the test, measuring the response time before the test, or by monitoring the ratio between two consecutive *X* RFs (See Section 5.3.5).

5.3.4 Response Time and RFs' Time Interval: Multi-Layered Walls

Heterogeneous multi-layered walls are common in buildings. The behaviour of RFs in terms of energy conservation is the same as for homogeneous walls: The overall heat applied to one side is stored and conducted to the other side. The magnitude of RFs and their profiles though are diverse. In this section, the behaviour of common two-layered walls is studied. The same principles are valid for walls of more than two layers. The instantaneous heat fluxes at two sides A and C, and at the contact surface B of a two-layered wall of layers (1) and (2), excited by a triangular surface temperature pulse at side A can be calculated based on the temperature history and the time series RFs (*X*, *Y*, and *Z*) as follows [106]:

$$\begin{cases} \dot{q}_A^t = [T_A^t \cdots T_A^{(t-n)}] \begin{bmatrix} X_0 \\ \vdots \\ X_n \end{bmatrix}_{(1)} - [T_B^t \cdots T_B^{(t-n)}] \begin{bmatrix} Y_0 \\ \vdots \\ Y_n \end{bmatrix}_{(1)} \\ \dot{q}_B^t = [T_A^t \cdots T_A^{(t-n)}] \begin{bmatrix} Y_0 \\ \vdots \\ Y_n \end{bmatrix}_{(1)} - [T_B^t \cdots T_B^{(t-n)}] \begin{bmatrix} X_0 \\ \vdots \\ X_n \end{bmatrix}_{(1)} = [T_B^t \cdots T_B^{(t-n)}] \begin{bmatrix} X_0 \\ \vdots \\ X_n \end{bmatrix}_{(2)} - [T_C^t \cdots T_C^{(t-n)}] \begin{bmatrix} Y_0 \\ \vdots \\ Y_n \end{bmatrix}_{(2)} \\ \dot{q}_C^t = [T_B^t \cdots T_B^{(t-n)}] \begin{bmatrix} Y_0 \\ \vdots \\ Y_n \end{bmatrix}_{(2)} - [T_C^t \cdots T_C^{(t-n)}] \begin{bmatrix} X_0 \\ \vdots \\ X_n \end{bmatrix}_{(2)} \end{cases} \tag{5.11}$$

Combining the second and the third equations with the first and the forth, a global form of equations can be derived:

$$\dot{q}_A^t = \left\{ X_{(1)} - \frac{Y_{(1)}^2}{Z_{(1)} + X_{(2)}} \right\} \left[T_A^t \ \cdots \ T_A^{t-n} \right] - \left\{ \frac{Y_{(1)} Y_{(2)}}{Z_{(1)} + X_{(2)}} \right\} \left[T_C^t \ \cdots \ T_C^{t-n} \right] = [U][T_A] - [V][T_C] \quad (5.12)$$

$$\dot{q}_C^t = \left\{ \frac{Y_{(1)} Y_{(2)}}{Z_{(1)} + X_{(2)}} \right\} \left[T_A^t \ \cdots \ T_A^{t-n} \right] - \left\{ Z_{(2)} - \frac{Y_{(2)}^2}{Z_{(1)} + X_{(2)}} \right\} \left[T_C^t \ \cdots \ T_C^{t-n} \right] = [V][T_A] - [W][T_C] \quad (5.13)$$

Where U, V, and W are the time-series RFs of a two-layered wall. The RFs in brackets are subjected to element-wise operations. In Fig 5.9, a COMSOL RF simulation of a two-layered wall with properties introduced in Table 5.3 is shown.

TABLE 5.3 Construction and properties of the two-layered wall used for simulation of RFs in multi-layered walls

Layer/property	L (m)	k [Wm^{-1}K^{-1}]	ρ [kgm^{-3}]	c [J kg^{-1}K^{-1}]	$\tau_r\|_{1\%}$ [min]	R_c [m^{2}KW^{-1}]
1: Concrete	0.1	0.7	1600	880	34	0.14
2: Polyurethane	0.05	0.02	35	1320	9	2.38

Note that this construction is shown for demonstration purposes. In practical conditions, the insulation layer is coated with plaster and finishing, whose effect is always included in the RFs of the wall, due to its short response time. The excitation pulse is applied once individually at each slab as a single-layer and then at the two-layered wall: once at side 1 (concrete, left) and once at side 2 (Polyurethane, right). The global $\tau_r\big|_{1\%}$ and the R_c-value are 43 min and 2.52 m^{2}KW^{-1} respectively.

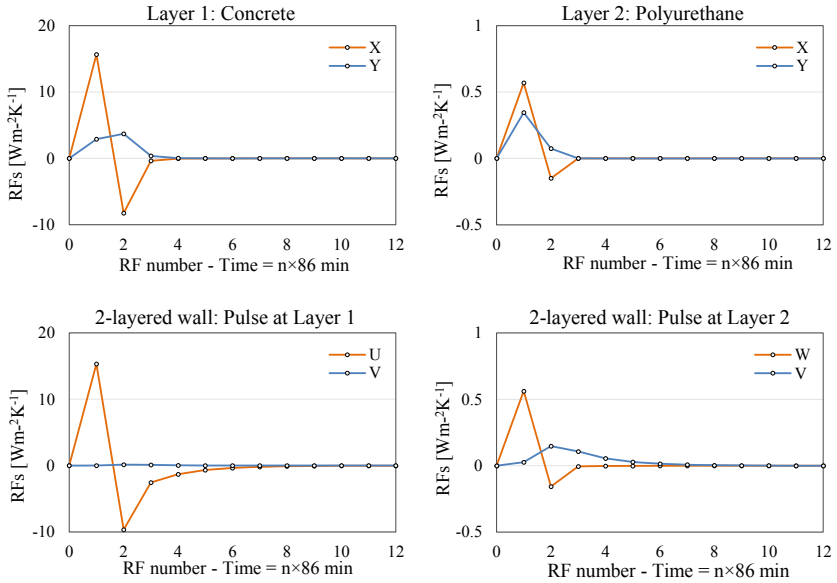

FIG. 5.9 RFs (dots) from two different layers of the 2-layered wall individually (top) and of the composed wall (bottom). The RFs of the composed wall are a combination of the two layers

The relationship between $\tau_r|_{1\%}$, t, and RFs as discussed in Section 5.3.3 can be extended to multi-layered walls. The pulse and the behaviour of its corresponding response are tied to the thermal response time of different layers. Consider the second surface of the first layer as the first surface of the second layer. The heat pulse will reach the second layer after a period of $\left(\tau_r|_{1\%}\right)_{(1)}$, the response time of the first layer. Therefore, similar to the outdoor surface for the homogeneous wall, the X curve can be affected by the second layer, only after $2\left(\tau_r|_{1\%}\right)_{(1)}$ is passed during the appearance of *X* RFs. Accordingly, the X curve of a multi-layered wall is partially/globally influenced by each layer and its opposite surface, depending on the response time $\tau_r|_{1\%}$ of each layer. Nevertheless, according to energy conservation, the extraction of the Rc- value from the RFs is independent from the aforementioned influence and can theoretically (with infinite number of RFs) take place, unless using a too short time interval where the error in the residuals are known to disturb the accuracy. In Table 5.4, the results of a simulation are shown in which a two-layered wall (polyurethane and concrete) is excited with pulses of different time intervals. Consider $\left(\tau_r|_{1\%}\right)_{(1)}$ and $\left(\tau_r|_{1\%}\right)_{(2)}$ the minimum response times of layers 1 and 2 respectively and $\tau_r|_{1\%}$ the total response time of the wall (the sum of the two response times).

TOC

TABLE 5.4 RFs corresponding to different conditions of time interval: The X_0 RFs represent both layers, only when the selected time interval is longer than twice the minimum response time of the first layer

	Pulse at Polyurethane Side			Pulse at Concrete Side		
	$(\tau_r\|_{1\%})_1 = 9$ [min] $(\tau_r\|_{1\%})_2 = 34$ [min] X_0 [Wm^{-2}K^{-1}]			$(\tau_r\|_{1\%})_1 = 34$ [min] $(\tau_r\|_{1\%})_2 = 9$ [min] X_0 [Wm^{-2}K^{-1}]		
Condition/Parameter	t [min]	X_0	$X_{0_{(1)}}$	t [min]	X_0	$X_{0_{(1)}}$
$t < (\tau_r\|_{1\%})_{(1)}$	2 5 7	2.0 2.1 1.9	2.0 2.1 1.9	5 10 25	63.5 45.0 28.2	64.0 45.0 28.5
$t = 2(\tau_r\|_{1\%})_{(1)}$	18	1	1.1	70	17.1	17.3
$2(\tau_r\|_{1\%})_{(1)} < t < \tau_r\|_{1\%}$	30	0.8	0.9	NAN	NAN	NAN
$t \approx 2\tau_r\|_{1\%}$	86	0.56	0.6	86	15.3	15.6
$t > 2\tau_r\|_{1\%}$	200 300 400 600 1000	0.46 0.44 0.43 0.42 0.41	0.51 0.47 0.46 0.44 0.43	200 300 400 600 1000	9.5 7.2 5.7 4.0 2.6	11.0 9.6 8.9 8.3 7.7

As seen in Table 5.4 and Fig 5.10, the X_0 RFs of the first layer and the whole wall are identical in short time intervals. The RFs are representative for the whole wall (The sum of the RFs is equal to the R_c-value of the whole wall and not the first layer or a part of the wall), when the time interval is longer than twice the total response time. This difference is larger when the pulse is applied at the concrete side, due to the fact that the insulation layer has a much higher influence on the heat transfer phenomenon in comparison with the concrete layer. As shown in Fig 5.10, the X_0 values for the whole wall and for the first layer deviate when a time interval longer than twice the response time (red dot) is applied.

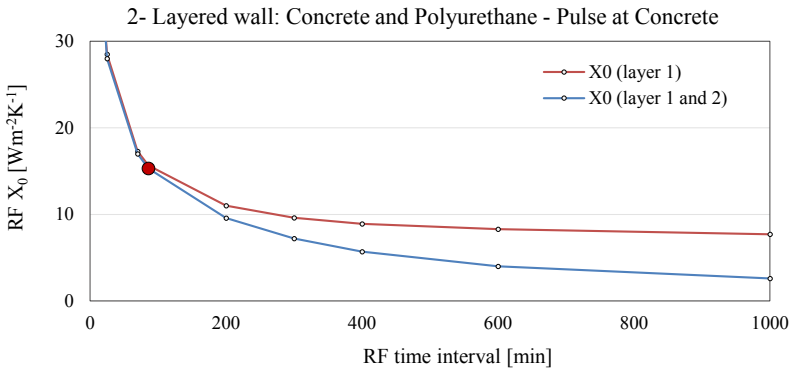

FIG. 5.10 Relationship between X_0 RF and the RF time interval for a double-layered (concrete and polyurethane) wall where the excitation pulse is applied to concrete side.

The aforementioned argument for X_0 is also valid for RFs with higher index. An *X* RF with any index is influenced by the second layer/opposite surface, only when the sum of time intervals (total time duration) before the appearance of that *X* RF, is longer than twice the minimum response time of the layer (s) ahead/ the whole wall.

Accordingly, in Fig 5.10, long before the red dot (when a time interval much shorter than $2\ \tau_r|_{1\%}$ is chosen), it may be that many more of the RFs are not representative for the whole wall, but only representative for the first layer. In this case, if a limited number of RFs are measured and used, the determination of the R_c-value will be associated with inaccuracy. This becomes more problematic when the front layer is non-insulated and the latter layer is an insulation layer, having a much larger influence than the first layer on the total thermal resistance while being excluded from the results. In such case, the inaccuracy level will be much higher than the case where the front layer is an insulation layer.

An accurate R_c-value can be obtained in such cases, only if at some point in the remaining RFs, the effect of the outdoor surface has appeared. This can be confirmed by observation of the rise in *Y* RFs during the test, measuring the $\tau_r|_{1\%}$ in advance, or by monitoring the ratio between two consecutive *X* RFs for a sufficiently long period of time (See Section 5.3.5).

TOC

5.3.5 High-Indexed RFs in Single-Layered and Multi-Layered Walls

In order to spare time in EPM, the *X* RFs with higher index ($n >> 2$) were not measured, but estimated. The fact that the higher indices form a series in the X graph, and that these RFs are based on the same equation, implies that the RFs with higher index be estimated based on the ones measured. This ratio, also called the common ratio, becomes constant after a certain index [141]. For a homogeneous slab the ratio of the two RFs is:

$$j \gg 2;\ \gamma_i = \exp\left(-\frac{i^2\pi^2 at}{L^2}\right);\qquad \frac{X_{j+1}}{X_j} = \frac{\sum_{i=1}^{\infty}[\left(\gamma_i^{j+2} - 2\gamma_i^{j+1} + \gamma_i^{j}\right)/\, i^2]}{\sum_{i=1}^{\infty}[\left(\gamma_i^{j+1} - 2\gamma_i^{j} + \gamma_i^{j-1}\right)/\, i^2]} = D = cte \tag{5.14}$$

Where a is thermal diffusivity, L is the thickness, t is the time interval, and j (the superscripts are powers) is the index of RFs [106]. Accordingly, knowing a limited number of *X* RFs, the rest can be calculated, provided that the ratio between the known RFs is constant. As this ratio is also found in the literature to have a relationship with properties such as thermal diffusivity, it can be used to determine them in case of interest. As discussed in Section 5.3.2, for estimation of the R_c-value in a homogeneous wall, the important condition is that the effect of the exterior surface is included in the results. In addition to what was discussed, the effect can be found through the ratio between every two RFs with an index higher than 2.
In a homogeneous wall, one can know if the results represent the whole sample, when the ratio X_{j+1} / X_j becomes constant. In Fig 5.11, a standard 21 cm brick wall (k=0.9 $Wm^{-1}K^{-1}$, ρc=136E5 $Jm^{-3}K^{-1}$) is shown. The wall is excited with pulses of different time intervals, resulting in different stabilizing points. The RFs of longer time interval reach a constant ratio of D at an earlier index, resulting in an R_c-value representative for the whole wall. For a very short time interval (5 min in dashed blue), the ratio is not yet constant, after 12 RFs. In this case, the R_c-value is smaller, representing only a part of the wall and therefore is inaccurate. In contrast, in the longer time intervals (solid lines), the ratio is constant and the accurate R_c-value has been extracted successfully. It is seen in all graphs that only after twice the response time (4 h) the ratio becomes constant, implying that the effect of the outdoor surface is included in the RFs. Note that in any time interval, the ratio becomes constant at a certain point (RF index m in equation 5.15). Considering the fact that the RFs reach a constant ratio at index m (large dots in Fig 5.11) of their time-series, R_c-value is achieved from the sum of RFs as follows:

$$R_c^{-1} = \sum_{j=0}^{n} X_j = \sum_{j=0}^{m} X_j + \sum_{j=m+1}^{n} X_j = \sum_{j=0}^{m} X_j + \sum_{i=0}^{n-m-1} D^i X_{m+1} = \sum_{j=0}^{m} X_j + X_{m+1}(1-D^n)(1-D)^{-1} \tag{5.15}$$

As the sum of the infinite geometric series converges to a limited value, for a large number of RFs, the sum of the RFs converges to the following value:

$$n \to \infty \ : \quad R_c^{-1} = \sum_{j=0}^{\infty} X_j = \sum_{j=0}^{m} X_j + X_{m+1}\left(1 - D\right)^{-1} \tag{5.16}$$

This implies that in theory, when it is possible to use large number of RFs, the sum of the RFs can be used to calculate the R_c-value, regardless of the time interval used.

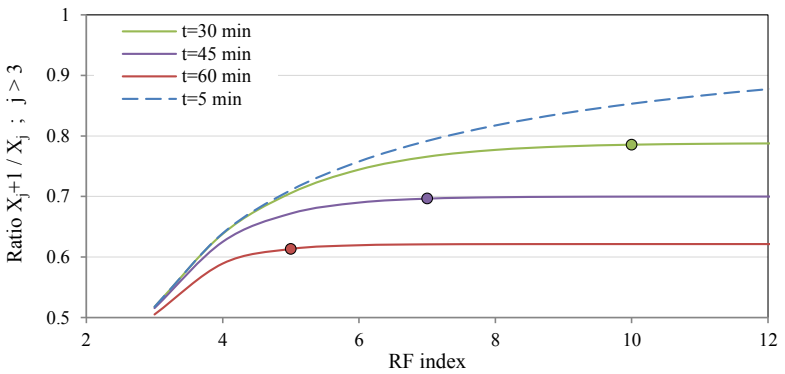

FIG. 5.11 The ratio between two consecutive RFs: In long time intervals where the R_c-value is calculated successfully, the slope becomes zero as the ratio is constant. The RFs are then representing the whole wall.

Similar to the single-layered walls, the effect of different layers and the exterior surface in a multi-layered wall are conditionally included in the ratio between measured RFs. This phenomenon takes place when the experiment time is longer than at least twice of the total thermal response time. The constant ratio found after $2\ \tau_r|_{1\%}$ (can be found from the rise in *Y* RFs) can be taken as the one to calculate the remaining RFs. In case the Y RFs are not observed, it is likely that the constant ratio changes to another constant value. This means that the effect of the later layer(s) is included in the *X* RFs. The effect of each layer is included in the *X* RFs, just after twice the response time before reaching that layer is passed. In Fig 5.12, this is shown by making a comparison between the X ratios in a 2, 3, 4, and a 6 – layered wall. For all four walls, the ratio is constant until the 10th RF. After the 10th, the effect of the fourth, fifth, and the sixth layers can be seen by the sudden change in the slope. This happens due to the fact that twice the total minimum response time of the layers before the 4th layer is covered at the point by which the mentioned RF ($j = 10$) has

TOC

appeared. The constant ratio moves then towards another constant, showing that the effect of later layers is included in the results. Note that such constructions (6 layers: three layers of brick-insulation) are only for demonstration of RFs and may be non-existent in practice.

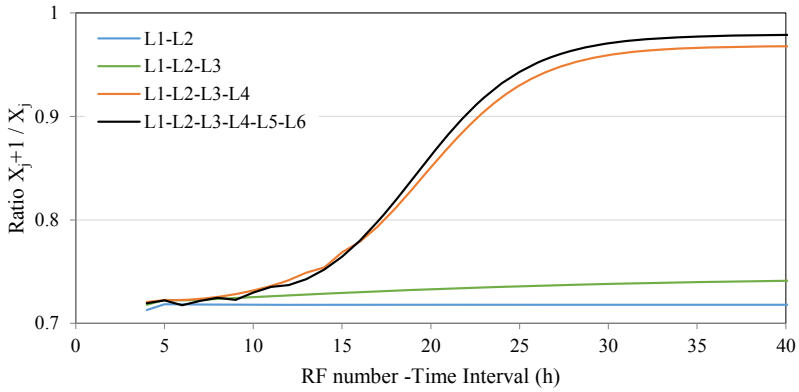

FIG. 5.12 The change in ratio between two consecutive RFs: X_{n+1} / X_n for $n > 3$ in higher indices in multi-layered walls: The ratio of the two RFs changes in higher indices in a multi-layered wall. The constant ratio moves to another constant value, where the influence of the latter layer(s) is included.

The change in the RF ratio slopes in Fig 5.12 show how the effect of different layers are included in the *X* RFs. Monitoring the slopes and observing the changes in the common ratio between *X* RFs, one can indicate the presence of different layers and therefore indication of the internal composition in a wall of unknown construction.

5.4 Inverse Determination of Thermo-Physical Characteristics Using EPM

Reflecting the necessity of reliable estimation of thermo-physical properties, in this section, the RFs are used to calculate the two main thermo-physical properties: thermal conductivity (k) and VHC (ρc). These two parameters are even more

important than the R_c-value because the R_c-value can be calculated when k is known (The thickness of a wall can be measured in several ways). The VHC can be used to achieve a more accurate estimation of the thermal behaviour and is needed in dynamic building simulations. Unlike the yearly heating demand, the heating and the cooling capacities and the size of the HVAC installations highly depend on this property [123]. Originally, the X RFs of index 0 to n are calculated for a homogeneous wall, based on the two properties k and VHC, L the thickness, and t the time interval [106]:

$$\begin{cases} X_0 = -\dfrac{kL}{at}\left(-\dfrac{1}{3}-\dfrac{at}{L^2}-\dfrac{2}{\pi^2}\sum_{i=1}^{\infty}\exp(-\dfrac{i^2\pi^2 at}{L^2})/i^2\right) \\ X_1 = -\dfrac{kL}{at}\left[\dfrac{1}{3}+\dfrac{2}{\pi^2}\sum_{i=1}^{\infty}\left(\left[\exp(-\dfrac{i^2\pi^2 at}{L^2})\right]^2-2\left[\exp(-\dfrac{i^2\pi^2 at}{L^2})\right]\right)/i^2\right] \\ X_j = -\dfrac{2kL}{at\pi^2}\left(\sum_{i=1}^{\infty}\left[\exp(-\dfrac{i^2\pi^2 at}{L^2})\right]^{j+1}-2\left[\exp(-\dfrac{i^2\pi^2 at}{L^2})\right]^{j}+\left[\exp(-\dfrac{i^2\pi^2 at}{L^2})\right]^{j-1}\right)/i^2 \quad \forall j \geq 2 \end{cases} \tag{5.17}$$

Where a is thermal diffusivity, On the contrary, in EPM, the RFs can be obtained directly from the measurements and therefore known. Since the wall's thickness is often measurable and the time interval is arbitrarily chosen, the above RF equations can be applied to calculate the thermal conductivity and the VHC of the tested sample. With an accurate estimation of thermal conductivity, the thermal resistance can also be calculated, based on the thickness of the wall. As the number of equations is much larger than the number of unknowns, an overdetermined system of equations needs to be tackled. Accordingly, the two unknowns, thermal conductivity and the VHC are found, solving the following optimization problem with at least two RFs (equations):

$$\begin{aligned} &\min_{k,\ \rho c} \sqrt[2]{\left|X_0^* - f_0(k,\ \rho c)\right|^2 + \left|X_1^* - f_1(k,\ \rho c)\right|^2 + \sum_{j=2}^{n}\left|X_j^* - f_j(k,\ \rho c)\right|^2} \\ &\text{s.t.} \quad k \in [0,2]\ ;\ \rho c \in [2\text{E}5,\ 2\text{E}6] \\ &\begin{cases} X_0 = f_0(k,\ \rho c) \\ X_1 = f_1(k,\ \rho c) \\ X_{j>1} = f_j(k,\ \rho c) \end{cases} \end{aligned} \tag{5.18}$$

Where f comes from (5.17) and the RFs are the ones estimated on site. The search

domains are taken between the minimum and the maximum possible values for building materials. The steps (mesh size) are taken as 1000 $Jm^{-3}K^{-1}$ for VHC and 0.01 $Wm^{-1}K^{-1}$ for thermal conductivity. Having an estimation of the materials used in a wall, shorter ranges can be applied. For this method, it is crucial that the RFs represent the desired layer/ wall. Therefore, it is essential to make sure the RFs are of corresponding time intervals. The optimization problem is stated, based on minimizing the RMSE (Root Mean Square Error) of the difference between measured RFs and the RFs calculated based on the wall's properties. The RMSE is chosen because it magnifies the tolerances of RFs (e.g. measurement errors) before the square-root and therefore it is more suitable than the MAE (Mean Absolute Error) for the aforementioned problem. However, on the tested samples, MAE has shown similar results. This may change in case of larger operational and equipment errors. In this problem, the objective function has many local minima. Due to the limitation domain (tolerance), the minimum required steps for the parameters, and the function itself, the computation time is inexpensive. Accordingly, the global minimum is found via Brute-force search [142]. This method solves the problem for all given possibilities to find the minimum of all the given solutions.

5.4.1 Single-Layered Homogeneous Walls

In homogeneous walls, in addition to the thermal conductivity and VHC, the thickness can also be obtained, solving the following problem for (minimum) three parameters:

$$\min_{k,\ \rho c} \sqrt[2]{\left|X_0^* - f_0\left(k,\ \rho C, L\right)\right|^2 + \left|X_1^* - f_1\left(k,\ \rho C, L\right)\right|^2 + \sum_{j=2}^{n}\left|X_j^* - f_j\left(k,\ \rho c, L\right)\right|^2}$$

$$\text{s.t.} \quad k \in \left[0,2\right];\ \rho c \in \left[2\text{E}5,\ 2\text{E}6\right];\ L \in \left[0.1,0.5\right] \tag{5.19}$$

$$\begin{cases} X_0 = f_0\left(k,\ \rho c, L\right) \\ X_1 = f_1\left(k,\ \rho c, L\right) \\ X_{j>1} = f_j\left(k,\ \rho c, L\right) \end{cases}$$

The step size for the thickness is taken as 1 cm. The outcomes of the optimization problem have shown to be more sensitive to X_0 and X_1 rather than to X RFs of higher indices (greater than 2). Regarding the time cost to measure the RFs, this is an advantage when applying large time intervals as it shortens the total measurement period (For k and VHC only 2 RFs can be required). Note that for an

TOC

additional determination of the thickness, at least 3 RFs are required. In Table 5.5, the method has been applied to a brick wall with known properties (Theory column), using 5, 3, and only 2 RFs, showing the accuracy of the computation method.

TABLE 5.5 Estimation of thermal conductivity (k), VHC (ρc), and thickness (L) using 5, 3, and 2 RFs (equations) for two standard brick walls of 0.2 m and 0.1 m thickness respectively. The effect of adding extra RFs in lighter walls and/or longer time intervals is negligible. (Here, the RFs used for property estimations are obtained by simulation)

Property	Theory	Estimation Using 5 RFs	Estimation Using 3 RFs	Estimation Using 2 RFs	$\tau_r\|_{1\%}$	t
k	**0.9**	0.9	0.9	0.9	642 [min]	1500 [min]
ρc	**1360000**	1360000	1360000	1360000		
L	**0.5**	0.5	0.5	N/A		
k	**0.9**	0.9	0.9	0.9	102 [min]	210 [min]
ρc	**1360000**	1360000	1360000	1360000		
L	**0.2**	0.2	0.2	N/A		
k	**0.9**	0.9	0.9	0.9	26 [min]	60 [min]
ρc	**1360000**	1360000	1360000	1360000		
L	**0.1**	0.1	0.1	N/A		

The difference between the estimated values and the actual ones depends on the representativeness of the used RFs. In Table 5.5, all values, from the extreme case of the 50 cm wall to the 10 cm one, have been determined with 100% accuracy due to the fact that the time interval is selected as such that all X RFs include information regarding the whole wall. Note that for such high accuracy, for the heavy 50 cm wall, 2×1500 min is required to measure the parameters. This time duration (2 days) in comparison to the standard method which requires minimum 3 days of measurements, is still shorter, especially because of high thermal mass in this case which leads to much longer measurement periods if the standard method is to be followed.

Determination of the thermo-physical properties in multi-layered walls requires the use of multi-layered wall equations. For a two-layered wall for instance, U and W in (5.12) and (5.13) can be used. Note that due to the larger number of unknowns in such cases, more RFs are needed to be measured. As the number of unknowns grows as a result of multi layers, the problem tends towards becoming ill-conditioned.

5.4.2 Multi-Layered Walls

In a multi-layered wall, properties of the outer single layers can be determined using EPM, provided that the corresponding RFs contain information only regarding that specific layer. As discussed in previous sections, this can occur in case of a time interval shorter than double the minimum response time of that single layer. An example of the wall introduced in Table 5.3 is shown below, where the pulse has been applied at the polyurethane once with a time interval of 5 min and once with 18 min (both shorter than the response time of first layer). As shown in Table 5.6, using RFs of 5 and 18 min time intervals, the optimization can reveal the properties of the first layer.

TABLE 5.6 Optimization results: Using RFs of the wall (demonstrated in Table 5.3) with time intervals shorter than the minimum response time of each layer results in determination of the properties of that single layer.

	Pulse at Polyurethane: $\tau_r\|_{1\%}$ = 9 min		Pulse at Concrete: $\tau_r\|_{1\%}$ = 34 min	
Property	**Theory**	**Estimation Using t=5 min**	**Theory**	**Estimation using t=25 min**
k [$Wm^{-1}K^{-1}$]	**0.02**	0.02	**0.7**	0.7
ρc [$Jm^{-3}K^{-1}$]	**46200**	43000	**1408000**	1321000

This fact is used in the next section to calculate the properties of the internal facing layer of a cavity wall.

5.4.3 Determination of k and ρc from the Results of the Experiments

The properties of the tested wall can be estimated through the RFs calculated from the results of an EPM experiment. Accordingly, the two main properties have been determined based on the RFs calculated from the experiments, by solving the following optimization problem using only the two first RFs.

$$\min_{k,\ \rho c} \sqrt[2]{\left|X_0^* - f_0\left(k,\ \rho c\right)\right|^2 + \left|X_1^* - f_1\left(k,\ \rho c\right)\right|^2}$$
$$\text{s.t.} \quad k \in \left[0,2\right];\ \rho c \in \left[2\text{E}5,\ 2\text{E}6\right]$$
$$\begin{cases} X_0 = f_0\left(k,\ \rho c\right) \\ X_1 = f_1\left(k,\ \rho c\right) \end{cases} \tag{5.20}$$

The selected time interval in all experiments has been shorter than $2\,\tau_r\big|_{1\%}$ of the first layer, the wood- cement board (146 min). Consequently, as discussed in Section 5.3.4, the measured RFs include only the properties of only the first layer (wood-cement in Table 5.1). In Fig 5.13, the problem, solved for the theoretical values (k = 0.35 $Wm^{-1}K^{-1}$ and VHC ρc = 1837500 $Jm^{-3}K$) is shown, finding the same values for both parameters.

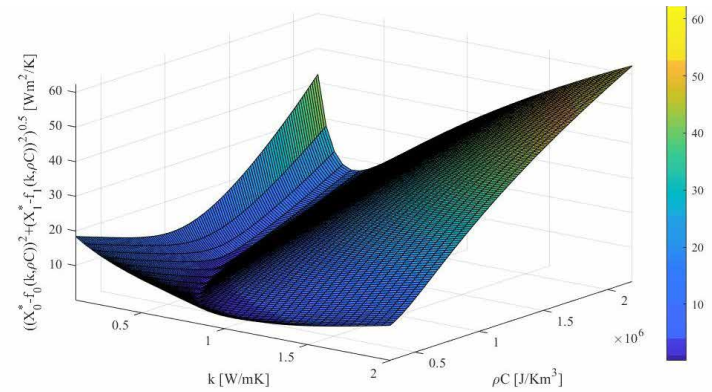

FIG. 5.13 The surface of RMSE ($\sqrt[2]{\left|X_0^* - f_0\left(k,\ \rho c\right)\right|^2 + \left|X_1^* - f_1\left(k,\ \rho c\right)\right|^2}$) as a function of thermal conductivity (k) and VHC (ρc). The minimum is found via the Brute-Force method

Solving the optimization problem for the results of the experiments leads to a prediction of the thermal conductivity and VHC. The results of the computations are shown in Table 5.7.

TOC

TABLE 5.7 Results of the determinations of thermal conductivity (k^*) and VHC (ρc^*) based on two RFs X_0^* and X_1^* with time interval t and pulse magnitude δ. The layer's minimum response time is $(\tau_r|_{1\%})_1 = 73\ min$. Theoretical properties of the tested layer are $k = 0.35$ Wm^{-1}K^{-1} and $\rho c = 1837500$ Jm^{-3}K

Test	1	2	3	4
t [min]	24	18	26	57
δ [K]	51	65	53	62
X_0^* [Wm^{-2}K^{-1}]	18.86	22.12	18.26	14.53
X_1^* [Wm^{-2}K^{-1}]	-12.74	-13.31	-12.62	-10.5
k^* [Wm^{-1}K^{-1}]	0.25	0.38	0.24	0.28
ρc^* [JK^{-1}m^{-3}]	1654000	1092000	1705000	2200000

Although closest to the expected value in thermal conductivity, the VHC has shown a large difference when a short time interval is used. This is in-line with the result from another test carried out on a case study whose thermal resistance was measured in [64].

5.4.4 Accuracy and Precision Analysis

For an estimation of the accuracy in determination of thermal conductivity and VHC, the results are analysed by making a comparison between the theoretical values of the wall being tested and the ones obtained from the experiments. It is assumed that the actual values are identical to the theoretical values. Note that as the response time of the first layer of the wall (73 min) is longer than any of the time intervals being used, the RFs obtained from EPM consequently refer only to the first layer. The departure (deviation from the expected value) is calculated via (5.21) and the results are summarized in Table 5.8:

$$Dep\ k = 100(k - k^*)/k \quad ; \quad Dep\ \rho c = 100(\rho c - \rho c^*)/\rho c \tag{5.21}$$

TABLE 5.8 The results of departure in estimation of thermal conductivity and VHC from the experiments, using only two RFs. The deviation is the highest for the VHC, when a short time interval is used.

Test	1	2	3	4	Average
Dep k	28.5 %	-8.5 %	31.4 %	20.0 %	17.1%
Dep ρc	9.9 %	40.5 %	7.3 %	-19.7 %	9.5%

As seen from Table 5.8, the thermal conductivity of the first layer has been found with 8.5%-31.4% deviation from the theoretical value. In comparison with the standard method [6] which declares an uncertainty between 14%-28% for determination of the R_c-value after many days, the difference is found acceptable. The deviation is expected to be a result of various factors including using only two RFs, the difference between actual and theoretical performance (e.g. moisture content and material aging), instrumental and operational error, and the imperfection of the excitation signals, especially in test 2. The prediction of VHC has shown to be poorest in the shortest time interval (18 min). In the other tests, the departure of VHC prediction has been below 20%. The accuracy of the method is expected to be highly improved by improving the control of the signal and therefore minimizing the imperfections seen before in Fig 5.5.

The instrumental error (based on the accuracy of the equipment) for determination of the thermo-physical characteristics in the experiments at its highest levels occurs at largest values of temperature and heat flux (according to the sensors' manual). Consequently, the final error has been calculated for RFs, using quadrature error computation. Including these errors in the new RFs for the thermal conductivity and VHC determination model (Equation 5.18), by solving the optimization problem with the uncertainty-included inputs, leads to a maximum total error of 11% in determination of thermal conductivity and 42% in the VHC. Note that this is the total error and therefore includes the already-existing error shown in Table 5.8 (e.g. operation error) of 8.5% and 40.5% for determination of thermal conductivity and VHC, respectively. Accordingly, instrumental error has leaded to a maximum of 1.5% (for VHC) and 2.5% (for k) additional uncertainty. This error is smaller, once a lower heat flux peak (longer time interval) is applied. For determination of the R_c-value, instrumental errors have been illustrated in [64].

Apart from the same range of results in different tests, the precision of the method in general is tested by repeating a test of similar time interval and pulse magnitude. Since the two tests 1 (red dotted) and 3 (blue dashed) are of such condition, they are compared in Fig 5.14 where the left graph shows the wall's interior surface temperature pulse (T_s) profiles and the right one shows the X RF curves.

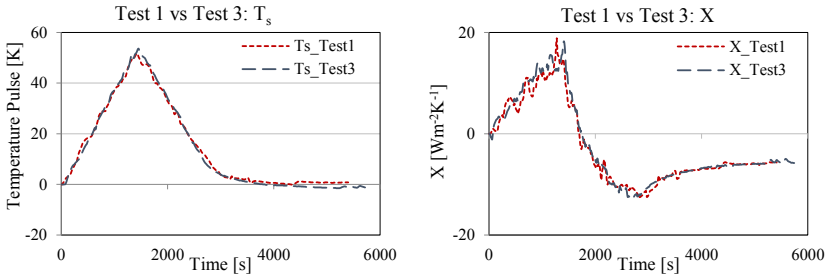

FIG. 5.14 Surface temperature and RFs measured from two similar tests (1 and 3), showing a good agreement between the trends and the values (a measure of precision of the method), despite the 2 minute difference in time intervals

As seen from Fig 5.14, the surface temperature profiles and the RFs are in agreement, showing the repeatability and therefore the precision of the method. In addition, the average deviations DEV of the two tests in calculation of thermal conductivity in [Wm^{-1}K^{-1}]and VHC in[Jm^{-3}K^{-1}] are calculated (See Table 5.5):

$$\begin{cases} \overline{k} = 0.24 \rightarrow DEV_k = \sum \dfrac{k - \overline{k}}{2} = \dfrac{0.2}{2} = 0.01 \; ; \\ \overline{\rho c} = 1672500 \rightarrow DEV_{\rho c} = \sum \dfrac{\rho c - \overline{\rho c}}{2} = \dfrac{37000}{2} = 18500 \end{cases} \tag{5.22}$$

The ratios between the deviations and the average values for k and ρc equal 2.6 % and 1% respectively, showing the precision of the method. The deviation between the k and ρc values in the four tests are expected to minimize when the control system and the heating and cooling equipment are improved.

5.5 Conclusion

In the first part of this chapter, aiming for in-situ determination of the thermal resistance of walls of unknown construction through EPM, a variety of aspects regarding the time interval, the thermal response time, and the excitation pulse

TOC

magnitude have been illustrated through simulations and experiments. In order to determine the R_c-value accurately, it is always necessary to consider the minimum thermal response time of the wall being studied by its RFs. The *X* RFs of a wall are representative for its whole construction only when at least double the total response time of the wall is passed. In an EPM experiment on an unknown wall, this can be confirmed in three ways:

1. A rise observed in *Y* RFs curve is an indication of passing the minimum thermal response time.
2. When the ratio between two consecutive *X* RFs becomes and stays constant for a long time, double the minimum response time is passed.
3. A test can take place in advance where the time required for the heat flux response at one side to a heat pulse at the other side is measured.

When confirmed, it can be concluded that information related to the composition of different layers and the thickness of a wall is included in its corresponding RFs.

In the second part of this chapter, it was shown that EPM can be applied to estimate two thermo-physical properties: thermal conductivity and VHC, and to determine the thickness of a homogeneous wall by solving an inverse modelling problem. In addition, in multi-layered walls, the method can be used with homogeneous walls' equations to estimate the aforementioned properties of the outer layers. Accordingly, EPM has been applied experimentally to estimate the thermo-physical properties of a tested case study wall with an acceptable (comparable to the standard method) accuracy and precision. The errors associated with the results are mainly suspected to be a result of poor signal control which was done via a manual dimmer.

Choice of time Interval and Pulse Magnitude

From the simulations and experiments, the possibility and advantage of combining different time intervals and pulse magnitudes has been demonstrated. For the majority of light to medium existing constructions (e.g. 0.1 m - 0.3 m brick wall), pulses with time intervals longer than 1 h result in a more stable curve (as a result of easier control and higher robustness) and therefore more reliable outcome. According to the experiments' results, short time intervals also result in poor estimation of VHC. For light-to-medium weighted walls, a time interval of 1h is found to be sufficient, provided that the considerations regarding the minimum thermal response time are taken into account. Except in light walls, the shorter time intervals (30-45 min) result in larger number of smaller RFs and therefore, make the result sensitive to the operational and instrumental errors. Furthermore, using a longer

time interval leads to a higher chance of having the effect of latter layers and the opposite surface included in the earlier RFs.

The pulse magnitude may be as large as reaching the surface temperature to 90 °C. Note that the larger pulse magnitudes in small heated areas increase the chances of 3D heat transfer and in that case, using longer time intervals is a more suitable option. Additionally, the location of the insulation in insulated walls can be estimated by comparing the *X* RFs at two sides. The side with smaller *X* RFs is closer to the insulation layer.

The Ratio between Two Consecutive *X* RFs

The ratio between two consecutive *X* RFs with high index ($j >> 2$) has shown to play an important role in the information that can be extracted regarding the construction of the walls. In a homogeneous wall, the first time this ratio becomes constant, is an indication of the fact that double the minimum response time is passed and the *X* RFs include information regarding the whole wall. This is an indication of the time when the test can stop and the rest of RFs can be calculated (based on the existing ones) instead of being measured. In multi-layered walls, the change in the constant ratio can give an indication about the presence of different layers. Here too, when the ratio becomes and stays constant, the rest of the *X* RFs can be calculated instead of being measured.

Determination of Characteristics Other than the R_c-Value

The results of the simulations have shown the possibility of determination of the thermo-physical characteristics of homogeneous walls by EPM and solving an inverse modelling problem which uses measured RFs and RF equations to estimate thermal conductivity, VHC, and thickness of a homogeneous wall.

In multi-layered walls, the aforementioned properties are expected to be found for each layer, using multi-layered walls' equations. However, this has not been tested so far. Experimentally tested, using only two first RFs and inverse determination, it has been possible to estimate the two thermal properties of the first layer of a cavity wall which has been tested by EPM in less than two hours. Except the short time interval which has resulted in poor estimation of VHC, the other tests have shown reasonably good accuracy and precision for the method.

Limitations in Specific Typologies

Heavily insulated walls interrupt the 1D heat transfer as they provide a high resistance in the thickness direction. This results in heat transfer in lateral directions. In case of very heavy insulation (this can be detected when no response from the other side of the wall is observed during the experiments), the RFs may represent the properties of the non-insulated layers and only partially the properties of the insulated layer. The part of the insulation being involved in the measured RFs cannot be known in a single test unless the time has passed twice the minimum thermal response time.

The method is not suitable for the cavity walls as the heat pulse cannot be conducted through the air appropriately. The applied heat at one side will dissipate in the air and through combined convection, the 1D heat transfer is interrupted. However, only in case of a 3-layered cavity wall, EPM can be applied on two sides separately. This way, relying on the *X* RFs of each side, the Rc-value of each side as well as their thermo-physical properties can be estimated. Accordingly, the thickness of the two solid layers can be estimated as well. Adding an estimated R_c-value of the air layer to the other two, the R_c-value of such cavity wall can be estimated.

Recommendations for the Future Studies

The EPM has shown even more potential for its application in future experiments. It is suggested that a more accurate control system is built and used. The size of the heated area as well as the size of the protected surface (at the outdoor side) should be as large as possible. Due to the limitation of the experiments, it is highly recommended to test the method on more constructions. The actual performance of the method on heavy constructions is of interest. Especially in multi-layered walls, the change of the ratio in the *X* RFs with higher indices can mean a change in the layer in terms of response. It is recommended to study further the ratio and to find more properties, using its constant value. It is recommended to test multi-layered walls to determine the thermal conductivity and VHC of their various layers. Execution of various tests on the same sample is expected to reveal further information about the properties and the construction of the tested sample. The method needs to be further tested in three-layered cavity walls where the pulse is applied at two sides of the cavity. It is recommended to use the method in other components (e.g. floors, roofs, and windows) following required modifications.

6 Determination of Buildings' Global Parameters Through Inverse Modelling and On-Board Monitored Data

At a final stage, in this chapter, a completely different approach is followed. Conducting in-situ measurements and experiments can be intrusive in occupied buildings and many households lose interest due to the hassle and costs associated with the in-situ methods. However, the recent rapid progress of sensor technologies has opened the door to automatic collection of the so-called on-board monitored data. In accordance with the increasing chance of the availability of such data (e.g. smart meter data and home automation systems), in this chapter, it is sought to use these data in combination with inverse modelling techniques to extract a whole building's global thermo-physical characteristics.

This chapter is based on a journal manuscript, submitted as:

Rasooli, A., & Itard, L. Automated In-Situ Determination of Buildings' Global Thermo-Physical Characteristics and Air Change Rates through Inverse Modelling of Smart Meter and Air Temperature Data

6.1 Introduction

Determination of buildings' thermo-physical characteristics is a necessary step in the assessment of buildings' thermal behaviour which results in an accurate estimation of building's energy saving potential. Along the same line, numerous studies have been dedicated to determine these characteristics using a whole range of completely different approaches. Of the most important thermo-physical characteristics, the thermal transmittance of the building envelope and the air tightness can be named. A large category of conventional methods involves direct measurement of these parameters using specific instrumentation. For instance, ISO 9869 [6] prescribes a standard method for determination of the thermal resistance and thermal transmittance of façades, using a heat flux meter and a set of two thermocouples installed on the two sides of the wall. Similarly, ISO 9972 [143] prescribes a fan-pressurization method to determine the permeability of the building, the results of which can be used for estimation of air infiltration rate. These specific methods generally require specialists, specific equipment, intrusion, investment, and long periods of measurement. For instance, following the measurement and data analysis procedure prescribed by the standard ISO 9869's Average Method [6], it can take more than a month of measurements to estimate only the thermal transmittance of a single wall [26]. Accordingly, many pieces of research have been conducted to analyse the results of these tests in alternative ways to obtain the properties quicker and more reliably [16, 19, 73]. Amongst the various methods of data analysis, inverse modelling has been widely researched. Opposite to forward modelling [144], where the inputs of a known system are fed to generate its outputs, in an inverse modelling problem, the system (e.g. a wall) is modelled as a box with unknown parameters. The system's governing equations are derived and fed by a large-enough set of known outputs and inputs to create a large set of equations. The model may be then identified by finding the parameters which can best satisfy the whole set of equations. As the number of equations are much more than the unknowns, a major challenge in inverse modelling is to research if the thermal system model is identifiable. This can be at risk when the problem does not have a unique solution [145]. Accordingly, the reversibility and the stability of the solution must be checked to identify whether the problem is ill-conditioned. Inverse modelling can be applied to different levels of construction.

6.2 State-of-the-art

Inverse Modelling at Component Level

On the element level (using surface boundary conditions), inverse modelling method with a harmonic approach [146] has been applied to estimate the thermal properties of walls. Chaffar et al. [24] used inverse method to characterize homogeneous walls by estimating their thermal conductivity and volumetric heat capacity. Similarly, Rasooli and Itard [147] applied an in-situ method and found the same properties through inverse modelling of a wall's thermal response factors. Šuklje et al. [126] used inverse modelling to characterise green façades. Deconinck and Roels [25] investigated the ability of stochastic grey-box modelling in characterization of the actual thermal performance of walls suffering from problems such as poor workmanship and consequent phenomena. The results showed good agreement between the calculated and the actual R-profiles on frequently-occurring surface temperature differences. Along the same line, Evangelisti et al. [125] used and calibrated a homogeneous wall equivalent to the multi-layered walls.

Inverse Modelling at Building Level

The advantage of using inverse modelling methods on the element level (e.g. walls) is obtaining individual results with high accuracy. However, this requires separate tests and measurements for each parameter in each component of interest. Many of these approaches do not take place due to the hassle and costs associated with their required procedure, calling for automated approaches. Following the advancement and growth of sensors and controllers, monitoring of buildings is a new trend [30], leading to the availability of the so called "on-board monitored" data. Many new buildings and HVAC systems thus are being equipped with sensors to monitor certain parameters such as air temperature, relative humidity (RH), and CO_2 concentration. Furthermore, with the introduction of smart meters, a huge potential of energy monitoring has been introduced [32, 148, 149]. With the availability of this amount of data, building models have become an alternative to component-level measurement methods, especially in cases where more information (e.g. ventilation rate, energy consumption) are simultaneously needed and a very high level of accuracy is not necessarily required. Buildings are accordingly first modelled and analysed to predict parameters such as energy consumption, indoor air temperatures, and thermo-physical characteristics.

Inverse modelling has been used in several pieces of research to estimate parameters which lead to a better prediction of energy behaviour. In addition to prediction and characterization of indoor climate [150], numerous studies have been dedicated to estimation of energy demand and energy load calculations through data-driven models. Zhang et al. [33] compared four Inverse Modelling methods for characterization of hot water energy consumption. Support Vector Machines [151] and Artificial Neural Networks [152] have been applied to predict energy consumption in commercial buildings. Similarly, An et al. [34] developed and calibrated an inverse PDE-ODE model and González-Vidal et al. [35] compared a black-box model with a grey-box one for better prediction of the buildings' energy demand. With the same aim, Lam et al. [153] used occupant behaviour data to calibrate an EnergyPlus model for an office building. Braun and Chaturvedi [154] applied a grey-box model and trained it with 2 weeks of data to accurately predict transient cooling and heating requirements of buildings. Despite a huge potential and interest in energy load predictions, the application of inverse modelling and machine learning is not limited to this area. Gori and Elell [36] showed the advantage of dynamic grey-box models in reducing the errors when finding the thermal transmittance. Nordström et al. [155] used the energy signature method to estimate the effective U-value of the buildings, showing the possibility of using static energy signature models for sufficiently large indoor and outdoor temperature differences. Most Recently, Senave et al. [31] investigated the level of accuracy in determination of heat loss coefficient through the Average Method [6], Energy Signature Method [156], Linear Regression, and ARX modelling [47]. Along the same line, through sensitivity analysis of the determination of the heat loss coefficient with these methods in another study [46], it was found that the selected input data has a higher impact than the applied data analysis method. Determination of the heat loss coefficient [43-45], also carried out in the current chapter, is a highlighted issue in the field. During 2017-2021, IEA Annex 71 [29] is dedicated to assess buildings' energy performance by determination of parameters as such. Methods such as QUB [128, 130, 157] and ISABELE [129] address the determination of this parameter by conducting in-situ tests. However, these methods require heating pulses to the buildings, implying their feasibility in vacant buildings.

The initial step in an inverse modelling problem is to choose and build the most appropriate model that suits the problem. Kramer et al. [158] has compared and categorized building thermal models, suggesting the use of simplified building models with physical meaning. On the one hand, simplified methods benefit from short computation time and lower risk of having multiple solutions. On the other hand, they often fail to present an accurate physical meaning to the identified parameters since they are lumped values of multiple physical parameters. Generally, the models are built and the order can be increased or reduced until a performance

criterion is met [37]. Literature shows that the best choices for the models are generally case sensitive and depending on the instance, some models can perform better than the rest. Along the same line, Berthou et al. [159], Hazyuk et al. [160], and Trčka and Hensen [161] showed that the complexity of the model does not necessarily decrease the errors associated with the predictions. Andrade-Cabrera et al. [37] have recently shown a trade-off between the complexity of the lumped parameter models and the energy forecasting accuracy by tracking the annual energy estimation error when reducing a model's complexity. To find the appropriate model, Bacher and Madsen [32] described a hierarchy model selection procedure by likelihood ratio tests and forward selection strategy. The procedure has been applied to a case study to estimate building characteristics such as thermal conductivity and heat capacity. An et al. [38] patented a method consisting of a static model which was achieved by integration of a dynamic model in a long period. By using data regarding temperature, RH and building's information, the thermal properties of the building have been determined. Park et al. [41] used a simple 1R1C (1 resistor-1 capacitor) model to study the internal gains from the appliances in low-energy buildings. A well-insulated room was modelled and measurements were applied to identify the global (lumped) thermal resistance and the global capacitance. The validity of the model led to a second study [42] where a 2R2C model was used in combination with an electrical heater to identify the same parameters this time for appliances and for the thermal (building) model. Zeifman et al. [39] used a second order model rather than a first order one to additionally separate the infiltrative heat loss from the conductive part. The circumstance of "which model works better" is case-specific and depends on the type and operation of the buildings. Accordingly, from 8 different RC models, Ramallo-González et al. [40] found the 2R1C model to work best for their case. The model was then applied to 6 case studies (houses) to find properties such as heat loss coefficients of the envelopes. Wang an Xu made an energy model consisting of 3R2C roof, a 2R2C internal mass, and 3R2C external wall to identify the parameters using genetic algorithm (GA) and validated it with an office building. They present the method to simplify energy models using easily available and short-period data. The GA has been often used as a promising optimization technique for the buildings' inverse modelling problems [162]. Costola et al. [149] used GA to optimize 34 parameters of their model, fed with smart meter energy data, to show the capability of this method in making reliable estimations. However, a trade-off was seen between the variables and the results sets which was said to be solved by using realistic bounds and multiple objective functions. Gupta [163] applied the same method (GA) and fed simulated energy data to a 2R1C, a 3R1C, and a 4R2C model and found the 3R1C to perform better than the other two, in determination of the resistance and capacitance of the buildings.

Over the studied literature, it has been evident that using actual data to estimate building's thermo-physical properties, especially in the occupied residential buildings, has been a well-known significant challenge. Large-scale measurements are always associated with numerous operational and instrumental errors. Accordingly, in comparison with simulated data, using actual data has often led to unsatisfactory results [48]. In the building level, many unidentified random disturbances introduced by occupants influence the energy consumption. Accordingly, many of the studies have dealt with office buildings and commercial buildings where the effects of occupants are better defined and therefore easier to model in comparison with residential buildings.

The advancement and progress of smart meters, sensors and monitoring technologies is leading the building sector to include more and more measurements in their HVAC installations and their control and automation systems. Besides comfort and energy, on-board data from the monitoring of parameters such as temperature, RH, and CO_2 concentrations is of high value in terms of revealing health-related aspects. The aim of this chapter is to investigate the possibilities of using such data, in combination with a simple thermal model and inverse modelling, to determine four critical global thermo-physical characteristics of a residential building. It is shown how the global values determining the heat loss coefficient leading to the determination of transmission and air exchange (heat transfer by air movement and mixing throgh ventilation and infiltration) losses, thermal mass effect, solar radiation effect can be used to understand buildings' thermal behaviour. Additionally, it is shown that by using the thermal resistance of buildings' components (either from construction data or from measurements), it is possible to estimate the daily air flow rates of a building in the winter. The effect of different time periods, period lengths, and granularity levels are demonstrated. The results are evaluated using information available from inspections and construction documents.

Unlike many studies on the same topic, in this research, the details regarding preparation and processing of the data are also explained, which can significantly help future similar studies.

6.3 Methodology

The framework of this study begins with measurement of certain parameters in a building. The work continues with construction of a simple 1R1C model representing the building and feeding it with data of different sizes, granularity levels, and time periods, to estimate its global key parameters. An optimization is solved and the parameters are estimated. Thereafter, the building construction information has been applied to find hourly air change rates. The findings are evaluated using the supplementary available information.

To prepare the feed data, initial steps have been taken. First, the indoor air and meteorological measurements were processed and the data has been aggregated in different levels. Then the indoor sensors' data have been calibrated, using the sensors' calibration curves. Thereafter, the energy data were cleaned and filtered using the other sensor's data. The procedure of preparing the data and dealing with missing data points are explained. The required feed data is then prepared: indoor and outdoor average air temperature, total heating consumption, and global solar radiation.

Thereafter, the general procedure of making an electrical circuit analogous to the thermal model - according to the available input data and the desired output - is explained briefly for the sake of understanding and examples are shown. With the aim of determination of the building's global thermo-physical characteristics, a 1st order model is built. The model's governing equation (energy conservation) is derived based on the main heat transfer processes. The system's detailed properties are lumped into four equivalent parameters: heat loss coefficient (inverse of global equivalent resistance), global equivalent capacitance, solar gain factor, and a constant parameter (e.g. internal heat generation and other unknown effects). The model is then fed to estimate the four parameters for different periods, durations, and granularity levels (hourly, daily, and weekly values). The parameters are found via inverse modelling of the main equation by defining an optimization problem. The accuracy of the determination of the four parameters cannot be examined as they are lumped parameters and the actual values do not exist. However, using supplementary information such as the construction documents, their range, order of magnitude, and behaviour can be evaluated.

Finally, the first parameter, the heat loss coefficient, includes a constant part (transmission) and a variable part (ventilation and infiltration). Accordingly the construction information (based on the building documents or obtained from the

measurements) are used to estimate the daily air flow rates in the winter. This is of high importance due to the fact that the ventilation and infiltration in winter times result in considerable values of airborne heat loss in the buildings.

In section 6.3, the raw data, measuring methods and equipment, and the required processes before feeding the data to the model are explained in detail. In section 6.4, the chosen model is shown and the inverse modelling of the 1st-order circuit through GA is presented. Thereafter, in section 6.5, the results are presented and the method is evaluated using the construction documents. Finally, in section 6.6, conclusions are drawn and recommendations are given.

6.4 Data: Sources, Cleaning, and Processing

The data used in this study is obtained during a large-scale measurement campaign of 12 months (See Appendix C), starting from June 2017. The raw data is obtained in different time intervals. The logging intervals, indoor [164] and outdoor [165] sensor types, instrumentation, and their corresponding accuracies are summarized in Table 6.1.

TABLE 6.1 The description of the sensors by which the data have been measured

Data	Source	Logging Interval	Sensor Type and Accuracy
Indoor Air Temperature	In-Situ Sensors	5 min	KT Thermistor – 1% per °C (0.15 °C - 0.3°C)
CO_2 Concentration	In-Situ Sensors	5 min	GE Telaire: 400 – 1250 ppm: 3% of reading
RH	In-Situ Sensors	5 min	Honeywell HiH5031: +/- 3%
Motion	In-Situ Sensors	5 min	Honeywell IR8M: 11 x 12 m (at 2.3m height)
RH Bathroom	In-Situ Sensors	5 min	Honeywell HiH5031: +/- 3%
Gas Consumption	Smart Meter	1 h	Technolution P1 port reader
Power Consumption	Smart Meter	10 s	Technolution P1 port reader
Outdoor Air Temperature	KNMI	1 h	RTD Pt 500: 0.1°C
Global Solar Radiation	KNMI	1 h	Pyranometer: 1%
Wind velocity	KNMI	1 h	Cup anemometer: 0.5ms^{-1}

All logging intervals are synchronized and aggregated to the smallest common available level (hourly data) in the analysis. Since each sensor starts logging at the

time it is powered, the logging times are different. Accordingly, the data has been synchronized in such a way that the time shift between the loggings are minimized for all sensors.

Indoor measurements have been carried out during a large-scale measurement campaign in the Netherlands (Appendix C). The details regarding the execution of the campaign can be found in [148]. During the campaign, the houses have been inspected and the sensors have been installed in the living room, the kitchen, and the two bedrooms of the houses to measure air temperature, CO_2 concentration, RH, and motion. The sensors used in the houses are shown in Fig 6.1.

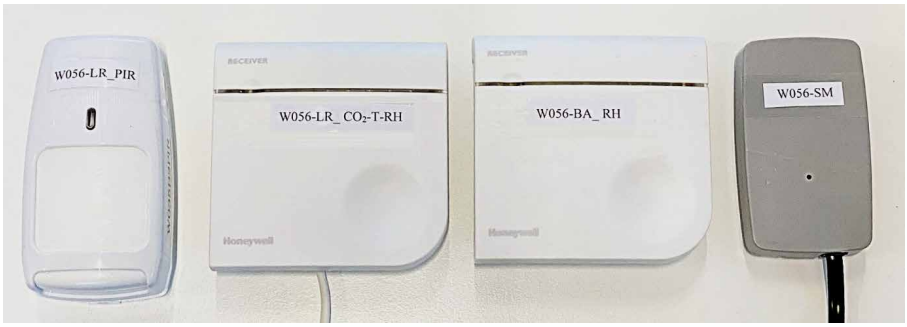

FIG. 6.1 Sensors used in the measurement campaign, from left to right: motion sensors (4 rooms), CO_2-air temperature-RH sensor (4 rooms), RH sensor (bathroom), and smart meter port reader

6.4.1 Indoor Air Measurements:

The indoor sensors were carefully placed in the most representative locations of the room, avoiding the areas in the vicinity of solar radiation, draught, and moisture. With a logging interval of 5 minutes, the data were logged for one year. No missing values have been found, thanks to the local memory of the data loggers attached with the sensors.

To ensure high accuracy, it is essential to have all sensors recalibrated every 1-2 years. All temperature and RH sensors have been calibrated via a set of pre-calibrated sensors which were individually calibrated in a climate chamber. The calibration has been carried out, having all sensors in a large enclosed environment, exposed to two state points, 20°C – RH 70% and 30°C – RH 40%. The selected

points are chosen based on the operation range of the sensors (indoor environment), assuming a linear correlation between the two points. The linear calibration correlations of the sensors are shown in Table 6.2.

TABLE 6.2 Calibration correlations for correction of the measured air temperatures

Sensor / Readings	Point 1 (°C)	Point 2 (°C)	Calibration Correlation
Pre-Calibrated Sensor	21.2	29.8	-
Temperature Sensor Living Room	22.7	31.9	$T_{correct}=0.93\ T_{measured}$
Temperature Sensor Kitchen	22.8	31.0	$T_{correct}=1.05\ T_{measured} - 2.7$
Temperature Sensor Bedroom 1	22.7	31.8	$T_{correct}=0.94\ T_{measured} - 0.2$
Temperature Sensor Bedroom 2	22.9	31.4	$T_{correct}=T_{measured} - 1.7$

The CO_2 sensors are self-calibrating type and therefore, not manually recalibrated. The instantaneous values of CO_2 concentrations were used only as an indication to the occupants and the evaluation of the findings. In Fig 6.2, the results of four parameters are presented. At the top, left to right, the average room air temperatures and the CO_2 concentration are shown respectively. At the bottom left and the bottom right, average room RH and motion (in binary) are shown for 1 week. The motion measurements help as an indication of presence, showing 0 as no motion and 1 as at least one motion during that hour.

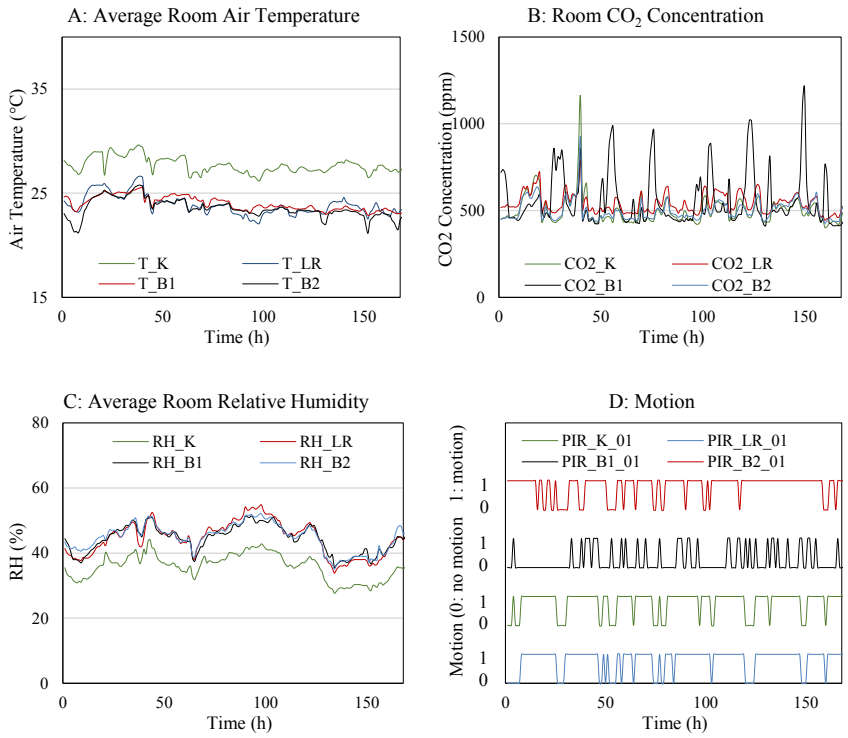

FIG. 6.2 First week of measurements: room air temperatures (A), room CO_2 concentrations (B), room RH (C) and occupant motion (D) are presented. (LR: Living Room, K: Kitchen, B1: Bedroom 1, B2: Bedroom 2)

6.4.2 Meteorological Measurements

Meteorological measurements including outdoor air temperature, wind velocity, and solar radiation are provided from the KNMI (Koninklijk Nederlands Meteorologisch Instituut: Royal Netherlands Meteorological Institute) [165]. The local meteorological data is approximated by averaging the measurement values between two nearest stations both located within 10 km range of the building. These values have shown to be the closest to the actual local values measured via a weather station which has been locally installed after the measurement campaign period. In Fig 6.3, local measurements are compared to the assumed (averaged) KNMI values during the same measurement period.

TOC

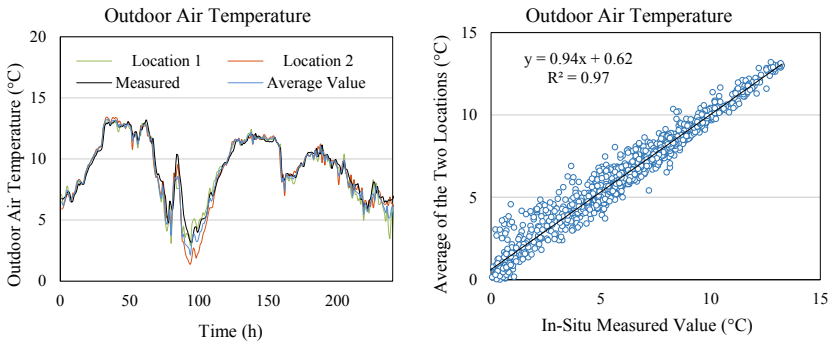

FIG. 6.3 Comparison between outdoor air temperature data from KNMI in two locations and their average value (the one used in the model) and the in-situ measured values (left -10 days) and the linear regression between the average value and in-situ measurements (right - 56 days).

The R^2 values regarding the fit between the KNMI location-based average value, the two locations, and the in-situ measurements for air temperature, solar radiation, and wind velocity are presented in Table 6.3:

TABLE 6.3 R^2 values in comparison between the parameters in two locations and their average values and the in-situ measured values. December 2018-February 2019

Location / Parameter	Outdoor Air Temperature	Solar Radiation	Wind Velocity
Location 1	R^2=0.96	R^2=0.90	R^2=0.78
Location 2	R^2=0.95	R^2=0.90	R^2=0.78
Average of the two locations	R^2=0.97	R^2=0.92	R^2=0.81

Despite the small difference, the average of the values reported for the two KNMI locations still shows to be the closest to the actual in-situ measurements. Accordingly, this value has been applied instead of performing in-situ measurements.

6.4.3 Energy Consumption Recordings and Filtering

Energy usage data has been gathered via a Technolution Cloudia smart meter port reader, connected to the P1 port of the smart meter. The logging intervals of the smart meter data from electrical power (kW) and the accumulated gas consumption (m^3) are 10 s and 1h respectively. The hourly rates of heating consumption is found by deducting two consecutive recordings and multiplying by the standard average

TOC

calorific value of the gas in the Netherlands (35.17 MJ/m^3). The long-time missing values (due to the port reader and comunication faults) of the gas and electricity consumption are left blank and not used in the analysis (See Fig 6.7). The short period missing values (3-5) hours are filled by the data of the points with similar conditions (e.g. air temperature and time of the day). For shorter periods, the gaps of the missing values have been filled by the average of the values at the beginning and the end of the gaps.

Separation of SH and DHW-Related Heating from the Total Heating Consumption

The smart meter data shows the hourly total amount of gas consumed for domestic hot water (DHW), space heating (SH), and noise (cooking and boiler set-point heating). Consequently, determination of each category in higher resolution (e.g. per minute) is not possible, unless separate measurements are carried out. Due to the availability of a whole year data, rough differentiation between different categories can take place aided by comparing the summer and winter period. During the summer, heating (gas) is not consumed for SH. This knowledge helps in filtering the data in the winter period where both SH and DHW take place. The data due to the DHW can be filtered simply by comparing the magnitude of its peaks in summer. The SH peaks observed in the winter are clearly much larger than the other peaks. The only peaks large enough to be confused with SH values are the shower DHW peaks. Accordingly, the shower times are detected via an RH sensor placed in the bathroom. By observing the data in different period lengths, much information is conveyed. In Fig 6.4, the bathroom RH (blue) and the total heat consumption (orange) are plotted for 21 days (left), one week (middle), and one day (right) in summer.

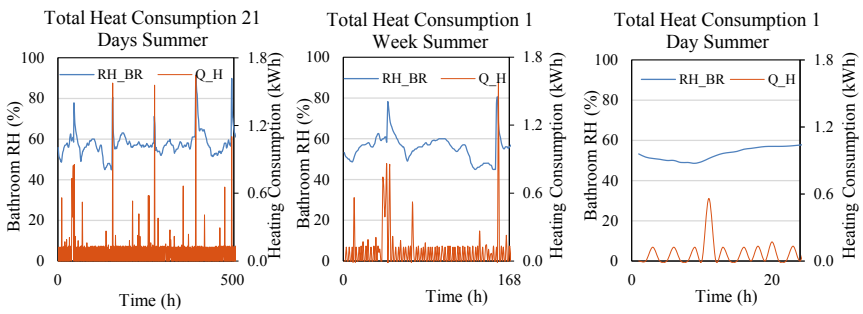

FIG. 6.4 Total heating consumption, Q_H (in orange) and bathroom RH, RH_BR (in blue) for 21 days of summer.

TOC

To estimate the SH-related heating consumption, the following procedure is carried out:

First, the noise regarding the frequent heating up of the boiler is filtered. This noise is the heat consumed by the boiler to maintain the minimum set point temperature to ensure instantaneous hot water supply. Note that the very short periods of using DHW cannot be distinguished from this noise and therefore are eliminated during the noise filtering. Second, all DHW-related heating consumption should be removed from the remaining data to achieve the SH-related heating consumption. Comparing the winter period (frequent SH) with the summer (no SH), the magnitude of the SH and the frequent DHW can be estimated. Ever since the frequent DHW consumption values are much smaller than the SH values and the shower time DHW data points, they can be filtered by omitting the values smaller than a certain level. For this case study, the observed range in summer was 0.9 kW for every hour section. This eliminates the majority of the small DHW-related consumptions except showering times. Finally, an approximation of the shower DHW consumption can be found following the high peaks of the bathroom RH profile. Accordingly, the heating consumption values taking place during the shower times (when the RH of the bathroom rises above 70%) have been filtered. The same procedure is repeated by filtering based on the RH level at one time step before. This repetition eliminates the consumption from a short period of the hour before.

In Fig 6.5, the bathroom RH (blue) and heat consumption (orange) raw data (left) and the DHW-filtered one (right) is presented for 21 days of summer.

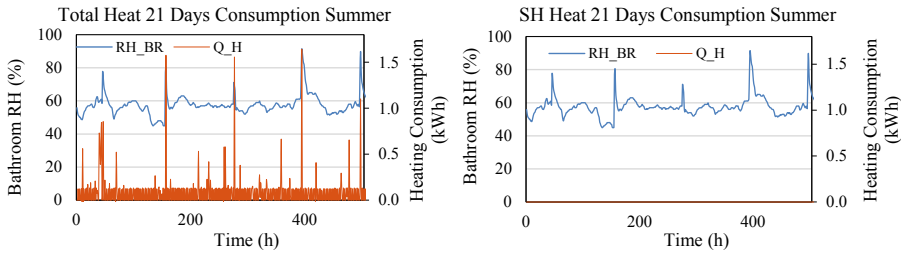

FIG. 6.5 bathroom RH (blue) and heat consumption (orange) raw data (left) and the DHW-filtered one (right)

Similarly, the bathroom RH (blue) and heat consumption (orange) raw data (left) and the DHW-filtered one (right) is presented in Fig 6.6 for 21 days (top), 1 week (middle), and 1 day (bottom) of winter.

TOC

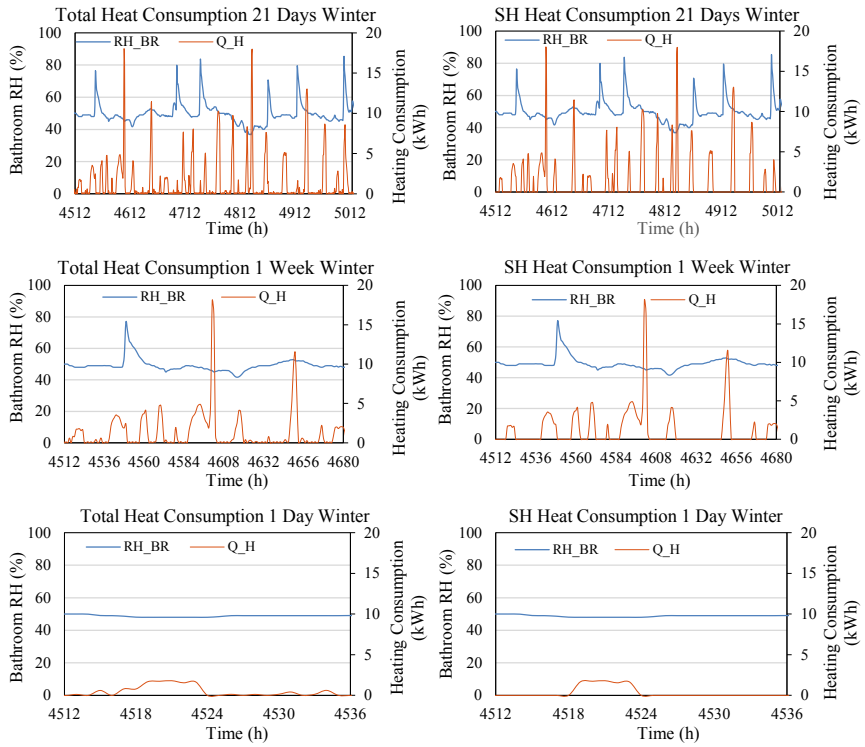

FIG. 6.6 Bathroom RH (blue) and heat consumption (orange) raw data (left) and the DHW-filtered one (right) for 21 days (top), 1 week (middle), and 1 day (bottom) of winter.

Filtering out (the majority of) the DHW-related heating consumption from the total heating consumption (left side in Fig 6.6), the SH-related heating consumption is presented (right side in Fig 6.6). To validate the filtering methods, the sum of the DHW-related gas consumption (filtered out) is presented as a percentage of the total consumption, in different periods and presented in Table 6.4. Note that the found values are half of what is assumed in the literature (approximately 20%). However, the difference is explainable due to the low frequency and the short duration of showers (as illustrated from the bathroom RH data and the answers in a seperate survey) which are lower than what is assumed in the literature.

TABLE 6.4 Total, SH-related and DHW-related gas consumption in different periods

Duration	Total heating consumption (kWh)	SH- related heating consumption (kWh)	DHW percentage of total gas consumption (%)
7 Days	230.21	211.62	8.07
21 Days	716.07	636.86	11.06
2 Months	1925.77	1747.20	9.27
3 Months	2849.30	2591.38	9.05

The limitation of using hourly data can be mentioned in possible scenarios where the DHW and SH cannot be separated correctly, causing uncertainty:

- The SH starting during a last short period of one hour (e.g. 10:50) and ending at an early period of the logging hour (e.g. 11:10). This results in the peak to break into two smaller peaks which can be confused with DHW use during two hours.
- The case where DHW and SH take place during the same hour.

6.4.4 Input Data for the Model

The raw data is processed before being fed to the model. The average indoor temperature has been obtained from the volume-based average value of the room temperatures. The hourly global solar radiation, initially available in (Jm^{-2}) is converted to (Wm^{-2}) and later to (W) using the transparent surface areas. Finally, the total heating consumption is filtered as explained in Section 6.3.3 to SH values. The data regarding indoor (top left) and outdoor (top right) air temperatures, total heating consumption (bottom right), and solar radiation (bottom left) are plotted in Fig 6.7.

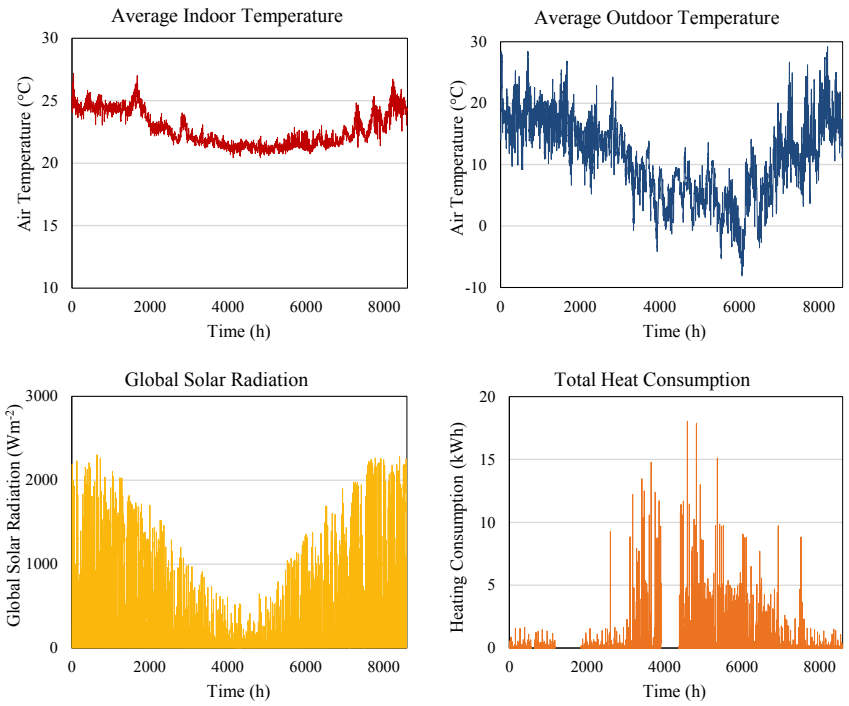

FIG. 6.7 Indoor (left top), outdoor (right top) air temperatures, Solar radiation (bottom left), and the total heating consumption (bottom right) for one year in the case study.

6.5 Inverse Modelling of the Building's Thermal Model

In addition to the statistical methods mentioned in the literature, the choice of model highly depends on the availability of the measured data, the range of parameters, and the desired level of outputs (e.g. lumped or local parameters). In Section 6.5.1, examples of thermal models are shown and in section 6.5.2 the case study is presented. In Sections 6.5.3 to 6.5.5, the chosen model and the types of analysis are explained.

6.5.1 The Choice of the Model

As already pointed out in Section 6.2, there is never a single way of describing the thermal behaviour of a building. The use of high-resolution thermal networks requires an abundance of input data and information, which is often not present or cannot be measured. Additionally, with a high-resolution of a model, the chance of finding multiple solutions increases. Accordingly, the accuracy of the estimations does not increase with the increase of the resolution. Therefore, lower resolution models are achieved through model reduction, in which some nodes are neglected or nodes of similar thermal behaviour are lumped. A dwelling in a form of detached house for instance, where the sides are in contact with outdoor air, can be modelled in a mid-resolution circuit as shown in Fig 6.8 with 11R4C (11 resistors- 4 capacitors) circuit. This model consists of 2 nodes placed on air and 9 on the surfaces of the roof, the floor, the façades (4 orientations). The capacitors (C) are placed on the construction and on the indoor air. Apart from the floor, all components are in contact with outdoor and indoor air. Accordingly, resistances R between the air and the components relate to convective (lumped with IR radiation), and the ones at the boundaries of a circle, relate to conductive heat transfer. Indices i and o denote indoor and outdoor air and indices H and V indicate horizontal and vertical alignments.

When reducing this model, the circles (components) can be taken as single nodes whose conductive resistances are lumped with convective resistance(s). Alternatively, parallel branches can be lumped into a single branch, following the resistance summation rules. Note that the resistance $R_{vent+inf}$ is a variable parameter and therefore has a different value in different periods. Accordingly, when lumping this branch with one with (approximately) constant resistance such as the wall's thermal transmittance, the lumped resistance is also a non-constant.

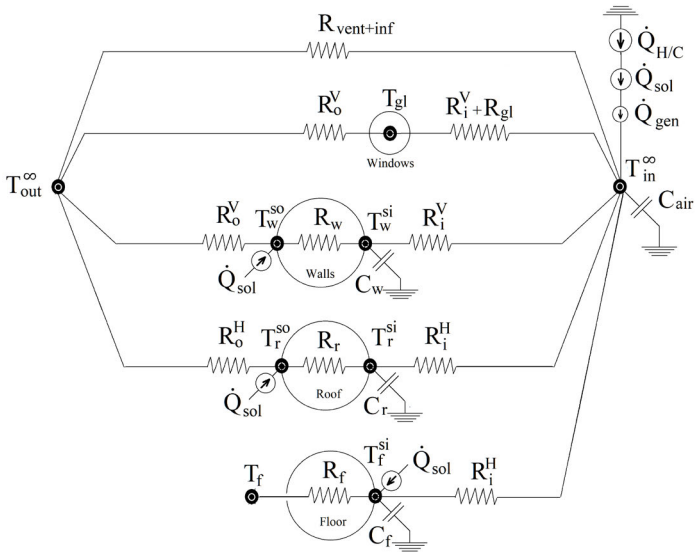

FIG. 6.8 The 11R4C model for a detached house: Thermal resistances and capacitances are moddeled as resistors and capacitors.

The same modelling procedure is standard to follow for any type of building. For an apartment, one wall (edge apartment), two walls (middle apartment), or three walls (mid-floor apartment with three neighbours), the floor and the roof (except the highest and lowest floors) are adjacent to the neighbour apartments. Assuming similar indoor temperature in these adjacent media, the heat transfer (air to air) and therefore the thermal resistance R from these components can be neglected in the calculations. In an apartment in the middle floors, two main nodes can be considered: the interior air and the exterior air. The nodes are connected via resistors and internal nodes, the surface temperatures. The thermal mass capacitors are the same as the house. In Fig 6.9, an example electrical circuit analogous example to the case study apartment is shown.

TOC

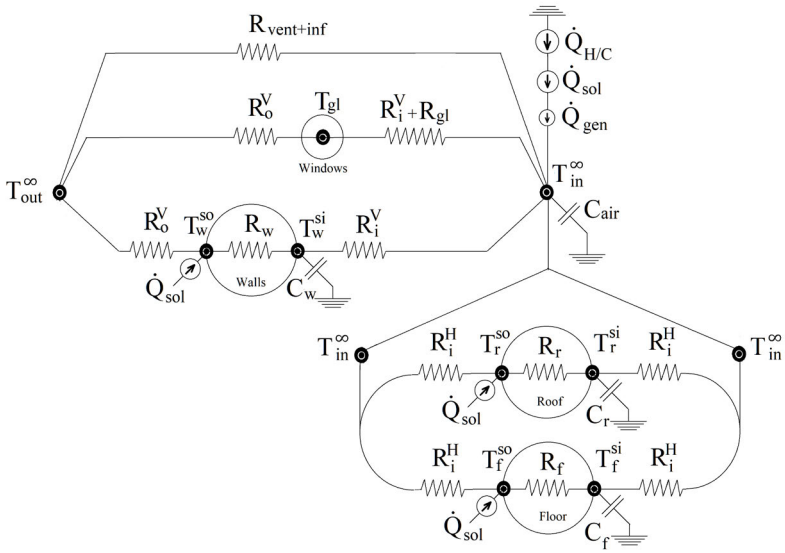

FIG. 6.9 The 12R4C model for a mid-floor apartment

According to Kirchhoff's current law, the sum of the currents towards a node (e.g. indoor air) are equal to zero:

$$\sum I = \frac{1}{R}\,\Delta V_0 + \mathrm{C}\,\frac{\partial V_0}{\partial t} + I_{source} = 0 \tag{6.1}$$

Where ΔV_0 is voltage drop, R is resistance, C is capacitance, and I is the electrical current. Following the analogy between the circuit and the thermal system (the building), the currents (heat flow) can be computed from the voltages (temperatures), resistances (thermal resistances), and capacitances (thermal masses). This is in fact a visualization of what was always done in building simulation.

Of the most important parameters defining the resolution of the model, is the feed data, which should match not only the physics involved, but also, the available level of detail in the input and output data. Finding a balance between the desired accuracy and level of outputs, the available data, and the potential of the model to be identifiable, one can make an appropriate choice of the model's resolution. Note that in high resolution models, the risk of finding multiple sets of answers increases and therefore these models are not always suitable for inverse modeling [158].

TOC

6.5.2 The Case Study

The case study building is one-floor, four-room apartment of 72 m^2, located in the West of the Netherlands. The building construction year is 2014 and certain standards regarding the energy efficiency have been carefully followed (Energy label A). The apartment unit is adjacent to two neighbours on west and east sides and has a south façade and a north façade which faces the patio. The heating system is a combination condensing boiler which heats all 4 rooms. The thermostat is set at 21°C at all times. The house is ventilated via a mechanical ventilation system at medium stand.

The indoor air temperature of four rooms are available whereas no surface temperature has been measured. Accordingly, a zonal model with four indoor air nodes as shown in Fig 6.10 is a better choice than the one previously shown in Fig 6.9.

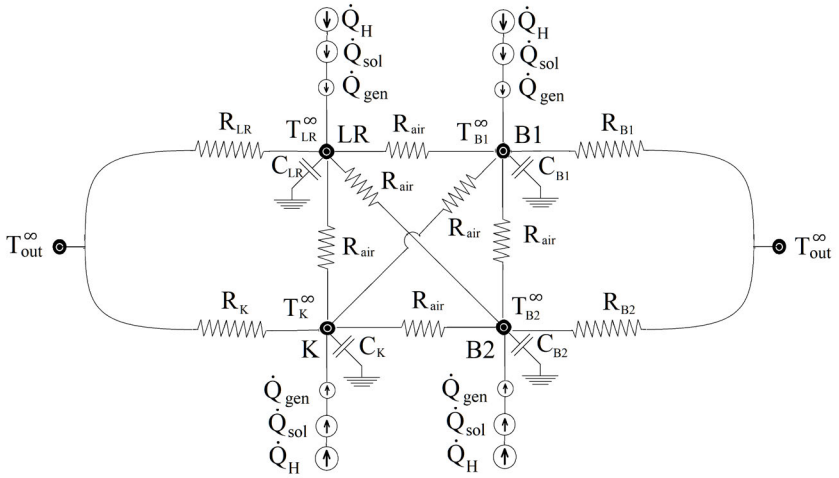

FIG. 6.10 The high-resolution electrical circuit model analogous to the case study, according to the available measured data

As seen in Fig 6.10, due to the lack of data of the surface temperatures, the corresponding nodes are omitted. Therefore, the capacitors and resistors are lumped parameters of more detailed actual ones.

TOC

6.5.3 Building the 1st - Order Circuit

The aim here is to apply the simplest model that can work with minimum measurements (e.g. no surface temperature data) to estimate parameters such as the heat loss coefficient. Reducing the circuit to the simplest possible dynamic model, a 1R1C model is built, shown in Fig 6.11. This model is used in the inverse modelling of its four global parameters, using the available input and output data. Analogous to the thermal system (the building), the building's resistance against transmission and air exchange heat loss/gains is translated into an equivalent global thermal resistance R_{eq} , including the resistance of all exterior walls, roof and floor, ventilation and infiltration. Similarly, equivalent thermal capacitance C_{eq}, represents the buildings total equivalent thermal mass, showing the dynamic ability of the system to accumulate/release heat. Note that this capacitance is not the air capacitance but reflects the behaviour of the building (air + construction). Other heat sources such as internal gains are taken as a separate flow source $\dot{Q}_{gen}$ in the circuit. S_0 indicates the portion of solar heat that enters the system.

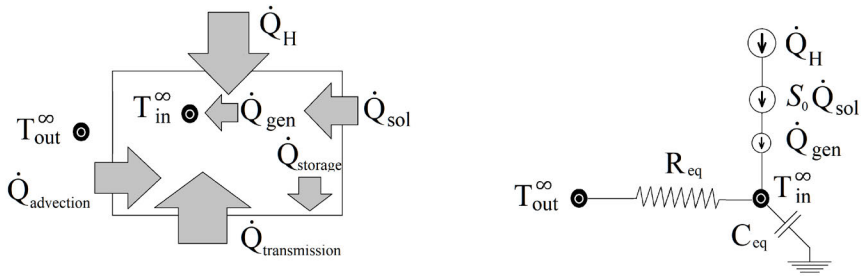

FIG. 6.11 The first order model: 1R1C analogized electrical circuit with two nodes of air temperatures (indoor and outdoor) heat transfer phenomena are the electrical currents towards the indoor air node.

The state equation of this system, based on energy conservation is as follows:

$$\left(\dot{Q}_{advection}+\dot{Q}_{transmission}\right)+\dot{Q}_{H}+\dot{Q}_{sol}+\dot{Q}_{gen}=\dot{Q}_{storage} \tag{6.2}$$

Where the sum of the heat flows are stored in the system. It is of high importance to state the model equation in such a way that in the governing equations, parameters would not have the possibility to compensate for each other during the inverse modelling. Deriving the energy conservation equation for indoor air, the following equation is obtained:

TOC

$$\left[\left(\rho c_p \dot{\forall}\right)_{air} + \sum_{i=1}^{4} \mathrm{U}_i A_i\right]\left[T_{out}^{\infty} - T_{in}^{\infty}\right] - \sum_i \frac{\partial T}{\partial t}\left(\rho c \forall\right)_i + \eta.\left[\dot{Q}_H\right] + \left[\dot{Q}_{sol}\right] + \left[\dot{Q}_{gen}\right] = 0 \qquad (6.3)$$

Where U is the thermal transmittance (air to air) of each building envelope component, T is the air temperature, ρ is the density, c_p is the specific heat capacity, $\forall$ is the volume, $\dot{Q}_H$ is the heating consumption recorded by the smart meter, η is the nominal efficiency of the boiler which according to the manual of the boiler is taken as 0.9, $\dot{Q}_{sol}$ is the global solar radiation, A is the surface area, t is time, and i is the index for different components which accumulate heat (walls, celling, floor, and air). Note that during the inverse modelling it is not possible to separate air heat transfer from transmission losses as the driving forces are the same. Taking a global equivalent resistance between indoor and outdoor air, R_{eq}, and a global capacitance C_{eq} which stores and releases the heat from/to the air and the construction, (6.3) can be translated to the following:

$$R_{eq}^{-1}\left[T_{out}^{\infty} - T_{in}^{\infty}\right] - C_{eq}\left[\frac{\partial T_{in}^{\infty}}{\partial t}\right] + \eta.\left[\dot{Q}_H\right] + S_0.\left[P_{sol}\right] + S_1 = 0 \qquad (6.4)$$

In which R_{eq}^{-1} is the heat loss coefficient, S_0 is the average fraction of the solar irradiance that enters the system and influences the indoor air, and S_1 is a constant for all the other effects including the internal heat gains. The global heat loss coefficient R_{eq}^{-1} is the equivalent summation of all transmission resistances and ventilation resistances:

$$R_{eq}^{-1} = \frac{1}{R_{vent}} + \sum \kappa_{f,\,r,\,w,\,g} = \left(\rho c_p \dot{\forall}\right)_{air} + \left(\mathrm{U}A\right)_w + \left(\mathrm{U}A\right)_r + \left(\mathrm{U}A\right)_{gl} \qquad (6.5)$$

Where floor is neglected due to the existance of adjacent unit with similar indoor temperature. The storage parameter C_{eq} is an indirect equivalent thermal mass of the system, roughly approximated by:

$$C_{eq} \equiv \left(\rho c_p \forall\right)_{construction} + \left(\rho c_p \forall\right)_{air} \qquad (6.6)$$

Where $\rho c_p \forall$ is the thermal mass of the construction (floor, roof, walls, and internal walls) and of the air.

The parameter S_0 is taken as a fraction of the global solar radiation transmitted through the windows. Accordingly, the heat penetration to the system via solar radiation can be computed as following:

$$Q_{sol} = S_o . A_{gl} . P_{sol} \tag{6.7}$$

Where A_{gl} is the total glass surface and P_{sol} is the global solar irradiance per unit area. Note that S_0 should not be confused with the g-value of the glass, in this building equal to 0.58 (HR++ type). The first, shows the seasonal/daily fraction of solar radiation, entering the house and affecting the heating consumption and indoor temperature, whereas the latter is a constant window property. The advantage of using S_0 rather than the g-value is that the S_0 is based on the specific building and not solely on the window.

6.5.4 Objective Function and Inverse modelling

The generic definition used for inverse modelling can be stated as following:

A recording the actual inputs $u(t)$ and outputs $\mu(t)$ is available. A prediction $\mu^{th}(t, \theta)$ is then generated by feeding $u(t)$ to a model consisting of parameters θ. Inverse modelling takes place by determining the parameter vector θ_{eq} that minimizes a (usually quadratic) norm (σ) of the predicted error [166]:

$$\theta_{eq} = \underset{\theta}{\operatorname{argmin}} \sum_{t} \sigma\left(\mu^{th}(t, \theta) - \mu(t)\right) \tag{6.8}$$

To incorporate the long-time dynamic effect of the thermal mass, the state equation targets indoor air temperature. Accordingly, for the current problem, θ_{eq} is the vector [R_{eq}^{-1} C_{eq} S_0 S_1] which is estimated from the input $u(t)$ being the heating consumption, outdoor temperature, and solar irradiance, and the output $\mu(t)$ the indoor air temperature. The prediction function is then as following:

$$T_{in}^{\infty}\Big|_{t}^{th} = \left(\eta \dot{Q}_H + \frac{1}{R_{eq}} \left[T_{out}^{\infty} \right] + S_0 \dot{Q}_{sol} + S_1 \right) + C_{eq} \left[T_{in}^{\infty}\Big|_{t-1}^{th} \right] \Bigg) \Bigg/ \left(\frac{1}{R_{eq}} + C_{eq} \right) \tag{6.9}$$

The objective is to minimize the norm (σ), taken as the RMSE (Root Mean Square Error) between actual and theoretical indoor air temperature. The objective function of the optimization problem is accordingly stated as follows:

$$\min_{\frac{1}{R_{eq}},\, C,\, S_0,\, S_1} \sqrt{\frac{1}{n}\sum_{i=1}^{n} \left(\left(\eta \dot{Q}_H + S_0 \dot{Q}_{sol} + S_1 + \frac{1}{R_{eq}} \left[T_{out}^{\infty} \right]_i + C_{eq} \left[T_{in}^{\infty}\Big|_{t-1}^{th} \right]_i \right) \left(\frac{1}{R_{eq}} + C_{eq} \right)^{-1} - T_i^{ac} \right)^2}$$

$$\text{s.t. } R_{eq}^{-1} \in [10,\, 180];\; C_{eq} \in [1\text{E}\,5,\, 1\text{E}\,9];\; S_0 \in [0,\, 1];\; S_1 \in [0,\, 2000] \tag{6.10}$$

Ranges of the global parameters presented in the constrains are estimated based on the possible ranges of the physical properties they are computed from. The possible ranges of the properties in building industry are presented in Table 6.5. Note that the global R and C are found case-specific since the surface areas are included in the calculation. The surface areas used in the calculations are presented later in Table 6.8 in Section 6.6.

TABLE 6.5 Upper and lower bounds of the parameters defined in the optimization problem

Parameter	Lower Bound	Upper Bound
R_w	0.2(m^2KW^{-1})	8 (m^2KW^{-1})
R_r	0.2(m^2KW^{-1})	8 (m^2KW^{-1})
R_{gl}	0.1 (m^2KW^{-1})	0.7 (m^2KW^{-1})
ACH	0.1 (h^{-1})	2 (h^{-1})
$\left(\rho c_p \dot{\forall}\right)_{air}$	6.8 (WK^{-1})	145 (WK^{-1})
$1/R_{eq}$	10 (WK^{-1})	180 (WK^{-1})
$\left(\rho c \forall\right)_{construction}$	8 E6 (JK^{-1})	4 E7 (JK^{-1})
S_0	0	1
S_1	0	2000

The optimization problem presented is solved using GA through MATLAB [52]. Using other methods including Quasi-Newton and interior-point have resulted in nearly the same values and therefore are not presented here. Customized settings used for the GA are population size of 20000, generations of 4000. The mutation and crossover values are the default ones in MATLAB [52]. The results of the optimization in this problem have shown to be insensitive to the changes of these values. As the GA, due to its stochastic nature, does not lead to a unique solution, the optimization is run multiple times and the solution with the lowest objective function value (RMSE) is reported. The variation in the results has not been significant.

6.5.5 Granularity Level, Time Period, and the Size of the Input Data

The model has been fed with the data from different periods and granularity levels. First, the data from the whole year and then the data from the available two months of winter period (January-February) are fed to the model. Then, the data is reduced from one month (February) to the data from two weeks, one week, and finally one day in February 2018. February is chosen here because it is statistically known to be the coldest month of the year in the Netherlands. Separately, data from November and January are used to examine the method's performance. The meteorological winter is defined as December – January- February. However, due to the large energy data gaps in December 2018, this month unfortunately could not be used.

For each period, hourly, daily, and weekly data has been fed to the model. Using different periods and granularity levels, the method can be validated in terms of precision and the performance of the method as a function of input data can be expressed.

6.6 Results and Discussion

The outcomes and the results of the inverse modelling are presented here. The findings and outcomes are later evaluated using the construction data taken from the energy and construction detailed reports and the floor plans available from the municipality. For this case, due to the construction year and the quality of the reports and the corresponding organizations, this data has appeared to be reliable.

6.6.1 Outcomes of the Inverse Modelling

For each of the mentioned periods, the problem has been solved using different granularity levels of hourly, daily and weekly (when applicable). The results of the optimization are presented in Table 6.6.

TABLE 6.6 Results of the optimization for different period lengths using different granularity levels

Duration	Granularity Level	R_{eq}^{-1} [WK^{-1}]	C_{eq} [JK^{-1}]	S_o [-]	S_1 [W]	RMSE [K]
Complete year June 2017-June 2018	Hourly	81	3.4E 8	0.10	98	0.95
	Daily	82	1.5E 7	0.10	114	0.89
	Weekly	81	1.6E 6	0.10	88	078
2 months winter: January -February 2018	Hourly	148	1.7E 8	0.30	994	0.21
	Daily	148	7.2E 7	0.55	676	0.18
	Weekly	149	1.0E 7	0.20	1399	0.05
1 month: February	Hourly	138	1.4E 8	0.25	914	0.26
	Daily	138	1.6E 7	0.20	1222	0.10
2 Weeks: February 1-14	Hourly	115	2.1E 8	0.48	60	0.19
	Daily	110	1.2E 7	0.31	310	0.02
1 Week: Feb 1-7	Hourly	157	2.0E 8	0.66	486	0.13
	Daily	148	1.1E 7	0.55	697	0.03
Day 1 Feb	Hourly	100	1.0E 8	0.34	72	0.10

To test the reliability of the method further, data sets from two other periods have been tested. In Table 6.7, the outcomes of the optimization for November 2017 and January 2018 are presented.

TABLE 6.7 Results of the optimization for November 2017 and January 2018 using different granularity levels

Duration	Granularity Level	R_{eq}^{-1} [WK^{-1}]	C_{eq} [JK^{-1}]	S_o [-]	S_1 [W]	RMSE [K]
November 2017	Hourly	101	2.0E 8	0.25	169	0.18
	Daily	108	2.9E 7	0.42	56	0.09
January 2018	Hourly	128	2.3E 8	0.80	125	0.21
	Daily	130	3.1E 7	0.90	44	0.13

As seen in Tables 6.6 and 6.7, the first parameter R_{eq}^{-1} takes different values when different periods are used. These differences are attributed to the different infiltration and ventilation rates in different periods. The average values of hourly, daily, and weekly heat loss coefficient are in a close range. Opposite to this, the values of

C_{eq} become smaller in lower granularities (e.g. weekly), showing the weakening of the dynamic effect when analysing longer time periods. From building physics point of view, it is known that the response time of the buildings is in the order of days. Accordingly, using low granularity levels (daily/weekly), the dynamics cannot be captured. Consequently, in terms of granularity level, the use of hourly data is expected to result in the best estimation of C_{eq} in this problem. Note that the determination of the second parameter, C_{eq} is not always reliable, due to its high magnitude in the equation: a small temperature measurement error (inevitable in measurement equipment) multiplied by the large C_{eq} results in a large difference in its term in the equation. Generally, when building a model with one capacitance, the C_{eq} will have a large quantity and therefore less accurate, whereas in a higher resolution of model, the capacitance breaks down into smaller ones in each component, leading to higher accuracy. This is in agreement with the findings of Bacher and Madsen [32]. The solar factor S_0 remains below 1 and varies in different values and when analysing hourly, daily, and weekly data due to the difference in averaged and detailed data points and the difference in gain in different periods of the year. Similarly, the last parameter, S_1 varies in different granularity levels and periods, giving an indication of the heat generation and other changes in the system (e.g. occupant behavior) which have no correlation with the air temperature, temperature change, and solar radiation.

The obvious sources of uncertainty for this method include:

- The choice of model in terms of resolution and lumped parameter modelling
- Limitation in addressing any level of the stochastic user behaviour in the model
- Assumption of constant parameters such as heat transfer coefficients and air exchange rates
- The uncertainty of the measured data and the choice of processing (e.g. using average indoor temperature)
- The uncertainty of the SH filtering of the heating consumption data.
- Averaging variable parameters including S_0, S_1, and R_{eq}^{-1}.

The method in general works best for the coldest months of the year (winter) attributable to the large sizes of peaks in energy data. Such data helps in better training of the model. Additionally, for the same reason, the filtering of the DHW is also more accurate during the winter period. Using warmer periods, the heating values are in a smaller range and steadier, which results in inaccurate DHW data filtering and a poorer training of the model. This issue amplifies especially in a well-insulated house, such as the case study, where the indoor air temperature is stable. The summer period is not discussed due to the lack of heating consumption data.

In the summer period, the heating is off, no cooling takes place (in the Netherlands), and manual ventilation generally occurs more often through the windows and doors.

Using the results of the optimization, a predicted temperature function is fitted to the actual one. The results of the comparisons are presented in Fig 6.12. The hourly (on top) and daily (bottom) data have been fed to the model. The estimated temperatures (in black) and the actual temperatures (in red) are shown for January 2018 (left), February 2018 (middle) and November 2017 (right). As seen in Fig 6.12, for the hourly data, opposite to the trend which is well captured, the peaks are not always well predicted. Using daily data, a good agreement is seen between the actual and theoretical (computed) values of temperature.

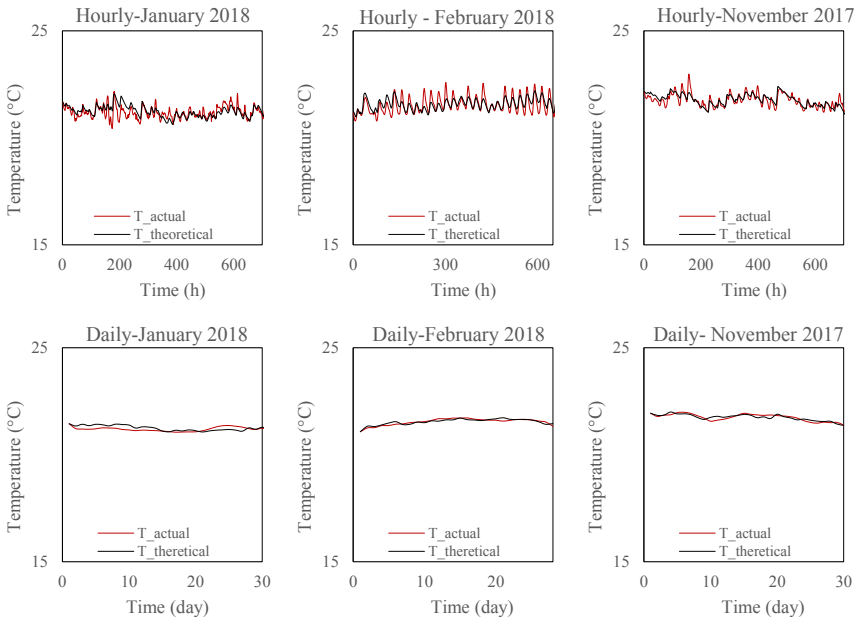

FIG. 6.12 Actual and computed hourly (top) and daily (bottom) estimated (in black) and actual (in red) temperatures for January 2018 (left), February 2018 (middle), and November 2017 (right).

The same procedure is repeated and shown in Fig 6.13, by using hourly (left), daily (middle), and weekly (right) data for two months of January 2018 and February 2018.

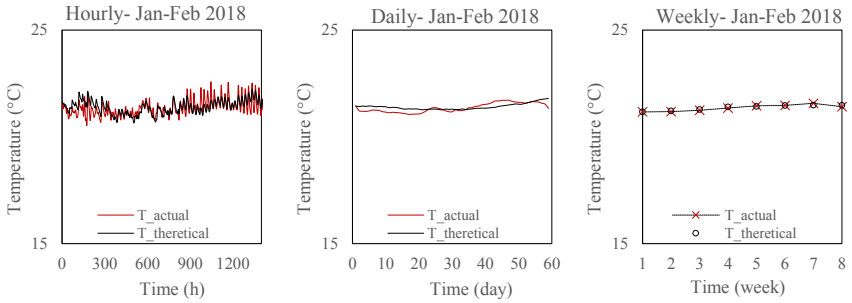

FIG. 6.13 Actual and computed hourly (left), daily (middle), and weekly (right) temperatures for two months of January 2018 and February 2018.

6.6.2 Evaluation based on the Construction Data

The outcomes of the optimization are only average values of variable parameters. To evaluate the findings of the models and analyses, the results are compared to the actual approximation of the parameters based on construction data. The properties of the components and parameters needed in the evaluation are obtained from the inspections and the official construction report documents (energy report) and are tabulated in Table 6.8. Note that the thermal capacitance values (right column) are roughly approximated from the construction materials and have not been mentioned in the reports. The missing values (e.g. floor's R_c-value) are the ones that have not been relevant for this case study.

TABLE 6.8 The building's components and their properties

Component	Area (m^2) – Volume (m^3)	Type-Configuration	R_c (m^2KW^{-1})	ρc_p (WK^{-1})
North window	8 (m^2)	HR ++ (4-15-4)	0.55	-
South window	5 (m^2)	HR ++ (4-15-4)	0.55	-
Side walls	52.4 (m^2)	Reinforced Concrete	-	3.3E7
Opaque façade	26.2 (m^2)	Insulated Brick and Gypsum	4	1.3 E7
Roof	72 (m^2) – 21.6 (m^3)	Insulated Concrete	5	4.5 E7
Floor	72 (m^2) – 21.6 (m^3)	Insulated Concrete	-	4.5 E7
Internal Walls	133.4 (m^2) – 14 (m^3)	Gypsum	-	1.1 E7
Indoor Air	195 (m^3)	Properties at 21° C	-	2.4 E5

TOC

As for the first parameter, the inverse equivalent resistance (heat loss coefficient) R_{eq}^{-1} should be equal to the inverse summation of the parallel resistances:

$$R_{eq}^{-1} = \left(\rho c_p \dot{\forall}\right)_{air} + \frac{A_r}{\alpha_{h,i}^{-1} + l_r / k_r + \alpha_{h,o}^{-1}} + \frac{A_w}{\alpha_{v,i}^{-1} + l_w / k_w + \alpha_{v,o}^{-1}} + \frac{A_{gl}}{\alpha_{v,i}^{-1} + l_{gl} / k_{gl} + \alpha_{v,o}^{-1}} \tag{6.11}$$

Where the α is the convective (lumped with IR radiation) heat transfer coefficient. Due to the small influence of this parameter in the R_{eq}^{-1} and its limited range, here it has been taken as a constant with the average values (common values often used in the literature and building simulation) shown in Table 6.9:

TABLE 6.9 Indoor and outdoor assumed average convective heat transfer coefficients

Property	Vertical α_v (Wm^{-2}K)	Horizontal α_h (Wm^{-2}K)
Indoor convective HTC	7.5	7.5
Outdoor convective HTC	25	18.5

According to the values of Table 6.8 and Table 6.9 in (6.11), the actual range of the heat loss coefficient R_{eq}^{-1} for the specific building can be estimated.

In this case study, the transmission part of the heat loss coefficient is relevant only for the North and South opaque façades, the roof, and the windows with a total value of 37 WK^{-1}. The expected range is therefore as follows:

$$\begin{cases} \dfrac{1}{R_{eq}} \approx 65 + 5.25 + 13.68 + 18 = 102 \ \ \mathrm{WK}^{-1} \quad at\ 1\ ACH \\ \dfrac{1}{R_{eq}} \approx 97.5 + 5.25 + 13.68 + 18 = 134.5 \ \ \mathrm{WK}^{-1} \quad at\ 1.5\ ACH \\ \dfrac{1}{R_{eq}} \approx 130 + 5.25 + 13.68 + 18 = 167 \ \ \mathrm{WK}^{-1} \quad at\ 2\ \ ACH \end{cases} \tag{6.12}$$

According to the building's air tightness report, the air rate is approximately 95 WK^{-1}. Summing up this value with the transmission resistance, an average heat loss coefficient of 132 WK^{-1} is expected. Values obtained from the model show a maximum of 23% deviation with this value. Note that the heat loss coefficient is not a constant due to the variable ventilation and infiltration rates in addition to

the occupant-related air exchange rates. Accordingly, the assumed value is just an indication of the possible range of this parameter.

Similarly, the global capacitance C_{eq} is roughly approximated from the summation of all heat storing components, assuming the indoor air and the construction as a single node and therefore the same behaviour:

$$C_{eq} \equiv \left(\rho c \forall\right)_f + \left(\rho c \forall\right)_w + \left(\rho c \forall\right)_{gl} + \left(\rho c \forall\right)_r + \left(\rho c \forall\right)_{internal\ \ walls} + \left(\rho C_p \forall\right)_{air} \tag{6.13}$$

In which the air has the smallest thermal mass. According to the values in Table 6.8, the global capacitance takes a minimum value of 1.5 E8 JK^{-1}. This value is expected to be higher due to the solids other than the construction (e.g. furniture). The values obtained from the model show to be in the expected range. However, the exact value of the capacitance cannot be discussed here as a consequence of the assumptions made and the simplicity of the model. The third parameter, the solar gain fraction S_0 requires in-situ measurements. However, the obtained range of [0 1] as expected from the physics point of view (only a fraction of solar radiation heats the building) confirms the relative validity of the findings. The last parameter S_1 is not evaluated due to the limited knowledge regarding the actual internal gains and unknown effects in the case study. In all cases, this value has taken a positive number, showing the positive rate of heat generation in the system.

6.6.3 Determination of Air Flow Rates

In the previous section, an average global heat loss coefficient was sought. This parameter includes a fixed part (relating to transmission losses assuming constant convection heat transfer coefficients) and variable parts relating to air exchange and movement (ventilation and infiltration). In the current case study, according to the survey, occupancy and the user behaviour during the weekdays is the same as in the weekends. Accordingly, here, it is assumed that the major part of the changes in the daily change of energy use are associated with variations in air change rates. Obtaining the global capacitance, solar fraction, and the internal gain from the optimization, the ventilation and infiltration rates can be estimated by recalculating the heat loss coefficient by the following equation:

$$\left[\frac{1}{R_{eq}}\right]_i = \frac{C_{eq}\left(\frac{\partial T_{in}^{\infty}}{\partial t}\right)_i - \eta.\left[\dot{Q}_H\right]_i - S_0.\left[\dot{Q}_{sol}\right]_i - S_1}{\left[T_{out}^{\infty}\right]_i - T_{in}^{\infty}\Big|_i^{th}} \tag{6.14}$$

In which, the differentiation has been approximated, using high-order approximation central difference, using 5 points (two before and two after):

$$\left(\frac{\partial T_{in}^{\infty}}{\partial t}\right)_i = \left(-T_{in}^{\infty}\Big|_{t+2} + 8\,T_{in}^{\infty}\Big|_{t+1} - 8\,T_{in}^{\infty}\Big|_{t-1} + T_{in}^{\infty}\Big|_{t-2}\right)/12\,\Delta t + \mathcal{O}\left(\Delta t\right)^4 \quad ; \quad \Delta t = 1\,(h) \tag{6.15}$$

Computation of the daily heat loss coefficient rates, term $\frac{1}{R_{eq}}$, can be found. Here, the daily rates are used rather than hourly rate due to the better fit shown in Fig 6.12 and the absence of undesired meaningless noise. The outcomes of (6.14) are presented in Fig 6.14. Note that the first and last two days are not presented here due to the discretization method used in (6.15) which uses 2 days before and after the current time. In case of using another discretization method (e.g. forward with one point), these days can also be added to the estimations. For lower granularity levels (e.g. week), the capacitance term can be neglected.

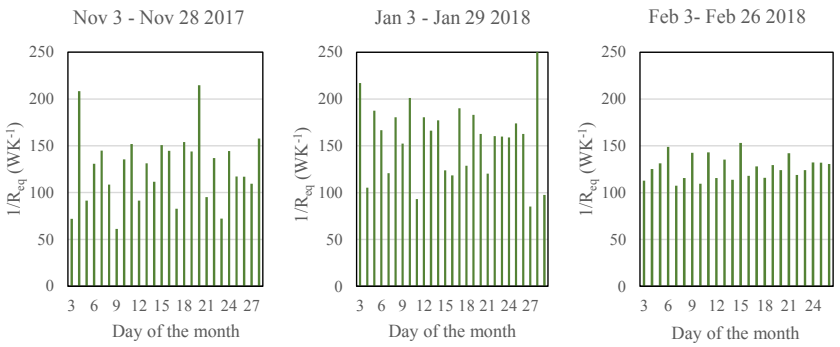

FIG. 6.14 The daily computation results of the heat loss coefficient for November 2017, January 2018, and February 2018

Using (6.11), and the resistance properties of the construction (the transmission part of 37 WK^{-1}), the air change rate fraction can be separated. Using (6.12), these values are converted to air flow rates (ACH) and plotted in Fig 6.15. Note that for

TOC

an old building where the construction is unknown, the thermal resistances or the thermal transmittances of the façades can be measured following a measurement method (e.g. ISO 9869 or EPM, See Chapters 2 and 3). This needs the same time as what is needed for training the model (one month).

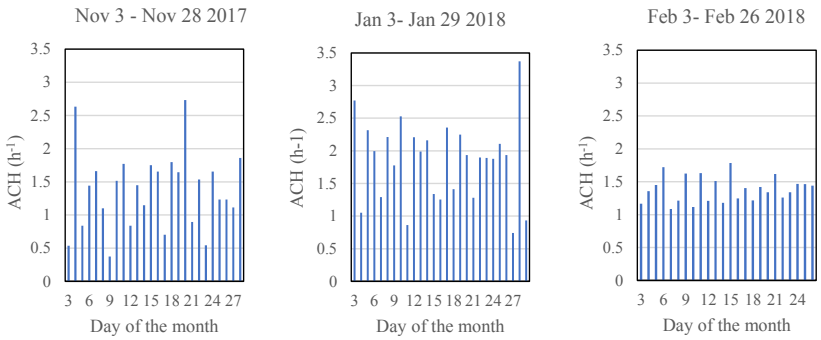

FIG. 6.15 Daily ACH rates obtained from the heat loss coefficient and the construction's thermal resistance.

As seen in Fig 6.15, the daily average approximations of air change rates are in the acceptable range of their values in reality. According to the inspection and the survey, the apartment is being manually and randomly ventilated 13-24 hours a day. For a personalized advice, the data in Fig 6.15 can be compared to the standard daily recommended ACH value for the specific building.

To investigate the validity of the results, the average monthly values found from Fig 6.15 are compared to the wind velocity. The wind velocity is known to have a direct influence on the infiltration rate and on outdoor convective heat transfer coefficient. As seen in Table 6.10 and Fig 6.16 (left), the higher wind velocities are associated with higher values of ACH. Furthermore, the CO_2 concentration values of the bedroom (where the highest peaks of CO_2 occur), show to be lower in the higher values of ACH, shown in Table 6.10 and Fig 6.16 (right). This is an indication of the validity of the ACH approximations.

TABLE 6.10 Monthly average values of estimated ACH, average wind velocity, and average CO_2 concentration

Parameter	November 2017	January 2018	February 2018
Average ACH (h^{-1})	1.37	1.84	1.38
Average Wind Velocity (ms^{-1})	4.3	5.7	4.7
Average CO_2 Concentration (ppm)	846	725	745

TOC

According to the building construction report, the average ventilation rate for this building is 1.84 ACH. The values found in Table 6.10 are in the same range of the assumed value and the average of the three months (1.53 ACH) leads to 3% deviation with the assumed average value, showing the reliability of the approximation. The values presented in Table 6.10 are depicted in Fig 6.16.

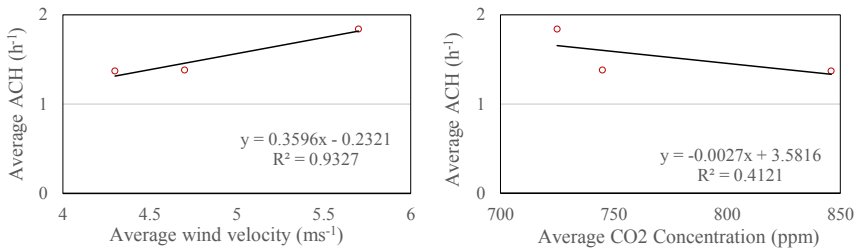

FIG. 6.16 The values and the trends of the monthly average of the daily ACH against average wind velocity (left) and average CO_2 concentration (right) showing a logical drift.

Note that the accurate real values of ACH cannot be obtained since apart from the actual air-tightness of the building, the ventilation rate changes manually by the occupant. In addition to what is known as ventilation rate, random unknown factors such as the openings of the doors, ventilation grilles, and windows and the cleanness of the exhaust air channels can highly influence the ACH.

6.7 Conclusion

6.7.1 Conclusions

The research reported in this chapter aimed to illustrate the extent to which it is possible to extract buildings' global thermo-physical characteristics, by measuring air temperature, and heating consumption data and feeding it to an inverse modelling problem of a simple 1R1C model.

From the entire process of measurement, collection, and handling the data and feeding it to the model, many important detailed practical lessons are learned. These are very important since in many pieces of research, the difference between computer-generated data and actual data and the consequent departures are underestimated. In the actual circumstances, the occupants can apply significant levels of changes in many important variables such as ventilation rates and thermostat settings, resulting in a system behaviour that is difficult to mathematically model. The details for data filtering and cleaning are shared and explained. For filtering the data, the RH level in the bathroom has shown a critical role in the separation of the DHW and SH gas consumption from the smart meter readings. The air temperature also showed to help in filling the short-term heating consumption data gaps. The use of pattern recognition algorithms in combination with the applied method is recommended in the future studies.

During the optimization, unlike using heating demand for the RMSE function, by using temperature, the dynamic nature of the temperature history effect can be fully incorporated in the model. This is due to the fact that discretization methods can only cover a limited number of time steps before the present time. The optimization showed to work at its best during the winter period. This is suspected to be the consequence of the fact that the winter period contains heating data with a long range of values (e.g. large peaks), leading to a better training of the model. This limitation is no a barrier since the air heat losses are mainly critical in the winter, as a consequence of a need for enough air exchange while minimizing the heat losses.

The feed of data to the 1R1C model with different granularity levels has shown different results. This, for the solar gains and for the internal gains are due to the differences in hourly values and aggregated values. The dynamic effect of thermal mass shows to weaken as the granularity level increases. This is also in-line with the physics involved since by averaging the heating during a longer time period, the dynamic effects fade. Consequently, using hourly data, a better estimation of the global capacitance, showing the ability of the building to store and release the heat, can be obtained. The estimation of the capacitance is expected to improve in houses with lower insulation, where the air temperature drifts are higher, improving the feed data to the model. The estimated heat loss coefficient showed very little differences when using different granularity level in the feed data. This is logical since a large part of this value is the transmission loss which is a static parameter. The differences in this value for different periods are due to the difference in different ventilation and infiltration rates. The range of this parameter, as well as the capacitance and solar fraction parameter is logical when evaluated with the construction data.

After finding the four parameters, the heat loss coefficient was recalculated using the other 3 and the feed data, assuming the majority of changes to be a result of the changes in ventilation and infiltration losses. Using temperature data, losses can also be estimated. This however, requires the thermal transmittance of the building envelope, which can be found from the construction data and or preferably by making in-situ measurements. The values found with this approach have been validated using CO_2 concentration, average wind velocity, and the building's documented average air change rate. The expected trends and the values have shown a good agreement with the findings of the model.

In this case study, the year's coldest months have shown to result in the best fit in the optimization. This is a consequence of the large quantity of heating hours with large variations in the heating consumption data. Note that 2018 was of the hottest winters in the Netherlands. Accordingly, the shown performance of the method is expected to improve if the cold period is longer and more extreme. Note that such study, by nature, does not lead to a high accuracy of parameter estimation.

6.7.2 Recommendations for future studies:

As the outcomes for the solar radiation cannot be validated, this data should be measured on site, preferably per orientation, since the unknown local circumstances (e.g. a balcony extension on the top floor) can highly influence the solar gains. It is highly recommended to use orientation-specific solar radiation data for the input and to break down the solar gain term into different orientations in the equation to increase the accuracy of the predictions. For the present research, this data has not been available. Following the difference between actual and theoretical material properties, it is recommended to measure the in-situ thermal transmittance for the building envelope, following a standard method, during the data acquisition. This can lead to a higher accuracy when estimating air exchange rates. Along the same line, the data from the surface temperatures and heat fluxes can be used to feed a model of higher resolution to separate the construction's thermal resistance. Comparing the results of such model with the one used in this research is highly recommended. Furthermore, it is recommended to test the models by feeding the indoor air temperature of the living room and compare the results with the ones obtained based on the average air temperature. From a more general perspective, it is recommended to explore a method to find the most important zone to measure its air temperature for the model.

TOC

7 Conclusion

7.1 Conclusions

This thesis was conducted to discover the possibilities for developing and studying new methods and approaches, solving the existing problems associated with in-situ determination of buildings' thermo-physical characteristics. A special attention was given to the thermo-physical properties of the exterior walls, forming the main fragment of the thesis. For the first time, the theory of response factors was brought to real life circumstances and its various theoretical and mathematical aspects were translated into in-situ experimental application. With regards to the core question posed in Chapter 1, a number of methods were developed, advanced, and modified to determine some of building's most critical thermo-physical characteristics. The tackled problems associated with the conventional characterization approaches can be summarized in measurement duration and effort.

In the second chapter, the most intuitive approach was followed to answer the first key question. The existing ISO 9869 standard method for in-situ determination of walls' thermal resistance was improved. Two problems associated with this method were pointed out: measurement duration and imprecision. The proposed solution was to modify the method by using an extra heat flux meter at the opposite side of the wall, facing the primary one. Measuring two heat flux profiles, three estimations of R_c-values could take place: based on indoor heat flux, outdoor heat flux, and the average of the two estimations. The event of the earliest convergence between the three estimates is not predictable in advance. For instance, in a two-layered wall with outdoor insulation, in disparity with the implied suggestion of the ISO 9869 in mounting the heat flux meter at the indoor surface, the R_c-value based on the outdoor heat flux resulted in a much quicker convergence to the actual R_c-value. Similarly, in a homogeneous and symmetric heavy wall, the average of the two estimates of R_c-values, resulted in a much earlier convergence. The duration of the measurement is determined by the side which results in an earlier convergence. Consequently, due to the unknown exact construction of the walls, it is clearly

TOC

advantageous to use two heat flux meters. Doing so, it was possible to measure the thermal resistance 10 times quicker than before. In addition to shortening the measurement duration, the average value showed a second advantage: increasing the precision. Following the convergence criteria, it was shown both in simulations and experiments that in a homogeneous wall, the two reportable estimates of the R_c-value can differ. This is an indication of poor precision due to unacceptable reproducibility, which can be solved following the suggested method. The extension bears an additional cost of approximately 5% to 20% compared to the original procedure. The statements were proven, using simulations on five typologies and two in-situ experiments. In Appendix B, two additional typologies are tested, leading to the same conclusions.

With the aforementioned approach, the shorter time duration (e.g. three days) could still be too long for actual circumstances and therefore a barrier to its application. Additionally, other limitations such as the validity domain of the method (e.g. minimum temperature gradients of 5K) could be an obstacle for its application. Hence, in the third chapter, reflecting the second key question, development of an alternative method was sought to determine the thermal resistance in a shorter period of time (hours instead of days). Inspired by the theory of response factors (RFs), a new rapid in-situ transient measurement method, the Excitation Pulse Method, EPM was developed. With this method, it was possible to measure the thermal resistance of three light walls of unknown construction within a couple of hours, with an accuracy comparable to the one of the ISO 9869. The method was tested as a proof-of-principle and the results were validated using the ISO 9869 on three samples. Using this method was found highly beneficial as it can allow quick measurements to take place when the available time is short. For instance, using this method as an alternative to the suggested estimations in the Dutch building energy labelling method, the overestimation of approximately 400% in determination of the thermal transmittance was resolved. The short time and the dynamic nature of the method, showed a great potential for its future application and high motivation for its further development and advancement.

The fourth chapter was dedicated to the experimental aspects of the EPM to reflect on the third key question. The details regarding the construction of the prototype needed for this method were demonstrated. The possibility of combining various pulse time intervals and pulse magnitudes was shown. The use of longer time intervals (e.g. 1 h instead of 15 min) was found a better alternative as the residuals of the RF curve are difficult to record due to their small values. The sensitivity of the results of the EPM to the number of RFs was further demonstrated. It was shown that for heavy constructions, a combination of largest possible signal and the longest possible time interval is the appropriate solution to follow. The analysis of

the three-dimensional heat transfer effects showed the effect of 3D heat transfer to be generally rather limited except in very heavy constructions. For heavy homogeneous walls, it was advised to heat an as large as possible area and measure the parameters in the center of this area in order to minimize the lateral heat transfer risk. The size of the pulse magnitude is dependent on the dimensions of the wall. Generally, surface temperatures up to 90 °C is acceptable, provided that no damage is delivered to the finishing of the wall in occupied residential buildings. A large pulse magnitude on thick walls results in 3D heat transfer disturbance, unless a very large area is heated.

In the fifth chapter, the application of the EPM was pursued in a higher level. First, special attention was given to the theory of RFs, on which the method was based. Simulations and experiments showed the relationship between the RF time interval, excitation pulse magnitude, and the thermal response time. The determination of the minimum thermal response time was shown to be a necessity for applying EPM and any other pulse-response-based method. The response from the excitation side, (*X* RFs) bears the thermo-physical properties of the whole sample, only if double the minimum response time is already passed. The event of this situation, simultaneous to the experiment, can be identified either by detection of a rise in *Y* RFs, or by observation of a constant slope in X curve. The ratio between two consecutive *X* RFs with a high index showed to determine wall's minimum thermal response time and to give an indication of the wall's composition.

Besides the R_c-value which was possible to determine before, two other properties, thermal conductivity (with an accuracy comparable to the standard method) and volumetric heat capacity (VHC) were shown possible to stem from the results of EPM. For a homogeneous wall, the thickness could additionally be determined. This outcome answered the fourth key question. The parameters were found via inverse modelling of the RF equations where the actual RFs were determined through the EPM. These equations, derived for the homogeneous slab can also be used to determine the thermal conductivity and the VHC of the exterior layers of walls. During the experiments ,the use of longer time intervals has shown to be advantageous in terms of the accuracy and the performance of the method. Generally, for a range of light to medium- weighted walls (e.g. 0.1-0.3m brick walls), time intervals longer than 1h result in more reliable outcomes. This way, the stability of the heat flux and temperature as due to the quality of the control process improves. Using a short time interval showed a poor estimation of VHC in one of the experiments. Using short time intervals, the tail of the *X* RF curve becomes longer and therefore, measurement of many more RFs are needed, increasing the total error. The accuracy of the experiments was expected to highly increase in the case of applying a better heat flux/temperature control and instruments of higher quality.

The limitation of the method includes cavity walls (except 3-layered ones with known dimension of the cavity layer) and very heavily insulated walls where the risk of lateral heat transfer in the conductive layer competes with the 1D heat transfer through the insulation layer. Without certain considerations regarding the size of the heated area, the accuracy of the method can drop in heavily insulated walls and massive walls. To both obstacles, the solution is to increase the test length or to repeat the test in different sides, both calling for longer measurement time (still considerably shorter than the time required for making measurements according to the current standard methods)

Reflecting the final key question, in the last chapter, the perspective from conducting in-situ measurements and tests was shifted to using only the available on-board monitored data (e.g. data from the smart meter and home automation systems). This approach, frequently followed in the recent years, solves the problems associated with the cost, intrusion, and effort of equipment delivery and experiments. Using indoor and outdoor air temperature, energy consumption, and solar radiation data, a building was modelled as a 1st order circuit. Data preparation methods were explained and through inverse modelling of the state equation, it was possible to determine the global thermo-physical characteristics of this building. The four parameters, the heat loss coefficient, the equivalent capacitance, the solar fraction parameter, and a constant were determined. The model worked best in the winter due to the quality of the training data. The feed of data to the model with different granularity levels showed different results in the last three parameters. For the solar gains and for the internal gains the different results are due to the differences in hourly values and aggregated values. For the capacitance, the difference reflects the decay of dynamic effects of thermal mass when longer periods are used. The ranges of the parameters were found logical when evaluated with the construction data.

Finally, using the results of the optimization, daily values of heat loss coefficient were determined and by using construction reports, the daily air change rates were determined and evaluated, showing acceptable trends and values. This way, estimations of air-born heat losses could also be followed.

7.2 General Remarks

The pieces of study of which this thesis was built from consist of numerous test simulations and test experiments. Many of these have not been published and yet they have served an important purpose in reaching the ones reported. Some of the practical lessons learned and general remarks are the following:

In the light walls, EPM has shown an excellent performance. Especially, in homogeneous cases, the application of the method is even simpler as the *X* RFs can be calculated using the constant ratio of the residual tail in the RF curve. This makes the test even shorter than what is needed according to the theory of RFs. Additionally, the location of the insulation layer can sometimes be estimated, using the RFs. Both protected (exterior) and excited (interior) areas should be as large as possible with measurements taking place in the middle, to minimize the risks of 3D heat transfer.

Comparing the ISO 9869 extension with EPM, a general conclusion can be drawn. In a stable weather condition with a temperature gradient of less than 5K between indoor and outdoor surfaces, on the one hand, the ISO 9869 standard method (and its extension) is not applicable. On the other hand, EPM takes advantage of such condition as it resembles boundary conditions which are closer to the one described in the theory of response factors. Thus, in contrast with ISO 9869, the EPM is especially suitable for mid-season and summer periods (with low temperature gradient across the wall) and is highly advantageous to be used in such cases, provided that the sample is not outside the methods working range.

Prior to any in-situ measurements with heat flux sensors and thermocouples, IR thermography is essential to inspect the homogeneity of the flux and temperature on the surface of the sample. Along the same line, using average values obtained from multiple sensors are clearly advantageous.

7.3 Recommendations for future studies

In-situ measurements are crucial to take place in different levels. Accordingly, this study and the ones alike are highly recommended to be pursued. To achieve rapid determination of exterior walls' thermo-physical properties, EPM is a suitable choice, provided that the conditions are within the method's application range. Upon construction of higher-quality instrumentation, further research on the application of EPM is recommended. It is highly recommended to advance and further study the EPM in multi-layered walls and study their properties through inverse modelling of the multi-layered walls' RFs equations in order to determine their thermal performance.

Where large-scale measurements are needed, more investment on simple methods such as the ISO 9869's "Average Method" and the extension provided in this thesis are recommended. Such approach, despite its existing shortcomings, has the advantage that it can be performed more often and by more professionals. This will lead to the promotion of in-situ measurements rather than relying on calculations or even worse, appearance-based guesses.

The use of actual residential building data showed many challenges ever since the users can and do highly affect the parameters in unknown unpredictable manners. Accordingly, it is recommended to invest and focus much more on the actual data obtained from the residential sector. Using synthesis data as shown in many pieces of research, leads to advancements of the characterization models and methods. However, since the computer programs fail to simulate the reality of user behavior, the use of this data cannot lead one to tackle the challenges associated with the actual system. Similarly, using office buildings' data, a model cannot be trained as difficult as the one from a residential building since the former bears a less sophisticated behavior than the latter, in terms of users and systems. This is due to the fact that commercial buildings and office buildings possess larger spaces, are centrally controlled, and have a well-defined occupancy profile.

Researchers working with real data are advised to share the details of the data cleaning and practicalities of building their models. Practical details regarding issues such as data gathering, data filtering, and model execution have often been missing in the literature.

To follow up the study conducted in chapter 6, measuring surface temperatures and heat fluxes in all components are recommended in the future as it can help in two ways: separation of transmission losses from the heat loss coefficient and validating higher resolution models. Furthermore, it is highly recommended to measure the solar radiation inside the buildings and find the necessity of using this data when following different characterization methods. Along the same line, the use of night data is recommended, provided that the dynamic continuity of the system is modelled properly. Similarly, measurement of rates via a number of air flow meters (e.g. anemometers) is beneficial as it can reveal the validity of the methods which are claimed to separate the air exchange losses from the transmission losses when the heat loss coefficient is determined.

Finally, from a broader perspective, researchers and practitioners are recommended to avoid “one fit for all” solutions as it weakens the accuracy and decreases the effectiveness of the work. For instance, when measuring the thermal resistance of a cavity wall of unknown number of layers, the Extension method is a much better choice than the EPM whereas in a light homogeneous wall, it is vice versa. When measuring the thermal resistance for the same light wall during large temperature drifts and large temperature gradient across the wall, EPM is a less suitable choice than the extension as the circumstances deviate from the one in the theory of the method. Accordingly, the choice of methods, models, and approaches must solely depend on the instance and the present conditions.

Detailed circumstances in different households lead to high unexpected discrepancies between the expected and actual thermal and energy performance of the components and thus the entire buildings. Therefore, when seeking accurate absolute values, customized in-situ measurements are highly recommended.

TOC

Appendices

APPENDIX A

Mathematical Representation of the Required Conditions for Convergence of the two R_c-values to the Actual R_c-value When Applying the Extension to ISO 9869

In this appendix, mathematics is demonstrated, leading to the fact that under the satisfaction of certain practical conditions during in-situ measurements, the two R_c-value graphs from inside and outside heat fluxes will converge to the same value. In this case, the effect of heat storage is decayed and the convergence point is closest to the actual R_c-value.

By definition, the boundary heat flux at any arbitrary moment for a homogeneous wall can be derived from the temperature time-series of two surfaces 1 and 2, and

the time-series of thermal Response Factors X_i and Y_i. Let n be the highest index for the minimum required number of response factors:

$$\dot{q}_1^t = \sum_{i=0}^{n} X_i T_1^{t-i} - \sum_{i=0}^{n} Y_i T_2^{t-i} \quad ; \quad \dot{q}_2^t = \sum_{i=0}^{n} Y_i T_1^{t-i} - \sum_{i=0}^{n} X_i T_2^{t-i} \tag{A.1}$$

The cumulative heat fluxes for a period of $m \gg n$ hours on two sides can be calculated as the sum of the heat flux histories, each for their past n hours:

$$\begin{aligned}\sum_{j=0}^{m} \dot{q}_1^{t-j} &= \sum_{i=0}^{n} X_i T_1^{t-i} - \sum_{i=0}^{n} Y_i T_2^{t-i} + \sum_{i=0}^{n} X_i T_1^{t-i-1} - \sum_{i=0}^{n} Y_i T_2^{t-i-1} + \ldots \\ &+ \sum_{i=0}^{n} X_i T_1^{t-i-j} - \sum_{i=0}^{n} Y_i T_2^{t-i-j} + \ldots + \sum_{i=0}^{n} X_i T_1^{t-i-m} - \sum_{i=0}^{n} Y_i T_2^{t-i-m}\end{aligned} \tag{A.2}$$

$$\begin{aligned}\sum_{j=0}^{m} \dot{q}_2^{t-j} &= \sum_{i=0}^{n} Y_i T_1^{t-i} - \sum_{i=0}^{n} X_i T_2^{t-i} + \sum_{i=0}^{n} Y_i T_1^{t-i-1} - \sum_{i=0}^{n} X_i T_2^{t-i-1} + \ldots \\ &+ \sum_{i=0}^{n} Y_i T_1^{t-i-j} - \sum_{i=0}^{n} X_i T_2^{t-i-j} + \ldots + \sum_{i=0}^{n} Y_i T_1^{t-i-m} - \sum_{i=0}^{n} X_i T_2^{t-i-m}\end{aligned} \tag{A.3}$$

Which can also be presented in matrix form:

$$\begin{aligned}\sum_{j=0}^{m} \dot{q}_1^{t-j} &= \left[T_1^t \ldots T_1^{t-n}\right] \begin{bmatrix} X_0 \\ \vdots \\ X_n \end{bmatrix} - \left[T_2^t \ldots T_2^{t-n}\right] \begin{bmatrix} Y_0 \\ \vdots \\ Y_n \end{bmatrix} + \left[T_1^{t-1} \ldots T_1^{t-1-n}\right] \begin{bmatrix} X_0 \\ \vdots \\ X_n \end{bmatrix} - \left[T_2^{t-1} \ldots T_2^{t-1-n}\right] \begin{bmatrix} Y_0 \\ \vdots \\ Y_n \end{bmatrix} + \ldots \\ &+ \left[T_1^{t-j} \ldots T_1^{t-j-n}\right] \begin{bmatrix} X_0 \\ \vdots \\ X_n \end{bmatrix} - \left[T_2^{t-j} \ldots T_2^{t-j-n}\right] \begin{bmatrix} Y_0 \\ \vdots \\ Y_n \end{bmatrix} + \ldots + \left[T_1^{t-m} \ldots T_1^{t-m-n}\right] \begin{bmatrix} X_0 \\ \vdots \\ X_n \end{bmatrix} - \left[T_2^{t-m} \ldots T_2^{t-m-n}\right] \begin{bmatrix} Y_0 \\ \vdots \\ Y_n \end{bmatrix}\end{aligned} \tag{A.4}$$

$$\begin{aligned}\sum_{j=0}^{m} \dot{q}_1^{t-j} &= \left[T_1^t + T_1^{t-1} + \ldots + T_1^{t-j} + \ldots + T_1^{t-m} \quad \ldots \quad T_1^{t-n} + T_1^{t-1-n} + \ldots T_1^{t-j-n} + \ldots + T_1^{t-m-n}\right]_{1\times n} \begin{bmatrix} X_0 \\ \vdots \\ X_n \end{bmatrix}_{n\times 1} \\ &- \left[T_2^t + T_2^{t-1} \ldots + T_2^{t-j} + \ldots + T_2^{t-m} \ldots \quad T_2^{t-n} + T_2^{t-1-n} + \ldots T_2^{t-j-n} + \ldots + T_2^{t-m-n}\right]_{1\times n} \begin{bmatrix} Y_0 \\ \vdots \\ Y_n \end{bmatrix}_{n\times 1}\end{aligned} \tag{A.5}$$

Similarly, $\sum_{j=0}^{m}\dot{q}_2^{t-j}$ and the subtraction of two heat cumulative fluxes can be calculated and presented in summation form:

$$\sum_{j=0}^{m}\dot{q}_1^{t-j}=\left[\sum_{j=0}^{m}T_1^{t-j}\ldots\sum_{j=0}^{m}T_1^{t-n-j}\right]\begin{bmatrix}X_0\\ \vdots\\ X_n\end{bmatrix}-\left[\sum_{j=0}^{m}T_2^{t-j}\ldots\sum_{j=0}^{m}T_2^{t-n-j}\right]\begin{bmatrix}Y_0\\ \vdots\\ Y_n\end{bmatrix} \tag{A.6}$$

$$\sum_{j=0}^{m}\dot{q}_2^{t-j}=\left[\sum_{j=0}^{m}T_1^{t-j}\ldots\sum_{j=0}^{m}T_1^{t-n-j}\right]\begin{bmatrix}Y_0\\ \vdots\\ Y_n\end{bmatrix}-\left[\sum_{j=0}^{m}T_2^{t-j}\ldots\sum_{j=0}^{m}T_2^{t-n-j}\right]\begin{bmatrix}X_0\\ \vdots\\ X_n\end{bmatrix} \tag{A.7}$$

$$\sum_{j=0}^{m}\dot{q}_1^{t-j}-\sum_{j=0}^{m}\dot{q}_2^{t-j}=\left[\sum_{j=0}^{m}\left(T_1+T_2\right)^{t-j}\quad\sum_{j0}^{m}\left(T_1+T_2\right)^{t-i-j}\ldots\sum_{j=0}^{m}\left(T_1+T_2\right)^{t-n-j}\right]\left(\begin{bmatrix}X_0-Y_0\\ \vdots\\ X_n-Y_n\end{bmatrix}\right) \tag{A.8}$$

$$\sum_{j=0}^{m}\dot{q}_1^{t-j}-\sum_{j=0}^{m}\dot{q}_2^{t-j}=\overline{T}_{1,2}^{0}\left(X_0-Y_0\right)+\ldots+\overline{T}_{1,2}^{i}\left(X_i-Y_i\right)+\ldots+\overline{T}_{1,2}^{n}\left(X_n-Y_n\right)=\sum_{i=0}^{n}\overline{T}_{1,2}^{i}\left(X_i-Y_i\right) \tag{A.9}$$

Where $\overline{T}_{1,2}^{i}=\sum_{j=0}^{m}\left(T_1+T_2\right)^{t-i-j}$, the summation of the n-hour history of two surface temperatures in different time sequences of m hours.

Mathematically, equation 11 can only be equal to zero (showing then a system for which all energy coming in during a certain period of m also comes out during the same period) in 3 cases:

1 If $\left(X_i-Y_i\right)=0$, which is physically impossible or implies there is no excitation

2 If $\overline{T}_{1,2}^{i}=0$,which is only possible if all temperatures are at absolute zero

3 If $\overline{T}_{1,2}^{i}$ is constant.

If $\overline{T}_{1,2}^{i}$ is constant, it is referred to as $\overline{T}_{1,2}^{**}$ and can be treated out of the matrix as a coefficient.

$$\overline{T}_{1,2}^{i} = \sum_{i=0}^{m}\left(T_1+T_2\right)^{t-i} = \sum_{i=0}^{m}\left(T_1+T_2\right)^{t-i-1} = \ldots = \sum_{i=0}^{m}\left(T_1+T_2\right)^{t-n-i} = \overline{T}_{1,2}^{**} \tag{A.10}$$

There are four conditions by which $\overline{T}_{1,2}^{**}$ is constant:

1 For cyclic temperature profiles during monitoring period (e.g. multiple of $24\ h$), $T_1+T_2=cte$ and $\overline{T}_{1,2}^{**}=cte$

2 For steady state condition: $\partial T/\partial t=0$, thus $T_1=cte$, $T_2=cte$ and therefore $\overline{T}_{1,2}^{**}=cte$

3 For a relatively long monitoring period ($\mathrm{m}\rightarrow\infty$): $T_1+T_2=cte$ and therefore $\overline{T}_{1,2}^{**}=cte$

4 A combination of each two or all aforementioned conditions

Although the assumptions above are all within the explicitly mentioned measurement conditions of ISO 9869, they often cannot be satisfied. Conditions 1 and 2 (and therefore 4), usually cannot be satisfied during in-situ measurements due to the dynamic effects and temperature random fluctuations and noise. Thus, condition 3 will be needed to compensate for the other three. Accordingly, it is often seen that the monitoring period needs to be considerably long, becoming problematic in terms of feasibility.

According to (A.9) and (A.10):

$$\sum_{i=0}^{m}\dot{q}_1^{t-i}-\sum_{i=0}^{m}\dot{q}_2^{t-i}=\left[\overline{T}_{1,2}^{**}\ \ \ldots\ \ \overline{T}_{1,2}^{**}\right]\begin{bmatrix}X_0-Y_0\\ \vdots\\ X_n-Y_n\end{bmatrix}=\overline{T}_{1,2}^{**}\left(\left[1\right]_{1\times n}\begin{bmatrix}X_0-Y_0\\ \vdots\\ X_n-Y_n\end{bmatrix}_{n\times 1}\right) \tag{A.11}$$

From the theory of thermal Response Factors and energy conservation:

$$\sum_{i=0}^{\infty}X_i-\sum_{i=0}^{\infty}Y_i=\sum_{i=0}^{m}X_i-\sum_{i=0}^{m}Y_i=\sum_{i=0}^{n}X_i-\sum_{i=0}^{n}Y_i=0 \tag{A.12}$$

According to (A.11) and (A.12), the subtraction of the two cumulative heat fluxes over a long-enough measurement period is equal to zero (also implied by conservation of energy):

$$\sum_{i=0}^{m}\dot{q}_1^{t-i}-\sum_{i=0}^{m}\dot{q}_2^{t-i}=\overline{T}_{1,2}^{**}\left(\left[1\right]_{1\times n}\begin{bmatrix}X_0-Y_0\\ \vdots \\ X_n-Y_n\end{bmatrix}_{n\times 1}\right)=\overline{T}_{1,2}^{**}\left(\sum_{i=1}^{n}X_i-\sum_{i=1}^{n}Y_i\right)=0 \tag{A.13}$$

$$\sum_{i=0}^{m}\dot{q}_1^{t-i}=\sum_{i=0}^{m}\dot{q}_2^{t-i} \tag{A.14}$$

Where q_1 and q_2 are heat fluxes at the interior and exterior sides of the wall respectively. According to the aforementioned measurement conditions and (A.14), in long term, the two cumulative R_c-value are equal. Consequently, the average R_c-value also converges to the same final value:

$$R_{c-in}=\sum_{t=0}^{m}\Delta T^t/\sum_{t=0}^{m}\left(\dot{q}^t\right)_1=R_{c-out}=\sum_{t=0}^{m}\Delta T^t/\sum_{t=0}^{m}\left(\dot{q}^t\right)_2=R_{c-ave}=\left(R_{c-in}+R_{c-out}\right)/2 \tag{A.15}$$

At the convergence point, three graphs $R_{c\text{-}in}$, $R_{c\text{-}out}$, and $R_{c\text{-}ave}$ are closest to the actual R_c-value. This however, because the aforementioned conditions often are not satisfied in practice, takes a very long time to occur.

APPENDIX B

Further Implications in the ISO 9869's Proposed Extension

In this appendix, as an extension to Chapter 2, the results of the analysis of two additional modelled typologies are presented.

The material used in this appendix is a part of the following conference paper:

Rasooli, A., & Itard, L. C. M. (2019). Quicker measurement of walls' thermal resistance following an extension to ISO 9869 average method. In *CLIMA 2019: REHVA 13th HVAC World Congress*.

The first case shown here is a homogeneous wall similar to types 1a and 1b in Chapter 2 and the second one is a symmetrical cavity wall. The details of the constructions of the simulated walls including their layers and materials as well as their theoretical R_c-values (R_c^{th}) are summarized in Table APP.B.1.

TABLE APP.B.1 Construction and material properties used in the simulated walls: thickness (L), thermal conductivity (k), density (ρ), and specific heat capacity (C) of each layer. The estimated Rc-value is based on thermal properties

Type	Typology	Material(s)	R_c^{th}[m^2KW^{-1}]	Layer	L [m]	k [$Wm^{-1}K^{-1}$]	ρ [kgm^{-3}]	c [$Jkg^{-1}K^{-1}$]
1	Homogeneous	L1: Heavy Brick	0.91	L1	0.55	0.6	2400	840
2	3-Layered Cavity Wall	L1-L3: Brick	0.62	L1, L3	0.2	0.9	2000	840
		L2: Air Cavity		L2	0.08	0.021	35	1320

The results of the simulations are presented in Fig APP.B.1. The left figure refers to the homogeneous wall. In addition to the high thermal mass in this construction, the homogeneity of this construction results in a quite stable symmetrical heat flux profile at two sides and therefore, symmetrical curves of Rc-values for inside and outside surfaces. Accordingly, the average of the two profiles, as derived in Chapter 2, converges much more quickly to an accurate Rc-value. In both figures red and blue curves refer to Rc-values derived from indoor and outdoor heat fluxes respectively. The dashed black curve is the average of the two. Curves Rc-in and Rc-out are Rc1 and Rc2 (See Chapter 2).

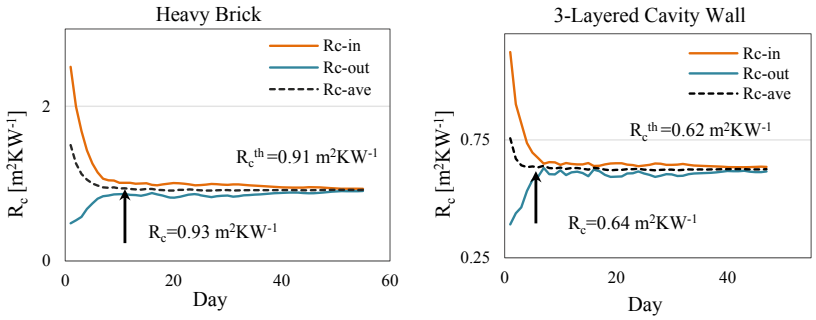

FIG. APP.B.1 The simulation results for the homogeneous heavy brick wall (left) and the 3-layered symmetrical cavity wall(right)

Note that in case of a thin homogeneous wall, the chance of finding symmetric profiles is lower. In such cases, with no problem of the measurement duration, the indoor heat flux results in a more stable R_c-value. In terms of the thermal resistance measurement, the behaviour of the common brickwork wall (Fig APP.B.1, left) is similar to the ones of red brick and concrete, reported in Chapter 2. As seen in Fig APP.B.1, the performance of the symmetrical cavity wall typology is similar to the one of homogeneous walls. Accordingly, the R_c-ave curve converges much more quickly to the correct value.

APPENDIX C

Set-Up and Execution of a Large-Scale Measurement Campaign

In this appendix, the setup of an extensive monitoring campaign (project OPSCHALER) of 100 houses in the Netherlands, from which the data is used in Chapter 6 is explained. The houses are inspected, the tenants fill in questionnaire and the measurement equipment are installed in all rooms by installers who are trained for the whole procedure. In addition to the smart data which is the pattern from the gas and electricity consumption, various parameters such as air properties (temperature, relative humidity, and CO_2 concentration), presence patterns of occupants, perceived comfort level of occupants, and more, are examined.

This appendix is an adapted version based on the following conference paper:

Rasooli, A., L. Itard, and A. Meijer, *Energy and Comfort Monitoring in Existing Buildings: A Large-Scale Measurement Campaign of 150 Dutch Dwellings*, in *ASHRAE 6th International Conference: ENERGY in BUILDINGS 2017*. 2017, ASHRAE: Athens, Greece.

C.1 Introduction

In the field of built environment, energy efficiency is a highlighted area, demanding special attention. Many studies have shown the difference between actual and theoretical energy consumption [4,167-170]. Follow-up studies have shown the most critical reasons for such difference, obtained by sensitivity analysis [2, 3, 171]. From the technical point of view, the thermo-physical properties, such as walls' thermal transmittance [64], and from behavioral point of view, occupant behavior due to thermal comfort have shown to play a significant role [172, 173]. Numerous researches have been carried out to study these matters through simulations. However, the accuracy of the input data being used, which are mostly assumed values, has always been under doubt. This is due to the difficulty of performing in-situ measurements in terms of time, costs, and effort. Therefore, projects including in-lab and in-situ experiments have become of high importance since they aid to collect more accurate data, directly measured from the field or in the lab. For the same reason, performing large scale measurement campaigns in the buildings are of high value. Of the main practical obstacles for performing such campaigns are the high expenses vs limited resources of funding and the willingness of people to participate and cooperate. Unlike other sections, in this appendix, the main focus is specially laid on the actual process of performing an extensive measurement campaign which took place in 100 Dutch houses. The step by step procedure is explained and the future plans and methods are briefly depicted.

ECOMMON (Energy and Comfort Monitoring) [17] is an on-going project from Delft University of Technology, started in 2014, aiming to measure, collect, and analyze data leading to more accurate energy consumption prediction in addition to better thermal comfort perceptions. The first phase of this project (2014-2016) had been accomplished in 35 houses [74, 174], where the scope was to especially focus on indoor air quality and thermal comfort monitoring. With the introduction of smart meters, there is now a huge potential available for analysis of the real-time energy consumption patterns. From the scientific point of view, the analysis of such patterns in parallel with real time measured data of other variables such as air temperature, can lead to invaluable information. Along the same line, measurement campaigns provide the opportunity to observe the correlations between measured data leading to thermal comfort, thermo-physical characteristics of the building, HVAC, and the energy consumption. Accordingly, at the second phase of ECOMMON [23], the aim was to lay a great emphasis on energy consumption, parallel to thermal comfort. With the introduction of smart meters, it is nowadays possible to log such data via the P1 port of the smart meters. Thus, the targeted houses for the latter phase of the project were the ones equipped with a smart meter. The houses were located in diverse areas in the Netherlands.

C.2 Execution of the Monitoring Campaign

The project consisted of two campaigns. The campaigns took place in different periods. In some of the houses, the measurements continued for a longer period. In a few houses, extensive measurements took place to gather more detailed data. The campaigns, the number of houses in each period, the number of long period measurements, and the number of extensive measurements is mentioned in Table APP.C.1.

TABLE APP.C.1 Detailed descriptions of the measurement campaigns

Campaign	Number of houses	Long-term	Extensive
Campaign 1	55	10	0
Campaign 2	45	0	5

The monitoring campaign consisted of various procedures. The first part was to inspect the houses in terms of energy efficiency and construction. This simply led to an approximated energy label. At the same time, the occupants filled in a questionnaire including questions about the salary scale, consumption habits, number of residents, hours of presence, and so on. Thereafter, the measurement sets were installed, according to a special protocol prepared for the installations. The whole procedure took in average, approximately 3 hours per house. In the following sections, the most relevant details and aspects of performing the measurement campaign are introduced and explained.

C.2.1 Team training

The installation team consisted of 20 students who were officially registered through university organizations providing students with part-time and short-term jobs. Before each campaign, the students followed a 2 full-day course. During the first day of the course, the students learned about building inspection, network connection and set up, and measurement equipment installation. They also learned about general aspects of energy and thermal comfort in buildings. During the second day, they practiced all they had learnt and were examined in a real house. This way, it was ensured that they were ready to go to people's houses. After this test, they were scheduled on a daily basis to visit houses for the campaign. Residents who wished

to participate in the campaign, had registered before on the corresponding website. Through the university, the appointments were scheduled for the installers to visit these houses. In each house, the following procedures took place.

C.2.2 Inspection of the houses

Before the installation began, the house was inspected in a variety of aspects. Floor plan, dimensions, types and thickness of the doors and windows and the insulation of the walls as well as the HVAC systems and the installations and many more relevant details were part of inspection. The inspection was energy-related and had theme similar to an energy labelling inspection. This, in addition to the valuable information (coupled with the measurement data) gave an opportunity for personalized advice to the occupants on how they can use their building more energy-efficient. Additionally, health-related (CO_2 concentration and temperature peaks) feedback and a corresponding advice were communicated.

C.2.3 Occupant survey

During the installation, the occupants were asked to fill in a survey. The questions of this survey were divided in four categories. The first part asked about general characteristics of the households, such as household composition, age and revenues. The second part was about the residents' heating and ventilation habits including thermostat settings, hours of ventilation in each room, and number of showers taken per day. The third part was about the overall comfort perception (warmth, cold, humidity, and draught) of their dwellings in winter and summer.

C.2.4 Installation for measurements

At the university, equipment fragments were prepared in boxes. Each box went to a house and the contents were installed in different rooms. Each box contained a router (to create an individual Wi-Fi network), a P1 port reader, a mini PC, a set of four TRHC (Temperature, Relative Humidity, CO_2) sensors (to measure air temperature, relative humidity, and CO_2 concentration), a set of four motion detectors, an RH (Relative Humidity) sensor for the bathroom, an electricity power

measurement apparatus (ELP), and antennas for making a wireless network. In Fig APP.C.1, the boxes and the contents are shown.

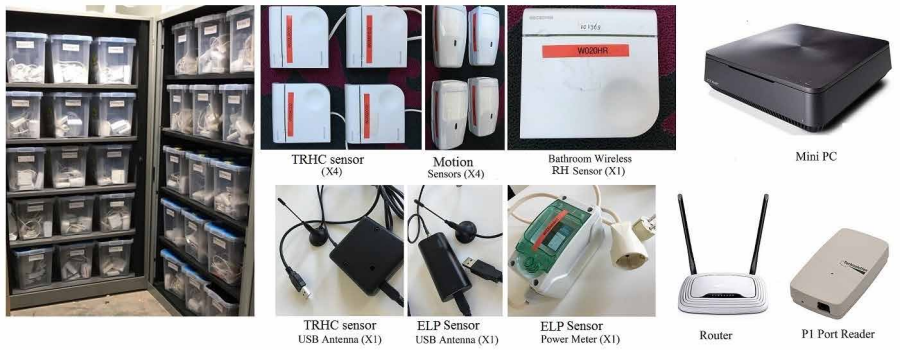

FIG. APP.C.1 The boxes with equipment inside: Each box was sent to one house and the equipment were installed. All the equipment are coded and labeled and coupled with the database.

C.2.5 Actual Energy Consumption

The main focus of the project was to collect and analyze the data from the actual energy consumption (from the P1 port of the smart meters). A P1 port reader [73] was installed at the P1 port of the smart meter to read out the gas and electricity consumption. This device communicates to the router through Wi-Fi. The P1 port reader streamed the data via a secure pathway to the university server, which stored them in the database

C.2.6 Indoor Air Properties

The TRHC sets measure the average air temperature, RH, and CO_2 concentration within the time intervals of 5 minutes. They connect via a wireless system to the antenna of the mini-PC. Each pair of these sensors with a motion sensor was installed in one room. The whole equipment was installed in 4 rooms: living room, kitchen, master bedroom, and secondary bedroom (child room or study room). The motion sensors detect motion, which in combination with CO_2 can lead to presence [175]. The measurements were logged every 5 minutes (Average value). Performing

such measurements provides data to be used in thermal comfort perception models as well as energy consumption predictions.

C.2.7 Electricity of the heating/ventilation system

The electricity (power) consumption for the heating system was measured via the ELP sensor. In case of an electrical heating system, combination of this data with the efficiency, leads to actual heating demand. In case of combination boilers which are very common, the separation of domestic hot water and space heating can be done using the power consumption of the boiler. In case of a balanced ventilation system, the fan's power consumption data next to the occupant survey, leads to a rough estimation of the ventilation rate.

C.2.8 Comfort Monitoring

The actual thermal comfort of the occupants is of high importance. Therefore, a Comfort App [76] was used to monitor the tenants' comfort. The occupants were provided with the app installed on their smartphones/tablets. They were given individual codes and instructions to log their relevant comfort related information. The comfort app asks about clothing, activities, and actual thermal comfort perception of the occupant. These data can be compared to the comfort prediction extracted from the data of the measurements. In Fig APP.C.2, an example of the aforementioned questions is shown.

FIG. APP.C.2 An example of the questions asked in the comfort app: The occupants fill the app occasionally and the data is saved in the servers for further comparison and analysis.

For privacy reasons, the app works only with specific codes, given to the occupants in order to keep the process anonymous. The code is coupled with the house number in order to analyze and compare the data with app responses.

C.2.9 Privacy

Within monitoring projects, privacy is a key issue. Therefore, the privacy measures were applied under the regulations of the university's ethical committee. The raw data contained private data such as address data that can relate the data to specific people. Before analysis, the address data were deleted and replaced by a random dwelling code. This code was used to combine data from different sources (meter readings, sensor data, comfort data and inspection data). During data collection, the sensor data were stored on a local computer and backed up via a secure internet connection to a server, specifically set up for this project. The meter readings were streamed via a secured internet connection to the same server and stored in a database. All data collection and handling complied to the Dutch privacy regulations.

In Fig APP.C.3, the installation setup is shown. The modem of the house is the interface between the university database and the measurement network. The data was sent on a daily basis to the servers of the university.

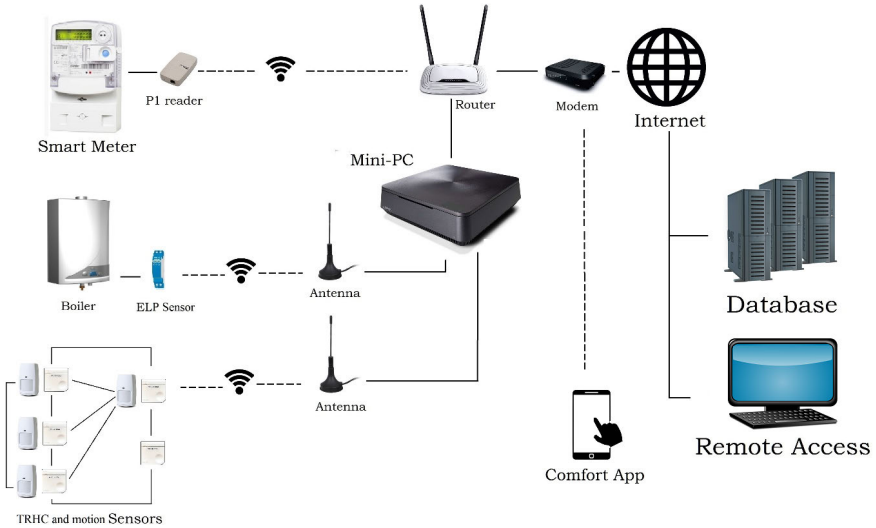

FIG. APP.C.3 Schematic representation of the equipment installed in each house. Dashed lines indicate wireless connection and the solid lines indicate wired connection. The data was stored daily at the database and live remote access had been available for assistance.

C.2.10 Uninstallation

After each campaign, teams were sent to uninstall the equipment. The teams followed special manuals on how to collect the equipment appropriately. The occupants were asked to give feedback and they were offered a small gift for their participation. This procedure was often quick and took approximately 30 minutes per house.

C.2.11 Accuracy of the measurements

Alongside every measurement to be carried out, there is always a concern for accuracy. Depending on the type of analysis, the importance of the accuracy level magnifies. In cases where the analysis is to be done using the absolute values rather than the profile trend, the accuracy is more critical.

TOC

Sensors' Accuracy

The CO_2 sensors were the NDIR (nondispersive infrared sensors) with +/- 50 ppm accuracy. The RH sensors had an accuracy of 3%. The temperature sensors were the KT Thermistor type with an accuracy of 1% per °C. Motion sensors covered a range of 11 × 12 m (range at 2.3 m mounting height) [174]. To ensure minimum measurement error, the sensors were mounted in each room at a location which is the most representative for the whole room in terms of air properties and motion.

Sensors' Calibration

The main challenge with calibration of sensors for such a large-scale campaign is the quantity vs the extremely-high costs for in-lab calibrations. The total number of sensors of temperature, relative humidity, and CO_2 equaled 780. This number of sensors could only be calibrated with a very careful and well-planned procedure. The calibration has taken place in a small room that is prepared to behave similar to a climate chamber. A convectional heater and a humidifier were placed in the middle of the room, under a main table where the sensors were placed with a certain distance with each other and the same conditions (Fig C.4). In the corners of the room, fans are placed to ensure perfect mixing of the air. At the same time, it was ensured that the sensors had not been exposed to any excess form of direct heat/humidity/air movement. Two pre-calibrated sensors (calibrated in a company with a calibration certificate) are placed on two different points of the table to assure consistency of air properties for the whole measurement area. A good agreement was observed between the values measured by the two pre-calibrated sensors, showing the consistency of the properties in the well-mixed air. The data has been measured and the average was logged every 5 minutes. The process, similar to the climate chamber, included hours of constant equilibrium for each calibration point.

FIG. APP.C.4 The setup of calibration: the sensors are placed with a certain distance with each other, measuring the changes in air properties. The air is well mixed to ensure consistency of its properties.

The calibration curves have been generated using two points, the first one related to high RH and low temperature and the second point related to low RH and high temperature (Table APP.C.2). The sensors were custom made and therefore, could not be tuned. However, by using the calibration curve (line), the measured data could be corrected before analysis.

TABLE APP.C.2 Two-Point Calibration Details

Calibration Points	Temperature	RH (%)	CO_2 (ppm)
Point 1	Low (20 °C)	High (70%)	Constant (~500 ppm)
Point 2	High (35 °C)	Low (40%)	Constant (~500 ppm)

C.2.12 Extensive measurements

In two sample houses, in the whole campaign, additional measurements took place. The R-value of a wall was measured following the ISO 9869 method [6]. From the thermal comfort aspect, the mean radiant temperature, air velocity, PMV, and PPD were measured via a local micro-climate unit. Furthermore, local meteorological measurements took place for one year in one of the houses. These buildings were selected from the ones under long-term monitoring. The tenants agreed with each and every step of this procedure since such measurements give a far better impression of the thermal behavior of the building and the comfort of its occupants.

C.3 Outcomes and Reflections

The project has led to a large set of data. The campaigns drew great attention from the researchers, professionals, and experts in the field of HVAC and energy efficiency as well as others who are interested in areas alike. The importance of large-scale in-situ measurements for collection of real-time accurate data is of no doubt.

The major process outcome of the campaigns related to the trade-off between expectations and reality during a practical work. The most critical aspects for performing the campaign included the logistics, planning, transport, equipment

numbering, labeling, training, organization, and communication. From the installations there are a variety of lessons learned. People generally tended to be cooperative with this research. Most people were very interested in the research and asked many relevant questions about measurements, data gathering and analysis outcomes. Few participants were slightly concerned about the motion sensors installed in their bedrooms. However, once explained by the installers that these sensors only log 0 and 1, they were convinced to have them running. People were mostly curious about the rooms' air temperature (as an indication for their energy use and their thermostat settings). Additionally, due to health concerns, people were also interested to know about their rooms' CO_2 levels during different times of the day.

References

[1] Recast, E., (2010) Directive 2010/31/EU of the European Parliament and of the Council of 19 May 2010 on the energy performance of buildings (recast). Official Journal of the European Union. 18(06).

[2] Majcen, D., L. Itard, and H. Visscher (2013), Actual and theoretical gas consumption in Dutch dwellings: What causes the differences? *Energy Policy*, . ***61***: 460-471.

[3] Ioannou, A. and L. Itard (2015), Energy performance and comfort in residential buildings: Sensitivity for building parameters and occupancy. *Energy and Buildings*. ***92***: 216-233.

[4] van den Brom, P., A. Meijer, and H. Visscher (2018), Performance gaps in energy consumption: household groups and building characteristics. *Building Research & Information,* ***46(1)***: 54-70.

[5] Majcen, D., L. Itard, and H. Visscher (2013), Theoretical vs. actual energy consumption of labelled dwellings in the Netherlands: Discrepancies and policy implications. *Energy policy*. ***54:*** 125-136.

[6] ISO, E. (2014), 9869: 1 Thermal insulation—Building elements—In-situ measurements of thermal resistance and thermal transmittance. International Organization for Standardization, Geneva.

[7] ASTM, C., 1046-95 (Reapproved 2001): Standard practice for in-situ measurement of heat flux and temperature on building envelope components. Annual Book of ASTM Standards, 2001. 4.

[8] ASTM, C., 1155-95 (Reapproved 2001): Standard practice for determining thermal resistance of building envelope components from the in-situ data. Annual Book of ASTM Standards, 2001. 4.

[9] Soares, N., Martins, C., Gonçalves, M., Santos, P., da Silva, L. S., & Costa, J. J. (2019). Laboratory and in-situ non-destructive methods to evaluate the thermal transmittance and behavior of walls, windows, and construction elements with innovative materials: A review. *Energy and Buildings*, ***182***, 88-110.

[10] ISO, E. (2007), 6946: Building components and building elements. Thermal resistance and thermal transmittance. Calculation method.

[11] ISO, E. (2007), 10211: Thermal bridges in building construction–Heat flows and surface temperatures–detailed calculations (ISO 10211: 2007), CEN.

[12] ISO, E. (2007), 13786: 2007-Thermal performance of building components--Dynamic thermal characteristics--Calculation methods. CEN. European Committee for Standardization. 27.

[13] ISO, E. (1991), 8302: Thermal Insulation –Determination of Steady-State Thermal Resistance and Related Properties –Guarded Hot Plate Apparatus, International Standard Organization, International Organization for Standardization.

[14] ISO, B. (1996), 8990: 1996, Thermal insulation. Determination of steady-state thermal transmission properties. Calibrated and guarded hot box, BSI, ISBN 0, . 580(26826): p. 8.

[15] ISO, E. (2018), 9869: 2 Thermal insulation — Building elements — In-situ measurement of thermal resistance and thermal transmittance — Part 2: Infrared method for frame structure dwelling. International Organization for Standardization, Geneva.

[16] Atsonios, I. A., Mandilaras, I. D., Kontogeorgos, D. A., & Founti, M. A. (2017). A comparative assessment of the standardized methods for the in–situ measurement of the thermal resistance of building walls. *Energy and Buildings*, ***154***, 198-206..

[17] Cesaratto, P.G., M. De Carli, and S. Marinetti (2011), Effect of different parameters on the in situ thermal conductance evaluation. *Energy and Buildings*, ***43(7)***:1792-1801.

[18] Wang, F., Wang, D., Wang, X., & Yao, J. (2010). A data analysis method for detecting wall thermal resistance considering wind velocity in situ. *Energy and Buildings*, ***42(10)***, 1647-1653.

[19] Deconinck, A.-H. and S. Roels (2016), Comparison of characterisation methods determining the thermal resistance of building components from onsite measurements. *Energy and Buildings*, ***130***: 309-320.

[20] Deconinck, A.-H. (2017), Reliable thermal resistance estimation of building components from on-site measurements. PhD Dissertation, KU Leuven: Belgium.

[21] Gori, V., Marincioni, V., Biddulph, P., & Elwell, C. A. (2017). Inferring the thermal resistance and effective thermal mass distribution of a wall from in situ measurements to characterise heat transfer at both the interior and exterior surfaces. *Energy and Buildings*, ***135***, 398-409..

[22] Ahmad, A., M. Maslehuddin, and L.M. Al-Hadhrami (2014), In situ measurement of thermal transmittance and thermal resistance of hollow reinforced precast concrete walls. *Energy and Buildings*, ***84***: 132-141.

[23] Desogus, G., S. Mura, and R. Ricciu (2011), Comparing different approaches to in situ measurement of building components thermal resistance. *Energy and Buildings*. ***43(10)***: 2613-2620.

[24] Chaffar, K., Chauchois, A., Defer, D., & Zalewski, L. (2014). Thermal characterization of homogeneous walls using inverse method. *Energy and buildings*, ***78***, 248-255..

[25] Deconinck, A.-H. and S. Roels (2017), The as-built thermal quality of building components: characterising non-stationary phenomena through inverse modelling. *Energy Procedia*. ***132***: 351-356.

[26] Baker, P. (2011), Technical Paper 10: U-values and traditional buildings-In situ measurements and their comparisons to calculated values. technical report.

[27] Lucchi, E. (2018), Applications of the infrared thermography in the energy audit of buildings: A review. *Renewable and Sustainable Energy Reviews*. ***82***: 3077-3090.

[28] ISO, E. (1983), 6781: Thermal insulation: Qualitative detection of thermal irregularities in building envelopes-Infrared method, International Organization for Standardization Berlín.

[29] Annex 71 (2017), IEA EBC Annex 71: building energy performance assessment based on in situ measurements.

[30] Lee, Y. M., An, L., Liu, F., Horesh, R., Chae, Y. T., & Zhang, R. (2013). Applying science and mathematics to big data for smarter buildings. *Annals of the NEW YORK Academy of Sciences*, ***1295(1)***, 18-25..

[31] Senave, M., Roels, S., Reynders, G., Verbeke, S., & Saelens, D. (2020). Assessment of data analysis methods to identify the heat loss coefficient from on-board monitoring data. *Energy and Buildings*, ***209***, 109706.

[32] Bacher, P. and H. Madsen (2011), Identifying suitable models for the heat dynamics of buildings. Energy and Buildings. ***43(7)***: 1511-1522.

[33] Zhang, Y., O'Neill, Z., Dong, B., & Augenbroe, G. (2015). Comparisons of inverse modeling approaches for predicting building energy performance. *Building and Environment*, ***86***, 177-190..

[34] An, L., Chae, Y. T., Horesh, R., Lee, Y., & Zhang, R. (2013, December). An inverse PDE-ODE model for studying building energy demand. In 2013 Winter Simulations Conference (WSC) (pp. 1869-1880). IEEE.

[35] González-Vidal, A., Ramallo-González, A. P., Terroso-Sáenz, F., & Skarmeta, A. (2017, December). Data driven modeling for energy consumption prediction in smart buildings. In 2017 IEEE International Conference on Big Data (Big Data) (pp. 4562-4569). IEEE.

[36] Gori, V. and C.A. Elwell (2018), Estimation of thermophysical properties from in-situ measurements in all seasons: Quantifying and reducing errors using dynamic grey-box methods. *Energy and Buildings*, ***167***: 290-300.

[37] Andrade-Cabrera, C., De Rosa, M., Kathirgamanathan, A., Kapetanakis, D. S., & Finn, D. (2018, May). A Study on the Trade-off between Energy Forecasting Accuracy and Computational Complexity in Lumped Parameter Building Energy Models. In The 10th Canada conference of International Building Performance Simulation Association (eSim 2018), Montreal, Canada, 9-10 May 2018. IBPSA.

[38] An, L., Chae, Y. T., Horesh, R., Lee, Y. M., & Reddy, C. K. (2013). U.S. Patent No. 8,620,632. Washington, DC: U.S. Patent and Trademark Office.

[39] Zeifman, M., A. Lazrak, and K. Roth (2019), Residential retrofits at scale: opportunity identification, saving estimation, and personalized messaging based on communicating thermostat data. *Energy Efficiency*.

[40] Ramallo-González, A. P., Brown, M., Gabe-Thomas, E., Lovett, T., & Coley, D. A. (2018). The reliability of inverse modelling for the wide scale characterization of the thermal properties of buildings. *Journal of Building Performance Simulation*, ***11(1)***, 65-83.

[41] Park, H., Ruellan, M., Bouvet, A., Monmasson, E., & Bennacer, R. (2011, October). Thermal parameter identification of simplified building model with electric appliance. In 11th International Conference on Electrical Power Quality and Utilisation (pp. 1-6). IEEE.

[42] Park, H., Martaj, N., Ruellan, M., Bennacer, R., & Monmasson, E. (2013). Modeling of a building system and its parameter identification. *Journal of Electrical Engineering & Technology*, ***8(5)***, 975-983.

[43] Farmer, D., D. Johnston, and D. Miles-Shenton (2016), Obtaining the heat loss coefficient of a dwelling using its heating system (integrated coheating). *Energy and Buildings*, ***117***: 1-10.

[44] Bauwens, G. (2015), In Situ Testing of a Building's Overall Heat Loss Coefficient-Embedding Quasi-stationary and Dynamic Tests in a Building Physical and Statistical Framework, PhD thesis, KU Leuven, Belgium.

[45] Roels, S., Bacher, P., Bauwens, G., Castaño, S., Jiménez, M. J., & Madsen, H. (2017). On site characterisation of the overall heat loss coefficient: Comparison of different assessment methods by a blind validation exercise on a round robin test box. *Energy and Buildings*, ***153***, 179-189..

[46] Senave, M., Roels, S., Verbeke, S., Lambie, E., & Saelens, D. (2019). Sensitivity of characterizing the heat loss coefficient through on-board monitoring: A case study analysis. *Energies*, ***12(17)***, 3322.

[47] Senave, M., Reynders, G., Bacher, P., Roels, S., Verbeke, S., & Saelens, D. (2019). Towards the characterization of the heat loss coefficient via on-board monitoring: Physical interpretation of ARX model coefficients. *Energy and Buildings*, ***195***, 180-194..

[48] van Schijndel, J. and S. Uittenbosch (2011). Determination of Hygrothermal Properties for Building Materials using Inverse Modeling Techniques. in 9th Nordic Symposium on Building Physics-NSB 2011, Tampere, Finland, 29 May-2 June, 2011.

[49] Annex 58 (2016), IEA-EBC Annex 58: Reliable building energy performance characterisation based on full scale dynamic measurements.

[50] Choi, D. S., & Ko, M. J. (2019). Analysis of Convergence Characteristics of Average Method Regulated by ISO 9869-1 for Evaluating In Situ Thermal Resistance and Thermal Transmittance of Opaque Exterior Walls. *Energies*, ***12(10)***, 1989.

[51] COMSOL Multiphysics® v. 5.3.a www.comsol.com. COMSOL AB, S., Sweden.

[52] MATLAB, M., MATLAB R2018b. The MathWorks: Natick, MA, USA, 2018.

[53] Belussi, L., Danza, L., Meroni, I., & Salamone, F. (2015). Energy performance assessment with empirical methods: Application of energy signature. *Opto-Electronics Review*, ***23(1)***, 85-89.

[54] Yang, Y. (2017), Innovative non-destructive methodology for energy diagnosis of building envelope, Bordeaux.

[55] Filippidou, F., Nieboer, N., & Visscher, H. (2019). Effectiveness of energy renovations: a reassessment based on actual consumption savings. Energy Efficiency, ***12(1)***, 19-35.

[56] Jiménez, M. J., Madsen, H., & Andersen, K. K. (2008). Identification of the main thermal characteristics of building components using MATLAB. Building and Environment, ***43(2)***, 170-180.

[57] Gutschker, O. (2008). Parameter identification with the software package LORD. Building and Environment, ***43(2)***, 163-169.

[58] Peng, C., & Wu, Z. (2008). In situ measuring and evaluating the thermal resistance of building construction. *Energy and Buildings*, ***40(11)***, 2076-2082.

[59] Cesaratto, P. G., & De Carli, M. (2013). A measuring campaign of thermal conductance in situ and possible impacts on net energy demand in buildings. *Energy and Buildings*, ***59***, 29-36.

[60] Biddulph, P., Gori, V., Elwell, C. A., Scott, C., Rye, C., Lowe, R., & Oreszczyn, T. (2014). Inferring the thermal resistance and effective thermal mass of a wall using frequent temperature and heat flux measurements. *Energy and Buildings*, ***78***, 10-16.

[61] Flood, C., L. Scott, and C. Architects (2016), In Situ Thermal Transmittance of Case Studies in Dublin.

[62] Peng, C., & Wu, Z. (2008). In situ measuring and evaluating the thermal resistance of building construction. *Energy and Buildings*, ***40(11)***, 2076-2082.

[63] Baker, P. (2008), Technical Paper 2: In situ U-value measurements in traditional buildings–preliminary results.

[64] Rasooli, A., Itard, L., & Ferreira, C. I. (2016). A response factor-based method for the rapid in-situ determination of wall's thermal resistance in existing buildings. *Energy and Buildings*, ***119***, 51-61.

[65] Meng, X., Luo, T., Gao, Y., Zhang, L., Shen, Q., & Long, E. (2017). A new simple method to measure wall thermal transmittance in situ and its adaptability analysis. *Applied Thermal Engineering*, ***122***, 747-757.

[66] Martín, K., Flores, I., Escudero, C., Apaolaza, A., & Sala, J. M. (2010). Methodology for the calculation of response factors through experimental tests and validation with simulation. *Energy and Buildings*, ***42(4)***, 461-467.

[67] Sala, J. M., Urresti, A., Martín, K., Flores, I., & Apaolaza, A. (2008). Static and dynamic thermal characterisation of a hollow brick wall: Tests and numerical analysis. *Energy and Buildings*, ***40(8)***, 1513-1520.

[68] Yesilata, B., & Turgut, P. (2007). A simple dynamic measurement technique for comparing thermal insulation performances of anisotropic building materials. *Energy and Buildings*, ***39(9)***, 1027-1034.

[69] Agarwal, K. N., & Verma, V. V. (1967). A quick method of measuring thermal conductivity and thermal diffusivity of building fabrics. *Building Science,* ***2(2)***, 165-172.

[70] Robinson, A. J., Lesage, F. J., Reilly, A., McGranaghan, G., Byrne, G., O'hegarty, R., & Kinnane, O. (2017). A new transient method for determining thermal properties of wall sections. *Energy and Buildings*, ***142***, 139-146.
[71] Baldinelli, G. (2010). A methodology for experimental evaluations of low-e barriers thermal properties: Field tests and comparison with theoretical models. *Building and Environment*, ***45(4)***, 1016-1024.
[72] Deconinck, A. H., & Roels, S. (2017). Is stochastic grey-box modelling suited for physical properties estimation of building components from on-site measurements?. *Journal of Building Physics*, ***40(5)***, 444-471.
[73] Gaspar, K., Casals, M., & Gangolells, M. (2016). A comparison of standardized calculation methods for in situ measurements of façades U-value. *Energy and Buildings*, ***130***, 592-599.
[74] Al-Homoud, M. S. (2005). Performance characteristics and practical applications of common building thermal insulation materials. *Building and environment*, ***40(3)***, 353-366.
[75] COMSOL Multiphysics® v. 5.2. www.comsol.com. COMSOL AB, S., Sweden.
[76] Kersten, B. and J. van Schijndel (2013). Modeling the Heat Exchange in Cavities of Building Constructions Using COMSOL Multiphysics®. in Excerpt from the proceedings of the 2013 COMSOL Conference in Rotterdam. Rotterdam, Netherlands.
[77] ISSO, 60, (2005), U en R-waarden van bouwkundige constructies ISSO publicatie.
[78] Hukseflux Thermal Sensors BV, www.hukseflux.com, Delft, the Netherlands.
[79] Rasooli, A., L. Itard, and C. Infante. Ferreira (2016), Rapid, transient, in-situ determination of wall's thermal transmittance. *REHVA European HVAC Journal*, ***53***: 16-20.
[80] ISSO, 82.3 (2011), Energieprestatie Advies Woningen Formulerstructuur, ISSO publicatie.
[81] ISSO, 60 (2005), U en R-waarden van bouwkundige constructies, ISSO publicatie
[82] ISSO, 82.1 (2011) , Energieprestatie Advies Woningen Energielabel + algemeen deel, ISSO publicatie.
[83] EBC. International Energy Agency's Energy in Buildings and Communities Programme. [cited 2014 December]; Available from: http://www.iea-ebc.org/.
[84] Mitalas, G. P. (1967). Room thermal response factors. *ASHRAE Transaction*, ***73***: 1-10.
[85] ORNL. Advanced Wall Systems: Hotbox Test R-value Database. [cited 2014 5 Dec]; Available from: http://web.ornl.gov/sci/roofs+walls/AWT/Ref/TechHome.htm.
[86] Kosny, J., Christian, J. E., Desjarlais, A. O., Kossecka, E., & Berrenberg, L. (1998). The performance check between whole building thermal performance criteria and exterior wall measured clear wall R-value, thermal bridging, thermal mass, and airtightness (No. ORNL/CP-98419; CONF-980650-). Oak Ridge National Lab., Buildings Technology Center, TN (United States).
[87] Baker, P. (2004), IQ-test—improving quality in testing and evaluation of solar and thermal characteristics of building components. Energy and buildings, ***36(5)***: 435-441.
[88] Jiménez, M.J., B. Porcar, and M.R. Heras (2009), Application of different dynamic analysis approaches to the estimation of the building component U value. *Building and Environment*, ***44(2)***: 361-367.
[89] Roulet, C., J. Gass, and I. Marcus (1987), In situ U-value measurement: reliable results in shorter time by dynamic interpretation of the measured data. Thermal Performance of the Exterior Envelopes of Buildings III, 777-784.
[90] Flanders, S. (1992), The Convergence Criterion in Measuring Building R-Values. Thermal Performance of the Exterior Envelopes of Buildings V, 204-209.
[91] Trust, E.S. (2015), Post-construction testing – a professionals guide to testing housing for energy efficiency (2005 edition).
[92] Genova, E., & Fatta, G. (2018). The thermal performances of historic masonry: In-situ measurements of thermal conductance on calcarenite stone walls in Palermo. *Energy and Buildings*, ***168***, 363-373.
[93] Doran, S., Kilbride, B. E., Director, P., & Kilbride, E. (2000). Field investigations of the thermal performance of construction elements as built 36/8/79 cc1637 Final Report.
[94] Asdrubali, F., D'Alessandro, F., Baldinelli, G., & Bianchi, F. (2014). Evaluating in situ thermal transmittance of green buildings masonries—A case study. *Case Studies in Construction Materials*, ***1***, 53-59.
[95] Rye, C., & Scott, C. (2012). The SPAB research report 1: U-value report. Society for the Protection of Ancient Buildings: London, UK.
[96] Stevens, G. and J.D. Russill (2013), U-value insulation England's field trial of solid wall insulation. ECEEE Summer Study: Rethink, Renew, Restart.

[97] Li, F. G., Smith, A. Z. P., Biddulph, P., Hamilton, I. G., Lowe, R., Mavrogianni, A., ... & Summerfield, A. J. (2015). Solid-wall U-values: heat flux measurements compared with standard assumptions. *Building Research & Information*, ***43(2)***, 238-252.

[98] Grinzato, E., Vavilov, V., & Kauppinen, T. (1998). Quantitative infrared thermography in buildings. *Energy and Buildings*, ***29(1)***, 1-9.

[99] Balaras, C. A., & Argiriou, A. A. (2002). Infrared thermography for building diagnostics. *Energy and buildings*, ***34(2)***, 171-183.

[100] Fokaides, P. A., & Kalogirou, S. A. (2011). Application of infrared thermography for the determination of the overall heat transfer coefficient (U-Value) in building envelopes. *Applied energy*, ***88(12)***, 4358-4365.

[101] Clarke, J. A., & Clarke, J. A. (2001). Energy simulation in building design. Routledge.

[102] Hittle, D. (1992), Response Factors and Conduction Transfer Functions, www.web.mit.edu.

[103] ISSO, Kleintje (2007), U en Rc-waarden van bouwkundige constructies, ISSO publicatie.

[104] Harrison, D.M. (2001), Error Analysis in Experimental Physical Science, Department of Physics, Editor, University Of Toronto.

[105] Rasooli, A., & Itard, L. (2018). In-situ characterization of walls' thermal resistance: An extension to the ISO 9869 standard method. *Energy and Buildings*, ***179***, 374-383.

[106] Stephenson, D. G., & Mitalas, G. P. (1967). Cooling load calculations by thermal response factor method. *ASHRAE Transactions*, ***73(1)***, 1-7.

[107] Kossecka, E., & Kosny, J. (2005). Three-dimensional conduction z-transfer function coefficients determined from the response factors. *Energy and Buildings*, ***37(4)***, 301-310.

[108] Stewart, D. B. (1981). Time-domain transient thermal response of structural elements. *Building and Environment*, ***16(2)***, 87-91.

[109] Filippidou, F., Nieboer, N., & Visscher, H. (2016). Energy efficiency measures implemented in the Dutch non-profit housing sector. *Energy and Buildings*, ***132***, 107-116.

[110] Evola, G., & Marletta, L. (2015). The Solar Response Factor to calculate the cooling load induced by solar gains. *Applied Energy*, ***160***, 431-441.

[111] Liu, Y., Yang, L., Zheng, W., Liu, T., Zhang, X., & Liu, J. (2018). A novel building energy efficiency evaluation index: Establishment of calculation model and application. *Energy conversion and management*, ***166***, 522-533.

[112] ASTM (1993), Standard test method for steady-state heat flux measurements and thermal transmission properties by means of the guarded-hot-plate apparatus.

[113] Asdrubali, F., & Baldinelli, G. (2011). Thermal transmittance measurements with the hot box method: Calibration, experimental procedures, and uncertainty analyses of three different approaches. *Energy and buildings*, ***43(7)***, 1618-1626.

[114] Ghosh, A., Ghosh, S., & Neogi, S. (2014). Performance evaluation of a guarded hot box U-value measurement facility under different software based temperature control strategies. *Energy Procedia*, ***54***, 448-454.

[115] Baldinelli, G., Bianchi, F., Lechowska, A. A., & Schnotale, J. A. (2018). Dynamic thermal properties of building components: Hot box experimental assessment under different solicitations. *Energy and Buildings*, ***168***, 1-8..

[116] Tadeu, A., Simoes, N., Simões, I., Pedro, F., & Škerget, L. (2015). In-situ thermal resistance evaluation of walls using an iterative dynamic model. *Numerical Heat Transfer, Part A: Applications*, ***67(1)***, 33-51.

[117] Aversa, P., Palumbo, D., Donatelli, A., Tamborrino, R., Ancona, F., Galietti, U., & Luprano, V. A. M. (2017). Infrared thermography for the investigation of dynamic thermal behaviour of opaque building elements: Comparison between empty and filled with hemp fibres prototype walls. *Energy and Buildings*, ***152***, 264-272.

[118] Albatici, R., Tonelli, A. M., & Chiogna, M. (2015). A comprehensive experimental approach for the validation of quantitative infrared thermography in the evaluation of building thermal transmittance. *Applied energy*, ***141***, 218-228.

[119] Buratti, C., & Moretti, E. (2005, April). Thermal resistance of masonry walls: in situ measurements. In 6th World Conference on Experimental Heat Transfer, Fluid Mechanics and Thermodynamics.

[120] Laurenti, L., Marcotullio, F., & De Monte, F. (2004). Determination of the thermal resistance of walls through a dynamic analysis of in-situ data. *International Journal of Thermal Sciences*, ***43(3)***, 297-306.

[121] Roulet, C., Gass, J., & Marcus, I. (1987). In situ U-value measurement: reliable results in shorter time by dynamic interpretation of the measured data. Thermal Performance of the Exterior Envelopes of Buildings III; ASHRAE Transactions: Atlanta, GA, USA, 777-784.

[122] Reilly, A., & Kinnane, O. (2017). The impact of thermal mass on building energy consumption. *Applied Energy*, ***198***, 108-121.

[123] Corrado, V., & Paduos, S. (2016). New equivalent parameters for thermal characterization of opaque building envelope components under dynamic conditions. *Applied energy*, ***163***, 313-322.
[124] Petojević, Z., Gospavić, R., & Todorović, G. (2018). Estimation of thermal impulse response of a multi-layer building wall through in-situ experimental measurements in a dynamic regime with applications. *Applied Energy*, ***228***, 468-486.
[125] Evangelisti, L., Guattari, C., Gori, P., & Asdrubali, F. (2018). Assessment of equivalent thermal properties of multilayer building walls coupling simulations and experimental measurements. *Building and Environment*, ***127***, 77-85.
[126] Šuklje, T., Hamdy, M., Arkar, C., Hensen, J. L., & Medved, S. (2019). An inverse modeling approach for the thermal response modeling of green façades. *Applied energy*, ***235***, 1447-1456.
[127] Ghiaus, C., & Alzetto, F. (2019). Design of experiments for Quick U-building method for building energy performance measurement. *Journal of Building Performance Simulation*, ***12(4)***, 465-479.
[128] Pandraud, G., Mangematin, E., Roux, D., & Quentin, E. (2013). QUB: a new rapid building energy diagnosis method. In Proceedings of CLIMA 2013.
[129] Boisson, P. and R. Bouchié (2014). ISABELE method: In-situ assessment of the building envelope performances. in 9th International Conference on System Simulation in Buildings.
[130] Sougkakis, V., Meulemans, J., Alzetto, F., Wood, C., Gillott, M., & Cox, T. (2017, September). An assessment of the QUB method for predicting the whole building thermal performance under actual operating conditions. International SEEDS Conference 2017: Sustainable Ecological EngineeringDesign for Society, Leeds Beckett University, Leeds, United Kingdom. ffhal-01589204
[131] Hiyama, K., Kato, S., & Ishida, Y. (2010, September). Thermal simulation: Response factor analysis using three-dimensional CFD in the simulation of air conditioning control. In Building Simulation (***Vol. 3,*** No. 3, pp. 195-203). Tsinghua Press.
[132] Varela, F., Aroca, S., González, C., & Rovira, A. (2014). A direct numerical integration (DNI) method to obtain wall thermal response factors. *Energy and buildings*, ***81***, 363-370..
[133] Ouyang, K., & Haghighat, F. (1991). A procedure for calculating thermal response factors of multi-layer walls? State space method. *Building and Environment*, ***26(2)***, 173-177.
[134] Pérez, J. S., Chicote, M. A., Díez, F. V., & Gómez, E. V. (2017). A new method for calculating conduction response factors for multilayer constructions based on frequency–Domain spline interpolation (FDSI) and asymptotic analysis. *Energy and Buildings*, ***148***, 280-297.
[135] Yu, G., Chen, H., Xiong, L., & Du, C. (2019). A simplified dynamic model based on response factor method for thermal performance analysis of capillary radiant floors. *Science and Technology for the Built Environment*, ***25(4)***, 450-463.
[136] Tittelein, P., Achard, G., & Wurtz, E. (2009). Modelling earth-to-air heat exchanger behaviour with the convolutive response factors method. *Applied Energy*, ***86(9)***, 1683-1691.
[137] Virseda, P., & Pinazo, J. M. (1997). Thermal behaviour in multilayer products by response factors. *Journal of food engineering*, ***33(3-4)***, 347-358.
[138] Rasooli, A. and L. Itard (2019), Properties of the Triangular Excitation Pulse and the 3D Heat Transfer Effects in the Excitation Pulse Method, in REHVA 13th HVAC World Congress: CLIMA 2019: Bucharest, Romania.
[139] EKO Instruments Europe B.V., www.eko-eu.com, Den Haag, Netherlands.
[140] FLIR Systems, I., www.flir.com, Wilsonville, USA.
[141] Underwood, C. P., & Yik, F. (2004). Modelling methods for energy in buildings. Oxford: Blackwell Science.
[142] Trakhtenbrot, B. A. (1984). A survey of Russian approaches to perebor (brute-force searches) algorithms. *Annals of the History of Computing*, ***6(4)***, 384-400.
[143] ISO, I. S. (2015). 9972: 2015 Thermal Performance of Buildings–Determination of Air Permeability of Buildings–Fan Pressurization Method. International Organization for Standardization: Geneva, Switzerland.
[144] ASHRAE, H. (2001). ASHRAE fundamentals handbook. American Society of Heating Refrigeration and Air-Conditioning Engineers. Atlanta GA.
[145] Raillon, L. (2018). Experimental Identification of Physical Thermal Models for Demand Response and Performance Evaluation, Doctoral dissertation, Saint Gobain, France.
[146] Ricciu, R., Ragnedda, F., Galatioto, A., Gana, S., Besalduch, L. A., & Frattolillo, A. (2019). Thermal properties of building walls: Indirect estimation using the inverse method with a harmonic approach. *Energy and Buildings*, ***187***, 257-268.
[147] Rasooli, A., & Itard, L. (2019). In-situ rapid determination of walls' thermal conductivity, volumetric heat capacity, and thermal resistance, using response factors. *Applied energy*, ***253***, 113539.

[148] Rasooli, A., L. Itard, and A. Meijer (2017), Energy and Comfort Monitoring in Existing Buildings: A LargeScale Measurement Campaign of 150 Dutch Dwellings, in ASHRAE 6th International Conference: ENERGY in BUILDINGS 2017, ASHRAE: Athens, Greece.

[149] Costola, D., A.P. Melo, and L. Jacob (2017), Development of Energy Simulation Models from Smart Meter Data using Inverse Modelling and Genetic Algorithms. Proceedings of the 15th IBPSA ConferenceSan Francisco, CA, USA, Aug. 7-9, 2017.

[150] Kramer, R., van Schijndel, J., & Schellen, H. (2013). Inverse modeling of simplified hygrothermal building models to predict and characterize indoor climates. *Building and Environment*, ***68***, 87-99.

[151] Dong, B., Cao, C., & Lee, S. E. (2005). Applying support vector machines to predict building energy consumption in tropical region. *Energy and Buildings*, ***37(5)***, 545-553.

[152] Karatasou, S., Santamouris, M., & Geros, V. (2006). Modeling and predicting building's energy use with artificial neural networks: Methods and results. *Energy and buildings*, ***38(8)***, 949-958.

[153] Lam, K. P., Zhao, J., Ydstie, E. B., Wirick, J., Qi, M., & Park, J. H. (2014). An EnergyPlus whole building energy model calibration method for office buildings using occupant behavior data mining and empirical data. *ASHRAE Journal*, 160-167.

[154] Braun, J. E., & Chaturvedi, N. (2002). An inverse gray-box model for transient building load prediction. *HVAC&R Research*, ***8(1)***, 73-99.

[155] Nordström, G., Johnsson, H., & Lidelöw, S. (2013). Using the energy signature method to estimate the effective U-value of buildings. In *Sustainability in Energy and Buildings* (pp. 35-44). Springer, Berlin, Heidelberg.

[156] Ghiaus, C. (2006). Experimental estimation of building energy performance by robust regression. *Energy and buildings*, ***38(6)***, 582-587.

[157] Ahmad, N., Ghiaus, C., & Thiery, T. (2020). Influence of Initial and Boundary Conditions on the Accuracy of the QUB Method to Determine the Overall Heat Loss Coefficient of a Building. *Energies*, ***13(1)***, 284.

[158] Kramer, R., Van Schijndel, J., & Schellen, H. (2012). Simplified thermal and hygric building models: A literature review. *Frontiers of architectural research*, ***1(4)***, 318-325.

[159] Berthou, T., Stabat, P., Salvazet, R., & Marchio, D. (2014). Development and validation of a gray box model to predict thermal behavior of occupied office buildings. *Energy and Buildings*, ***74***, 91-100..

[160] Hazyuk, I., Ghiaus, C., & Penhouet, D. (2012). Optimal temperature control of intermittently heated buildings using Model Predictive Control: Part I–Building modeling. *Building and Environment*, ***51***, 379-387.

[161] Trčka, M., & Hensen, J. L. (2010). Overview of HVAC system simulation. Automation in Construction, 19(2), 93-99.

[162] Mihail–Bogdan, C. Ă. R. U. Ţ. A. Ş. I. U., Constantin, I. O. N. E. S. C. U., & Horia, N. E. C. U. L. A. (2016). The influence of Genetic Algorithm parameters over the efficiency of the energy consumption estimation in a low–energy building. *Energy Procedia*, ***85***, 99-108.

[163] Gupta, P. (2017). Inverse Modelling for Determination of Resistance & Capacitance of Typical Dutch Residences Using Genetic Algorithms, MSc thesis, Electrical Engineering, Mathematics and Computer Science. 2017, Delft University of Technology, Netherlands.

[164] Ioannou, A. (2018). Thermal comfort and energy related occupancy behavior in Dutch residential dwellings. A+ BE| Architecture and the Built Environment, (27), 242-242., PhD Thesis, Delft University of technology, the Netherlands.

[165] (KNMI), K.N.M.I. The Royal Netherlands Meteorological Institute. Available from: https://www.knmi.nl/over-het-knmi/about.

[166] Royer, S., Thil, S., Talbert, T., & Polit, M. (2014). A procedure for modeling buildings and their thermal zones using co-simulation and system identification. *Energy and buildings*, ***78***, 231-237..

[167] van den Brom, P. I. (2020). Energy in Dwellings: A comparison between Theory and Practice. A+ BE| Architecture and the Built Environment, PhD Thesis, Delft University of technology, the Netherlands.

[168] Sunikka-Blank, M., & Galvin, R. (2012). Introducing the prebound effect: the gap between performance and actual energy consumption. *Building Research & Information*, ***40(3)***, 260-273.

[169] Balaras, C. A., Dascalaki, E. G., Droutsa, K. G., & Kontoyiannidis, S. (2016). Empirical assessment of calculated and actual heating energy use in Hellenic residential buildings. *Applied Energy*, ***164***, 115-132.

[170] Menezes, A. C., Cripps, A., Bouchlaghem, D., & Buswell, R. (2012). Predicted vs. actual energy performance of non-domestic buildings: Using post-occupancy evaluation data to reduce the performance gap. *Applied energy*, ***97***, 355-364.

[171] Delghust, M. (2015). Improving the predictive power of simplified residential space heating demand models: a field data and model driven study, Doctoral dissertation, Ghent University, Belgium.
[172] Ioannou, A., & Itard, L. C. M. (2014). Thermal comfort in residential buildings: sensitivity to building parameters and occupancy. In BauSIM 2014: Proceedings of the 5th German-Austrian IBPSA conference" Human-centred building (s)", Aachen, Germany, 22-24 September 2014. RWTH.
[173] van den Brom, P., Meijer, A., & Visscher, H. (2018). Performance gaps in energy consumption: household groups and building characteristics. *Building Research & Information*, ***46(1)***, 54-70.
[174] Itard, L., Ioannou, T., Meijer, A., & Rasooli, A. (2016). Development of improved models for the accurate prediction of energy consumption in dwellings. Monicair report, 111.
[175] Ioannou, A., & Itard, L. (2017). In-situ and real time measurements of thermal comfort and its determinants in thirty residential dwellings in the Netherlands. *Energy and Buildings*, ***139***, 487-505.

Biographical Note

Arash Rasooli was born in 1989 in Tehran, Iran. He began his academic life in 2007. He did a bachelor of science in Mechanical Engineering, solid design, in the Faculty of Mechanical and Aerospace Engineering, Tehran Science and Research Branch of IAU. In 2012, seeking higher education, he decided to experience living abroad. He moved to the Netherlands where he did a master of science in Mechanical Engineering, this time, specialization Energy Technology, at Delft University of Technology. During a master course “Indoor Climate Control Fundamentals” he met Prof. L. Itard, who agreed to supervise his internship project at OTB, a research institute for the built environment. Subsequently, he continued the internship project for his master thesis entitled: “Computational and Experimental Investigation of Walls’ Thermal Transmittance in Existing Buildings”. Following the success of the research, he was extremely eager to follow up the findings. He was offered to continue his research in the framework of a PhD research, under supervision of Prof. L. Itard. In 2016, he won the 1st prizes in TVVL national and REHVA international (EU) Student Competitions with his MSc thesis. He later won the 1st prize of the World HVAC Student Competition, which led to his cooperation with TVVL as the student competition jury member and with REHVA as the coordinator of "REHVA Community of Young Professionals". Parallel to his PhD research, Arash has been teaching in an MSc course “Indoor Climate Control Fundamentals” in the faculty of Mechanical, Maritime, and Materials Engineering at Delft University of Technology. This, later, led to his activity as an instructor in an online program in edX platform.

Having finished the PhD research, Arash will partly continue it in other ways alongside his future career, in research and development for thermal conductivity and heat flux instrumentation in EKO Instruments Europe B.V.

List of Publications

Patent

Itard, L. ,Rasooli, A., & Infante Ferreira, C. (2017). Method and Instrumentation for Determining at Least One Thermal Parameter of a Wall, NL Patent No. 2014467

Journal Articles

Rasooli, A., Itard, L., & Ferreira, C. I. (2016). A response factor-based method for the rapid in-situ determination of wall's thermal resistance in existing buildings. Energy and Buildings, 119, 51-61.

Rasooli, A., & Itard, L. (2018). In-situ characterization of walls' thermal resistance: An extension to the ISO 9869 standard method. Energy and Buildings, 179, 374-383.

Rasooli, A., & Itard, L. (2019). In-situ rapid determination of walls' thermal conductivity, volumetric heat capacity, and thermal resistance, using response factors. Applied Energy, 253, 113539.

Rasooli, A., & Itard, L. Automated In-Situ Determination of Buildings' Global Thermo-Physical Characteristics and Air Change Rates through Inverse Modelling of Smart Meter and Air Temperature Data. (Submitted)

Conference Papers

Rasooli, A., Itard, L. C. M., & Infante Ferreira, C. A. (2016, May). Introduction to an in-situ method for rapid measurement of the walls' thermal resistance in existing buildings. In CLIMA 2016-12th REHVA World Congress. Aalborg University.

Rasooli, A., & Itard, L. (2019, May). Quicker Measurement of Walls' Thermal Resistance Following an Extension to ISO 9869 Average Method. In E3S Web of Conferences (Vol. 111, p. 04019). EDP Sciences.CLIMA 2019: REHVA 13th HVAC World Congress, Bucharest, Romaina

Rasooli, A., & Itard, L. (2019, May). Properties of the triangular excitation pulse and the 3D heat transfer effects in the excitation pulse method. In E3S Web of Conferences (Vol. 111, p. 04018). EDP Sciences. CLIMA 2019: REHVA 13th HVAC World Congress, Bucharest, Romaina

Rasooli, A., L. Itard, and A. Meijer, (2017). Energy and Comfort Monitoring in Existing Buildings: A Large-Scale Measurement Campaign of 150 Dutch Dwellings, in ASHRAE 6th International Conference: ENERGY in BUILDINGS 2017, ASHRAE: Athens, Greece.

Professional Journal Paper

Rasooli, A., Itard, L., & Infante Ferreira, C. (2016). Rapid, transient, in-situ determination of wall's thermal transmittance. REHVA European HVAC Journal, 53, 16-20.

20#07

In-Situ Determination of Buildings' Thermo-Physical Characteristics

Method Development, Experimentation, and Computation

Arash Rasooli

Accurate determination of building's critical thermo-physical characteristics such as the walls' thermal resistance, thermal conductivity, and volumetric heat capacity is essential to indicate effective and efficient energy conservation strategies at building level. In practice, the values of these parameters, which determine not only possible energy savings, but also related costs, are rarely available because the current determination methods are time-and-effort-expensive, and consequently seldom used. This thesis combines theories, simulations, computations, and experiments to develop and improve methods and approaches for determination of a number of buildings' most important thermo-physical characteristics. First, a modification to the existing standard method, "ISO 9869 Average Method" is proposed to measure the walls' thermal resistance. Two current problems are solved: long measurement duration (weeks) and imprecision. To further shorten the measurement period to a few hours, a new transient in-situ method, Excitation Pulse Method, EPM (Patent No. 2014467), is then developed and tested. This method allows the determination of the walls' response factors which can be applied directly in dynamic models. More importantly, it is used to extract critical construction information including walls' thermal resistance, thermal conductivity, volumetric heat capacity, and the possible layer composition. Finally, in an attempt to reduce the hassle, cost, and intrusion associated with locally-conducted experiments, the use of data from smart meters and home automation systems is explored. Building's global characteristics including heat loss coefficient, global heat capacitance and daily air change rates are accordingly determined.

A+BE | Architecture and the Built Environment | TU Delft BK